UNIVERSITY OF CALIFORNIA, SAN DIEGO

Gas Sensing Mechanisms in Chemiresistive Metal Phthalocyanine Nanofilms

A Thesis submitted in partial satisfaction of the

Requirements for the degree Doctor of Philosophy

in

Chemistry

by

Forest I. Bohrer

Committee in charge:

Professor William C. Trogler, Chair
Professor Seth M. Cohen
Professor Clifford P. Kubiak
Professor Andrew C. Kummel
Professor Lawrence E. Larson

2008

The dissertation of Forest I. Bohrer is approved, and it is acceptable in quality and form for publication on microfilm.

_____

_____

_____

_____

_____

Chair

University of California, San Diego

2008

DEDICATION

This work is dedicated to my parents, for providing the utmost support throughout my life;

My brother, for his constant companionship;

And my wife, whose love has helped me to become who I am today.

TABLE OF CONTENTS

LIST OF SYMBOLS AND ABBREVIATIONS

Å	Angstrom
A	Ampere
AC	alternating current
AChE	acetylcholinesterase
AFM	atomic force microscopy
ANOVA	analysis of variance
β_2^H	hydrogen bond basicity scale
BF_3	boron trifluoride
CCl_4	carbon tetrachloride
CH_2Cl_2	dichloromethane
chemFET	chemically sensitive field effect transistor
Cl_2	chlorine (diatomic)
$cm^2\ V^{-1}\ s^{-1}$	centimeter squared per volt per second (unit of charge mobility)
CME	chemically modified electrode
CO	carbon monoxide
CoPc	cobalt phthalocyanine
CuCN	copper cyanide
CuPc	copper phthalocyanine
CW	chemical warfare
Δ	delta, change
DBU	1,8-diazabicyclo[5.4.0] undec-7-ene
DC	direct current
DCP	diethyl chlorophosphate
DFT	density functional theory
$dm^3\ mol^{-1}$	decimeter cubed per mole
DMAE	*N*,*N*-dimethylaminoethanol
DMF	*N*,*N*-dimethylformamide
DMMP	dimethyl methyl phosphonate
DMSO	dimethyl sulfoxide
e^-	electron
EPR	electron paramagnetic resonance
$FeCl_3$	ferric chloride
Fe_2O_3	ferric oxide
FePc	iron phthalocyanine
FET	field effect transistor
FTIR	Fourier transform infrared spectroscopy
G^o	Gibbs free energy
GC/MS	gas chromatography/mass spectrometry
H^o	enthalpy
$-\Delta H^o_{BF_3}$	Lewis basicity scale

H_2O_2	hydrogen peroxide
H_2Pc	metal-free phthalocyanine
HCl	hydrochloric acid
HFA	hexafluoroacetone
HFIP	1,1,1,3,3,3-hexafluoropropan-2-ol
HMTD	hexamethylene triperoxide diamine
HOMO	highest occupied molecular orbital
HPLC	high performance liquid chromatography
I_0	initial current
I_f	final current
I_2	iodine (diatomic)
IDE	interdigitated electrode
IR	infrared
I-V	current-voltage
K	Kelvin
K	equilibrium constant
k	rate constant
KBr	potassium bromide
kJ mol^{-1}	kilojoules per mole
λ	lambda (wavelength)
LC/MS	liquid chromatography/ mass spectrometry
LDA	linear discriminant analysis
LIDAR	light detection and ranging
Li_2Pc	dilithium phthalocyanine
$LnPc_2$	lanthanide bis(phthalocyanine)
LSER	linear solvation energy relationships
LUMO	lowest unoccupied molecular orbital
μL	microliter ($L*10^{-6}$)
μm	micrometer ($m*10^{-6}$)
MOEP	metallooctaethyl porphyrin
MOSFET	metal-oxide-semiconductor field effect transistor
MPc	metallophthalocyanine
MTPP	metallotetraphenyl porphyrin
ng	nanogram ($g*10^{-9}$)
$NaHCO_3$	sodium bicarbonate
$NaNO_2$	sodium nitrite
NH_3	ammonia
NiPc	nickel phthalocyanine
NIR	near-infrared
nm	nanometer ($m*10^{-9}$)
NMR	nuclear magnetic resonance
NO	nitric oxide
NO_x	nitrogen oxide species
NO_2	nitrogen dioxide
O_2	oxygen (diatomic)
O_3	ozone

OFET	organic field effect transistor
$^{\bullet}OH$	hydroxyl radical
OMBE	organic molecular beam epitaxy
OP	organophosphate
OPH	organophosphate hydrolase
π	pi; bond or orbital
π^*	pi-star; anti-bonding π orbital
% ppm^{-1}	percent current change per ppm
PbPc	lead phthalocyanine
PCA	principal component analysis
PCB	printed circuit board
pH	$pH = -\log[H^+]$
ppb	part per billion
ppm	part per million
QCM	quartz crystal microbalance
R	gas constant
redox	reduction/oxidation
RH	relative humidity
RMS	root mean square
s	second
s^{-1}	reciprocal second (i.e. per second)
S^o	entropy
S cm^{-1}	Siemens per centimeter
SAM	self assembled monolayer
SAW	surface acoustic wave
sccm	standard cubic centimeter per minute
SCE	standard carbon electrode
SCLC	space-charge limited conductivity
SiO_2	silicon dioxide
S/N	signal to noise ratio
SnO_2	stannic oxide
SWNT	single-walled carbon nanotube
T	temperature
$t_{90}^{'}$	time required for the sensor to recover 90% of baseline current
TATP	triacetone triperoxide
THF	tetrahydrofuran
TiOPc	titanyl phthalocyanine
UHV	ultrahigh vacuum
UV/Vis	ultra-violet/visible radiation
V	Volt
VOC	volatile organic compound
VOPc	vanadyl phthalocyanine
XRD	X-ray diffraction
ZnPc	zinc phthalocyanine

LIST OF FIGURES

Chapter I

Chapter II

Chapter III

Chapter IV

Chapter V

Chapter VI

LIST OF SCHEMES

Chapter I

Chapter II

Chapter III

Chapter IV

LIST OF TABLES

Chapter I

Chapter III

Chapter IV

Chapter V

ACKNOWLEDGEMENT

It has been wonderful to work with and learn from my advisor, Professor Bill Trogler, and his close collaborator, Professor Andy Kummel. I have benefited immeasurably from their scientific knowledge, practical laboratory experience, and career advice. I can think of no better mentors in the field of chemistry. My undergraduate advisor, Professor Susan Kauzlarich, has likewise been indispensable in my career development; she helped start me on my way to my doctorate, and to this day provides me with valuable advice and friendship.

I would like to thank Dr. Karla Miller for helping get me started on my graduate study. I am indebted to Dr. Amos Sharoni for scientific consultation and guiding me through my first difficult attempts at writing a scientific paper. His advice throughout my graduate study has been invaluable. I am grateful to Professor Ivan Schuller for his expert organization and management of the Integrated Nanosensors Laboratory and the AFOSR MURI project.

I would also like to thank my fellow researchers on the nanosensors project, including Cornel Colesniuc for his sense of humor and willingness to deposit endless numbers of films, Jeongwon Park for his cheerfulness and tireless efforts towards device fabrication, and Ngoc Tran for her friendship and theoretical expertise. I have also benefited from working with Richard Yang, Thomas Gredig, and Dr. Bernd Fruhberger.

I thank also the Trogler lab, including Sarah Toal, Sara Urbas, Jason Sanchez, Paul Martinez, Kristina Pohaku, and Zheng Wang. I have learned much working with

this group of individuals and have had a wonderful time doing so. I also am grateful to the many friends I have made in the chemistry department, including Ben, Anne, Shannon, Mike, Byron, Ilya, Stephen, Sara, Amanda, Becky, and many others.

I would like to thank my family for their endless support throughout my education. The generosity and hospitality of my parents cannot be exaggerated, and their encouragement has helped me through many difficulties. My brother has been a great friend and sympathetic ear for the trials of graduate school, a labor which he is also completing. Finally, I thank my wife for her unending support and love. Our relationship is the best thing in my life, and I look forward to embarking on the next phase of our life together at last.

Chapter 3 is a reprint in full of the material as it appears in the *Journal of the American Chemical Society*, **2007**, *129*(*17*), 5640-5646. Coauthors included A. Sharoni, C. Colesniuc, J. Park, I. K. Schuller, A. C. Kummel, and W. C. Trogler. Chapter 4 is a reprint in full of the material as it has been submitted to the *Journal of the American Society*, **2008**. Coauthors included C. Colesniuc, J. Park, M. E. Ruidiaz, I. K. Schuller, A. C. Kummel, and W. C. Trogler. Chapter 5 is a reprint in full of the material as it has been submitted to the *Journal of Materials Chemistry*, **2008**. Coauthors included C. Colesniuc, J. Park, I. K. Schuller, A. C. Kummel, and W. C. Trogler. The dissertation author was the primary investigator and author of these publications.

VITA

2003	Bachelor of Science, Chemistry, University of California, Davis
2003 – 2004	Teaching Assistant, Department of Chemistry and Biochemistry, University of California, San Diego
2005	Master of Science, Chemistry, University of California, San Diego
2008	Doctor of Philosophy, Chemistry, University of California, San Diego

PUBLICATIONS

Bohrer, F. I.; Sharoni, A.; Colesniuc, C.; Park, J.; Schuller, I. K.; Kummel, A. C.; Trogler, W. C. "Gas Sensing Mechanism in Chemiresistive Cobalt and Metal-Free Phthalocyanine Thin Films," *J. Am. Chem. Soc.* **2007**, *129*, 5640-5646.

Bohrer, F. I.; Colesniuc, C. N.; Park, J.; Schuller, I. K.; Kummel, A. C.; Trogler, W. C. "Selective Detection of Vapor Phase Hydrogen Peroxide with Phthalocyanine Chemiresistors," *J. Am. Chem. Soc.* **2008**, *130*, 3712-3713.

Bohrer, F. I.; Colesniuc, C. N.; Park, J.; Schuller, I. K.; Kummel, A. C.; Trogler, W. C. "Selective Vapor-Phase Detection of Peroxides with Chemiresistive Phthalocyanine Nanofilms," *J. Mater. Chem.* **2008** *submitted for publication*.

Bohrer, F. I.; Colesniuc, C. N.; Park, J.; Ruidiaz, M. E.; Schuller, I. K.; Kummel, A. C.; Trogler, W. C. "Comparative Gas Sensing in Cobalt, Nickel, Copper, Zinc, and Metal-Free Phthalocyanine Chemiresistors" *J. Am. Chem. Soc.* **2008** *manuscript in preparation*.

ABSTRACT OF THE DISSERTATION

Gas Sensing Mechanisms in Chemiresistive Metal Phthalocyanine Nanofilms

By

Forest I. Bohrer

Doctor of Philosophy in Chemistry

University of California, San Diego, 2008

Professor William C. Trogler, Chair

Chemiresistive films of metallophthalocyanines (MPcs; M = Fe, Co, Ni, Cu, Zn, and H_2) are shown to be sensitive to gas phase electron donors and acceptors. The mechanism of sensing occurs through coordination of the analyte molecule to metal center of the phthalocyanine; electron donors cause film current losses by trapping of charge carriers, while electron acceptors causes current gains by generation of charge

carriers within the film. Vapor phase peroxides may cause gains or losses of film current by electrocatalytic processes dependent on the metal center.

MPcs featuring varied metal centers and peripheral substituents are prepared via literature procedures. A novel route is devised for synthesis of a copper phthalocyanine incorporating the 1,1,1,3,3,3-hexafluoropropan-2-ol (HFIP) group. MPc films are deposited by organic molecular beam epitaxy (OMBE) and spin-coating; film morphologies are examined by atomic force microscopy (AFM). It is demonstrated that substrate temperature during OMBE deposition can significantly alter grain morphology. Spin-coating offers a cost-effective alternative to OMBE, with soluble, functionalized phthalocyanines. The roles of solvent and functional group are explored and procedures for preparing uniform amorphous films are described.

The differing mechanisms of sensing in metal-free phthalocyanine (H_2Pc) and metalated phthalocyanines (MPc) are examined with respect to electron-donating (basic) analytes. MPc sensitivities to vapor phase electron donors are correlated exponentially with analyte basicity as described by binding enthalpy, consistent with the van't Hoff equation and the standard free energy of reaction. Coordination of analytes to the phthalocyanine metal center (MPc) or inner protons (H_2Pc) is the dominant mechanism of chemical sensing for basic analytes. Sensor recovery times $t_{90}^{'}$ are demonstrated to depend exponentially on binding enthalpy. Linear discriminant analysis is used to identify analytes. Single sensor normalization of analyte concentration leads to excellent discrimination and identification of analytes.

MPc sensing arrays are shown to be redox-selective vapor sensors of hydrogen peroxide and di-*t*-butyl peroxide. These peroxides cause unique current losses in CoPc sensors and current gains in FePc, NiPc, CuPc, ZnPc, and H_2Pc sensors. Detection limits of 50 ppb and 250 ppb are achieved for hydrogen peroxide and di-*t*-butyl peroxide, respectively. Oxidation and reduction of peroxides via catalysis at the phthalocyanine surface is consistent with the pattern of sensor responses. Differential analysis by redox contrast of a small array of sensors thus uniquely identifies peroxide vapors.

Chemically sensitive field-effect transistors (ChemFETs) of ZnPc are evaluated for use as vapor sensors. The average carrier mobility is 1.3×10^{-4} cm^2 V^{-1} s^{-1}, comparable to previously reported phthalocyanine mobility values. ZnPc ChemFETs display persistent photoconductivity, lasting up to 1.5 months, which induces significant baseline drift. Persistent photoconductivity and sensor instability require improvements to the ZnPc ChemFET architecture before its implementation as vapor sensors.

CHAPTER I

REVIEW OF METALLOPHTHALOCYANINE CHEMISTRY AND CHEMIRESISTIVE GAS SENSING

1.1 METALLOPHTHALOCYANINE CHEMISTRY

Phthalocyanines, both metalated (MPc) and metal-free (H_2Pc), are a class of coordination complexes composed of a dianionic macrocyclic ring with a central metal center (MPc) or two central protons (H_2Pc, Figure 1-1). MPcs are used industrially as dyes[1-2] and catalysts,[3-4] and as components of recordable media,[5] photovoltaics,[6] and vapor sensors.[7] MPcs generally behave as p-type semiconductors sensitive to environmental gas species; indeed, MPcs have little intrinsic conductivity and their observed conductivity arises from doping by gas-phase oxidants such as oxygen and ozone.[8-10] Phthalocyanine chemical and electronic properties may be tuned through variation of the metal center,[11-12] or through organic functionalization of the macrocycle.[13]

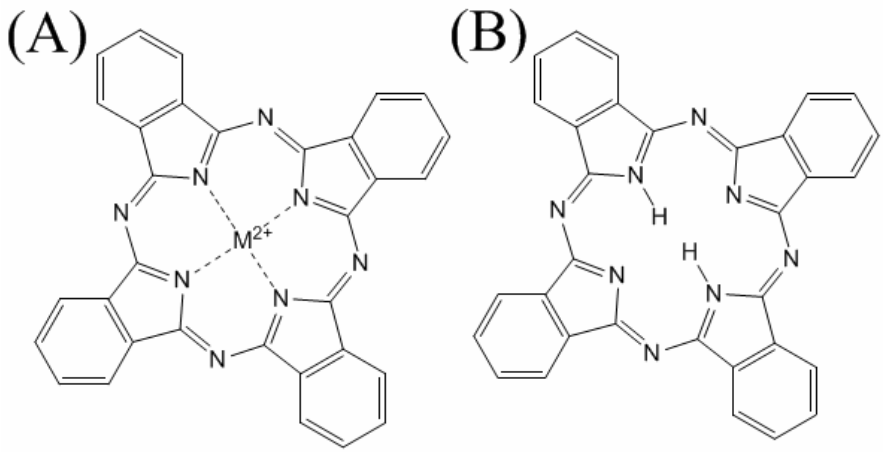

Figure 1-1 (A) Metallophthalocyanine and (B) metal-free phthalocyanine.

1.1.1 Syntheses of Metallophthalocyanines

MPcs may be prepared by several synthetic methods (Scheme 1-1), which generally involve the reaction of derivatives of phthalic acid and a divalent metal salt (MX_2*yH_2O) in a high-boiling alcohol solvent. Examples include (**1**) reaction of diiminoisoindole with formamide and MX_2, (**2**) reaction of phthalimide with formamide and MX_2, (**3**) molybdenum trioxide-catalyzed reaction of phthalic anhydride with urea and MX_2, (**4**) condensation of *ortho*-cyanobenzamide around a M^{2+} center, and (**5**) base-catalyzed cyclization of phthalonitrile around a M^{2+} center.[14-19]

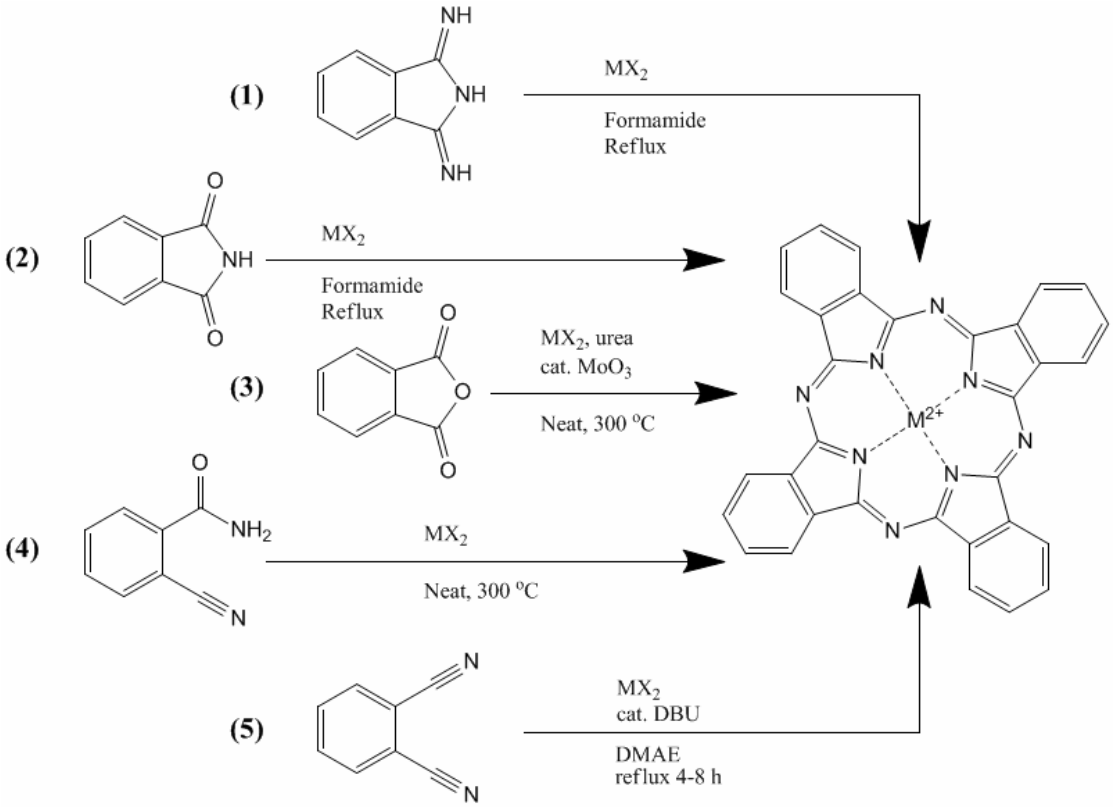

Scheme 1-1 Pathways for the synthesis of metallophthalocyanines.

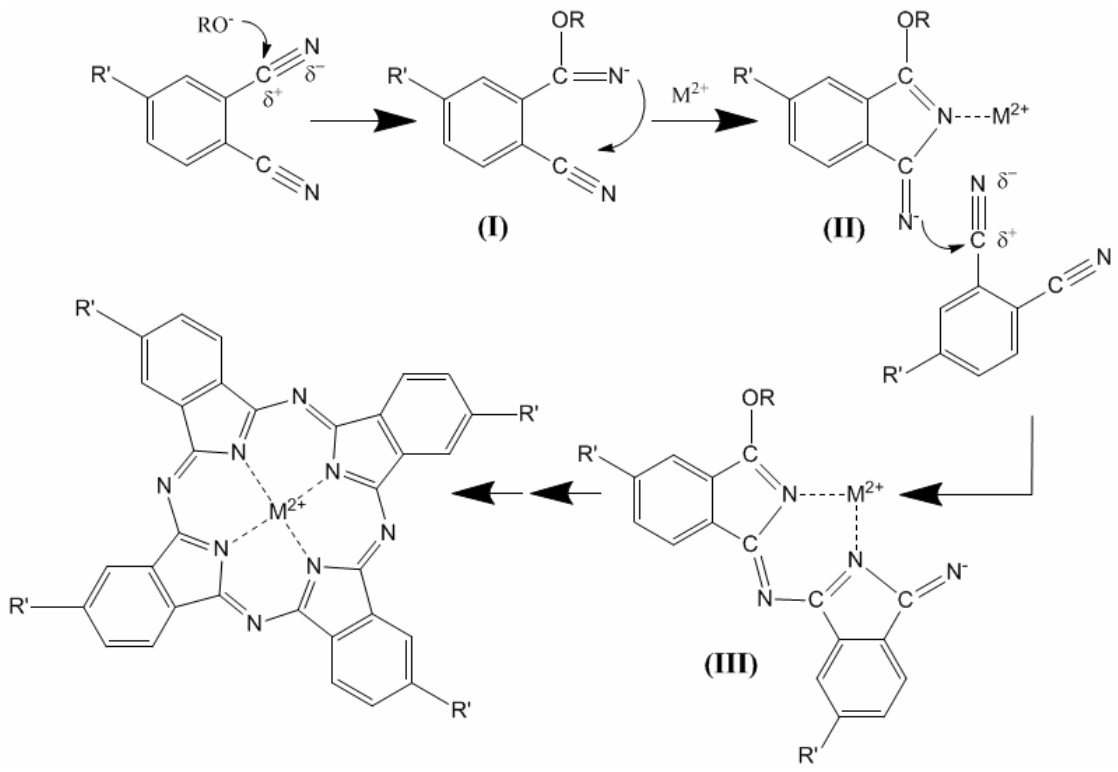

Scheme 1-2 Mechanism of phthalocyanine formation from phthalonitrile.

A convenient synthetic pathway is (**5**), the cyclization of phthalonitrile around a metal center of choice in *N*,*N*-dimethylaminoethanol (DMAE), a high-boiling, basic alcohol, with a catalytic amount of 1,8-diazabicyclo[5.4.0]undec-7-ene (DBU), a strong organic base.[20] The mechanism of this reaction involves nucleophilic attack of an alkoxide anion (Scheme 1-2 **I**; formed by deprotonation of the solvent by DBU) on the electron deficient carbon of one of the nitrile groups, leading to the formation of a 1-alkoxy-3-iminoisoindolenine intermediate (Scheme 1-2 **II**).[21] This intermediate may coordinate weakly to a metal, and sequential nucleophilic attack of the anionic nitrogen of the iminoisoindolenine intermediate on the nitrile group of another phthalonitrile (Scheme 1-2 **III**) leads to the formation of a phthalocyanine molecule

around the templating metal center.[21-22] This template effect is crucial to phthalocyanine formation; H_2Pc is prepared by first making the dilithium complex Li_2Pc, which is then hydrolyzed to form H_2Pc.[22]

1.1.1.1 Monophthalocyanines

MPcs have been synthesized with nearly every transition metal in the periodic table, as well as with lanthanides and some main group elements. MPcs containing late first-row transition metal centers (M = Fe, Co, Ni, Cu, and Zn) are widely used in catalysis, sensor applications, and molecular electronics studies.[4,7-10] Metal-free H_2Pc is also commonly employed in sensing and dye applications.[22-24] Early first-row transition metals (M = Ti, V, Cr, Mn) have also been incorporated into phthalocyanines; these MPcs often exhibit varied oxidation states (e.g. Mn^{3+}, Ti^{4+}).[25-27] Titanyl and vanadyl phthalocyanines in particular exhibit interesting chemistry; the central metals are in the +4 oxidation state and are thus capped with axial oxo ligands.[28-29] TiOPc is of particular interest for photovoltaic and photoconductivity applications.[30-31]

Second and third row transition metals are less widely studied, with the exception of PbPc, a common material for sensor and photovoltaic applications.[32-35] The central lead cation is large enough that it buckles the plane of the phthalocyanine, leading to unique crystalline structures. Ruthenium phthalocyanine has been studied for structural and catalytic properties,[36-37] while palladium phthalocyanine is of interest for its magnetic and electrochemical activities.[38-39] Main group metalloids

have also been incorporated into phthalocyanines, most notably with aluminum and silicon.[40-42]

1.1.1.2 Bis(phthalocyanines)

MPcs have also been synthesized using lanthanides (Ln) as metal centers; these large, heavy f-block metals (M = Pr, Nd, Sm, Gd, Tb, Dy, Ho, Er, Yb, Lu) are too large to fit within the central cavity of the Pc molecule, and so generally form bis(phthalocyanine) sandwich complexes ($LnPc_2$, Figure 1-2 A).[43-45] Lanthanide bis(phthalocyanines) are synthesized using similar methods to monophthalocyanines (Scheme 1-1 **5**), but considerable amounts of H_2Pc often form as a by-product. The ease of synthesis of $LnPc_2$ is greatest for Lu, becoming more difficult as one approaches La.[45] Triple phthalocyanine stacks involving two lanthanide centers have also been prepared (Figure 1-2 B).[46-47] The $LnPc_2$ compounds are easily oxidized materials, having blue (neutral) and green (radical cation) forms.[48] They have been studied for applications as electrochromic materials, gas sensors, and single molecule magnets.[49-53]

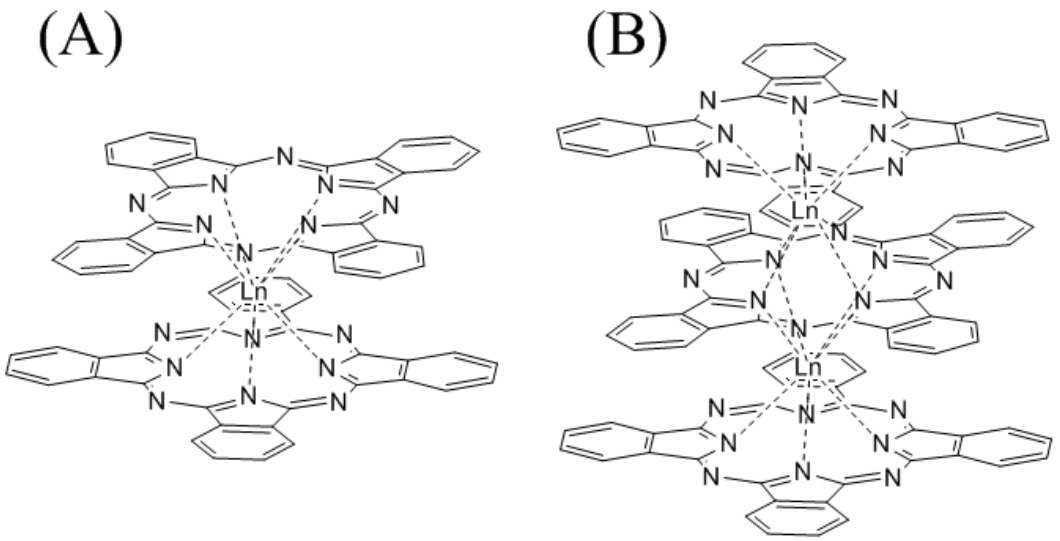

Figure 1-2 (A) Lanthanide bis(phthalocyanine) and (B) dilanthanide tris(phthalocyanine).

1.1.1.3 Substituted MPcs

The phthalocyanine ring itself has been modified by using differing template sizes, as well as organic functional groups. The standard phthalocyanine ring contains four diiminoisoindolenine units (Scheme 1-2), but subphthalocyanines with three such subunits have been prepared around small boron cations, and superphthalocyanines with five subunits have been templated around large uranium cations.[54-55] The external ring of the phthalocyanine can be functionalized at the periphery by using the appropriate phthalonitrile (Scheme 1-2); the most commonly functionalized position is the 4(5) position, leading to tetra- and octa-substitution.[56-57] The primary effect of this type of functionalization is to impart solubility; the functional groups may also alter the chemistry of the phthalocyanine significantly. The phthalocyanine ring has also been functionalized in the 3(6) position, but steric effects may present difficulties.[15] In the case of tetrasubstituted phthalocyanines, four isomers arise, leading to amorphous

solids and a lack of crystallinity, with separation of the isomers being very difficult.[58] It is also possible to complete substitution (hexadecasubstitution).[13]

The most popular substituents are alkyl and alkoxy groups.[56-58] Fluorinated MPcs are of significant interest because the strongly electron-withdrawing fluorine groups can significantly alter the electronic structure of the phthalocyanine; hexadecafluorinated MPcs are n-type semiconductors, which have been used for vapor sensors and molecular electronics. Chlorinated phthalocyanines have also been explored for similar applications.[63] Functional groups alter phthalocyanine chemistry, leading to spectroscopic changes,[64] increased solubility,[65] and ring annulation.[66-68]

1.1.2 Structural Properties of MPcs

1.1.2.1 MPc Crystal Structures

Standard MPcs are highly crystalline materials. MPcs are known to stack in a herringbone-type structure, with the z-axis in the direction of the metal center column (Figure 1-3).[7-10] The most common MPcs (M = H_2, Fe, Co, Ni, Cu, Zn) exhibit two monoclinic crystalline phases, denoted the α and β phases.[69-70] The stabilities of the two phases are temperature dependent, with α phase forming at lower temperatures (below 100 ^{o}C) and β phase forming at elevated temperatures (above 100 ^{o}C).[71] These phases differ in the tilt angle of the molecular plane to the stack axis; the α phase has a tilt angle of 26.5^{o} and β phase has a tilt angle of 46.8^{o}.[72] These crystal forms are adopted by the large number of unsubstituted MPcs that are essentially planar;

however, phthalocyanines with large central metals (PbPc), axially coordinating ligands (TiOPc), or lanthanide bis(phthalocyanines) have unique crystal structures.

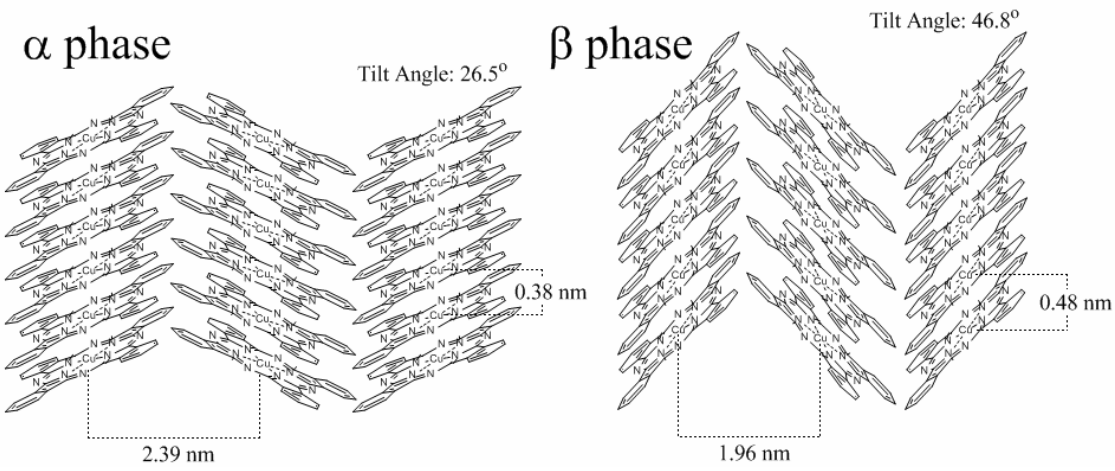

Figure 1-3 Copper phthalocyanine crystalline phases (data from Ashida et al).[72]

PbPc is a well-studied non-planar phthalocyanine that forms a "shuttlecock," with the lead cation buckled out of the plane of the phthalocyanine ligand.[9] This loss of ring planarity leads to alteration of the crystal packing; PbPc exhibits both monoclinic and triclinic polymorphs.[73-74] Similarly, TiOPc and VOPc are non-planar due to axially coordinated oxo ligands. TiOPc exhibits both monoclinic and triclinic crystalline phases, while VOPc forms multiple triclinic phases.[28,75-76] Lanthanide bis(phthalocyanines) exhibit an array of crystal phases ranging from monoclinic to orthorhombic.[77]

1.1.2.2 Mesostructures of MPcs

Crystalline phthalocyanines can form a range of solid phase mesostructures. Structural control is important for thin film applications because the mesostructure can

alter sensing and conduction parameters of MPc-based devices. MPc films form as agglomerations of small crystalline grains with diameters ranging from 50 nm to several μm. MPc grain size is strongly affected by the deposition method, substrate identity, substrate temperature during deposition, and post-deposition annealing. Thermal deposition is the most popular method of depositing MPc films.[7-10] Other methods of deposition include spin-coating of solubilized MPcs and Langmuir-Blodgett film deposition.[78-79]

A deposition method that is well-adapted for fabricating electronic devices is organic molecular beam epitaxy, offering nanometer-scale control of film thickness and deposition rate control down to 0.1 Å s^{-1}.[80] The temperature of the substrate on which the film is deposited affects both the crystal phase and the film mesostructure.[71,81] Films deposited at or below 100 ^{o}C exhibit small, ellipsoid α phase grains (diameter ≈ 50 nm), while films deposited at temperatures above 100 ^{o}C display much larger β phase grains.[71,82] These larger grains may form long crystallites or whisker-like formations.[83] Extended ribbon- and wire-like structures can be achieved using special deposition techniques.[84]

Substrate identity can also affect the size and structure of MPc grains. MPc molecules orient perpendicular to gold surfaces, leading to highly ordered epitaxial growth,[83-85] while on amorphous SiO_2 MPc molecules may orient perpendicular or parallel to the surface.[86] High-temperature annealing of the films can lead to alteration of the grain structure, but in general the substrate temperature during deposition determines the mesostructure of the film.[71,83-85]

Mesostructure and morphology control are important for applications in molecular electronics and sensing technologies. Higher mobilities ($1.6*10^{-2}$ cm^2 V^{-1} s^{-1}) have been achieved in organic field effect transistors (OFETS) of CuPc when the molecular stacking axis is oriented parallel to the electric field as opposed to perpendicular to the field ($1.2*10^{-2}$ cm^2 V^{-1} s^{-1}) or randomly oriented ($1.1*10^{-2}$ cm^2 V^{-1} s^{-1}).[87] Even higher mobilities (0.1-0.2 cm^2 V^{-1} s^{-1}) have been achieved in OFETs using single CuPc nano-ribbons for the conducting channel.[84,88] Porous MPc films with larger grain structures are found to respond faster and more sensitively to analyte vapors, but these sensors exhibit larger current drifts and are less reproducible.[89-91]

1.1.3 Electronic Properties of MPcs

1.1.3.1 MPc Electronic Structures

The electronic structures of MPcs have been studied both experimentally and theoretically. Experimental data includes spectroscopic and electrochemical studies, while the theoretical aspect has been explored by density functional theory (DFT) calculations. Electronic spectra (UV/Vis) of phthalocyanines have been recorded in the vapor phase,[92] the solution phase (DMSO),[93] and the solid state (borosilicate matrices).[94] Two major absorption bands are present in the UV/Vis spectra of MPcs, which give rise to the characteristic blue color of phthalocyanine dyes: the Soret (B) band (λ = 300-350 nm) and the Q band (λ = 600-700 nm). Other minor absorptions are present below λ = 300 nm, designated the N, L, and C bands. The Q band is attributed to π-π^* transitions of the phthalocyanine ring and may be split into Q_x and

Q_y bands.[92] Recently, a weak n-π^* transition has also been identified in the Q-band.[95] Some metal-dependent d-π^* transitions have been noted in the N, L, and C bands, particularly for NiPc.[92-93] The size of the central metal has been correlated with shifts in absorption wavelengths among MPcs.[94]

Oxidation and reduction potentials have been explored by electrochemical techniques, usually cyclic voltammetry, in a variety of solvents.[96-97] Oxidation potentials of MPcs generally increase in the order Fe < Co < Ni, Cu, Zn, H_2 (Table 1-1).[98] Phthalocyanines with redox-active metal centers (Fe, Co) exhibit oxidation at the metal center, while those with less redox-active metal centers (Ni, Cu, Zn, H_2) display oxidation of the organic ring.[98-99] Similar oxidation potentials among NiPc, CuPc, ZnPc, and H_2Pc are consistent with this behavior. Oxidation potentials have been correlated with electronic spectra (UV/Vis) and charge transfer bands (NIR).[100-101] Reduction potentials have also been determined (Table 1-1); again, reductions were reported to occur at the metal center for MPcs with redox-active metal centers and at the organic ring for MPcs without.[102]

Table 1-1 Reported oxidation and reduction potentials for MPcs (M = Fe, Co, Ni, Cu, Zn, H_2); reduction potentials for FePc could not be determined precisely.[98,102]

MPc	Oxidation Potential (V vs. SCE)	Reduction Potential (V vs. SCE)	Type of electron transfer
FePc	0.19	-	Metal $2^+ \leftrightarrow 3^+$
CoPc	0.77	-0.37	Metal $2^+ \leftrightarrow 3^+$
NiPc	1.05	-0.85	Ligand red/ox
CuPc	0.98	-0.84	Ligand red/ox
ZnPc	0.68	-0.89	Ligand red/ox
H_2Pc	1.10	-0.66	Ligand red/ox

MPc electronic structures have been calculated using density functional theory. Liao and Scheiner showed that HOMOs in FePc, CoPc, and CuPc are metal 3*d*-centered while HOMOs in NiPc and ZnPc are localized on the organic ring; LUMOs in all cases are ring centered.[12] However, $1e^-$ oxidations were reported to occur at the A_{1u} (ligand-centered) orbital in all cases, including those with a metal-centered HOMO.[12,103] The 3*d*-like HOMOs of FePc and CoPc are extremely close in energy to the ligand A_{1u} orbital, so there may be significant orbital mixing to account for experimental evidence of metal oxidation and reduction.[98-99] Reductions occur at the metal for FePc and CoPc, and at the ring for NiPc, CuPc, ZnPc, and H_2Pc, consistent with experimental results.[12,103-104] In general, DFT calculational studies agree well with experimental data.[12,103-106]

1.1.3.2 Conductivity in MPcs

MPc conduction mechanisms have been studied using a variety of device geometries, including interdigitated electrodes (IDEs), field effect transistors (FETs), and vertical "sandwich" devices (an MPc layer deposited between two electrode layers). Standard MPcs are p-type semiconductors.[7-10] However, addition of electron withdrawing functional groups, particularly fluorine, can alter the molecular orbital structure drastically, leading to n-type phthalocyanines.[60,107] This inversion of the conductivity mechanism affects gas sensing behaviors.[108-109]

P-type conductivity in MPcs is well understood. It has been found that MPcs are highly resistive in dark, high-vacuum environments.[110-111] On exposure to O_2,

conduction increases drastically; this behavior has been attributed to the formation of charge transfer complexes by coordination of O_2 to MPc metal centers at the air/phthalocyanine interface, leading to MPc^+ and O_2^- species and injection of charge carriers into the bulk solid.[61,111] Superoxide adducts have been directly detected by EPR studies.[112-114] The crystal structures of MPcs are generally unaffected by exposure to air, so it is assumed that this reaction occurs via adsorption of O_2 to surface MPc molecules. Bulk absorption of O_2 has been detected experimentally only for ruthenium phthalocyanine.[37] Gas effusion studies on ZnPc suggest a ratio of approximately one O_2 molecule for every twenty phthalocyanines; correlation with capacitance-voltage plots suggests that only one superoxide adduct is present for every 10,000 O_2 molecules on the film.[115]

Conduction in organic semiconductors can be described by one of two mechanisms: (1) carrier hopping between localized molecular states and (2) carrier delocalization within a band structure. The conduction mechanism is related to the carrier mobility; Gould reports that band theory is generally appropriate for mobilities greater than 10^{-4} m^2 V^{-1} s^{-1}, while for lower mobilities hopping dominates.[10] The conduction mechanism in MPc thin films is a topic of extensive debate. Results from A.C. conduction studies by Shihub and Gould led to the conclusion that the conduction mechanism was temperature dependent, with hopping dominating at temperatures below 233 K and delocalization into a band structure at higher temperatures.[116] More recent experimental work has supported a purely hopping model, while theoretical studies may be found arguing for either a hopping model or a

band model.[117-119] Clearly, more research is needed to resolve this argument; until the exact mechanism is resolved it may be useful to consider MPc conduction through both mechanistic interpretations.

In addition to dual conduction mechanisms, two conduction regimes are known for MPcs. Ohmic conductivity occurs when the "intrinsic" carrier density in the film (generated thermally or by oxidant doping) is greater than the carrier density injected from the electrodes, while space-charge limited conductivity (SCLC) occurs when the injected carrier density is greater than the intrinsic density.[120] In the ohmic regime the current varies linearly with the voltage, while in the SCLC regime the current depends exponentially on voltage.[121] These conduction regimes have a direct impact on the sensing properties of MPc chemiresistors; the ohmic contact resistance that may occur between the electrode and the film may be removed by operating the sensor in the SCLC regime, leading to more consistent and stable sensor behavior.[120-122]

1.2 GAS AND VAPOR SENSING WITH METALLOPHTHALOCYANINE CHEMIRESISTORS

1.2.1 Interaction Mechanisms

Development of chemical sensors for detection of gas molecules requires optimization of a number of interrelated parameters: sensitivity, selectivity, reversibility and repeatability. Sensitivity and selectivity may imparted by use of strong interactions between the sensing element and the analyte of interest at the expense of reversibility and repeatability. Reversibility and repeatability can be

maximized by using weak intermolecular interactions, requiring other techniques to impart selectivity and sensitivity. Sensitivity can be increased through use of technological improvements, such as preconcentrators or specialized device geometries.[123-124] Selectivity is more difficult to achieve, usually requiring the use of cross-reactive sensor arrays with pattern recognition software.[125] Cross-reactive sensor arrays combine a number of sensors with varied sensitivities to a range of analytes, and analysis of patterns of sensitivity across the array can be used to identify analytes.

Accordingly, strong chemical interactions (such as covalent and ionic bonding) are unsuitable for use in these types of sensors, requiring use of weak intermolecular forces such as van der Waals forces and hydrogen bonding. Interactions between the sensing films and analyte vapors may be modeled using linear solvation energy relationships (LSER).[126] The partition coefficient K (eq. 1) of the sensor film is defined as the ratio of the concentration of analyte in the film (C_s) to the concentration of analyte in the vapor phase (C_v). The LSER equation (eq. 2) equates a linear combination of relevant intermolecular forces to log$K$.[127-128]

$$K = C_s/C_v \tag{1}$$

$$\log K = c + rR_2 + s\pi_2^* + a\alpha_2^H + b\beta_2^H + l\log L^{16} \tag{2}$$

Intermolecular forces include hydrogen bond acidity α_2^H and basicity β_2^H, dispersion interactions L^{16}, polarizability R_2, and dipole-dipole interactions π_2^*, with coefficients c, r, s, a, b, and l representing characteristics of the sensor film used.

The dominant mechanism of interaction in a sensing film can be predicted from relative interaction strengths.[129] Dispersion interactions (van der Waals forces

and induced dipole interactions) are the weakest, being generally less than 5 kJ mol^{-1}. Dipole-dipole and π-π interactions are slightly stronger, ranging from 5 to 50 kJ mol^{-1}. Hydrogen bond interactions present an even wider range, from 4 to 120 kJ mol^{-1}. For metal complexes such as phthalocyanines, ion-dipole and coordinative (dative) interactions are the strongest, with strengths of 50-200 kJ mol^{-1}. Additional forces can be exploited for sensing, such as the fluorophobic effect.[130]

Redox interactions can also lead to significant sensor responses. The majority of MPc sensing studies have focused on the detection of oxidizing gases, such as ozone, NO_x, and Cl_2.[131-133] MPc (M = H_2, Pb, Fe, Co, Ni, Cu, Zn, and others) films universally exhibit current increases on exposure to strongly oxidizing gases; the sensor films are partially oxidized, forming charge-transfer complexes which inject holes and increase film currents. These oxidants have been proposed to bind at the metal center and on the outer carbons of the organic rings.[7-10] MPcs offer particularly interesting sensor behavior arising from contrasting redox behavior when dosed with hydrogen peroxide. It has been found that MPc sensors show either oxidation or reduction on exposure to H_2O_2, depending on the metal center of the MPc.[134] Hydrogen peroxide was shown to decrease currents in CoPc sensors while it increased currents in NiPc, CuPc, and H_2Pc sensors, with a detection limit of 50 ppb. Oxidation and reduction of peroxides via catalysis at the phthalocyanine surface is consistent with the pattern of sensor responses. Consequently, differential analysis by redox contrast of a small array of sensors may be used to uniquely identify peroxide vapors, as peroxides are the only analytes observed to exhibit this behavior.

1.2.2 Sensor Platforms

MPc sensing films have been used with multiple readout modes. MPcs have been applied to adsorption detectors such as quartz crystal microbalances (QCM) and surface acoustic wave (SAW) devices.[135] Mass changes on the piezoelectric surface thereby lead to an alteration of the resonant frequency of the device. SAW devices have been shown to be effective for detection of weakly interacting organic molecules, which are detected poorly by electronic sensors.[136] MPc SAWs have also been effective in detecting strong oxidants and reductants such as NO_2 and NH_3.[137] However, SAWs lack the ability to distinguish between these two very different classes of analytes, recording only the mass change of the film.

Electronic and physical attributes of MPcs have been exploited for electrical chemosensors. Chemiresistors are the most common of these sensors, generally consisting of interdigitated electrodes (IDEs) with a phthalocyanine sensing layer spanning the area between the electrodes. Chemiresistors have been used to detect a broad array of analytes, including NO_x, O_3, Cl_2, volatile organic vapors, and strong bases such as NH_3.[7-10,121-122,131-133] Field effect transistors (FETs) are a more elaborate version of the standard two-terminal IDEs, with a third (gate) electrode separated from the semiconducting MPc channel by a thin layer of gate oxide. The electric field generated by this backside gate allows for greater control of the conductivity through the MPc sensing film, leading to high carrier mobilities and reduced current drifts.[138-139] Chemically sensitive FETs (chemFETs) display increased sensitivity to analytes; significant currents can be achieved even in ultrathin MPc films (four MPc

monolayers thick), leading to an increased analyte to charge carrier ratio and increasing the device sensitivity.[124,133]

1.2.3 Mechanism of Analyte Interactions with MPcs

Conductivity in MPc films depends strongly on atmospheric chemical species, particularly oxidants and reductants.[108-109] MPc conductivity has been attributed to coordination of O_2 to surface MPc metal centers, forming superoxide adducts which extract electrons, generating charge carriers (holes) in the bulk film.[61,111] Other oxidizing gases (O_3, NO_x, Cl_2, and others) generate holes in p-type MPc films through the charge transfer or redox reactions.[131-133]

MPc interactions with electron donating (reducing) gases, including Lewis bases such as NH_3, have the opposite effect. Current losses reported on dosing with Lewis bases have been attributed to hole trapping within the p-type film by electrons donated from the chemisorbed analyte.[108] Sensor interactions with electron donating analytes may be understood by using linear solvation energy relationships (LSER), which account for weak intermolecular forces such as dispersion interactions (van der Waals forces and π–π interactions), polarizability, dipolarity, and hydrogen bond acidity and basicity (*vide supra*).[126-128] Though not included in general LSER theory, metal coordinative bonds are the strongest intermolecular binding force for adsorption of Lewis bases onto MPcs.[140] As a surface dopant, O_2 occupies only a fraction of the binding sites on the film;[115] therefore strong Lewis bases could bind either to oxygen-free surface metal centers or could displace O_2 from occupied metal surface sites

(Scheme 1-3). Non-coordinating weak bases may be physisorbed on the organic regions of the MPc molecule through van der Waals forces and polarization interactions.

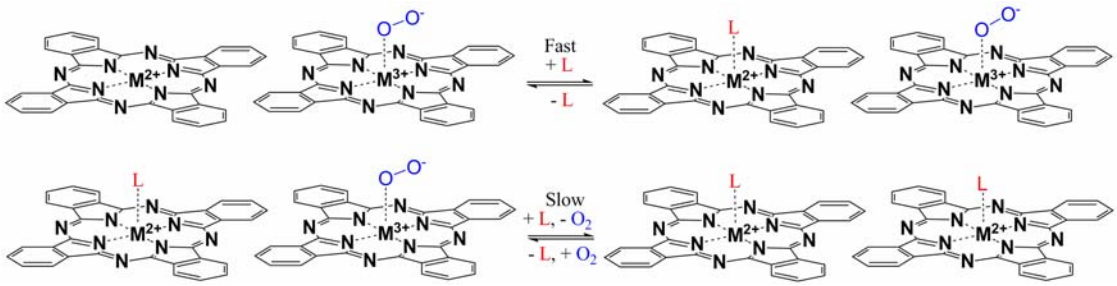

Scheme 1-3 Model of chemisorption onto MPc film by coordinating analyte L. Analytes may bind at open metal sites or may compete for oxygen bound sites.

Detection of electron donating analytes by MPc sensing films (M = Co, Ni, Cu, Zn) was found to be governed primarily by analyte coordination to the metal center (Chapters 3, 4).[141] MPc sensor responses to these analytes were generally correlated to the Lewis basicity of the analyte, described by the binding enthalpy scale $-\Delta H^{o}_{BF_3}$.[142] The $-\Delta H^{o}_{BF_3}$ scale is determined from calorimetrically measured enthalpies of formation (kJ mol^{-1}) of 1:1 adducts of Lewis bases to the Lewis acid BF_3 in dichloromethane, and thereby directly probes basicity through the free energy of binding. Detection of electron donors by an H_2Pc sensor was better correlated with the hydrogen bond basicities of the analytes as tabulated in the β_2^H scale.[143] Values for the β_2^H scale are determined using log K values (dm^3 mol^{-1}) of the analyte bases hydrogen bonding with reference acids such as 4-fluorophenol in CCl_4. Therefore, the

β_2^H scale is an indirect probe of hydrogen bond basicity and binding enthalpy through reaction equilibria. The sensor responses were found to approximate an exponential dependence on analyte basicity, in agreement with the van't Hoff equation and the expected standard free energy of reaction.[144-145]

1.2.4 Other Sensing Materials

1.2.4.1 Porphyrins

Porphyrins are macrocyclic molecules composed of four pyrrole units connected by methine bridges (Figure 1-4). The porphyrin macrocycle is a dianion; the central cavity of the molecule may contain two protons or a divalent metal cation. Porphyrins are insoluble in most solvents, but solubility may be imparted by the substitution of organic groups on the outer ring.[146] Functionalization of the outer carbons of the porphyrin molecule may be realized through a variety of synthetic pathways.[147] For example, phenyl groups may be added to the methine carbons to form metallotetraphenylporphyrin (MTPP) by the condensation of benzaldehyde and pyrrole. Additional functional groups may be added through the use of appropriate pyrrole and benzaldehyde precursors (e.g. 3,4-diethylpyrrole and *p*-nitrobenzaldehyde). Metallooctaethylporphyrin (MOEP) is prepared by the condensation of 3,4-diethylpyrrole and formaldehyde. In general, sensing is most often performed using MTPP and MOEP thin films.

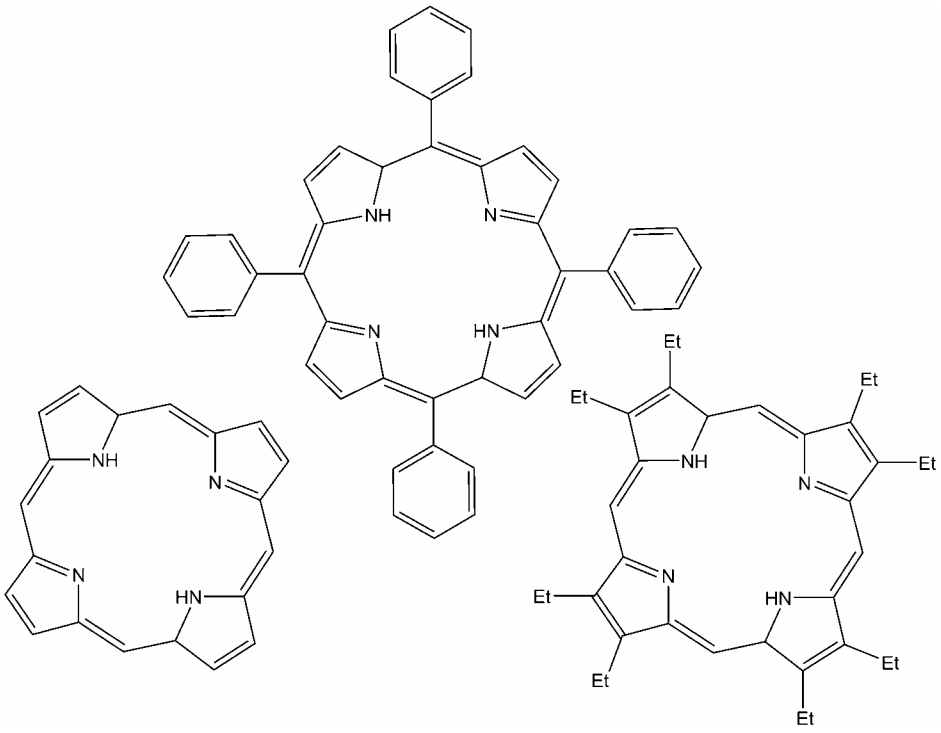

Figure 1-4 Molecular structures of porphyrin (left), metal-free tetraphenylporphyrin (H_2TPP, center) and metal-free octaethylporphyrin (H_2OEP, right).

Porphyrin thin films have been applied to different sensing platforms. Porphyrin sensing layers have been interfaced with SAW and QCM devices as well as with chemiresistive sensors for the detection of weakly interacting volatile organic compounds (VOCs).[148] Porphyrins are well-suited for optical detection of analytes, through monitoring of optical absorbance[149] or photoluminescence.[150] Porphyrin sensing layers are generally deposited as self-assembled monolayers (SAMs) or Langmuir-Blodgett films,[151] although evaporative deposition and spin-coating may also be used.[152]

The mechanism of chemiresistive porphyrin vapor sensing is generally similar to that of phthalocyanines. Chemically sensitive thin films interact with analyte

molecules through weak intermolecular forces, which imparts a reversibility that would be lost if strong covalent interactions were used. Linear solvation energy relationships (LSER)[126-128] are again an applicable model for interactions between the analyte and the porphyrin film, with hydrogen bonding dominating metal-free porphyrin interactions and axial coordination determining metalloporphyrin interactions. Axial coordination of porphyrin metal centers has been explored with a variety of methods, including electrochemistry,[153] UV/Vis spectroscopy,[154] NMR, X-ray crystallography,[155] EPR,[156] and DFT calculations,[157] for coordinating gas molecules including electron acceptors (O_2, NO_x, CO) and electron donors (pyridine and other Lewis bases). For electron donors it has been found that the axial ligation constants scale with the Lewis basicity of the analyte.[154]

Chemiresistive sensing requires the use of highly conjugated porphyrin derivatives. H_2TPP films spin-coated onto gold IDEs have shown standard p-type semiconductivity, displaying current gains upon exposure to nitric oxide (hole generation via electron extraction) and current losses upon exposure to triethylamine (hole trapping via electron donation).[148] Other studies based on TPPs have been somewhat more ambiguous, with p-type ZnTPP and n-type perfluoroZnTPP each showing current gains after exposure to amine electron donors. This increase in current may be due to solvent effects in the film leading to better molecular packing and hole conduction, rather than electronic effects arising from the analyte-porphyrin interaction.[158] Highly conjugated diyne-bridged NiOEP dimers have also shown current gains after exposure to both NO and NH_3.[159] A proposed mechanism relates

the current gains upon dosing with NH_3 to electron transfer from the porphyrin to NH_3, contrary to the expected electron donating character of ammonia.[160]

1.2.4.2 Polymers

Polymeric chemiresistors are well-studied, as typified by polyaniline and polythiophene. Polyaniline is one of the most widely studied conducting polymers; it is easily synthesized by oxidative polymerization of aniline in acidic media. Polyaniline displays a broad range of oxidation states; in its fully reduced form it is an insulator, and it becomes a p-type semiconductor when oxidized.[161-162] Polyaniline may also be protonated to give salts, depending on the oxidation state of the polymer and the pH of the acidic medium. Oxidation states of polyaniline are referred to as leucoemeraldine (fully reduced), emeraldine (partially oxidized), and pernigraniline (fully oxidized), while the unprotonated form is denoted the base and the protonated form is denoted the salt (e. g. emeraldine base versus emeraldine salt).[163] Oxidized polyanilines may be highly conductive, with conductivities approaching 3.0 S cm^{-1} for the emeraldine base.[164]

Polyaniline gas sensing may be correlated with its redox behavior. Most studies of polyaniline sensing films involve the conductive emeraldine salt. High porosity films of polyaniline nanofibers offer improved kinetics over conventional films.[165] Nanofiber films of the emeraldine salt have been shown to be highly sensitive to reducing gases such as NH_3; the mechanism involves deprotonation and reduction of the oxidized film, leading to irreversible current loss.[166] Other reducing agents have

similar effects; hydrazine rapidly reduces emeraldine salts to the leucoemeraldine (completely reduced) form, irreversibly converting the film to an insulator.[165] These films are also sensitive to HCl vapors by the opposite mechanism: protonation and hole doping of the film leading to current gains. These effects are irreversible for large doses (100 ppm), but may be reversible for small, short doses.[167] Weakly interacting analytes have also been explored. Water and alcohols have been shown to cause modest losses in conductivity, attributed to various mechanisms, including polymer swelling and hydrogen bonding interactions that donate electron density into the film.[167-168]

Another widely studied conductive polymer is polythiophene, which is generally used as short chain oligomers of 6 (sexithiophene) to 10 thiophene units. Polythiophene was initially synthesized by nickel-catalyzed polymerization of Grignard reagents derived from dibromothiophenes.[169] Polythiophenes can also be generated through polymerization of thiophene with $FeCl_3$ in chloroform. More recent synthetic methods include use of Suzuki coupling of thiophene boronic esters with palladium catalysts, or Stille coupling of tin-derived thiophenes.[170]

Like polyaniline, polythiophenes are insulating in their neutral (reduced) state, and become semiconducting on the introduction of oxidative dopants.[171] Polythiophenes may be self-doped[172] or externally doped.[173] Charge conduction occurs through polaron and bipolaron hopping from chain to chain; the polaron extends over approximately five thiophene units.[174] Oligomer length plays a role in the mechanism of conductivity, with hexamers giving rise to polaronic conduction and octamers and

decamers exhibiting bipolaronic conduction.[175] Bipolarons are thought to be structurally paired on adjacent π-stacked thiophene chains.[176]

Film morphology plays a large role in mediating the chemical sensitivity of polythiophenes. Oligomers (thiophene n = 5, 6, 8, 10) are preferred over long chain polymers due to the ability of oligomers to form ordered crystalline grains which lead to better conductivity.[174-176] Vapor adsorption occurs at the surface of crystalline grains; films with smaller grains and more grain boundaries show increased film porosity and improved vapor sensitivity.[177] Addition of sidechains on the thiophene units can lead to improved porosity and increased vapor sensitivity.[178] Alteration of sidechain chemistry can modulate the chemical sensitivity at these grain boundaries. Polythiophenes functionalized with alkoxy sidechains were found to be more sensitive to polar molecules such as alcohols, while those with alkyl groups showed increased sensitivity to nonpolar analytes.[179]

Sensing mechanisms in polythiophene resemble those of polyaniline. The analyte NO_2 has been extensively studied, and 100 ppm doses were shown to give 500% increases in sensor current,[180] attributed to the formation of NO_2 charge-transfer complexes in the film leading to the generation of charge-carrying bipolarons.[181] These charge transfer complexes have been observed through UV-Vis and IR spectroscopic studies.[182] Polythiophene sensitivities have also been examined with regards to reducing gases, primarily NH_3. Ammonia adsorption leads to current losses, with lower sensitivities and longer recovery times than with NO_2.[181] These responses have been attributed to polaron trapping by the non-bonding lone pair on

ammonia molecules. At higher doses ammonia may deprotonate and dedope the HCl-doped thiophene polymer, restoring the oxidized polymer to its neutral state.[183] Polythiophene sensing of VOCs has also been explored; trapping of polarons was reported as the sensing mechanism.[184-185] At high VOC concentrations (e.g. 5000 ppm methanol) the polythiophene films are partially dissolved, leading to permanent current losses.[184-186]

1.2.4.3 Carbon Nanotubes

Carbon nanotubes are molecular wires resembling rolled sheets of graphite. They display molecular properties such as high tensile strength, optical refraction, and conduction behavior ranging from semiconducting to metallic. They have been applied to such applications as nanoelectronics,[187] scanning microscopy nanoprobes,[188] and chemical sensors.[189] Carbon nanotubes present challenges in manipulation and orientation; lack of control of nanotube morphology leads to significant variance in device behavior. Recent developments in nanotube alignment include directional drying of aqueous nanotube suspensions and orientation in electric field gradients.[190-191]

Carbon nanotube chemiresistive sensors generally use single-walled carbon nanotubes (SWNTs), which are p-type semiconductors.[187] As such, basic chemiresistive sensing is dominated by redox effects, including carrier generation through electron extraction by oxidants. Strong electron acceptors such as NO_2 have been shown to drastically increase nanotube conduction via charge carrier

generation.[189,192] Electron donors such as NH_3 cause losses in sensor current which are attributed to hole trapping by electron donation.[189] Electron donor detection has been enhanced by organic functionalization of the nanotubes with hydrogen bonding groups such as poly-(*m*-aminobenzene sulfonic acid).[193] Carbon nanotubes may be interfaced with catalytic metal species for enhanced detection of gases; palladium nanoparticles attached to SWNTs have been used to detect hydrogen and methane, while similarly attached Fe_2O_3 particles have the ability to catalytically detect hydrogen peroxide.[194-196]

1.2.4.4 Pentacene

Pentacene is the most widely-studied organic semiconductor for organic electronics. FETs with pentacene semiconducting channels are well-behaved and reproducible. Pentacene conduction is highly dependent on film morphology, which can be controlled precisely with deposition techniques.[197] Like most conductive organics, pentacene is a p-type semiconductor, and high conductivities can be achieved by doping with electron acceptors such as I_2.[198]

Conductivity in pentacene depends strongly on atmospheric doping. When deposited in vacuo, pentacene exhibits low conductivity, which is increased by an order of magnitude on exposure to air.[199] This is attributed to the generation of charge carriers by atmospheric oxidants, particularly O_2.[200] Other strong oxidants such as NO_2 and Cl_2 lead to significant current gains by carrier generation through electron extraction.[201] Conversely, atmospheric humidity is found to reduce pentacene film

currents by trapping charge carriers via electron donation.[202-203] Pentacene exhibits broad sensitivity to weakly electron donating VOCs such as 1-pentanol, methanol, ethanol, acetone, toluene, and chloroform; low concentrations of these chemicals trap charge carriers, while larger doses cause solvation and reorganization of the film.[204-205] Stronger bases or electron donors, such as NH_3, have not been thoroughly examined.

1.3 ORGANOPHOSPHATE TOXICITY AND DETECTION METHODS

1.3.1 Organophosphate Neurotoxicity

Toxic chemical warfare (CW) agents are important target analytes for chemical sensing. Organophosphate neurotoxins (Figure 1-5) are an important class of CW agents (sarin, soman) and pesticides (methyl paraoxon, dimethyl methylphosphonate). Organophosphate neurotoxicity arises from potent inhibition of acetylcholinesterase (AChE) activity through phosphorylation and phosphonylation of the serine residue in the active site of the enzyme.[206-207] Sarin and soman contain an easily hydrolyzed phosphorus-fluoride bond, thereby enabling AChE phosphorylation.[227] Sarin may be inhaled or travel across mucous membranes in the gastrointestinal tract, eyes, or skin. Death rapidly occurs by respiratory arrest from muscle seizures. Secondary effects include chronic memory decline, fatigue, and blurred vision.[209] Recent uses of sarin gas include low-level exposures of U. S. personnel during the 1991 Gulf War and the terrorist attack on the Tokyo subway system on March 30, 1995.[210-211]

Organophosphates have found widespread agricultural use as insecticides, which are also hazardous to humans. Organophosphate pesticides may affect humans

by AChE inhibition, leading to seizures and death by respiratory paralysis.[206] Additionally, there is a high risk of acute necrotizing pancreatitis, which can be lethal.[212] Diagnosis of organophosphate poisoning relies on clinical observations, including a history of organophosphate exposure, characteristic clinical symptoms of exposure, clinical improvement upon treatment with atropine, and decreased acetylcholinesterase activity in the blood panel.[213]

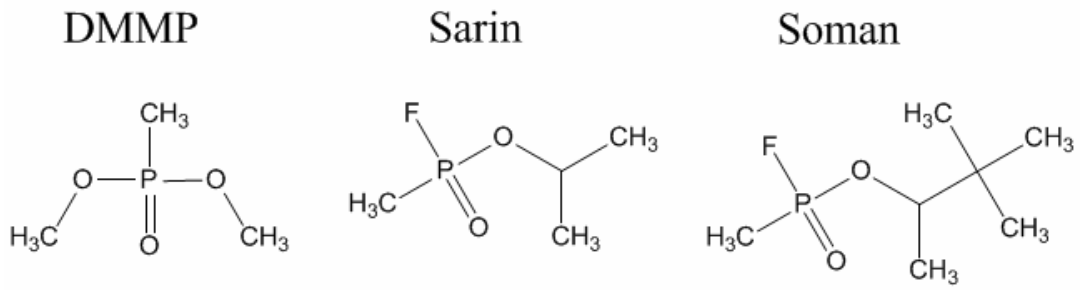

Figure 1-5 Organophosphate neurotoxin simulant dimethyl methylphosphonate (DMMP), and the CW agents O-isopropyl methylphosphonofluoridate (sarin), and O-pinacolyl methylphosphono-fluoridate (soman).

1.3.2 Organophosphate Detection Methods

Practical detection methods for organophosphate neurotoxins have had limited success. The use of sarin on the Tokyo subway in 1995 is an example of this; one hour after the attack the police reported the toxin to be acetonitrile, and three hours later the use of sarin had been confirmed.[210] The detection methods employed at the time (GC/MS, HPLC) failed to identify sarin in part because it had not been included in the responding agencies' chemical libraries.[214] Since this incident, a large number of detection instruments have been deployed across Japan; these are generally bulky,

complex instrument systems, including GC/MS, HPLC, and X-ray fluorescence, with high power and computing demands.[215] Other large instruments used to detect organophosphates include LIDAR, which can identify organophosphate spectral features from a distance of 300 m to 1 km.[216] Miniaturization of sensing platforms is desirable to facilitate deployment and use by nonscientific personnel. A significant amount of research has since been devoted to developing small, versatile sensor platforms for detection of organophosphates.

Optical sensors for organophosphates make use of physical detection methods involving diffraction, refraction, and surface plasmon resonance. Pesticides (Atrazine and Triadimenol) have been detected through microcapillary condensation in porous silica; changes in the reflectivity resonant frequency and refractive index allow identification of organophosphates in the presence of water and other environmental species.[217] Another pesticide, methyl paraoxon, has been detected using photonic arrays of polystyrene spheres immobilized in a hydrogel and functionalized with organophosphate hydrolase enzyme (OPH). Hydrolysis of methyl paraoxon by OPH alters the pH of the photonic array, altering the hydrogel structure and the diffraction wavelength.[218] Surface plasmon resonances have also been exploited for organophosphate detection; a variety of organophosphates were identified by surface plasmon resonance changes in Zn-functionalized Au nanoparticles on silica gel.[219]

Luminescent compounds have been used for organophosphate detection. Organic fluorophores such as fluoresceinamine immobilized on silica gel have been shown to detect halogenated organophosphates such as diethyl chlorophosphate (DCP)

preferentially over non-halogenated organophosphates such as DMMP. The halogen-phosphorus bond is hydrolyzed, leaving the phosphate group free to bind to the amine moiety of fluoresceinamine, leading to an irreversible increase in fluorescence (100% fluorescence gain in the presence of 13 ppm DCP) in the solution phase.[220] Fluorescent metal complexes have been shown to detect organophosphates. Arrays of luminescent metal ions (Zn^{2+}, La^{3+}, Eu^{3+}) bound to fluorescent ligands show a transition between metal-centered and ligand-centered luminescence when organophosphates bind to the metal.[221] Selectivity has been imparted through use of molecularly imprinted polymers containing Eu^{3+} ions bound to chelating β-diketonate moieties; upon binding of low ppb concentrations of organophosphates to the Eu^{3+} center a strong increase in fluorescence is seen, with minimal interference from other species.[222]

Electronic sensors interfaced with biomolecules are a major area of organophosphate detection in the aqueous and vapor phases. Biological substrates, such as AChE and OPH, exhibit a high selectivity for organophosphates; AChE, the primary site where organophosphate poisoning occurs, possesses a high binding affinity for these neurotoxins, while OPH selectively catalyzes organophosphate hydrolysis. Carbon nanotubes with attached AChE molecules have been used as the semiconducting channel in chemFETs; binding of organophosphates to AChE can be detected by changes in the transfer curves.[223] Carbon nanotubes applied to screen-printed carbon electrodes can electrochemically detect organophosphate-bound AChE in solution.[224] Carbon nanotubes have also been interfaced with OPH through non-

specific binding in a chemiresistive device. Enzymatic decomposition of the pesticide paraoxon by OPH leads to significant conductance losses; the mechanism is as yet unclear.[225]

OPH and AChE bound to a much simpler substrate, silica gel, can be used to detect organophosphates. Detection of organophosphate binding may be accomplished by pH monitoring[226] or infrared spectral analysis of phosphonate products.[227] Organophosphates can be detected electrochemically by binding them to AChE and oxime substrates.[228-229] AChE has even been attached to the backside of a silicon microcantilever; binding of aqueous phase organophosphates to the AChE causes a deflection of the cantilever which may be detected by standard AFM software.[230]

1.4 PEROXIDE BASED IMPROVISED EXPLOSIVES AND DETECTION METHODS

1.4.1 Peroxide Based Explosives

Recent terrorist incidents in England and Germany have involved improvised peroxide-base explosives.[231-232] The two common peroxide-based explosives are triacetone triperoxide (TATP)[233] and hexamethylene triperoxide diamine (HMTD).[234] These explosives are easily synthesized with widely available materials. TATP may be prepared by adding aqueous hydrogen peroxide (30%, 35%, or 50%) to a stirred solution of sulfuric acid and acetone; care must be taken to keep the temperature of the reaction low (-20 ^{o}C) to prevent spontaneous detonation of the product.[235] HMTD is

produced by simply combining hexamethylenetetramine with 30% hydrogen peroxide, again stirring at low temperature.[236] Both compounds are highly volatile and easily sublimed, but are sensitive to shock and heat.[233-237] Due to this instability, they are extremely dangerous to handle, so neither compound has any legitimate military or commercial application.

1.4.2 Peroxide Based Explosive Detection Methods

TATP is the most widely used peroxide-based improvised explosive, and as such is the most studied for detection methods. TATP may be detected by standard laboratory methods such as FTIR and LC/MS.[238] The C-O infrared stretch of TATP is easily detected in ambient air at high concentrations, but trace TATP concentrations may be overshadowed by background signals from naturally occurring species.[239] FTIR sensitivity can be increased by interfacing the detector with chromatographic separation apparatuses such as HPLC.[240] LC/MS is also an excellent method for identifying trace amounts (10 ng in 100 μL of solution) of peroxide-based explosives; liquid chromatography is preferred to gas chromatography as it has greater retention times and can achieve better separation.[241] Desorption electrospray ionization mass spectrometry (DESI-MS) is the preferred mass spectrometric method for identifying TATP.[242] This technique relies of the complexation of TATP with alkali metal ions; upon fragmentation of the explosive, the metal ions are retained by the fragments, allowing for identification.[243] A drawback to these detection methods is that they

require relatively bulky instrumentation systems with significant power and computing demands.

To overcome this obstacle, small, deployable TATP sensing systems have been developed. Electrochemical cells have undergone miniaturization for field deployment for detection of peroxides and peroxide-based explosives.[244] Electrochemical detection is a sensitive way of identifying H_2O_2 and TATP in solution, and real time detection of TATP has been achieved.[245-246] Other detection methods for peroxide based explosives rely on the photochemical reaction of the organic peroxide with UV light (λ = 254 nm) to form H_2O_2. The samples are then analyzed through the use of HPLC in combination with fluorescence detectors[247] or enzymatic fluorochemical assays.[248-249]

1.5 OBJECTIVES OF THE DISSERTATION

The objective of the research presented herein is to demonstrate the ability of metallophthalocyanines to be used as chemical sensors, specifically for vapor-phase detection of volatile organic compounds, organophosphate neurotoxins, and peroxides. This work builds on prior research into the electronic and physical structures of MPcs, and their conductivity behavior in response to atmospheric species. Analyte coordination to the phthalocyanine metal centers and electrocatalytic redox behavior of MPcs allow for sensitive and selective detection of a variety of electron donors and acceptors.

Chapter 2 accounts for synthetic preparation of a wide range of MPcs of varied metal centers and organic functionalities. A synthetic method was devised to prepare the novel compound 2(3),9(10),16(17),23(24)-tetrakis(1,1,1,3,3,3-Hexafluoropropan-2-ol)phthalocyaninato copper. Deposition methods of MPcs were explored, and the physical structures of phthalocyanine films were examined in order to improve sensor characteristics.

Chapter 3 explores the mechanism of chemical sensing in cobalt (CoPc) and metal-free phthalocyanine (H_2Pc) with respect to analyte basicity (electron donor ability). The influence of O_2 on the sensing behavior of these MPcs was studied. It was found that the magnitude of the sensor response correlates with the Lewis basicity of the analyte for CoPc chemiresistors and the hydrogen bond basicity for H_2Pc chemiresistors.

Chapter 4 continues this study by expanding the number of MPcs to include nickel, copper, and zinc phthalocyanines. It was found that analyte basicity is exponentially correlated with the sensor response; this is explained with regards to the van't Hoff equation and the free energy of binding. In order to obtain selectivity for analyte identification, linear discriminant analysis is applied to a sensor array of CoPc, NiPc, CuPc, ZnPc, and H_2Pc.

Chapter 5 extends the investigation of MPc sensing to volatile peroxides, including hydrogen peroxide and di-*t*-butyl peroxide, by redox contrast. These peroxides are found to decrease currents in CoPc and increase currents in FePc, NiPc, CuPc, ZnPc, and H_2Pc; oxidation and reduction of hydrogen peroxide via catalysis at

the phthalocyanine surface is consistent with the pattern of sensor responses. Differential analysis by redox contrast of a small sensor array was used to uniquely identify hydrogen peroxide vapor down to part per billion concentrations.

Chapter 6 examines field effect transistor devices featuring ZnPc as the semiconducting channel. Output and transfer curves are presented in order to understand the electronic behavior of these devices. Persistent photoconductivity is found to affect these devices for a period of up to one month.

1.6 REFERENCES

(1) Spaeth, M. L.; Sooy, W. R. *J. Chem. Phys.* **1968**, *48*, 2315-2323.

(2) de la Torre, G.; Claessens, C. G.; Torres, T. *Chem. Comm.* **2007**, 2000-2015.

(3) Gantchev, T. G.; Sharman, W. M.; Lier, J. E. *Photochem. Photobiol.* **2003**, *77*, 469-479.

(4) Zagal, J. H. *Coord. Chem. Rev.* **1992**, *119*, 89-136.

(5) Yokota, C.; Sasakawa, T.; Hyakutake, H. *Proc. SPIE-Int. Soc. Opt. Eng.* **1995**, *2514*, 249-257.

(6) Uchida, S.; Xue, J.; Rand, B. P.; Forrest, S. R. *Appl. Phys. Lett.* **2004**, *84*, 4218-4220.

(7) Snow, A. W.; Barger, W. R. Phthalocyanine Films in Chemical Sensors. *Phthalocyanines: Properties and Applications;* Lever, A. B. P., Ed.; John Wiley and Sons: New York, 1989; Vol. 1, p. 341.

(8) Wright, J. D. *Prog. Surf. Sci.* **1989**, *31,* 1-60.

(9) Guillaud, G.; Simon, J.; Germain, J. *Coord. Chem. Rev.* **1998**, *178,* 1433-1484.

(10) Gould, R. D. *Coord. Chem. Rev.* **1996**, *156,* 237-274.

(11) Whalley, M. *J. Chem. Soc.* **1961**, 866-869.

(12) Liao, M. S.; Scheiner, S. *J. Chem. Phys.* **2001**, *114*, 9780-9791.

(13) Eberhardt, W.; Hanack, M. *Synthesis* **1997**, 95-100.

(14) Schultz, H.; Lehmann, H.; Rein, M.; Hanack, M. *Struct. Bond.* **1991**, *74*, 41-146.

(15) Hanack, M.; Lang, M. *Adv. Mater.* **1994**, *6*, 819-833.

(16) Brach, P. J.; Grammatica, S. J.; Ossanna, O. A.; Weinberger, L. *J. Heterocycl. Chem.* **1970**, *7*, 1403-1405.

(17) Byrne, G. T.; Linstead, R. P.; Lowe, A. R. *J. Chem. Soc.* **1934**, 1017-1022.

(18) Brumfield, S. N.; Foltz, V. W.; McGhee, C. M.; Thomas, A. L. *J. Org. Chem.* **1962**, *27*, 2266-2267.

(19) Brumfield, S. N.; Mays, B. C.; Thomas, A. L. *J. Org. Chem.* **1964**, *29*, 2484-2486.

(20) Tomoda, H.; Saito, S.; Ogawa, S.; Shiraishi, S. *Chem. Lett.* **1980**, *9*, 1277-1280.

(21) Baumann, F.; Bienert, B.; Rosch, G.; Vollmann, H.; Wolf, W. *Angew. Chem.* **1956**, *68*, 133-168.

(22) Baker, S.; Petty, M. C.; Roberts, G. G.; Twigg, M. V. *Thin Solid Films* **1983**, *99*, 53-59.

(23) Agbabiaka, A. A.; Mukhopadhyay, S.; Dukherjee, D.; Thorpe, S. C. *Supramol. Sci.* **1997**, *4*, 185-190.

(24) Sadaoka, Y.; Jones, T. A.; Gopel, W. *J. Mater. Sci. Lett.* **1989**, *8*, 1288-1290.

(25) Muranaka, A.; Okuda, M.; Kobayashi, N.; Somers, K.; Ceulemans, A. *J. Am. Chem. Soc.* **2004**, *126*, 4596-4604.

(26) Ercolani, C.; Neri, C.; Porta, P. *Inorg. Chim. Acta.* **1967**, *1*, 415-418.

(27) Lever, A. B. P.; Wilshire, J. P.; Quan, S. K. *Inorg. Chem.* **1981**, *20*, 761-768.

(28) Mizuguchi, J.; Rihs, G.; Karfunkel, H. R. *J. Phys. Chem.* **1995**, *99*, 16217-16227.

(29) Barlow, D. E.; Hipps, K. W. *J. Phys. Chem. B*, **2000**, *104*, 5993-6000.

(30) Tsuzuki, T.; Hirota, N.; Noma, N.; Shirota, Y. *Thin Solid Films* **1996**, *273*, 177-180.

(31) Tsuzuki, T.; Shirota, Y.; Rostalski, J.; Meissner, D. *Sol. Energy Mater. Sol. Cells* **2000**, *61*, 1-8.

(32) Tracey, S. M.; Hodgson, S. N. B.; Ray, A. K. *J. Sol-Gel Sci. Tech.* **1998**, *13*, 219-222.

(33) Liu, C. J.; Hsieh, J. C.; Ju, Y. H. *J. Vac. Sci. Technol., A* **1996**, *14*, 753-756.

(34) Tongpool, R.; Yoriya, S. *Thin Solid Films* **2005**, *477*, 148-152.

(35) Sadaoka, Y.; Jones, T. A.; Gopel, W. *Sens. Actuators, B* **1990**, *1*, 148-153.

(36) Doeff, M. M.; Sweigart, D. A. *Inorg. Chem.* **1981**, *20*, 1683-1687.

(37) Generosi, A.; Paci, B.; Albertini, V. R.; Perfetti, P.; Pennesi, G.; Paoletti, A. M.; Rossi, G.; Capobianchi, A.; Caminiti, R. *Appl. Phys. Lett.* **2005**, *86*, 114106/1-3.

(38) Chen, W. H.; Rieckhoff, K. E.; Voigt, E. M. *Chem. Phys.* **1986**, *102*, 193-203.

(39) Brown, R. J. C.; Kucernak, A. R.; Long, N. J.; Mongay-Batalla, C. *New J. Chem.* **2004**, *28*, 676-680.

(40) Ho, Z. Z.; Peyghambarian, N. *Chem. Phys. Lett.* **1988**, *148*, 107-111.

(41) Lowbry, M. K.; Starshak, A. J.; Esposito, J. N.; Krueger, P. C.; Kenney, M. E. *Inorg. Chem.* **1965**, *4*, 128.

(42) Kobayashi, N.; Furuya, F.; Yug, G. C.; Wakita, H.; Yokomizo, M.; Ishikawa, N. *Chem. Eur. J.* **2002**, *8*, 1474-1484.

(43) Padilla, J.; Hatfield, W. E. *Inorg. Chim. Acta* **1990**, *172*, 241-245.

(44) Vertsimakha, Y. *Synth. Met.* **2000**, *109*, 287-289.

(45) Clarisse, C.; Riou, M. T. *Inorg. Chim. Acta* **1987**, *130*, 139-144.

(46) Ishikawa, N.; Iino, T.; Kaizu, Y. *J. Am. Chem. Soc.* **2002**, *124*, 11440-11447.

(47) Ishikawa, N. *J. Porphyrins Phthalocyanines* **2001**, *5*, 87-101.

(48) Gobernado-Mitre, M. I.; Tomilova, L. G.; Aroca, R.; DeSaja, J. A. *J. Mol. Struct.* **1993**, *297*, 49-55.

(49) Collins, G. C. S.; Schiffrin, D. J. *J. Electroanal. Chem.* **1982**, *139*, 335-369.

(50) Passard, M.; Blanc, J. P.; Maleysson, C. *Thin Solid Films* **1995**, *271*, 8-14.

(51) Rodriguez-Mendez, M. L.; Gorbunova, Y.; de Saya, J. A. *Langmuir* **2002**, *18*, 9560-9565.

(52) Ishikawa, N.; Sugita, M.; Ishikawa, T.; Koshihara, S. Y.; Kaizu, Y. *J. Phys. Chem. B* **2004**, *108*, 11265-11271.

(53) Ishikawa, N.; Sugita, M.; Ishikawa, T.; Koshihara, S. Y.; Kaizu, Y. *J. Am. Chem. Soc.* **2003**, *125*, 8694-8695.

(54) Kasuga, K.; Idehara, T.; Handa, M. *Inorg. Chim. Acta* **1992**, *196*, 127-128.

(55) Cuellar, E. A.; Marks, T. J. *Inorg. Chem.* **1981**, *20*, 3766-3770.

(56) Metz, J.; Schneider, O.; Hanack, M. *Inorg. Chem.* **1984**, *23*, 1065-1071.

(57) Wu, Y.; Tian, H.; Chen. K.; Liu, Y.; Zhu, D. *Dyes Pigm.* **1998**, *37*, 317-325.

(58) Gorlach, B.; Dachtler, M.; Glaser, T.; Albert, K.; Hanack, M. *Chem. Eur. J.* **2001**, *7*, 2459-2465.

(59) Bao, Z.; Lovinger, A. J.; Brown, J. *J. Am. Chem. Soc.* **1998**, *120*, 207-208.

(60) Keizer, S. P.; Mack, J.; Bench, B. A.; Gorun, S. M.; Stillman, M. J. *J. Am. Chem. Soc.* **2003**, *125*, 7067-7085.

(61) Hiller, S.; Schlettwein, D.; Armstrong, N. R.; Wohrle, D. *J. Mater. Chem.* **1998**, *8*, 945-954.

(62) Michaelis, W.; Wohrle, D.; Schlettwein, D. *J. Mater. Res.* **2004**, *19*, 2040-2048.

(63) Pakhomov, L. G.; Zakamov, V. R.; Pakhomov, G. L. *J. Mater. Sci.* **2005**, *40*, 3279-3281.

(64) Burnham, P. M.; Cook, M. J.; Gerrard, L. A.; Heeney, M. J.; Hughes, D. L. *Chem. Comm.* **2003**, 2064-2065.

(65) Li, H.; Jensen, T. J.; Fronczek, F. R.; Vicente, M. G. H. *J. Med. Chem.* **2008**, *51*, 502-511.

(66) Vagin, S.; Frickenschmidt, A.; Kammerer, B.; Hanack, M. *Eur. J. Org. Chem.* **2005**, 3271-3278.

(67) Kudrik, E. V.; Shaposhnikov, G. P.; Balakirev, A. E. *Russ. J. Gen. Chem.* **1999**, *69*, 1321-1324.

(68) Balakirev, A. E.; Maizlish, V. E.; Shaposhnikov, G. P. *Russ. J. Gen. Chem.* **2002**, *72*, 311-314.

(69) Hoshino, A.; Takenaka, Y.; Miyaji, H. *Acta Crystallogr., Sect. B: Struct. Sci.* **2003**, *B59*, 393-403.

(70) Heutz, S.; Bayliss, S. M.; Middleton, R. L.; Rumbles, G.; Jones, T. S. *J. Phys. Chem. B* **2000**, *104*, 7124-7129.

(71) Miller, C. W.; Sharoni, A.; Liu, G.; Colesniuc, C. N.; Fruhberger, B.; Schuller, I. K. *Phys. Rev. B* **2005**, *72*, 104113/1-6.

(72) Ashida, M.; Uyeda, N.; Suito, E. *J. Cryst. Growth* **1971**, *8*, 45-56.

(73) Ukei, K. *Acta Crystallogr., Sect. B: Struct. Sci.* **1973**, *B29*, 2290-2292.

(74) Iyechika, Y.; Yakushi, K.; Ikemoto, I.; Kuroda, H. *Acta Crystallogr., Sect. B: Struct. Sci.* **1982**, *B38*, 766-770.

(75) Griffiths, C. H.; Walker, M. S.; Goldstein, P. *Mol. Cryst. Liq. Cryst.* **1976**, *33*, 149-170.

(76) Ziolo, R. F.; Griffiths, C. H. *J. Chem. Soc., Dalton Trans.* **1980**, 2300-2302.

(77) de Cian, A.; Moussavi, M.; Fischer, J.; Weiss, R. *Inorg. Chem.* **1985**, *24*, 3162-3167.

(78) Wang, B.; Zuo, X.; Wu, Y.; Chen, Z.; Li, Z. *Mater. Lett.* **2005**, *59*, 3073-3077.

(79) Cook, M. J. *Pure. Appl. Chem.* **1999**, *71*, 2145-2151.

(80) Forrest, S. R. *Chem. Rev.* **1997**, *97*, 1793-1896.

(81) Narayanan Unni, K. N.; Menon, C. S. *Mater. Lett.* **2000**, *45*, 326-330.

(82) Iwatsu, F. *J. Phys. Chem.* **1988**, *92*, 1678-1681.

(83) Lee, Y. L.; Tsai, W. C.; Maa, J. R. *Appl. Surf. Sci.* **2001**, *173*, 352-361.

(84) Tong, W. Y.; Djurisic, A. B.; Xie, M. H.; Ng, A. C. M.; Cheung, K. Y.; Chan, W. K.; Leung, Y. H.; Lin, H. W.; Gwo, S. *J. Phys. Chem. B* **2006**, *110*, 17406-17413.

(85) Lee, Y. H.; Tsai, W. C.; Chang, C. H.; Yang, Y. M. *Appl. Surf. Sci.* **2001**, *172*, 191-199.

(86) Resel, R.; Ottmar, M.; Hanack, M.; Keckes, J.; Leising, G. *J. Mater. Res.* **2000**, *15*, 934-939.

(87) Ofuji, M.; Ishikawa, K.; Takezoe, H.; Inaba, K.; Omote, K. *Appl. Phys. Lett.* **2005**, *86*, 062114/1-3

(88) Tang, Q.; Li, H.; He, M.; Hu, W.; Liu, C.; Chen, K.; Wang, C.; Liu, Y.; Zhu, D. *Adv. Mater.* **2006**, *18*, 65-68.

(89) Liu, C. J.; Shih, J. J.; Ju, Y. H. *Sens. Actuators, B* **2004**, *99*, 344-349.

(90) Lee, Y. L.; Hsiao, C. Y.; Hsiao, R. H. *Thin Solid Films* **2004**, *468*, 280-284.

(91) Lee, Y. L.; Chang, C. H. *Sens. Actuators, B* **2006**, *119*, 174-179.

(92) Edwards, L.; Gouterman, M. *J. Mol. Spectrosc.* **1970**, *33*, 292-310.

(93) Stillman, M. J.; Thomson, A. J. *J. Chem. Soc. Faraday Trans. 2* **1974**, *70*, 790-804.

(94) Kumar, G. A.; Jose, G.; Thomas, V.; Unnikrishnan, N. V.; Nampoori, V. P. N. *Spectrochim. Acta, Part A* **2003**, *59*, 1-11.

(95) Mack, J.; Stillman, M. J. *Inorg. Chem.* **2001**, *40*, 812-814.

(96) Lever, A. B. P.; Wilshire, J. P. *Inorg. Chem.* **1978**, *17*, 1145-1151.

(97) Campbell, R. H.; Heath, G. A.; Hefter, G. T.; McQueen, R. C. S. *J. Chem. Soc., Chem. Commun.* **1983**, 1123-1125.

(98) Wolberg, A.; Manassen, J. *J. Am. Chem. Soc.* **1970**, *92*, 2982-2991.

(99) Cahill, A. E.; Taube, H. *J. Am. Chem. Soc.* **1951**, *73*, 2847-2851.

(100) Rollmann, L. D.; Iwamoto, R. T. *J. Am. Chem. Soc.* **1968**, *90*, 1455-1463.

(101) Lever, A. B. P.; Pickens, S. R.; Minor, P. C.; Licoccia, S.; Ramaswamy, B. S.; Magnell, K. *J. Am. Chem. Soc.* **1981**, *103*, 6800-6806.

(102) Clack, D. W.; Hush, N. S.; Woolsey, I. S. *Inorg. Chim. Acta* **1976**, *19*, 129-132.

(103) Toman, P.; Nespurek, S.; Yakushi, K. *Macromol. Symp.* **2004**, *212*, 327-334.

(104) Zhang, X.; Zhang, Y.; Jiang, J. *J. Mol. Struct.* **2004**, *673*, 103-108.

(105) Schlettwein, D.; Hesse, K.; Gruhn, N. E.; Lee, P. A.; Nebesny, K. W.; Armstrong, N. R. *J. Phys. Chem. B* **2001**, *105*, 4791-4800.

(106) Gantchev, T. G.; van Lier, J. E.; Hunting, D. J. *Radiat. Phys. Chem.* **2005**, *72*, 367-379.

(107) Peisert, H.; Knupfer, M.; Schwieger, T.; Fuentes, G. G.; Olligs, D.; Fink, J.; Schmidt, T. *J. Appl. Phys.* **2003**, *93*, 9683-9692.

(108) Schollhorn, B.; Germain, J. P.; Pauly, A.; Maleysson, C.; Blanc, J. P. *Thin Solid Films* **1998**, *326*, 245-250.

(109) Germain, J. P.; Pauly, A.; Maleysson, C.; Blanc, J. P.; Schollhorn, B. *Thin Solid Films* **1998**, *333*, 235-239.

(110) de Haan, A.; Debliquy, M.; Decroly, A. *Sens. Actuators, B* **1999**, *57*, 69-74.

(111) Martin, M.; Andre, J. J.; Simon, J. *J. Appl. Phys.* **1983**, *54*, 2792-2794.

(112) Zwart, J.; van Wolput, J. H. M. C. *J. Molec. Catal.* **1979**, *5*, 51-64.

(113) Barbon, A.; Brustolon, M.; van Faassen, E. E. *Phys. Chem. Chem. Phys.* **2001**, *3*, 5342-5347.

(114) Yahiro, H.; Naka, T.; Kuramoto, T.; Kurohagi, K.; Okada, G.; Shiotani, M. *Microporous Mesoporous Mater.* **2005**, *79*, 291-297.

(115) Kerp, H. R.; Westerduin, K. T.; van Veen, A. T.; van Faassen, E. E. *J. Mater. Res.* **2001**, *16*, 503-511.

(116) Shihub, S. I.; Gould, R. D. *Thin Solid Films* **1995**, *254*, 187-193.

(117) Misevich, A. V.; Pochtenny, A. E. *Electron Tech. Internet J.* **2000**, *33*, 167-170.

(118) Coehoorn, R.; Pasveer, W. F.; Bobbert, P. A.; Michels, M. A. J. *Phys. Rev. B* **2005**, *72*, 155206/1-20.

(119) Norton, J. E.; Bredas, J. L. *J. Chem. Phys.* **2008**, *128*, 034701/1-7.

(120) Silveira, W. R.; Marohn, J. A. *Phys. Rev. Lett.* **2004**, *93*, 116104/1-4.

(121) Miller, K. A.; Yang, R. D.; Hale, M. J.; Park, J.; Fruhberger, B.; Colesniuc, C. N.; Schuller, I. K.; Kummel, A. C.; Trogler, W. C. *J. Phys. Chem. B* **2006**, *110*, 361-366.

(122) Wilson, A.; Collins, R. A. *Sens. Actuators* **1987**, *12*, 389-403.

(123) Grate, J. W.; Anheier, N. C.; Baldwin, D. L. *Anal. Chem.* **2005**, *77*, 1867-1875.

(124) Yang, R. D.; Gredig, T.; Colesniuc, C. N.; Park, J.; Schuller, I. K.; Trogler, W. C.; Kummel, A. C. *Appl. Phys. Lett.* **2007**, *90*, 263506/1-3.

(125) Albert, K. J.; Lewis, N. S.; Schauer, C. L.; Sotzing, G. A.; Stitzel, S. E.; Vaid, T. P.; Walt, D. R. *Chem. Rev.* **2000**, *100*, 2595-2626.

(126) Kamlet, M. J.; Aboud, J. L. M.; Taft, R. W. *Progr. Phys. Org. Chem.* **1981**, *13*, 485-630.

(127) Grate, J. W. *Chem. Rev.* **2000**, *100*, 2627-2648.

(128) Grate, J. W.; Abraham, M. H. *Sens. Actuators, B* **1991**, *3*, 85-111.

(129) Steed, J. W.; Atwood, J. L. *Supramolecular Chemistry* J. Wiley and Sons, Ltd.: New York, 2000.

(130) Leeder, S. M.; Gagne, M. R. *J. Am. Chem. Soc.* **2003**, *125*, 9048-9054.

(131) Brunet, J.; Pauly, A.; Mazet, L.; Germain, J. P.; Bouvet, M.; Malezieux, B. *Thin Solid Films* **2005**, *490*, 28-35.

(132) Miyata, T.; Minami, T. *Appl. Surf. Sci.* **2005**, *244*, 563-567.

(133) Bouvet, M.; Guillaud, G.; Leroy, A.; Maillard, A.; Spirkovitch, S.; Tournilhac, F. G. *Sens. Actuators, B* **2001**, *73*, 63-70.

(134) Bohrer, F. I.; Colesniuc, C. N.; Park, J.; Schuller, I. K.; Kummel, A. C.; Trogler, W. C. *J. Am. Chem. Soc.* **2008**, *130*, DOI: 10.1021/ja710324f

(135) Wohltjen, H. *Sens. Actuators* **1984**, *5*, 307-325.

(136) Urbanczyk, M.; Jakubik, W.; Kochowski, S. *Sens. Actuators, B* **1994**, *22*, 133-137.

(137) Nieuwenhuizen, M. S.; Nederlof, A. J.; Barendsz, A. W. *Anal. Chem.* **1988**, *60*, 230-235.

(138) Bao, Z.; Lovinger, A. J.; Dodabalapur, A. *Appl. Phys. Lett.* **1996**, *69*, 3066-3068.

(139) Yang, R. D.; Park, J.; Colesniuc, C. N.; Schuller, I. K.; Trogler, W. C.; Kummel, A. C. *J. Appl. Phys.* **2007**, *102*, 034515/1-7.

(140) Liao, M. S.; Kar, T.; Gorun, S. M.; Scheiner, S. *Inorg. Chem.* **2004**, *43*, 7151-7161.

(141) Bohrer, F. I.; Sharoni, A.; Colesniuc, C.; Park, J.; Schuller, I. K.; Kummel, A. C.; Trogler, W. C. *J. Am. Chem. Soc.* **2007**, *129*, 5640-5646.

(142) Maria, P. C.; Gal, J. F. *J. Phys. Chem.* **1985,** *89,* 1296-1304.

(143) Abraham, M. H.; Grellier, P. L.; Prior, D. V.; Morris, J. J.; Taylor, P. J. *J. Chem. Soc. Perkins Trans 2* **1990,** 521-529.

(144) Garrone, E.; Areán, C. O. *Chem. Soc. Rev.* **2005**, *34*, 846-857.

(145) Espenson, J. H. *Chemical Kinetics and Reaction Mechanisms* McGraw-Hill, Inc.: New York, 1981.

(146) Micali, N.; Villari, V.; Castriciano, M. A.; Romeo, A.; Scolaro, L. M. *J. Phys. Chem. B* **2006**, *110*, 8289-8295.

(147) Smith, K. M. *J. Porphyrins Phthalocyanines* **2000**, *4*, 319-324.

(148) Di Natale, C.; Macagnano, A.; Repole, G.; Saggio, G.; D'Amico, A. D.; Paolesse, R.; Boschi, T. *Mater. Sci. Eng., C* **1998**, *5*, 209-215.

(149) Dunbar, A. D. F.; Richardson, T. H.; McNaughton, A. J.; Hutchinson, J.; Hunter, C. A. *J. Phys. Chem. B* **2006**, *110*, 16646-16651.

(150) Huo, C.; Zhang, H.; Zhang, H.; Zhang, H.; Yang, B.; Zhang, P.; Wang, Y. *Inorg. Chem.* **2006**, *45*, 4734-4742.

(151) Di Natale, C.; Paolesse, R.; Macagnano, A.; Mantini, A.; Goletti, C.; D'Amico, A. *Sens. Actuators, B* **1998**, *52*, 162-168.

(152) Tonezzer, M.; Quaranta, A.; Maggioni, G.; Carturan, S.; Della Mea, G. *Sens. Actuators, B* **2007**, *122*, 620-626.

(153) Walker, F. A.; Beroiz, D.; Kadish, K. M. *J. Am. Chem. Soc.* **1976**, *98*, 3484-3489.

(154) Yamamoto, K. *Inorg. Chim. Acta* **1986**, *113*, 181-186.

(155) Smith, P. D.; James, B. R.; Dolphin, D. H. *Coord. Chem. Rev.* **1981**, *39*, 31-75.

(156) Cunningham. K. L.; McNett, K. M.; Pierce, R. A.; Davis, K. A.; Harris, H. H.; Falck, D. M.; McMillin, D. R. *Inorg. Chem.* **1997**, *36*, 608-613.

(157) Atanasov, M.; Daul, C. A.; Rohmer, M. M.; Venkatachalam, T. *Chem. Phys. Lett.* **2006**, *427*, 449-454.

(158) Ma, X.; Sun, J.; Wang, M.; Hu, M.; Li, G.; Chen, H.; Huang, J. *Sens. Actuators, B* **2006**, *114*, 1035-1042.

(159) Tepore, A.; Serra, A.; Manno, D.; Valli, L.; Micocci, G.; Arnold, D. P. *J. Appl. Phys.* **1998**, *84*, 1416-1420.

(160) Arnold, D. P.; Manno, D.; Micocci, G.; Serra, A.; Tepore, A.; Valli, L. *Langmuir* **1997**, *13*, 5951-5956.

(161) Renkuan, Y.; Yuxue, L.; Hong, Y.; Yongbin, W. ; Xiangqin, Z.; Jian, X. *Synth. Met.* **1993**, *55-57*, 4087-4092.

(162) Huang, W. S.; MacDiarmid, A. G. *Polymer* **1993**, *34*, 1833-1845.

(163) MacDiarmid, A. G.; Epstein, A. J. *Faraday Discuss. Chem. Soc.* **1989**, *88*, 317-332.

(164) Han, C. C.; Chen, H. Y. *Macromolecules* **2007**, *40*, 8969-8973.

(165) Virji, S.; Huang, J.; Kaner, R. B.; Weiller, B. H. *Nano Lett.* **2004**, *4*, 491-496.

(166) Xu, K.; Zhu, L.; Li, J.; Tang, H. *Electrochim. Acta* **2006**, *52*, 723-727.

(167) Wang, J.; Chan, S.; Carlson, R. R.; Luo, Y.; Ge, G.; Ries, R. S.; Heath, J. R.; Tseng, H. R. *Nano Lett.* **2004**, *4*, 1693-1697.

(168) Li, G.; Josowicz, M.; Janata, J.; Semancik, S. *Appl. Phys. Lett.* **2004**, *85*, 1187-1189.

(169) McCullough, R. D. *Adv. Mater.* **1998**, *10*, 93-116.

(170) Barbarella, G.; Melucci, M.; Sotgiu, G. *Adv. Mater.* **2005**, *17*, 1581-1593.

(171) Berlin, A.; Pagani, G. A.; Sannicolo, F. *J. Chem. Soc., Chem. Commun.* **1986**, *22*, 1663-1664.

(172) Ikenoue, Y.; Chiang, J.; Patil, A. O.; Wudl, F.; Heeger, A. J. *J. Am. Chem. Soc.* **1998**, *110*, 2983-2985.

(173) Yuen, J. D.; Dhoot, A. S.; Namdas, E. B.; Coates, N. E.; Heeney, M.; McCulloch, I.; Moses, D.; Heeger, A. J. *J. Am. Chem. Soc.* **2007**, *129*, 14367-14371.

(174) *Semiconducting Polymers* Hadziioannou, G., van Hutten, P. F., Eds.; Wiley-VCH: New York, 2000; pp.481-486.

(175) Zotti, G.; Schiavon, G.; Berlin, A.; Pagani, G. *Adv. Mater.* **1993**, *5*, 551-554.

(176) Graf, D. D.; Campbell, J. P.; Miller, L. L.; Mann, K. R. *J. Am. Chem. Soc.* **1996**, *118*, 5480-5481.

(177) Someya, T.; Katz, H. E.; Gelperin, A.; Lovinger, A. J.; Dodabalapur, A. *Appl. Phys. Lett.* **2002**, *81*, 3079-3081.

(178) Torsi, L.; Lovinger, A. J.; Crone, B.; Someya, T.; Dodabalapur, A.; Katz, H. E.; Gelperin, A. *J. Phys. Chem., B* **2002**, *106*, 12563-12568.

(179) Torsi, L.; Tanese, M. C.; Cioffi, N.; Gallazzi, M. C.; Sabbatini, L.; Zambonin, P. G.; Raos, G.; Meille, S. V.; Giangregorio, M. M. *J. Phys. Chem., B* **2003**, *107*, 7589-7594.

(180) Rella, R.; Siciliano, P.; Quaranta, F.; Primo, T.; Valli, L.; Schenetti, L. *Colloids Surf., A* **2002**, *198-200*, 829-833.

(181) Rella, R.; Siciliano, P.; Quaranta, F.; Primo, T.; Valli, L.; Schenetti, L.; Mucci, A.; Iarossi, D. *Sens. Actuators, B* **2000**, *68*, 203-209.

(182) Ram, M. K.; Yavuz, O.; Aldiss, M. *Synth. Met.* **2005**, *151*, 77-84.

(183) Jang, J.; Chang, M.; Yoon, H. *Adv. Mater.* **2005**, *17*, 1616-1620.

(184) Dan, Y.; Cao, Y.; Mallouk, T. E.; Johnson, A. T.; Evoy, S. *Sens. Actuators, B* **2007**, *125*, 55-59.

(185) Sotzing, G. A.; Briglin, S. M.; Grubbs, R. H.; Lewis, N. S. *Anal. Chem.* **2000**, *72*, 3181-3190.

(186) Mabrook, M. F.; Pearson, C.; Petty, M. C. *Appl. Phys. Lett.* **2005**, *86*, 013507/1-3.

(187) Tans, S. J.; Verschueren, A. R. M.; Dekker, C. *Nature* **1998**, *393*, 49-52.

(188) Dai, H.; Hafner, J. H.; Rinzler, A. G.; Colbert, D. T.; Smalley, R. E. *Nature* **1996**, *384*, 147-150.

(189) Kong, J.; Franklin, N. R.; Zhou, C.; Chapline, M. G.; Peng, S.; Cho, K.; Dai, H. *Science* **2000**, *287*, 622-625.

(190) Lay, M. D.; Novak, J. P.; Snow, E. S. *Nano Lett.* **2004**, *4*, 603-606.

(191) Kumar, M. S.; Lee, S. H.; Kim, T. Y.; Kim, T. H.; Song, S. M.; Yang, J. W.; Nahm, K. S.; Suh, E. K. *Solid-State Electron.* **2003**, *47*, 2075-2080.

(192) Li, J.; Lu, Y.; Ye, Q.; Cinke, M.; Han, J.; Meyyappan, M. *Nano Lett.* **2003**, *3*, 929-933.

(193) Bekyarova, E.; Davis, M.; Burch, T.; Itkis, M. E.; Zhao, B.; Sunshine, S.; Haddon, R. C. *J. Phys. Chem. B* **2004**, *108*, 19717-19720.

(194) Lu, Y.; Li, J.; Han, J.; Ng, H. T.; Binder, C.; Partridge, C.; Meyyappan, M. *Chem. Phys. Lett.* **2004**, *391*, 344-348.

(195) Sayago, I.; Terrado, E.; Aleixandre, M.; Horrillo, M. C.; Fernandez, M. J.; Lozano, J.; Lafuente, E.; Maser, W. K.; Benito, A. M.; Martinez, M. T.; Gutierrez, J.; Munoz, E. *Sens. Actuators, B* **2007**, *122*, 75-80.

(196) Sljukic, B.; Banks, C. E.; Compton, R. G. *Nano Lett.* **2006**, *6*, 1556-1558.

(197) Knipp, D.; Street, R. A.; Volkel, A. R. *Appl. Phys. Lett.* **2003**, *82*, 3907-3909.

(198) Minakata, T.; Nagoya, I.; Ozaki, M. *J. Appl. Phys.* **1991**, *69*, 7354-7356.

(199) Parisse, P.; Picozzi, S.; Passacantando, M.; Ottaviano, L. *Thin Solid Films* **2007**, *515*, 8316-8321.

(200) Jurchescu, O. D.; Baas, J.; Palstra, T. T. M. *Appl. Phys. Lett.* **2005**, *87*, 052102/1-3.

(201) Minakata, T. *Polym. Adv. Technol.* **1995**, *6*, 607-610.

(202) Li, D.; Borkent, E. J.; Nortrup, R.; Moon, H.; Katz, H.; Bao, Z. *Appl. Phys. Lett.* **2005**, *86*, 042105/1-3.

(203) Zhu, Z. T.; Mason, J. T.; Dieckmann, R.; Malliaras, G. G. *Appl. Phys. Lett.* **2002**, *81*, 4643-4645.

(204) Wang, L.; Fine, D.; Dodabalapur, A. *Appl. Phys. Lett.* **2004**, *85*, 6386-6388.

(205) Wang, X.; Someya, T.; Sekitani, T.; Kato, Y.; Iba, S. *Mol. Cryst. Liq. Cryst.* **2007**, *462*, 29-36.

(206) Marrs, T. C. *Pharmacol. Ther.* **1993,** *58,* 51-66.

(207) Worek, F.; Aurbek, N.; Thiermann, H. *J. Appl. Toxicol.* **2007**, *27*, 582-588.

(208) Holmstedt, B. *Pharmacol. Rev.* **1959**, *11*, 567-688.

(209) Abu-Qare, A. W.; Abou-Donia, M. B. *Food Chem. Toxicol.* **2002,** *40,* 1327-1333.

(210) Okumura, T.; Hisaoka, T.; Yamada, A.; Naito, T.; Isonuma, H.; Okumura, S.; Miura, K.; Sakurada, M.; Maekawa, H.; Ishimatsu, S.; Takasu, N.; Suzuki, K. *Toxicol. Appl. Pharmacol.* **2005,** *207,* S471-S476.

(211) Brown, M. A.; Brix, K. A. *J. Appl. Toxicol.* **1998**, *18*, 393-408.

(212) Panieri, E.; Krige, J. E.; Bornman, C.; Linton, D. M. *J. Clin. Gastroenterol.* **1997**, *25*, 463-465.

(213) Ikizceli, I.; Yurumez, Y.; Avsarogullari, L.; Kucuk, C.; Sozuer, E. M.; Soyuer, I.; Yavuz, Y.; Muhtaroglu, S. *Regul. Toxicol. Pharmacol.* **2005**, *42*, 260-264.

(214) Okumura, T.; Ninomiya, N.; Ohta, M. *Prehosp. Disaster Med.* **2003**, *18*, 189-192.

(215) Stan, H. J.; Kellner, G. *Biomed. Environ. Mass Spectrom.* **1989**, *18*, 645-651.

(216) Leonard, D. A.; Driscoll, T. A.; Sweeney, H. E. *Proc. SPIE-Int. Soc. Opt. Eng.* **1996**, *2832*, 20-31.

(217) De Stefano, L.; Moretti, L.; Rendina, I.; Rotiroti, L. *Sens. Actuators, B* **2005**, *111-112*, 522-525.

(218) Walker, J. P.; Kimble, K. W.; Asher, S. A. *Anal. Bioanal. Chem.* **2007**, *389*, 2115-2124.

(219) Newman, J. D. S.; Roberts, J. M.; Blanchard, G. J. *Anal. Chem.* **2007**, *79*, 3448-3454.

(220) Bencic-Nagale, S.; Sternfeld, T.; Walt, D. R. *J. Am. Chem. Soc.* **2006**, *128*, 5041-5048.

(221) Knapton, D.; Burnworth, M.; Rowan, S. J.; Weder, C. *Angew. Chem. Int. Ed.* **2006**, *45*, 5825-5829.

(222) Southard, G. E.; Van Houten, K. A.; Ott, E. W.; Murray, G. M. *Anal. Chim. Acta* **2007**, *581*, 202-207.

(223) Ishii, A.; Takeda, S.; Hattori, S.; Sueoka, K.; Mukasa, K. *Colloids Surf., A* **2008**, *313-314*, 456-460.

(224) Wang, J.; Timchalk, C.; Lin, Y. *Environ. Sci. Technol.* **2008**, *42*, doi: 10.1021/es702335y.

(225) Liu, N.; Cai, X.; Lei, Y.; Zhang, Q.; Chan-Park, M. B.; Li, C.; Chen, W.; Mulchandani, A. *Electroanalysis* **2007**, *5*, 616-619.

(226) Simonian, A. L.; Grimsley, J. K.; Flounders, A. W.: Schoeniger, J. S.; Cheng, T. C.; DeFrank, J. J.; Wild, J. R. *Anal. Chim. Acta* **2001**, *442*, 15-23.

(227) Luckarift, H. R.; Greenwald, R.; Bergin, M. H.; Spain, J. C.; Johnson, G. R. *Biosens. Bioelectron.* **2007**, *23*, 400-406.

(228) Skladal, P. *Anal. Chim. Acta* **1992**, *269*, 281-287.

(229) Oh, I.; Masel, R. I. *Electrochem. Solid-State Lett.* **2007**, *10*, J19-J22.

(230) Yan, X.; Tang. Y.; Ji, H.; Lvov, Y.; Thundat, T. *Instrum. Sci. Technol.* **2004**, *32*, 175-183.

(231) *Report of the Official Account of the Bombings in London on 7th July 2005.* HC series, 2005-06 1087; House of Commons, Parliament, Great Britain; Stationary Office, London, 2006.

(232) Landler, Mark. German police arrest 3 in terrorist plot. *New York Times* 09/06/07; http://www.nytimes.com/2007/09/06/world/europe/06germany.html

(233) Bellamy, A. J. *J. Forensic Sci.* **1999**, *44*, 603-608.

(234) Oxley, J. C.; Smith, J. L.; Chen. H.; Cioffi, E. *Thermochim. Acta* **2002**, *388*, 215-225.

(235) Oxley, J. C.; Smith, J. L.; Shinde, K.; Moran, J. *Propellants, Explos., Pyrotech.* **2005**, *30*, 127-130.

(236) Schaefer, W. P.; Fourkas, J. T.; Tiemann, B. G. *J. Am. Chem. Soc.* **1985**, *107*, 2461-2463.

(237) Evans, H. K.; Tulleners, F. A. J.; Sanchez, B. L.; Rasmussen, C. A. *J. Forensic Sci.* **1986**, *31*, 1119-1125.

(238) Pacheco-Londono, L.; Primera, O. M.; Ramirez, M.; Ruiz, O.; Hernandez-Rivera, S. *Proc. SPIE-Int. Soc. Opt. Eng.* **2005**, *5778*, 317-326.

(239) Pacheco-Londono, L.; Premera, O. M.; Hernandez-Rivera, S. *Proc. SPIE-Int. Soc. Opt. Eng.* **2004**, *5617*, 190-201.

(240) Schulte-Ladbeck, R.; Edelmann, A.; Quintas, G.; Lendl, B.; Karst, U. *Anal. Chem.* **2006**, *78*, 8150-8155.

(241) Widmer, L.; Watson, S.; Schlatter, K.; Crowson, A. *Analyst* **2002**, *127*, 1627-1632.

(242) Sigman, M. E.; Clark, C. D.; Caiano, T.; Mullen, R. *Rapid Commun. Mass Spectrom.* **2008**, *22*, 84-90.

(243) Cotte-Rodriguez, I.; Chen, H.; Cooks, R. G. *Chem. Commun.* **2006**, 953-955.

(244) Dräger Inc. Safety Website, DrägerSensor® H_2O_2 LC Chemical Sensor Data Sheet. http://www.draeger.com/ST/internet/pdf/Master/En/gt/9023492h2o2lcde.pdf (accessed July 2007).

(245) Lu, D.; Cagan, A.; Munoz, R. A. A.; Tangkuaram, T.; Wang, J. *Analyst* **2006**, *131*, 1279-1281.

(246) Laine, D. F.; Roske, C. W.; Cheng, I. F. *Anal. Chim. Acta* **2008**, *608*, 56-60.

(247) Schulte-Ladbeck, R.; Kolla, P.; Karst, U. *Anal. Chem.* **2003**, *75*, 731-735.

(248) Schulte-Ladbeck, R.; Kolla, P.; Karst, U. *Analyst* **2002**, *127*, 1152-1154.

(249) Schulte-Ladbeck, R.; Karst, U. *Anal. Chim. Acta* **2003**, *482*, 183-188.

CHAPTER II

SYNTHESES AND THIN FILM DEPOSITIONS OF METALLOPHTHALOCYANINES AND FUNCTIONALIZED DERIVATIVES

2.1 ABSTRACT

Metallophthalocyanines (MPcs) were prepared through a templated reaction of phthalonitrile and metal cations catalyzed by a strong organic base. Functionalization of the organic ring was achieved by using appropriately functionalized phthalonitriles. A novel phthalocyanine incorporating the 1,1,1,3,3,3-hexafluoropropan-2-ol (HFIP) group was prepared through Friedel-Crafts addition of hexafluoroacetone sesquihydrate to 2-bromoaniline to produce 4-(HFIP)-2-bromoaniline. Copper tetrakis-(HFIP)-phthalocyanine was prepared by sequential cyanation of 4-(HFIP)-2-bromoaniline using the Sandmeyer and Rosenmund-von Braun reactions, yielding a highly soluble deep blue complex. Deposition methods for MPc sensing films were also studied. Highly ordered films of MPcs were deposited by organic molecular beam epitaxy (OMBE). The influence of substrate temperature and metal center on the thin film grain structure was examined by atomic force microscopy (AFM). It was found that, among late first-row transition metals (M = Fe, Co, Ni, and Cu), the metal center did not play a significant role in grain size, but elevated substrate temperature during deposition can significantly alter grain morphology. Spin-coating was studied as a cost-effective alternative to OMBE using soluble functionalized phthalocyanines.

The role of solvent and functional groups were explored by AFM and relatively uniform amorphous nanofilms were achieved.

2.2 INTRODUCTION

Metallophthalocyanines (MPcs) and the metal-free derivative (H_2Pc) are a class of macrocyclic coordination complexes that have been the subject of extensive study. MPcs are used as dyes, catalysts,[1] photovoltaics,[2] and vapor sensors.[3-5] MPc chemical properties may be tuned through variation of the metal center as well as functionalization of the organic macrocycle.[6] A large variety of synthetic processes have been developed to achieve this goal.

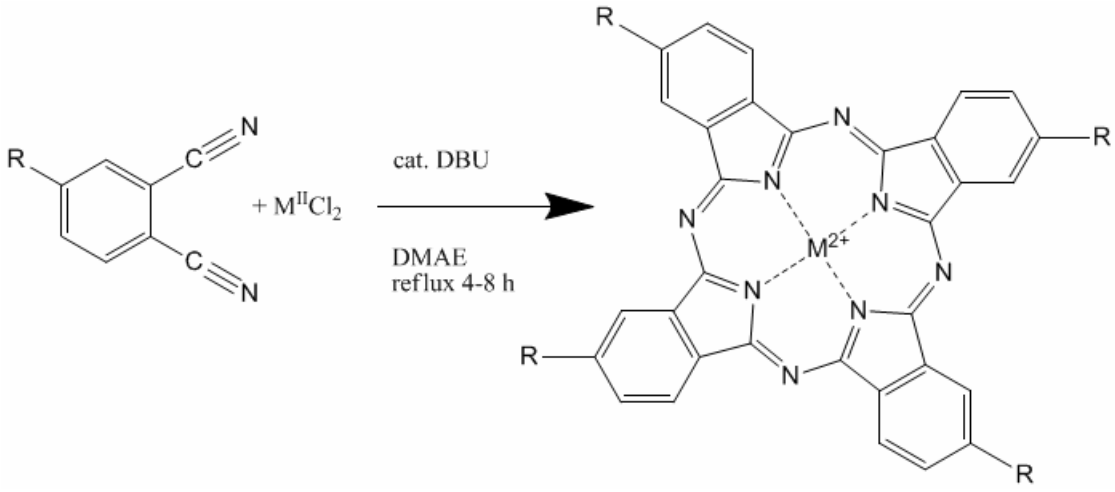

Scheme 2-1 Synthesis of metallophthalocyanine from phthalonitrile and a metal salt.

The most common synthesis of metallophthalocyanines involves a templated reaction of phthalonitrile (1,2-dicyanobenzene) around a metal center (Scheme 2-1). Phthalonitrile is dissolved with an appropriate metal salt, generally chlorides or sulfates, in a high-boiling, basic solvent, usually an alcohol such as pentanol or *N*,*N*-

dimethylaminoethanol (DMAE). The reaction is completed by addition of a catalytic amount of a strong organic base (usually 1,8-diazabicyclo[5.4.0]undec-7-ene, DBU) and refluxing for 4 h or more.[7] Other synthetic pathways have been explored, including the cyclization of diiminoisoindolenine, the condensation of phthalic anhydride and urea, and the reaction of phthalimide with formamide.[8-9] Microwave heating has been proposed as a method to avoid solvents and long reflux times.[10]

Metallophthalocyanines have been exhaustively explored in the literature, incorporating nearly all transition metals, lanthanides, and alkali earth metals, as well as some non-metals. The most actively researched MPcs in catalysis applications include FePc, CoPc, and ZnPc.[11-12] A large number of MPcs have been studied for gas sensing applications, with late first-row transition metals being most popular (M = Fe, Co, Ni, Cu, Zn, Pb).[13] Photoactive MPcs for photovoltaic applications include CuPc, ZnPc, and titanyl phthalocyanine (TiOPc), which has an axially coordinated oxygen bound to the titanium center.[14-16] Large lanthanide metal ions form sandwich complexes incorporating two or more Pc rings, which are redox-active and display potential for use as single-molecule magnets.[17-19] Phthalocyanines incorporating main group elements (silicon and aluminum) generally contain axial halide ligands for charge neutrality, and are of interest for phthalocyanine polymers.[20-22]

Phthalocyanine rings have been functionalized in a variety of ways. Functionalization of the organic ring can be accomplished by using the appropriately substituted phthalonitrile (Scheme 2-1); tetrasubstituted[23] and octasubstituted[24]

phthalocyanines have been widely used for soluble phthalocyanines, and this trend has been extrapolated out to complete substitution (i.e. hexadecasubstitution).[25]

A functional group of interest for thin film sensors that has not yet been applied to MPcs is 1,1,1,3,3,3-hexafluoropropan-2-ol, or the hexafluoroisopropyl (HFIP) group.[26] This functional group has been studied in polymer-based surface acoustic wave (SAW) vapor sensors, where it has been shown to be both hydrogen-bond acidic and hydrophobic; this offers potential for sensing of basic, electron donating analytes, while simultaneous rejecting polar, protic analytes such as water or alcohols.[27-28] The HFIP group is usually added to phenyl groups through Friedel-Crafts or Grignard reactions.[29] The electron deficient phenyl ring of phthalonitrile is deactivated to these types of electrophilic aromatic substitution, requiring use of a different starting material.

A variety of deposition methods are available for producing metallophthalocyanine thin films. The thermal stability of MPcs makes sublimation the most popular method for film deposition, capable of producing a wide variety of physical structures.[30] In particular, organic molecular beam epitaxy (OMBE) produces extremely well-controlled films ideal for gas sensing applications.[31] Soluble functionalized phthalocyanines may be deposited by spin-coating, which is an inexpensive method for preparation of nanoscale films.[32-33] Films may also be produced using Langmuir-Blodgett techniques.[34]

In the following chapter synthetic and deposition methods like those described above were explored for producing MPc thin films for vapor sensing materials. A

variety of phthalocyanines were synthesized with varied metal centers and organic functional groups. A synthetic pathway for the preparation of 2(3),9(10),16(17),23(24)-tetrakis(HFIP)phthalocyaninato copper ($Cu(HFIP)_4Pc$) is reported. Thin films were deposited by OMBE and spin-coating methods, and analyzed using atomic force microscopy (AFM).

2.3 RESULTS AND DISCUSSION

2.3.1 Synthesis of Metallophthalocyanines

A series of MPcs was synthesized using the standard method (Scheme 2-1).[7] Several MPcs are available commercially, including FePc, CoPc, NiPc, CuPc, ZnPc, PbPc, and H_2Pc, so these were not prepared. Vanadyl (VOPc) (**1A**) and titanyl (TiOPc) (**1B**) phthalocyanines are of interest as photoconductive compounds; they diverge chemically from standard MPcs because the metal centers are in the +4 oxidation state and are capped with double-bonded oxo-ligands.[35] VOPc was prepared from phthalonitrile and vanadium pentoxide (V_2O_5), yielding a bright purple powder, which is easily purified by sublimation.[36] TiOPc was synthesized in a similar manner, using titanium isopropoxide to yield an iridescent purple powder. Manganese phthalocyanine (**1C**) has a redox-active metal center which is sensitive to atmospheric oxygen. MnPc was prepared by reacting phthalonitrile with manganese sulfate. The blue-black powder gradually reacted with air to yield a black solid that was difficult to sublime, likely due to the formation of μ-oxo species.[37] Palladium phthalocyanine (**1D**) is of interest for magnetic, catalytic, and electrochemical studies.[38-39] It was

prepared in poor yield from palladium chloride and phthalonitrile; the failure of this synthesis may be due to palladium reacting catalytically with phthalonitrile to form polymeric species.

MPcs are generally insoluble in organic solvents, and are only truly soluble in concentrated sulfuric acid. Solubility may be imparted by the addition of organic groups to the outer phenyl rings of the phthalocyanine, generally achieved by using appropriately substituted phthalonitriles (Scheme 2-1). Tetrakis(methyl) phthalocyanines (**2A-H)** were synthesized with a variety of metal centers (M = V, Ti, Mn, Co, Ni, Cu); however, it was found these compounds were still somewhat insoluble, and so tetrakis(*t*-butyl)phthalocyanines (M = V, Ti, Mn, Fe, Co, Ni, Cu) (**3A-H**) were prepared. These phthalocyanines were found to be quite soluble in a wide range of solvents, including acetone, toluene, THF, and CH_2Cl_2, among others.

The addition of the functional group 1,1,1,3,3,3-hexafluoropropan-2-ol (HFIP) is of considerable interest for phthalocyanine sensors, as it is both hydrogen bond acidic and hydrophobic. The compound 2(3),9(10),16(17),23(24)-tetrakis(HFIP) phthalocyaninato copper (**7**) was prepared in a three step synthesis (Scheme 2-2). 2-Bromoaniline was refluxed at 100 ^{o}C for 24 h with hexafluoroacetone sesquihydrate (HFA*1.5 H_2O) and a catalytic amount of p-toluenesulfonic acid; this reaction produced 4-(HFIP)-2-bromoaniline (**4)** in 24% yield as large white crystals.[40-41]

The amine of **4** was then converted to the nitrile using the Sandmeyer reaction.[42] The amine was diazotized by treatment with nitrous acid; the diazonium moiety was then replaced by the nitrile via reaction with CuCN, producing 4-(HFIP)-

2-bromocyanobenzene (**5**) in 77% yield. 1,2-Phenylenediamine cannot be used in this synthesis because adjacent aromatic amines, when treated with nitrous acid to form diazonium salts, cyclize to form a triazole ring.[43] Compound **5** was then converted to **7** through the intermediate 4-(HFIP)-phthalonitrile (**6**) by refluxing **5** with CuCN in anhydrous DMF.[44] CuCN catalyzes the replacement of the bromine on **5** with a nitrile group to form **6**; in the presence of basic CN^- anions in refluxing DMF the cyclization of **6** around Cu^{2+} cations occurs (Scheme 2-1), leading to the formation of **7**, a deep blue solid. The composition of **7** was confirmed by ^1H NMR, IR, UV-Vis, and LC-MS methods.

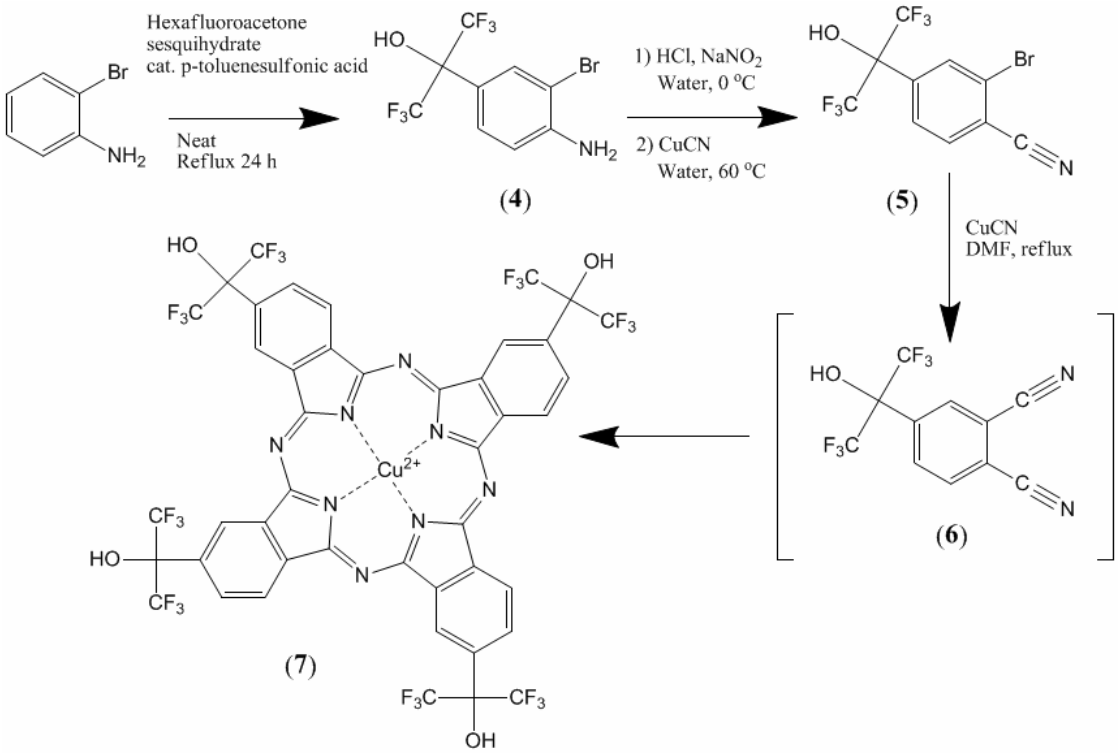

Scheme 2-2 Synthesis of 2(3),9(10),16(17),23(24)-tetrakis(HFIP)phthalocyaninato copper (**7**).

2.3.2 Deposition of Thin Films

MPc thin films used in the majority of gas sensing studies (Chapters 3-6) were deposited by organic molecular beam epitaxy (OMBE).[45] MPcs were purified by multiple sublimations at 400 ^{o}C and 10^{-5} Torr. Films were grown by subliming the source material from an effusion cell in a vacuum of $2x10^{-10}$ Torr. This material is then collimated into a molecular beam and deposited on the surface of interdigitated electrodes (IDEs) at a growth rate of 0.2 to 0.5 Å s^{-1}. The average film thickness was 50 nm, monitored by quartz crystal microbalance (QCM).

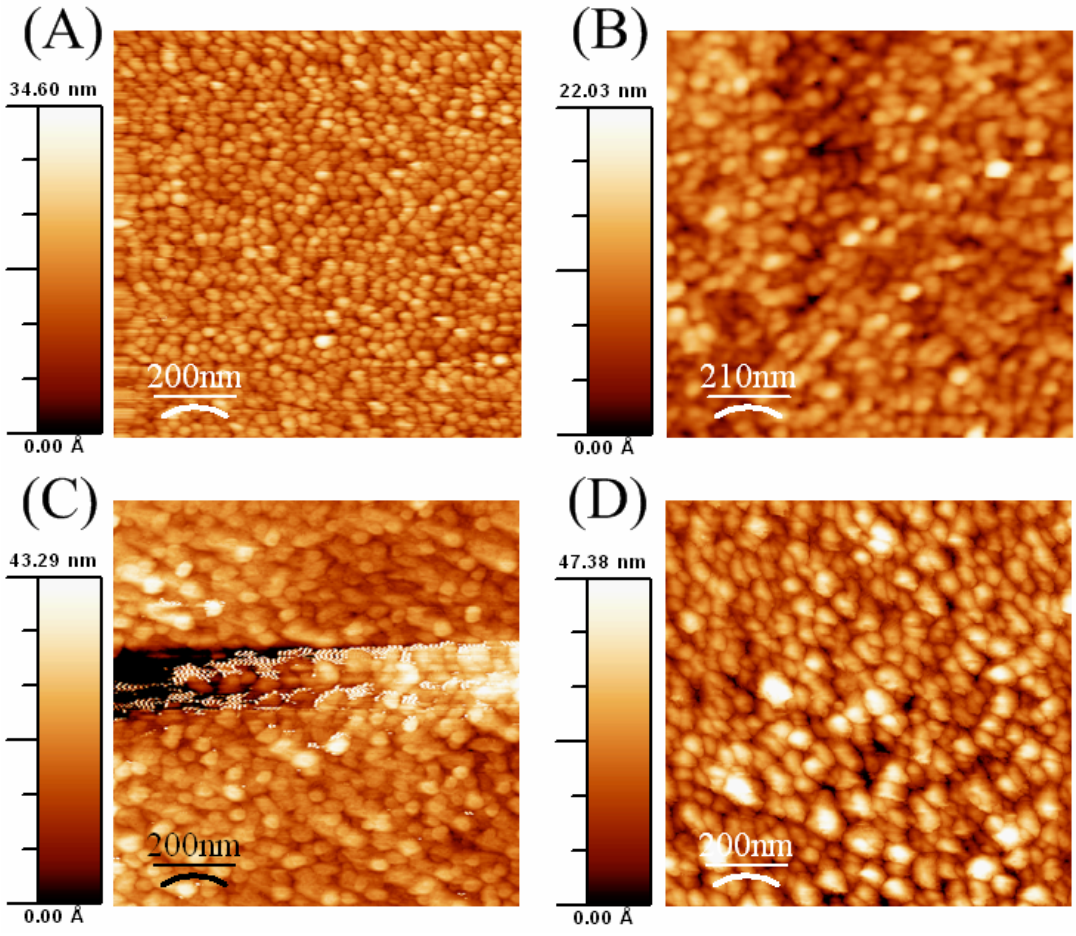

Figure 2-1 AFM images of grain structures of 50 nm MPc films. (A) FePc, (B) CoPc, (C) NiPc, (D) CuPc.

Grain structure in MPc films may be altered by variation of the substrate temperature. Low substrate temperatures (~25 ^{o}C) lead to small, ellipsoidal α-phase grains, while higher temperatures (>100 ^{o}C) lead to growth of much longer crystallites.[30-31] The metal center may also play a role in granular variability; this was explored by depositing 50 nm films of FePc, CoPc, NiPc, and CuPc at 25 ^{o}C and analyzing them via AFM (Figure 2-1). The grain structures across all MPcs are relatively similar, ranging from 40-80 nm on the long axis, with the smallest grains formed by FePc and largest grains by CuPc.

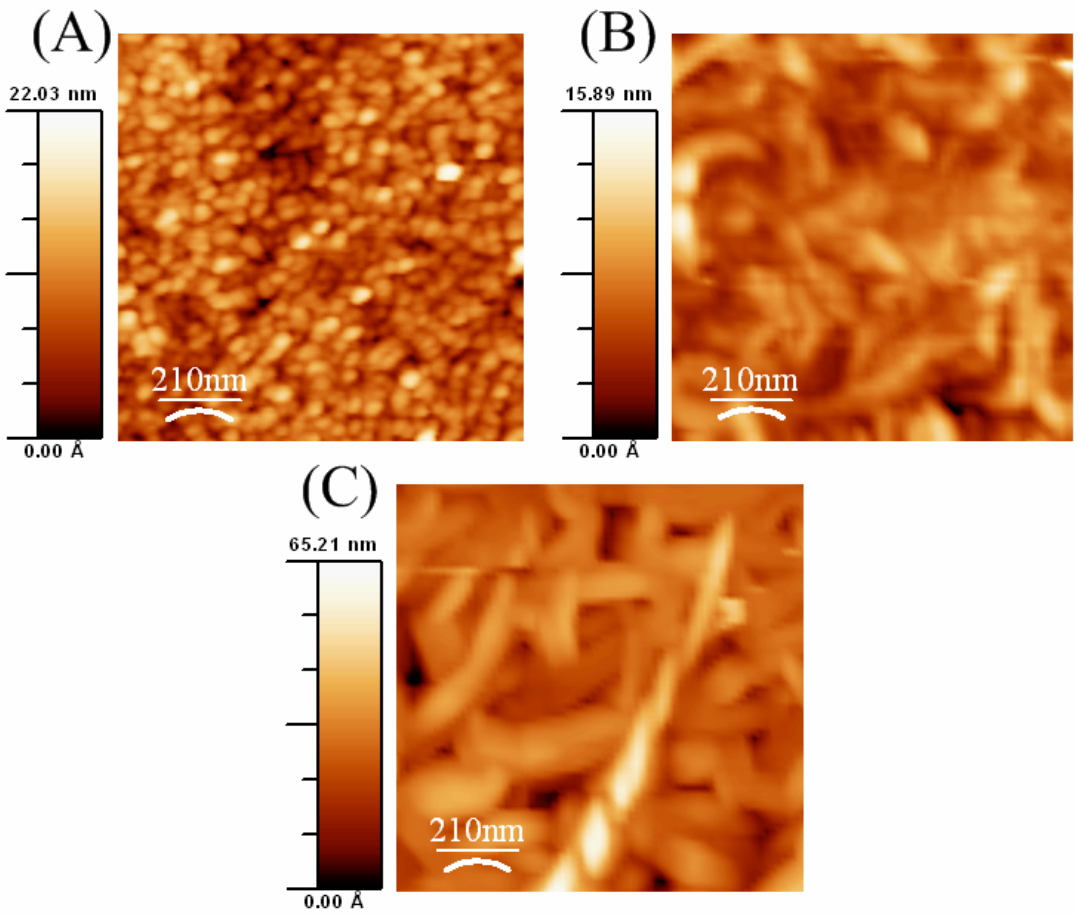

Figure 2-2 AFM images of grain structures of 50 nm CoPc films deposited at (A) 25 ^{o}C, (B) 160 ^{o}C, and (C) 200 ^{o}C.

The effect of grain size on chemical sensing was explored by holding the metal center (CoPc) constant and varying substrate temperature during deposition. Grain structures were studied at 25, 80, 160, 200, and 230 ^{o}C. The films were imaged by AFM (Figure 2-2); significant granular variation was found at the different temperatures. At 25 ^{o}C small ellipsoidal grains are seen, which become slightly larger (~100 nm on the long axis) when the temperature is raised to 80 ^{o}C. At 160 ^{o}C elongated crystallites (200 nm on the long axis) are evident; these are exaggerated further at 200 and 230 ^{o}C. No discernible pattern in chemical sensing could be related to the grain size of the films; however, it was found that the electrical drift generally increased with the substrate deposition temperature and grain size, so that sensors with the largest grains were the most unreliable sensors.

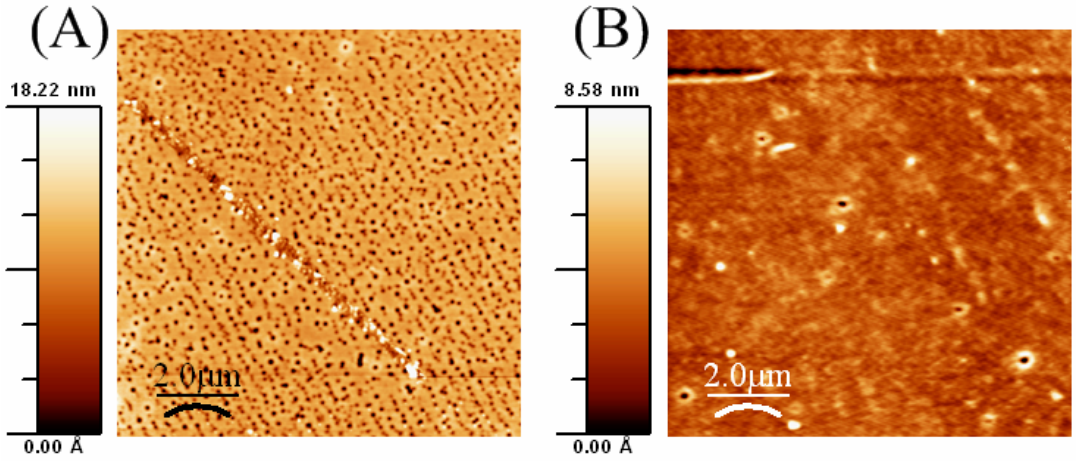

Figure 2-3 AFM images of spin-coated films of (A) $Co(tBu)_4Pc$ and (B) $Cu(tBu)_4Pc$.

Spin coating was explored as a cost-effective alternative to OMBE using soluble functionalized phthalocyanines. **3A-H** were dissolved in multiple solvents (including THF, 2-butanone, and toluene) at a variety of concentrations and spin-

coated onto cleaned glass slides and IDEs. The highest quality films were obtained by spin casting toluene solutions at concentrations of 20 or 25 mg/mL and using a spin rate of 3000 rpm. These films were imaged by AFM (Figure 2-3). The films show some defects, such as pinholes, but are quite uniform and smooth overall. Film thicknesses range from 60 to 100 nm. The lack of any grain structure is attributed to the fact that tetra-substituted MPcs exhibit four conformational isomers which inhibit crystallization and lead to amorphous films.

Spin-coating of **7** was also studied. The compound was readily soluble in toluene, but on spin-coating a non-uniform film was obtained (Figure 2-4A). This highly granular structure may be attributed to the fluorophobic effect; poly-fluorinated organics are known to be both hydrophobic and lipophobic.[46] The fluorophobic effect can be overcome by using partially fluorinated solvents or surfactants.[47] Thus, **7** was dissolved in trifluoroethanol and spin-coated at 3000 rpm, leading to highly uniform films like those seen in for **3A-H** spin-coated from toluene (Figure 2-4B).

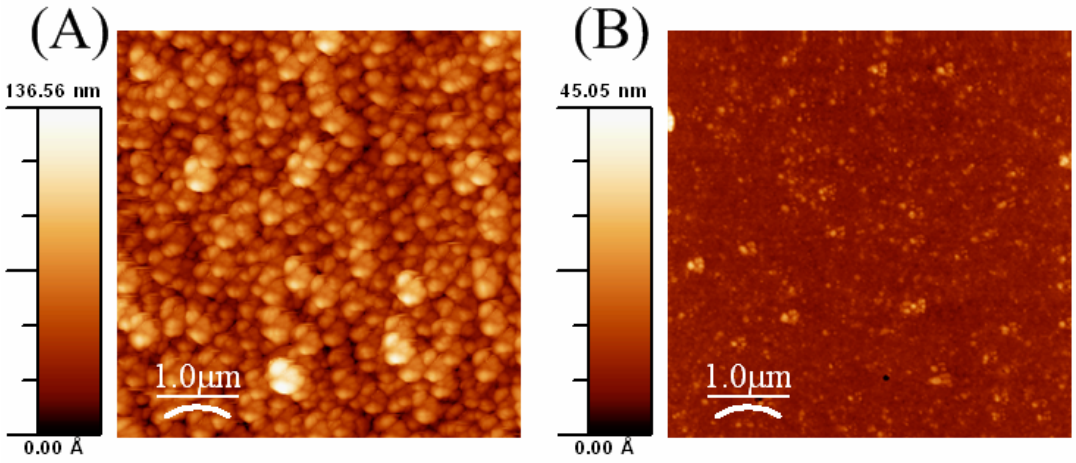

Figure 2-4 AFM images of spin-coated films of **7** using A) toluene and B) trifluoroethanol as the solvent.

The electrical behavior of spin-coated films was examined for use in chemiresistive sensors. Crystalline MPcs stack in a herring-bone formation, and conductivity is reported to occur along the z-axis of the crystal (the direction of overlapping metal centers).[13] There is no ordered overlap of molecules in amorphous MPc films, so the conductivity can be reduced by as much as three orders of magnitude. Amorphous MPc films therefore may be effective for detecting strong oxidants such as NO_2, but are not useful sensors for electron donors such as organophosphate neurotoxins, which decrease current in the films.[48-49] Currents in the spin-coated films detailed in this report were generally extremely low, in the range of 1.0-5.0x10^{-10} A; the signal-to-noise ratio for sensing was very low, and so the films were not used further for chemical sensing.

2.4 EXPERIMENTAL

2.4.1 General Synthetic and Characterization Techniques

All synthetic manipulations were carried out in a dry Ar atmosphere using standard Schlenk techniques. Compounds are labeled by metal center as follows: V^{4+} (**A**), Ti^{4+} (**B**), Mn^{2+} (**C**), Pd^{2+} (**D**), Fe^{2+} (**E**), Co^{2+} (**F**), Ni^{2+} (**G**), Cu^{2+} (**H**). Purification by sublimation was accomplished using a diffusion pump at a pressure of 10^{-3} Torr. ^{1}H NMR data were collected with a Varian Mercury 300 or 400 MHz spectrometer (300.1 or 400.1 MHz). IR data were recorded from KBr pellets using a Nicolet Magna-IR 550 spectrometer. UV/Vis spectra were obtained using evaporated films of

MPcs on glass slides (glass absorption below 250 nm) on an HP 8452A diode array spectrophotometer. GC/MS data were recorded on a ThermoFinnegan Trace GC/MS. LC/MS spectra were obtained on a Finnegan LCQDECA. AFM images were collected using a Nanoscope IV Scanning Microscope in tapping mode with a Mikromasch NSC15 325 kHz probe.

2.4.2 Thin Film Deposition Methods

Thin films were deposited using two different methods: organic molecular beam epitaxy (OMBE) and spin-coating. 50 nm thick films were deposited on interdigitated electrodes (IDEs; 50 nm Au electrodes on SiO_2 substrates) by OMBE in a UHV chamber with a base pressure of $2x10^{-10}$ Torr. The deposition rate of the MPc films ranged from 0.2 to 0.5 Å s^{-1}, and the deposition pressure was $5x10^{-9}$ Torr. Film growth rate and thickness were monitored with a quartz crystal microbalance (QCM). The IDEs were mounted on a temperature-controlled stage monitored with two thermocouples. After deposition, the devices were stored under vacuum at 10^{-3} Torr or less until use.

Spin-coated films were fabricated using a Laurell WS-400A-6NPP/Lite Single Wafer Spin Processor. Glass slides were cleaned by ultrasonication in acetone for 5 min followed by ultrasonication in methanol for 5 min. MPc films were spun onto glass slides and IDEs using toluene solutions (containing 20 or 25 mg/mL of MPc) at 3000 rpm for 1 min. Films of best quality were achieved by initiating the spin and then applying a single drop slowly to the spinning surface. MPc solutions were pre-

filtered using Millipore PTFE 0.20 μm syringe filters. Residual solvent in the films was removed under vacuum (10^{-3} Torr) before AFM imaging.

2.4.3 Synthesis of Metallophthalocyanines (1A-D)

Phthalonitrile (1,2-dicyanobenzene, 2.0 g, 15.6 mmol) was dissolved in 40 mL of anhydrous *N*,*N*-dimethylaminoethanol (DMAE) with the appropriate metal salt (7.8 mmol) and 0.5 mL of 1,8-diazabicyclo[5.4.0]undec-7-ene (DBU). The solution was refluxed for 4-8 h under a dry Ar atmosphere. The reaction mixture was cooled and the product was precipitated in a 50:50 water/methanol solution. The precipitate was suction filtered and washed several times with the 50:50 water/methanol solution. The resulting solid was then purified by sublimation at 450 ^{o}C and 10^{-3} Torr. Yields were generally 40% to 80%.

Phthalocyaninato oxovanadium (1A): 3.0 g (23.4 mmol) of phthalonitrile were reacted with 0.98 g (5.9 mmol) of V_2O_5. The resulting purple solid was sublimed at 450 ^{o}C and $5x10^{-3}$ Torr. Yield: 1.42 g (42%). IR (KBr): ν = 1610 cm^{-1} (m), 1500 cm^{-1} (s), 1480 cm^{-1} (w), 1415 cm^{-1} (m), 1330 cm^{-1} (s), 1290 cm^{-1} (s), 1160 cm^{-1} (m), 1120 cm^{-1} (s), 1065 cm^{-1} (s), 950 cm^{-1} (w), 900 cm^{-1} (s), 810 cm^{-1} (m), 780 cm^{-1} (s), 735 cm^{-1} (s).

Phthalocyaninato oxotitanium (1B): 5.0 g (39.0 mmol) of phthalonitrile were reacted with 6 mL (19.8 mmol) of titanium isopropoxide, Ti(*i*-PrO)$_4$. The resulting

iridescent purple solid was sublimed at 450 ^{o}C and 10^{-3} Torr. Yield: 4.88 g (87%). IR (KBr): ν = 1600 cm^{-1} (m), 1500 cm^{-1} (m), 1480 cm^{-1} (w), 1430 cm^{-1} (m), 1340 cm^{-1} (s), 1280 cm^{-1} (m), 1150 cm^{-1} (m), 1120 cm^{-1} (s), 1070 cm^{-1} (s), 970 cm^{-1} (m), 810 cm^{-1} (w), 740 cm^{-1} (s), 730 cm^{-1} (s).

Phthalocyaninato manganese (1C): 1.49 g (11.7 mmol) of phthalonitrile were reacted with 1.16 g (5.8 mmol) of $MnCl_2$*$4H_2O$. The resulting black solid was sublimed at 450 ^{o}C and 10^{-3} Torr. Yield: 0.80 g (48%). IR (KBr): ν = 1645 cm^{-1} (w), 1605 cm^{-1} (m), 1502 cm^{-1} (m), 1480 cm^{-1} (w), 1420 cm^{-1} (m), 1332 cm^{-1} (s), 1288 cm^{-1} (m), 1140 cm^{-1} (m), 1130cm^{-1} (s), 1079 cm^{-1} (s), 903 cm^{-1} (w), 780 cm^{-1} (m), 740 cm^{-1} (m), 710 cm^{-1} (s).

Phthalocyaninato palladium (1D): 1.0 g (7.8 mmol) of phthalonitrile were reacted with 0.71 g (4.0 mmol) of $PdCl_2$. A brown solid was isolated; upon sublimation at 450 ^{o}C and 10^{-3} Torr a tiny amount of purple powder was purified. Yield: 10 mg (< 0.1%). IR (KBr): ν = 1597 cm^{-1} (m), 1490 cm^{-1} (m), 1441 cm^{-1} (w), 1330 cm^{-1} (w), 1251 cm^{-1} (s), 1096 cm^{-1} (s), 980 cm^{-1} (s), 859 cm^{-1} (w), 801 cm^{-1} (m), 757 cm^{-1} (w), 695 cm^{-1} (m).

2.4.4 Synthesis of Metal Tetrakis(methyl)phthalocyanines (2A-H)

4-Methylphthalonitrile (2.0 g, 14.1 mmol) was dissolved in 40 mL of anhydrous DMAE with the appropriate metal salt (7.1 mmol) and 0.5 mL of DBU.

The solution was refluxed for 4-8 h under a dry Ar atmosphere. The product was cooled and then precipitated in a 50:50 water/methanol solution, suction filtered, and washed several times with the 50:50 water/methanol solution. The resultant solid was then purified by Soxhlet filtration in an appropriate solvent, usually acetone. Yields ranged from 10% to 90%.

2(3),9(10),16(17),23(24)-Tetrakis(methyl)phthalocyaninato oxovanadium (2A): 1.0 g (7.0 mmol) of 4-methylphthalonitrile were reacted with 0.30 g (1.8 mmol) of V_2O_5. The resulting blue-purple solid was purified by Soxhlet filtration in THF. Yield: 0.40 g (36%). ^{1}H NMR (300.1 MHz, $CDCl_3$ (δ = 7.26)): δ = 7.9-8.2 (broad m, Ar-H), 0.9 (s, -CH_3); IR (KBr):): ν = 3020 cm^{-1} (s), 2940 cm^{-1} (m), 1610 cm^{-1} (m), 1500 cm^{-1} (s), 1480 cm^{-1} (w), 1415 cm^{-1} (m), 1330 cm^{-1} (s), 1290 cm^{-1} (s), 1160 cm^{-1} (m), 1120 cm^{-1} (s), 1065 cm^{-1} (s), 950 cm^{-1} (w), 900 cm^{-1} (s), 810 cm^{-1} (m), 780 cm^{-1} (s), 735 cm^{-1} (s).

2(3),9(10),16(17),23(24)-Tetrakis(methyl)phthalocyaninato oxotitanium (2B): 0.94 g (6.6 mmol) of 4-methylphthalonitrile were reacted with 1 mL (3.3 mmol) of Ti(*i*-PrO)$_4$. The resulting deep blue solid was purified by Soxhlet filtration in THF. Yield: 0.09 g (8%). ^{1}H NMR (300.1 MHz, $CDCl_3$ (δ = 7.26)): δ = 7.8 (dd, 2H, Ar-H), 7.4 (s, 1H, Ar-H), 1.1 (s, 3H, -CH_3); IR (KBr): ν = 3020 cm^{-1} (s), 2940 cm^{-1} (m), 1600 cm^{-1} (m), 1500 cm^{-1} (m), 1480 cm^{-1} (w), 1430 cm^{-1} (m), 1340 cm^{-1} (s), 1280 cm^{-1} (m),

1150 cm^{-1} (m), 1120 cm^{-1} (s), 1070 cm^{-1} (s), 970 cm^{-1} (m), 810 cm^{-1} (w), 740 cm^{-1} (s), 730 cm^{-1} (s).

2(3),9(10),16(17),23(24)-Tetrakis(methyl)phthalocyaninato manganese (2C): 1.01 g (7.0 mmol) of 4-methylphthalonitrile were reacted with 0.61 g (3.6 mmol) of $MnSO_4*H_2O$. The resulting green-black solid was purified by Soxhlet filtration in acetone. Yield: 0.79 g (72%). ^1H NMR (300.1 MHz, $CDCl_3$ (δ = 7.26)): δ = 7.9-8.2 (broad m, Ar-H), 0.9 (s, $-CH_3$); IR (KBr): ν = 3000 cm^{-1} (s), 2960 cm^{-1} (m), 1615 cm^{-1} (m), 1597 cm^{-1} (m), 1490 cm^{-1} (m), 1435 cm^{-1} (w), 1330 cm^{-1} (w), 1250 cm^{-1} (s), 1080 cm^{-1} (s), 980 cm^{-1} (s), 840 cm^{-1} (w), 800 cm^{-1} (m), 760 cm^{-1} (w), 690 cm^{-1} (m).

2(3),9(10),16(17),23(24)-Tetrakis(methyl)phthalocyaninato cobalt (2F): 1.50 g (10.6 mmol) of 4-methylphthalonitrile were reacted with 1.26 g (5.3 mmol) of $CoCl_2*6H_2O$. The resulting blue-green solid was purified by Soxhlet filtration in acetone. Yield: 0.43 g (26%). ^1H NMR (300.1 MHz, $CDCl_3$ (δ = 7.26)): δ = 7.7-7.9 (broad m, Ar-H), 0.9 (s, $-CH_3$); IR (KBr): ν = 3000 cm^{-1} (s), 2950 cm^{-1} (m), 1615 cm^{-1} (m), 1532 cm^{-1} (m), 1450 cm^{-1} (m), 1322 cm^{-1} (m), 1276 cm^{-1} (w), 1130 cm^{-1} (m), 1095 cm^{-1} (s), 930 cm^{-1} (w), 820 cm^{-1} (m), 740 cm^{-1} (m); UV/Vis spectrum (evaporated film on SiO_2): λ_{max} (ε) = 292 nm (0.64), 340 nm (0.62), 602 nm (0.35), 686 nm (0.25).

2(3),9(10),16(17),23(24)-Tetrakis(methyl)phthalocyaninato nickel (2G): 1.50 g (10.6 mmol) of 4-methylphthalonitrile were reacted with 1.34 g (5.6 mmol) of $NiCl_2*6H_2O$. The resulting blue-black solid was purified by Soxhlet filtration in acetone. Yield: 1.49 g (90%). ^{1}H NMR (300.1 MHz, $CDCl_3$ (δ = 7.26)): δ = 7.7 (dd, 2H, Ar-H), 7.5 (s, 1H, Ar-H), 0.9 (s, 3H, -CH_3); IR (KBr): ν = 3020 cm^{-1} (s), 2910 cm^{-1} (m), 1610 cm^{-1} (m), 1540 cm^{-1} (m), 1315 cm^{-1} (m), 1280 cm^{-1} (w), 1130 cm^{-1} (m), 1100 cm^{-1} (s), 942 cm^{-1} (w), 830 cm^{-1} (m), 710 cm^{-1} (m); UV/Vis spectrum (evaporated film on SiO_2): λ_{max} (ε) = 436 nm (2.07), 634 nm (1.45), 758 nm (1.75).

2(3),9(10),16(17),23(24)-Tetrakis(methyl)phthalocyaninato copper (2H): 1.50 g (10.6 mmol) of 4-methylphthalonitrile were reacted with 0.90 g (5.3 mmol) of $CuCl_2*2H_2O$. The resulting blue-black solid was purified by Soxhlet filtration in acetone. Yield: 1.02 g (61%). ^{1}H NMR (300.1 MHz, $CDCl_3$ (δ = 7.26)): δ = 7.7-7.9 (broad m, Ar-H), 0.9 (s, -CH_3); IR (KBr): ν = 3020 cm^{-1} (s), 2940 cm^{-1} (m), 1620 cm^{-1} (m), 1530 cm^{-1} (m), 1290 cm^{-1} (w), 1222 cm^{-1} (w), 1115 cm^{-1} (m), 1080 cm^{-1} (s), 960 cm^{-1} (w), 810 cm^{-1} (m), 750 cm^{-1} (m); UV/Vis spectrum (evaporated film on SiO_2): λ_{max} (ε) = 278 nm (1.06), 380 nm (1.31), 644 nm (0.75), 734 nm (0.91).

2.4.5 Synthesis of Metal Tetrakis(*t*-butyl)phthalocyanines (3A-H)

4-*t*-butylphthalonitrile (2.0 g, 10.9 mmol) was dissolved in 40 mL of anhydrous DMAE with the appropriate metal salt (5.4 mmol) and 0.5 mL of DBU. The solution was refluxed for 4-8 h under a dry Ar atmosphere. The product was

cooled and then precipitated in a 50:50 water/methanol solution, suction filtered, and washed several times with the 50:50 water/methanol solution. The resultant solid was then purified by Soxhlet filtration in an appropriate solvent, usually acetone. Yields ranged from 20% to 90%.

2(3),9(10),16(17),23(24)-Tetrakis(*t*-butyl)phthalocyaninato oxovanadium (3A): 1.82 g (9.9 mmol) of 4-*t*-butylphthalonitrile were reacted with 0.47 g (2.8 mmol) of V_2O_5. The resulting bright blue solid was purified by Soxhlet filtration in THF. Yield: 0.67 g (34%). ^{1}H NMR (300.1 MHz, $CDCl_3$ (δ = 7.26)): δ = 7.8-8.1 (broad m, Ar-H), 0.9 (s, -CH_3); IR (KBr):): ν = 3010 cm^{-1} (s), 2960 cm^{-1} (s), 1610 cm^{-1} (m), 1530 cm^{-1} (s), 1470 cm^{-1} (w), 1350 cm^{-1} (s), 1270 cm^{-1} (s), 1140 cm^{-1} (m), 1060 cm^{-1} (s), 930 cm^{-1} (w), 900 cm^{-1} (s), 830 cm^{-1} (m), 790 cm^{-1} (s), 735 cm^{-1} (s).

2(3),9(10),16(17),23(24)-Tetrakis(*t*-butyl)phthalocyaninato oxotitanium (3B): 1.22 g (6.6 mmol) of 4-*t*-butylphthalonitrile were reacted with 1 mL (3.3 mmol) of Ti(*i*-PrO)$_4$. The resulting deep blue solid was purified by Soxhlet filtration in THF. Yield: 0.24 g (18%). ^{1}H NMR (300.1 MHz, $CDCl_3$ (δ = 7.26)): δ = 7.7 (dd, 2H, Ar-H), 7.5 (s, 1H, Ar-H), 1.0 (s, 3H, -CH_3); IR (KBr): ν = 3000 cm^{-1} (s), 2930 cm^{-1} (m), 1610 cm^{-1} (m), 1530 cm^{-1} (m), 1470 cm^{-1} (w), 1430 cm^{-1} (m), 1310 cm^{-1} (s), 1250 cm^{-1} (m), 1170 cm^{-1} (m), 1090 cm^{-1} (s), 970 cm^{-1} (m), 800 cm^{-1} (w), 740 cm^{-1} (s), 730 cm^{-1} (s).

2(3),9(10),16(17),23(24)-Tetrakis(*t*-butyl)phthalocyaninato manganese (3C): 0.89 g (4.8 mmol) of 4-*t*-butylphthalonitrile were reacted with 0.43 g (2.5 mmol) of $MnSO_4*H_2O$. The resulting blue solid was purified by Soxhlet filtration in CH_2Cl_2. Yield: 0.36 g (38%). ^{1}H NMR (300.1 MHz, $CDCl_3$ (δ = 7.26)): δ = 7.8-8.3 (broad m, Ar-H), 1.0 (s, -CH_3); IR (KBr): ν = 3010 cm^{-1} (s), 2940 cm^{-1} (m), 1600 cm^{-1} (m), 1580 cm^{-1} (m), 1490 cm^{-1} (m), 1440 cm^{-1} (w), 1310 cm^{-1} (w), 1240 cm^{-1} (s), 1080 cm^{-1} (s), 980 cm^{-1} (s), 830 cm^{-1} (w), 790 cm^{-1} (m), 760 cm^{-1} (w), 710 cm^{-1} (m).

2(3),9(10),16(17),23(24)-Tetrakis(*t*-butyl)phthalocyaninato iron (3E): 2.0 g (10.9 mmol) of 4-*t*-butylphthalonitrile were reacted with 1.53 g (5.5 mmol) of $FeSO_4*7H_2O$. The resulting blue-black solid was purified by Soxhlet filtration in acetone. Yield: 0.76 g (35%). ^{1}H NMR (300.1 MHz, $CDCl_3$ (δ = 7.26)): δ = 7.7-8.1 (broad m, Ar-H), 1.1 (s, -CH_3); IR (KBr): ν = 2950 cm^{-1} (m), 1610 cm^{-1} (m), 1532 cm^{-1} (m), 1502 cm^{-1} (m), 1478 cm^{-1} (m), 1333 cm^{-1} (s), 1286 cm^{-1} (m), 1095 cm^{-1} (s), 930 cm^{-1} (w), 820 cm^{-1} (m), 740 cm^{-1} (m); UV/Vis (evaporated film on SiO_2): λ_{max} (ε) = 298 nm (1.30), 344 nm (1.32), 566 nm (0.52), 644 nm (0.71).

2(3),9(10),16(17),23(24)-Tetrakis(*t*-butyl)phthalocyaninato cobalt (3F): 4.96 g (26.8 mmol) of 4-*t*-butyl-phthalonitrile were reacted with 3.23 g (13.5 mmol) of $CoCl_2*6H_2O$. The resulting blue solid was purified by Soxhlet filtration in CH_2Cl_2. Yield: 3.66 g (69%). ^{1}H NMR (300.1 MHz, $CDCl_3$ (δ = 7.26)): δ = 7.7-8.1 (broad m, Ar-H), 1.0 (s, -CH_3); IR (KBr): ν = 2970 cm^{-1} (m), 1615 cm^{-1} (m), 1532 cm^{-1} (m),

1450 cm^{-1} (m), 1322 cm^{-1} (m), 1280 cm^{-1} (m), 1163 cm^{-1} (w), 1119 cm^{-1} (s), 1090 cm^{-1} (s), 926 cm^{-1} (w), 775 cm^{-1} (m), 750 cm^{-1} (m), 723 cm^{-1} (s); UV/Vis spectrum (evaporated film on SiO_2): λ_{max} (ε) = 294 nm (0.85), 330 nm (0.93), 620 nm (0.56), 680 nm (0.46).

2(3),9(10),16(17),23(24)-Tetrakis(*t*-butyl)phthalocyaninato nickel (3G): 1.50 g (8.1 mmol) of 4-*t*-butyl-phthalonitrile were reacted with 1.08 g (4.6 mmol) of $NiCl_2*6H_2O$. The resulting blue solid was purified by Soxhlet filtration in CH_2Cl_2. Yield: 1.43 g (89%). ^{1}H NMR (300.1 MHz, $CDCl_3$ (δ = 7.26)): δ = 7.7 (dd, 2H, Ar-H), 7.5 (s, 1H, Ar-H), 1.1 (s, 9H, -CH_3); IR (KBr): ν = 3010 cm^{-1} (s), 2910 cm^{-1} (m), 1640 cm^{-1} (m), 1560 cm^{-1} (m), 1325 cm^{-1} (s), 1150 cm^{-1} (m), 1080 cm^{-1} (s), 942 cm^{-1} (m), 710 cm^{-1} (m); UV/Vis spectrum (evaporated film on SiO_2): λ_{max} (ε) = 436 nm (2.28), 626 nm (1.66), 768 nm (1.96).

2(3),9(10),16(17),23(24)-Tetrakis(*t*-butyl)phthalocyaninato copper (3H): 1.00 g (10.6 mmol) of 4-*t*-butyl-phthalonitrile were reacted with 0.90 g (5.3 mmol) of $CuCl_2*2H_2O$. The resulting blue-black solid was purified by Soxhlet filtration in acetone. Yield: 1.02 g (61%). ^{1}H NMR (300.1 MHz, $CDCl_3$ (δ = 7.26)): δ = 7.7-7.9 (broad m, Ar-H), 0.9 (s, -CH_3); IR (KBr): ν = 3020 cm^{-1} (s), 2940 cm^{-1} (m), 1620 cm^{-1} (m), 1530 cm^{-1} (m), 1290 cm^{-1} (w), 1222 cm^{-1} (w), 1115 cm^{-1} (m), 1080 cm^{-1} (s), 960 cm^{-1} (w), 810 cm^{-1} (m), 750 cm^{-1} (m); UV/Vis spectrum (evaporated film on SiO_2): λ_{max} (ε) = 288 nm (1.27), 360 nm (1.52), 632 nm (0.96), 744 nm (1.12).

2.4.6 Synthesis of 4-(1,1,1,3,3,3-Hexafluoropropan-2-ol)-2-Bromoaniline (4): 1.8 mL (15.9 mmol) of 2-bromoaniline and 200 mg p-toluenesulfonic acid were combined in a round-bottom flask under an inert Ar atmosphere. 2.0 mL (17.5 mmol) of hexafluoroacetone sesquihydrate (HFA*1.5H_2O) were added, and the mixture was refluxed at 100 ^oC for 24 h. Product was isolated from the red solution by extraction into diethyl ether, and washed 3x with water; product was recrystallized by slow evaporation of the ether to form pale red crystals. These crystals were further purified by column chromatography using toluene as the solvent. Product was isolated from the toluene by rotary evaporation of solvent and collected by sublimation onto a cold finger, affording white crystals. Yield: 1.26 g (24%). MP: 132 ^oC; ^1H NMR (300.1 MHz, $CDCl_3$ (δ = 7.26)): δ = 7.8 (s, 1H, Ar-H), 7.4 (d, 1H, Ar-H), 6.8 (d, 1H, Ar-H), 4.2 (broad s, -NH_2), 3.3 (broad s, 1H, -OH); IR (KBr): ν = 3390 cm^{-1} (s), 3320 cm^{-1} (s), 3130 cm^{-1} (s), 2830 cm^{-1} (m), 2690 cm^{-1} (w), 2400 cm^{-1} (w), 1620 cm^{-1} (m), 1570 cm^{-1} (w), 1510 cm^{-1} (s), 1450 cm^{-1} (w), 1270 cm^{-1} (s), 1150 cm^{-1} (s), 962 cm^{-1} (s), 880 cm^{-1} (s), 830 cm^{-1} (s), 730 cm^{-1} (w), 685 cm^{-1} (s), 640 cm^{-1} (m); GC-MS *m/z* (% relative intensity, ion): 337 (48%, M^+), 268 (100%, M^+ - CF_3), 198 (95%, M^+ - 2CF_3), 189 (35%, M^+ - CF_3, Br), 171 (30%, M^+ - $CF_3C(OH)CF_3$).

2.4.7 Synthesis of 4-(1,1,1,3,3,3-Hexafluoropropan-2-ol)-2-Bromocyanobenzene (5): Conversion of the amine of **4** to the nitrile was done using literature procedures for the Sandmeyer reaction.[42] 1.89 g (5.6 mmol) of **4** was dissolved in 20 mL of a 19%

HCl solution and cooled to 0 ^{o}C in an ice bath. 0.41 g (6.0 mmol) of $NaNO_2$ was dissolved in 10 mL of water and added dropwise to the acid solution to form the diazonium salt of **4**. Keeping the solution cold, the remaining HCl was slowly neutralized with $NaHCO_3$. After neutralization the diazonium solution was added dropwise to a 40 mL solution of 0.55 g (6.1 mmol) CuCN and 0.39 g (5.9 mmol) KCN in water held at 60 ^{o}C. The resulting brown solution and precipitate were stirred for a further 1.5 h. Product was isolated by extraction into CH_2Cl_2, affording a red-brown solid. Yield: 1.50 g (77%). MP: 120 ^{o}C; ^{1}H NMR (300.1 MHz, $CDCl_3$ (δ = 7.26)): δ = 8.1 (s, 1H, Ar-H), 7.8 (m, 2H, Ar-H), 3.7 (s, 1H, -OH); IR (KBr): ν = 3300 cm^{-1} (s), 2970 cm^{-1} (w), 2930 cm^{-1} (w), 2250 cm^{-1} (m), 1600 cm^{-1} (w), 1490 cm^{-1} (w), 1410 cm^{-1} (w), 1270 cm^{-1} (s), 1220 cm^{-1} (s), 1180 cm^{-1} (m), 1050 cm^{-1} (w), 976 cm^{-1} (s), 949 cm^{-1} (s), 895 cm^{-1} (m), 837 cm^{-1} (s), 806 cm^{-1} (s), 733 cm^{-1} (m); GC-MS *m*/*z* (% relative intensity, ion): 347 (40%, M^+), 278 (90%, M^+ - CF_3), 210 (95% M^+ - 2CF_3), 180 (40%, M^+ - $CF_3C(OH)CF_3$).

2.4.8 Synthesis of 4-(1,1,1,3,3,3-Hexafluoropropan-2-ol)-Phthalonitrile (6):

Conversion of the bromine of **5** to the nitrile was done using literature procedures for the Rosenmund von Braun reaction.[44] 0.49 g (1.4 mmol) of **5** were dissolved in 20 mL DMF with 0.29 g (3.2 mmol) of CuCN; the dark red solution was refluxed for 17 h. The product was isolated by addition of CH_2Cl_2 and washing with water, followed by rotary evaporation. DMF was removed by evaporation on a Kugelrohr apparatus, yielding an oily red solid. Yield: 0.11 g (27%). ^{1}H NMR (300.1 MHz, $CDCl_3$ (δ =

7.26)): δ = 8.3 (s, 1H, Ar-H), 7.95 (d, 1H, Ar-H), 7.85 (d, 1H, Ar-H); 2.8 (s, 1H, -OH); IR (KBr): ν = 3290 cm^{-1} (s), 2940 cm^{-1} (w), 2250 cm^{-1} (s), 1630 cm^{-1} (w), 1600 cm^{-1} (s), 1490 cm^{-1} (m), 1400 cm^{-1} (s), 1270 cm^{-1} (s), 1220 cm^{-1} (s), 1180 cm^{-1} (s), 1050 cm^{-1} (m), 976 cm^{-1} (s), 949 cm^{-1} (s), 895 cm^{-1} (m), 837 cm^{-1} (s), 733 cm^{-1} (s); GC-MS *m*/*z* (% relative intensity, ion): 295 (11% M + 1), 269 (7% M^+ -CN), 226 (98% M + 1 - CF_3).

2.4.9 Synthesis of 2(3),9(10),16(17),23(24)-Tetrakis(1,1,1,3,3,3-Hexafluoropropan-2-ol)phthalocyaninato Copper (7): 0.99 g (2.9 mmol) of **5** and 0.31 g (3.5 mmol) of CuCN were dissolved in 20 mL DMF. The solution was refluxed vigorously for 19 h. DMF was removed from the resultant deep blue solution by evaporation on a Kugelrohr apparatus. The product was dissolved in 30% methanol solution, and slowly acidified; a dark blue-purple solid precipitated out of solution at pH ~ 4. Yield: 0.89 g (66%). ^{1}H NMR (400.1 MHz, Acetone-d_6 (δ = 2.09)): δ = 7.5-8.5 (broad m, Ar-H), 2.8 (s, -OH); IR (KBr): ν = 3350 cm^{-1} (s), 3230 cm^{-1} (s), 2250 cm^{-1} (w), 1710 cm^{-1} (s), 1640 cm^{-1} (s), 1560 cm^{-1} (m), 1450 cm^{-1} (w), 1370 cm^{-1} (w), 1270 cm^{-1} (s), 1220 cm^{-1} (s), 1150 cm^{-1} (m), 968 cm^{-1} (s), 903 cm^{-1} (w), 837 cm^{-1} (w), 725 cm^{-1} (m); UV/Vis spectrum (evaporated film on SiO_2): λ_{max} (ε) = 210 nm (1.62), 344 nm (1.79), 370 nm (1.78), 388 nm (1.84), 600 nm (0.33), 636 nm (0.33), 666 nm (1.22); LC-MS *m*/*z* (% relative intensity, ion): 1239 (10%, M^+ - H), 1169 (100%, M^+ - CF_3), 1099 (9% M^+ - $2CF_3$).

2.5 ACKNOWLEDGEMENT

The author would like to thank Dr. Karla Miller and Dr. Amos Sharoni for insights and assistance with the work presented above.

2.6 REFERENCES

(1) Gilmartin, M. A. T.; Ewen, R. J.; Hart, J. P.; Honeybourne, C. L. *Electroanalysis* **1995**, *7*, 547-555.

(2) Uchida, S.; Xue, J.; Rand, B. P.; Forrest, S. R. *Appl. Phys. Lett.* **2004**, *84*, 4218-4220.

(3) Eley, D. *Nature* **1948**, *162,* 819.

(4) Wright, J. D. *Prog. Surf. Sci.* **1989**, *31,* 1-60.

(5) Guillaud, G.; Simon, J.; Germain, J. *Coord. Chem. Rev.* **1998**, *178,* 1433-1484.

(6) Snow, A. W.; Barger, W. R. Phthalocyanine Films in Chemical Sensors. *Phthalocyanines: Properties and Applications;* Lever, A. B. P., Ed.; John Wiley and Sons: New York, 1989; Vol. 1, p. 341.

(7) Tomoda, H.; Saito, S.; Ogawa, S.; Shiraishi, S. *Chem. Lett.* **1980**, *9*, 1277-1280.

(8) Hanack, M.; Lang, M. *Adv. Mater.* **1994**, *6*, 819-833.

(9) Brach, P. J.; Grammatica, S. J.; Ossanna, O. A.; Weinberger, L. *J. Heterocycl. Chem.* **1970**, *7*, 1403-1405.

(10) Davies, D. A.; Schnik, C.; Silver, J.; Sosa-Sanchez, J. L.; Riby, P. G. *J. Porphyrins Phthalocyanines* **2001**, *5*, 376-380.

(11) Gantchev, T. G.; Sharman, W. M.; Lier, J. E. *Photochem. Photobiol.* **2003**, *77*, 469-479.

(12) Korzhenevskii, A. B.; Shikova, T. G.; Bykova, V. V.; Koifman, O. I. *Russ. J. Gen. Chem.* **2002**, *72*, 1123-1127.

(13) Gould, R. D. *Coord. Chem. Rev.* **1996**, *156,* 237-274.

(14) Loi, M. A.; Denk, P.; Hoppe, H.; Neugebauer, H.; Winder, C.; Meissner, D.; Brabec, C.; Sariciftci, N. S.; Gouloumis, A.; Vazquez, P.; Torres, T. *J. Mater. Chem.* **2003**, *13*, 700-704.

(15) Tsuzuki, T.; Shirota, Y.; Rostalski, J.; Meissner, D. *Sol. Energy Mater. Sol. Cells* **2000**, *61*, 1-8.

(16) Zhang, Q.; Wang, D.; Xu, J.; Cao, J.; Sun, J.; Wang, M. *Mater. Chem. Phys.* **2003**, *82*, 525-528.

(17) Ishikawa, N.; Iino, T.; Kaizu, Y. *J. Am. Chem. Soc.* **2002**, *124*, 11440-11447.

(18) Ishikawa, N.; Sugita, M.; Ishikawa, T.; Koshihara, S.; Kaizu, Y. *J. Phys. Chem. B* **2004**, *108*, 11265-11271.

(19) Collins, G. C. S. *J. Electroanal. Chem.* **1982**, *139*, 335-369.

(20) Ho, Z. Z.; Peyghambarian, N. *Chem. Phys. Lett.* **1988**, *148*, 107-111.

(21) Lowbry, M. K.; Starshak, A. J.; Esposito, J. N.; Krueger, P. C.; Kenney, M. E. *Inorg. Chem.* **1965**, *4*, 128.

(22) Kobayashi, N.; Furuya, F.; Yug, G. C.; Wakita, H.; Yokomizo, M.; Ishikawa, N. *Chem. Eur. J.* **2002**, *8*, 1474-1484.

(23) Gorlach, B.; Dachtler, M.; Glaser, T.; Albert, K.; Hanack, M. *Chem. Eur. J.* **2001**, *7*, 2459-2465.

(24) Lux, A.; Rozenberg, G. G.; Petritsch, K.; Moratti, S. C.; Holmes, A. B.; Friend, R. H. *Synth. Met.* **1999**, *102*, 1527-1528.

(25) Eberhardt, W.; Hanack, M. *Synthesis* **1997**, 95-100.

(26) Snow, A. W.; Sprague, L. G.; Soulen, R. L.; Grate, J. W.; Wohltjen, H. *J. Appl. Polym. Sci.* **1991**, *43*, 1659-1671.

(27) Wohltjen, H.; Snow, A. W.; Barger, W. R.; Ballantine, D. S. *IEEE Trans. Ultrason. Ferroelectr. Freq. Control* 1987, *34*, 172-178.

(28) Grate, J. W.; Patrash, S. J.; Kaganove, S. N.; Wise, B. M. *Anal. Chem.* **1999**, *71*, 1033-1040.

(29) Farah, B. S.; Gilbert, E. E.; Sibilia, J. P. *J. Org. Chem.* **1965**, *30*, 998-1001.

(30) Tong, W. Y.; Djurisic, A. B.; Xie, M. H.; Ng, A. C. M.; Cheung, K. Y.; Chan, W. K.; Leung, Y. H.; Lin, H. W.; Gwo, S. *J. Phys. Chem. B* **2006**, *110*, 17406-17413.

(31) Miller, C. W.; Sharoni, A.; Liu, G.; Colesniuc, C. N.; Fruhberger, B.; Schuller, I. K. *Phys. Rev. B* **2005**, *72*, 104113/1-6.

(32) Hassan, B. H.; Li, H.; McKeown, N. B. *J. Mater. Chem.* **2000**, *10*, 39-45.

(33) Cook, M. J. *J. Mater. Chem.* **1996**, *6*, 677-689.

(34) Cook, M. J. *Pure Appl. Chem.* **1999**, *71*, 2145-2151.

(35) Tsuzuki, T.; Hirota, N.; Noma, N.; Shirota, Y. *Thin Solid Films* **1996**, *273*, 177-180.

(36) Assour, J. M.; Goldmacher, J.; Harrison, S. E. *J. Chem. Phys.* **1965**, *43*, 159-165.

(37) Canham, G. W. R.; Lever, A. B. P. *Inorg. Nucl. Chem. Lett.* **1973**, *9*, 513-517.

(38) Brown, R. J. C.; Kucernak, A. R.; Long, N. J.; Mongay-Batalla, C. *New J. Chem.* **2004**, *28*, 676-680.

(39) Chen, W. H.; Rieckhoff, K. E.; Voigt, E. M. *Chem. Phys.* **1986**, *102*, 193-203.

(40) Gilbert, E. E.; Jones, E. S.; Sibilia, J. P. *J. Org. Chem.* **1965**, *30*, 1001-1003.

(41) Masciadri, R.; Kamer, M.; Nock, N. *Eur. J. Org. Chem.* **2003**, 4286-4291.

(42) Vogel, A. *Textbook of Practical Organic Chemistry* 4th Ed. Furniss, B. S., Hannaford, A. J., Rogers, V., Smith, P. W. G., Tatchell, A. R., Eds.; John Wiley and Sons: New York, 1978; pp. 698-703.

(43) Misko, T. P.; Schilling, R. J.; Salvemini, D.; Moore, W. M.; Currie, M. G. *Anal. Biochem.* **1993**, *214*, 11-16.

(44) Friedman L.; Shechter, H. *J. Org. Chem.* **1961**, *26*, 2522-2524.

(45) Forrest, S. R. *Chem. Rev.* **1997**, *97*, 1793-1896.

(46) Leeder, S. M.; Gagne, M. R. *J. Am. Chem. Soc.* **2003**, *125*, 9048-9054.

(47) Hoang, K. C.; Mecozzi, S. *Langmuir* **2004**, *20*, 7347-7350.

(48) Qiu, W.; Hu, W.; Liu, Y.; Zhou, S.: Xu, Y.; Zhu, D. *Sens. Actuators, B* **2001**, *75*, 62-66.

(49) Wang, B.; Zuo, X.; Wu, Y.; Chen. Z.; Li, Z. *Mater. Lett.* **2005**, *59*, 3073-3077.

CHAPTER III

GAS SENSING MECHANISMS IN CHEMIRESISTIVE COBALT AND METAL-FREE PHTHALOCYANINE THIN FILMS

3.1 ABSTRACT

The gas sensing behaviors of cobalt phthalocyanine (CoPc) and metal-free phthalocyanine (H_2Pc) thin films were investigated with respect to analyte basicity. Chemiresistive sensors were fabricated by deposition of 50 nm thick films on interdigitated gold electrodes via organic molecular beam epitaxy (OMBE). Time-dependent current responses of the films were measured at constant voltage during exposure to analyte vapor doses. The analytes spanned a range of electron donor and hydrogen bonding strengths. It was found that, when the analyte exceeded a critical base strength, the device responses for CoPc correlated with Lewis basicity, and device responses for H_2Pc correlated with hydrogen-bond basicity. This suggests that the analyte-phthalocyanine interaction is dominated by binding to the central cavity of the phthalocyanine, with analyte coordination strength governing CoPc sensor responses and analyte hydrogen bonding ability governing H_2Pc sensor responses. The interactions between the phthalocyanine films and analytes were found to follow first order kinetics. The influence of O_2 on the film response was found to significantly affect sensor response and recovery. The increase of resistance generally observed for analyte binding can be attributed to hole destruction in the semiconductor film by oxygen displacement, as well as hole trapping by electron donor ligands.

3.2 INTRODUCTION

Phthalocyanines (Pcs), both metalated (MPcs) and metal-free (H_2Pc), are organic semiconductors that have been identified as promising candidates for gas sensors.[1,6-7] They are chemically sensitive to reactive gases and show potential for chemical selectivity via manipulation of the metal center and substitution of functional groups on the organic ring.[1-5] Conductivity in Pc films is influenced strongly by atmospheric "dopants," primarily O_2.[8] It has been reported that Pcs are insulating in a dark high vacuum environment.[9] However, when Pc thin films are exposed to O_2, the films become doped and the conductivity increases dramatically.

This air-induced conductivity has been attributed to different mechanisms. For polycrystalline films it is assumed that O_2 absorbs only at the air/MPc interface and at grain boundaries because the MPc crystal structure is very tight and unaffected by exposure to air.[2-4] It has been reported that the formation of charge transfer complexes by coordination of O_2 to MPc metal centers at the air/phthalocyanine interface leads to the formation of oxidized MPc^+ and O_2^- species and injection of hole charge carriers into the bulk solid.[8,10-11] The presence of the superoxide adduct of CoPc has been detected in several electron paramagnetic resonance (EPR) studies.[12-13] There is also evidence that weaker O_2 adsorption may occur on the four *meso*-nitrogens of free base H_2Pc, leading to conductivity increases that are not as large as those for the MPcs.[2-4] As a surface dopant, O_2 occupies only a fraction of the binding sites on the film;[8] therefore interactions with analyte vapors in air could result in two different mechanisms of analyte binding (Scheme 3-1). Analytes could either bind to open

surface metal coordination sites, or could compete with O_2 for occupied metal surface sites. There is the additional possibility of weak binding (physisorption) to the organic region of the Pc molecule for noncoordinating analytes, which may be governed by weak hydrophobic and possibly charge transfer interactions.

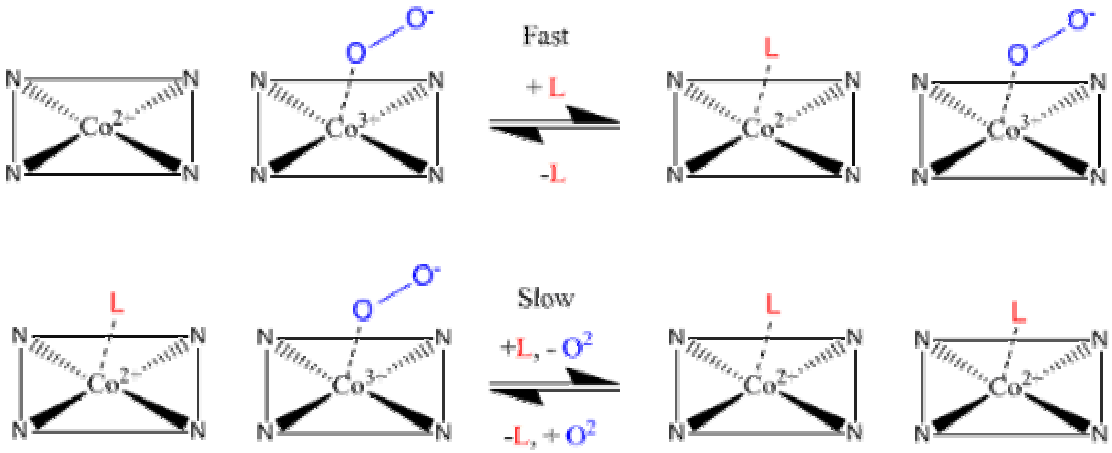

Scheme 3-1 Chemisorption model of CoPc interaction with oxygen and coordinating analytes L. For noncoordinating analytes, rapid reversible adsorption on the Pc rings is attributed to the weak sensor responses observed.

Previous mechanistic studies of solid state gas sensors have been studied in the context of both conduction mechanisms and molecular interactions. The responses of metal oxide gas sensors, primarily SnO_2, have been widely explored with respect to surface adsorption, chemical reaction, and resulting conductivity changes.[14-15] These sensors are operated at elevated temperatures (100-500 ^{o}C) and reactive oxygen species (O_2^-, O^-, and O^{2-}) are present at the surface of the SnO_2 grains.[16] These oxygen species engage in redox reactions with analytes such as water, carbon monoxide, and methane. The subsequent changes in grain surface charge alters the film conductivity, which has been rationalized using a band-bending model.[17]

Organic thin film sensors rely on weak intermolecular interactions rather than redox chemistry. Organic coatings encompass a wide variety of structures, including molecular crystals, liquid crystals, molecular cages, nanotubes, and polymers.[18] A variety of detection methods have been applied to organic sensors: these include spectroscopic detection,[19-20] surface acoustic wave (SAW) technology,[21] and chemiresistive devices.[22] Linear solvation energy relationships (LSER) have been used to understand analyte interactions in thin film polymer sensors; this model incorporates such molecular properties as dispersion (van der Waals forces and π stacking), polarizability, dipolarity, and hydrogen bond basicity and acidity.[23-24] These intermolecular interactions have been probed directly via FT-IR spectroscopy.[25] Resistive sensing studies with p-type Pc thin films have focused primarily on their interaction with oxidizing gases, such as ozone and NO_X.[26-30] Pc films are easily oxidized by NO_X, forming charge transfer complexes, which inject holes and increase film currents. The interaction of Pcs with reducing gases, such as NH_3, has the opposite effect. Decreased current upon analyte binding to these films has been attributed to electron donation from the reducing gas to trap charge carriers.[31] Attempts have been made to relate MPc sensing to band theory.[32-34] However, the magnitude of sensor response has not been quantitatively correlated with molecular properties of the analyte.

One postulate is that metal-analyte coordination strength should primarily govern analyte binding and therefore the response of CoPc chemiresistive sensors to non-oxidizing gases. Similarly, for H_2Pc chemiresistive sensors, the hydrogen

bonding of analyte to the two interior NH protons should primarily govern sensor responses. In order to test whether the anticipated molecular interactions between analytes and surface Pc molecules dominated the sensor response, we measured the CoPc and H_2Pc sensor responses to analytes with a wide range of established Lewis basicities and hydrogen-bond acceptor abilities.

Much research has been devoted to developing empirical scales of electron donation and basicity in molecules. Kamlet and Taft established the pK_{HB} scale of hydrogen bond basicity using log K values ($dm^3 \cdot mol^{-1}$) of complexation of bases with 4-fluorophenol in CCl_4.[35-36] This scale has been expanded using a variety of reference acids to create the extensive β_2^H scale of hydrogen bond basicities used in the present study.[37] Gutmann quantified Lewis basicities of aprotic electron donors as the molecular donor number (DN).[38-39] The donor number is defined as the enthalpy ($kcal \cdot mol^{-1}$) of formation of a 1:1 adduct of a Lewis base to the Lewis acid $SbCl_5$. Unfortunately there are several notable inaccuracies in this scale.[40] Maria and Gal improved on the DN concept by establishing the $-\Delta H^o_{BF_3}$ scale, a rigorous, calorimetrically determined enthalpy scale ($kJ \cdot mol^{-1}$) of adducts with the Lewis acid BF_3.[41] This was used in the present study as an experimental measure of electron pair donor ability, with the possible shortcoming that the softer Lewis acid character of cobalt(II) as compared to boron(III) would require using donor ligands of similar hard/soft character.[42]

3.3 EXPERIMENTAL

3.3.1 Electrode Fabrication

Interdigitated electrodes (IDEs) were prepared by standard photolithography and lift-off processing on thermally grown SiO_2 (thickness of 1 μm) on (100) Si substrates. The electrodes consist of 45 pairs of gold fingers, spaced 5 μm apart, with an electrode width of 2 mm. The electrodes were deposited by electron beam evaporation. An adhesion layer of 5 nm Ti was applied first, followed by 45 nm of Au for a total electrode thickness of 50 nm. Six pairs of electrodes were grown on each substrate to verify sensor reproducibility and increase yield.

3.3.2 Thin Film Deposition

CoPc (Aldrich, 97%) and H_2Pc (Aldrich, 98%) were purified via multiple zone sublimations at 400 ^oC and 10^{-5} torr. Films of a thickness of 50 nm were deposited on six IDEs per substrate by organic molecular beam epitaxy (OMBE) in a UHV chamber with a base pressure of $2x10^{-10}$ Torr. The deposition rate of the Pc films ranged from 0.2 to 0.5 Å s^{-1}, and the deposition pressure was $5x10^{-9}$ Torr. Film growth rate and thickness were monitored with a quartz crystal microbalance (QCM). The IDEs were mounted on a temperature-controlled stage monitored with two thermocouples. Substrate temperature during deposition was held constant at 25.0 ± 1.0 ^oC. After deposition, the devices were stored under vacuum at 10 mTorr or less until use. The thickness of the films was confirmed by low angle XRD measurements performed on a Rigaku RU-200B diffractometer using Cu K_α radiation.[43]

3.3.3 Device Measurements

Chemical responses of CoPc and H_2Pc IDE sensors were measured inside a test chamber of stainless steel coated with a passivating layer of SiO_2. The internal volume of the chamber was 15 cm^3. The IDEs were placed in ceramic chip mounts purchased from Spectrum Semiconductor Technologies L.L.C. Gold leads were wirebonded from the IDEs to the mounts. Two sensor arrays could be placed in the chamber at a time, for simultaneous mounting of six CoPc and six H_2Pc IDE devices. Contacts were made to the chip mounts via electrical feedthroughs in the top of the test chamber. The internal temperature of the chamber was monitored by a thermocouple and maintained at 50.0 ± 0.1 ^oC by coolant lines connected to a Haake F8 constant temperature bath. A Keithley 6517/6521 multi-channel electrometer was used both as voltage source and ammeter, enabling ten sensors to be tested simultaneously. The devices were placed in the chamber in the absence of light for 24 h before being tested to ensure the decay of residual photoconductivity. Analyte vapors were introduced into the sensor chamber by a system of bubblers and mass flow controllers. Zero grade air (< 0.1 ppm of NO_X and SO_X and < 5 ppm H_2O) and ultra high purity (UHP) nitrogen were used as carrier gases. A constant flow rate of 500 sccm (standard cm^3 per minute) was applied during the dosing/purging cycle. Analytes were introduced into the flow by bubblers immersed in a Haake F8 constant temperature bath. Mass flow controllers (MKS Instruments, Inc. 1479A, 10 sccm and 1000 sccm) were used in conjunction with the bubblers and a four-way valve to

saturate the carrier gas with a known concentration of analyte before introduction into the sensor chamber. Solenoid valves were placed before and after each bubbler to prevent cross contamination of analytes. A Labview VI program was used to control all instruments and record data.

Analytes were chosen to span both β_2^H and $-\Delta H^o_{BF_3}$ scales, including dichloromethane, nitromethane, acetonitrile, 2-butanone, di-*n*-butyl ether, trimethyl phosphate, water, isophorone, dimethyl methylphosphonate (DMMP, a neurotoxin simulant),[44] dimethyl sulfoxide (DMSO), N,N-dimethylformamide (DMF), and triethylamine, in order of increasing $-\Delta H^o_{BF_3}$ values. All analytes were of analytical purity (99.5+%) and dried over 4Å molecular sieves (Fisher). All analytes were purchased from Aldrich except isophorone (Acros) and DMMP (Strem). Table 3-1 lists analytes and their β_2^H and $-\Delta H^o_{BF_3}$ values. Analyte doses were delivered as saturated vapors at specific flow rates and then diluted to 500 sccm. The ratio of vapor from the bubbler to dilution gas was controlled with mass flow controllers. Vapor pressure data[45] were used with the Clausius-Clapeyron equation to calculate the concentration of each dose in parts per million (ppm). Dichloromethane, nitromethane, acetonitrile and 2-butanone were dosed at 225, 450, 675, and 900 ppm. Di-*n*-butyl ether, trimethyl phosphate, water, isophorone, DMMP, DMSO, DMF, and triethylamine were dosed at 90, 135, 180 and 225 ppm. Before dosing, the devices were annealed at 70 ^oC in order to drive off any adsorbed molecules and achieve a stable baseline current.

Table 3-1 Lewis basicities ($-\Delta H^{o}_{BF_3}$)[39] and hydrogen bond basicities (β_2^H)[35] for analytes studied.

Analyte	$-\Delta H^{o}_{BF_3}$ **(kJ·mol^{-1})**	β_2^H
Dichloromethane	10.0	0.05
Nitromethane	37.63	0.25
Acetonitrile	60.39	0.31
2-butanone	76.07	0.48
Di-*n*-butyl ether	78.57	0.46
Trimethyl phosphate	84.79	0.76
Water	--	0.38
Isophorone	90.56	0.52
DMMP[a]	--	0.81
DMSO	105.34	0.78
DMF	110.49	0.66
Triethylamine	135.87	0.67

[a] The β_2^H value for DMMP was estimated from experimental values for dimethyl ethylphosphonate and diethyl methylphosphonate.

3.4 RESULTS AND DISCUSSION

3.4.1 Film Characterization

Surface morphology was measured by atomic force microscopy (AFM) using a Nanoscope IV Scanning Microscope in tapping mode and a Veeco 200 kHz probe. The films had a granular structure with ellipsoidal grains of approximately 50 nm diameter on the long axis and an RMS roughness of 5 nm. XRD revealed the films deposited at 25 ^{o}C to be textured α phase.[43] I-V measurements were recorded in the test chamber at 5 degree increments in a range from 5 to 50 ^{o}C. Voltage was stepped from 10 V to -10 V in 0.1 V increments. The devices were allowed to equilibrate at each temperature and voltage. All devices reported had good ohmic behavior at low voltages. Space charge limited conductivity (SCLC) was found to occur, in general, above 5 V. Miller and coworkers showed that operation of MPc IDEs in the SCLC regime removes influence of the electrode/MPc interface on the chemical sensing.[46] Device responses were measured at 8 V, which is well within the SCLC regime. At 8 V the CoPc devices had a base current on the order of 1 μA, while the H_2Pc devices had a base current of approximately 1 nA.

Figure 3-1 shows the CoPc sensor response to a 40 min dose of DMMP (78 ppm) using zero grade air as the carrier gas. In many studies, 40 min is sufficient time at room temperature to reach the saturation region of the sensor response.[9,11,28,47-49] This figure illustrates that there are two temporal components to sensor response and recovery. There is an initial fast region, which accounts for the largest change in the sensor current (A, C), followed by a slower saturation region (B, D). The fast

response (A) is approximately equivalent to the fast recovery (C), while the slow saturation response (B) is approximately equivalent to the slow recovery (D).

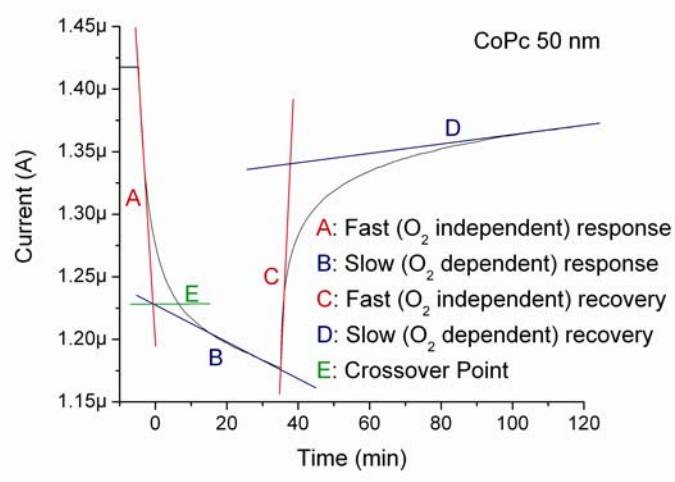

Figure 3-1 A 40 min DMMP pulse in air with both fast (oxygen independent) and slow (oxygen dependent) portions labeled. The crossover point is determined as the point where the response shifts from fast to slow, which occurs at ~5 min.

A mechanism involving O_2 binding to weak and strong sites has been previously suggested for NiPc sensors exposed to NO.[11] Our model assigns the fast portion of the response to binding of analyte at oxygen-free sites and the slow portion to competitive displacement of oxygen-bound sites (Scheme 3-1). This is supported by the vapor phase O_2 dependence of the sensor responses (*vide infra*). At room temperature, the crossover point between the oxygen independent (fast) and oxygen dependent (slow) sensor response occurs near 5 min (E). In order to reduce recovery times, the oxygen independent response was examined by using 5 min doses at a temperature of 50 ^{o}C.

3.4.2 Sensor Response Kinetics

Responses of the CoPc and H_2Pc IDE sensors were determined from the time-dependent current plots of the films when dosed with analyte. The weaker analytes (dichloromethane through 2-butanone) were dosed with a 20% duty cycle (5 min doses with 20 min recovery times). The stronger analytes (di-*n*-butyl ether through triethylamine) were dosed with a 5% duty cycle (5 min doses with 90 min recovery). Raw data for both sensors are shown in Figure 3-2.

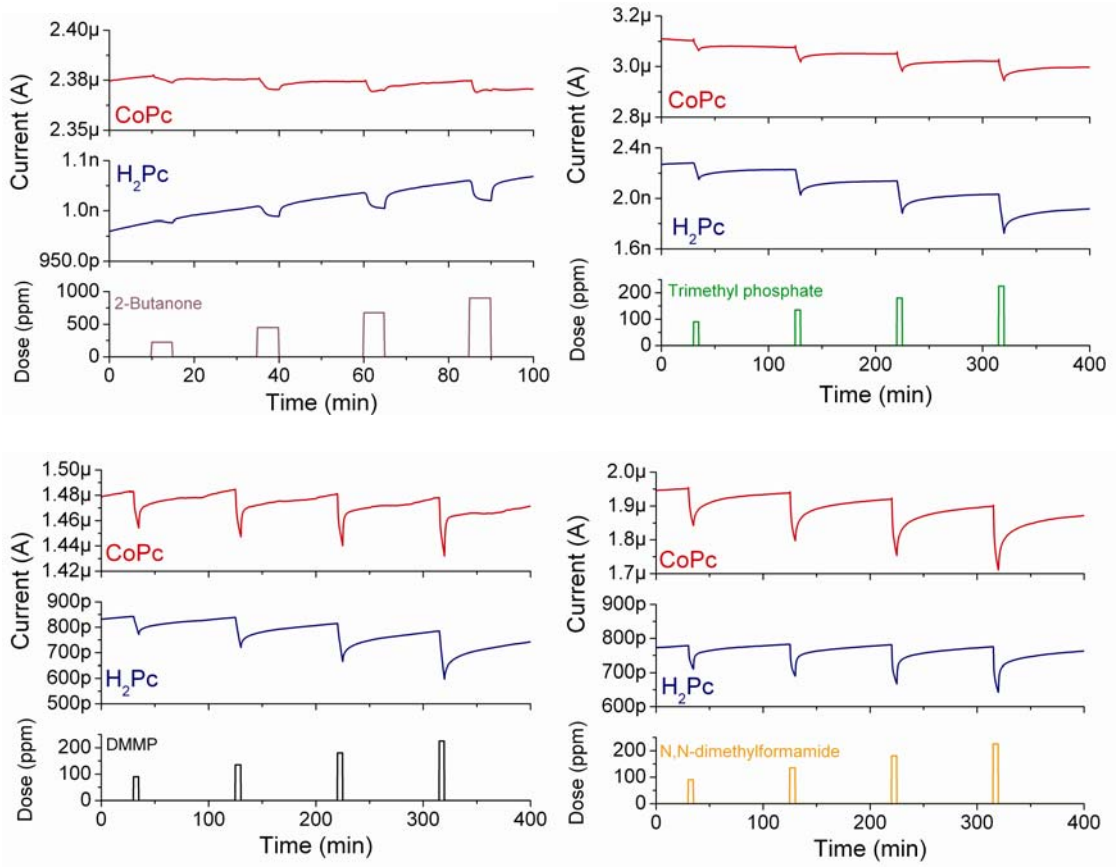

Figure 3-2 Sensor responses for CoPc (red) and H_2Pc (blue) to analytes 2-butanone (purple), trimethyl phosphate (green), DMMP (black) and DMF (orange). The top two traces in each graph represent the time-dependent current plots of the two sensors, while the bottom rectangular pulses in each represent the dosing of analyte as a function of time.

It can be seen qualitatively in Figure 3-2 that the changes in film current scale with analyte concentration. It should be noted that some oxygen dependent effects are seen in the sensor recoveries from strong analytes (those above the critical threshold; *vide infra*). Thus we should consider the fast portion of the response and recovery *primarily* oxygen independent, with some oxygen dependent character. In order to quantitatively analyze the sensor responses, the percent current change was calculated for each dose, using equation [1]

$$\% \text{ current change} = [(I_0 - I_f)/I_0] * 100 \qquad [1]$$

where I_0 is the current at the start of the dose and I_f is the current at the end of the 5 min dose. This value is designated as the sensor response. It can be seen in Figure 3-3 that CoPc sensor responses are linear with respect to analyte concentration (in general $R^2 \geq 0.97$), suggesting first order analyte-film interaction kinetics. H_2Pc sensor responses are similarly linear. The slopes R_C ($\%\cdot ppm^{-1}$) of the linear fits for each analyte increase with sensor response, and are used as device sensitivities combining data from all doses.

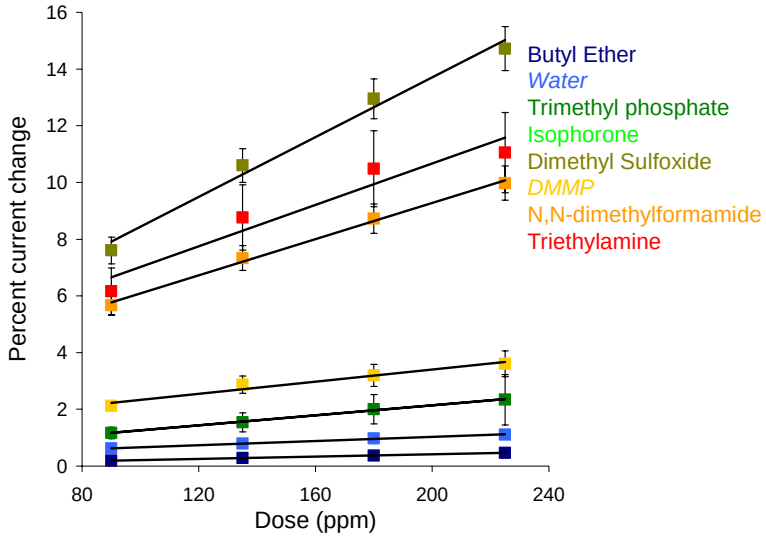

Figure 3-3 CoPc sensor response varies linearly with analyte concentration; slope R_C (%·ppm^{-1}, $R^2 \geq 0.97$) for each may be used as a measure of sensor response.

First order kinetics analysis as developed by Tongpool et al. was used to model the kinetics of gas-MPc sensor interactions.[50] The response curves appear to follow a first-order decay process; the reaction rate equation, *r*, is

$$r = -d[A]/dt = k[A] \qquad [2]$$

with *k* as the sensor response rate constant and [A] as the concentration of species A.[51] By integration this equation becomes

$$\ln[A_t] = \ln[A_0] - k(t-t_0) \qquad [3]$$

where $[A_0]$ is the initial concentration of A and $[A_t]$ is the concentration of A at time *t*. This may be adapted to the sensors by defining $[A_t]$ as $(I_t - I_f)$ where I_t is the current at time *t* and I_f is the final current of the dose. Consequently, if the plot of $\ln(I_t - I_f)$ versus *t* is linear, the reaction is first order and the slope of the line is *-k*. Figure 3-4 shows plots of $\ln(I_t - I_f)$ versus *t* for the strong analytes. Examination of these plots shows that the rates of sensing for all analytes are similar, with a range of 0.17 min^{-1} ≤

$k \leq 0.45$ min^{-1}. The H_2Pc sensor responses also obey first order kinetics, with rate constants in the range 0.15 min^{-1} $\leq k \leq$ 0.60 min^{-1}. These data suggest that sensor adsorption mechanisms are similar for all analytes.

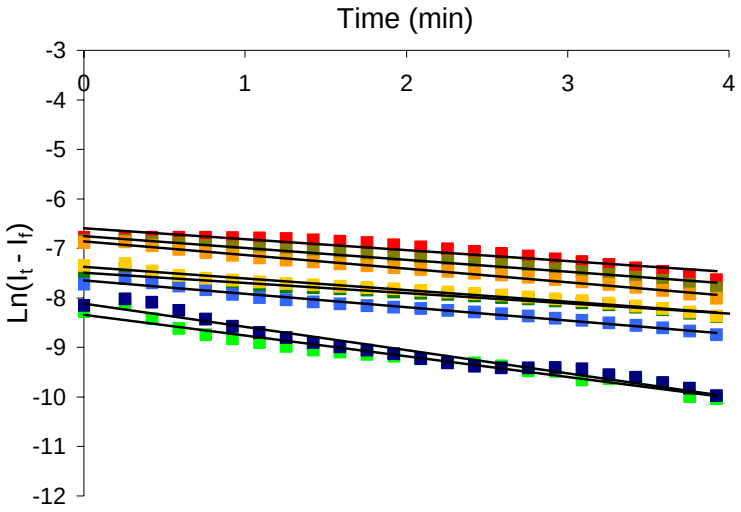

Figure 3-4 CoPc kinetics plots: ln($I_t - I_f$) vs. time is predominantly linear for all analytes, suggesting first order kinetics.

3.4.3 CoPc Sensitivity

CoPc sensitivity was analyzed by correlating the slopes R_C (%·ppm^{-1}, Figure 3-3) of all analytes to the $-\Delta H^o_{BF_3}$ scale. Figure 3-5 plots R_C versus $-\Delta H^o_{BF_3}$ for all analytes. It can be seen that above the threshold value of 73.7 kJ·mol^{-1} there is a strong linear dependence of sensor response with Lewis basicity. The sensor is relatively insensitive to analytes with $-\Delta H^o_{BF_3}$ values below this threshold, with small (< 0.2%) and completely reversible sensor responses. There are two outliers to the observed correlation, DMSO and isophorone; however, these outliers can be attributed

to inconsistencies within the $-\Delta H^{o}_{BF_3}$ scale. DMSO possesses a soft, electron-rich sulfur center that can bind more strongly to the partially soft cobalt center of CoPc. The $-\Delta H^{o}_{BF_3}$ scale is based on BF_3, a very hard Lewis acid, which is expected to bind at the oxygen of DMSO; this discrepancy in coordination explains the enhanced response of CoPc sensors to DMSO. Isophorone (3,5,5-trimethyl-2-cyclohexene-1-one, 90.56 kJ·mol^{-1}) is unusual because it has a high reported $-\Delta H^{o}_{BF_3}$ value as compared to cyclohexanone (76.37 kJ·mol^{-1}). BF_3 has subsequently been shown to bind to alkenes with an enthalpy of 11.8 kJ·mol^{-1}, which may lead to overestimation of the $-\Delta H^{o}_{BF_3}$ value initially reported for isophorone.[52]

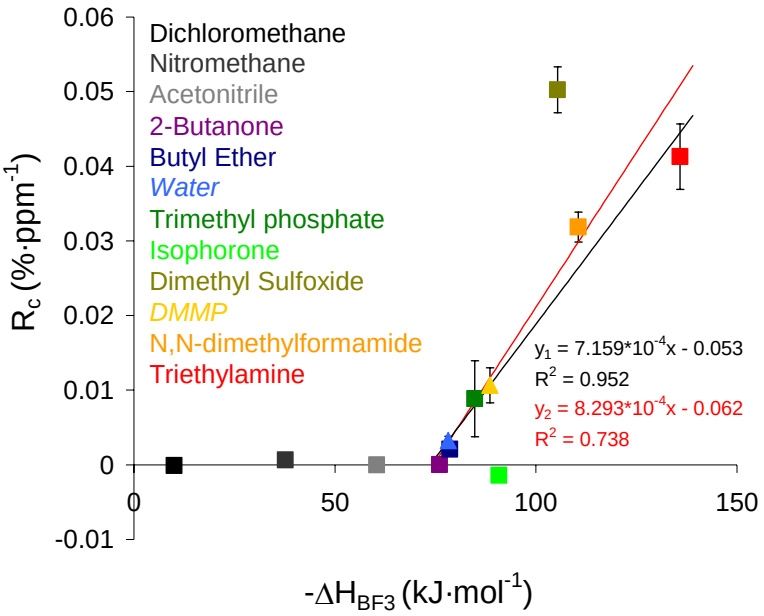

Figure 3-5 CoPc response slopes R_C vs. $-\Delta H^{o}_{BF_3}$ for all analytes. Least squares fits y_1 = neglecting outliers; y_2 = including outliers. Analytes represented by triangles have predicted $-\Delta H^{o}_{BF_3}$ values from the best fit line (y_1); error bars are present for all points.

The sensor response follows a bilinear model and an excellent least squares fit (bilinear $R^2 = 0.952$) can be made by disregarding the two outliers discussed above. Including the outliers also gives a correlation (bilinear $R^2 = 0.738$) with a similar slope. By interpolation, relative basicity values can be predicted for water = 78.2 $kJ \cdot mol^{-1}$ and DMMP = 88.6 $kJ \cdot mol^{-1}$. We attribute this bilinear sensor response to competing physisorptive and chemisorptive effects.[53] Physisorption generally occurs for analyte absorption energies less than 40 $kJ \cdot mol^{-1}$; above this threshold chemisorptive processes occur.[49,54] Below the critical threshold, we propose that weak physisorption of analytes to the entire MPc molecular surface is occurring, which causes small resistance changes. Above the threshold chemisorption at the metal and displacement of metal-bound O_2 are occurring, which provide the large resistance changes that correlate with analyte basicity. This is also supported by the fact that oxygen dependent effects are only observed with analytes above the critical threshold and strongest in the absence of O_2, while for analytes below this threshold only rapid oxygen independent sensor responses are seen even in the presence of O_2. These data show that the Lewis basicity of an analyte has a profound effect on the interaction between the analyte and the CoPc film. Comparison of sensor responses to bulk ligand parameters, such as vapor pressure and dipole moment, show no such correlation (Figure 3-6).

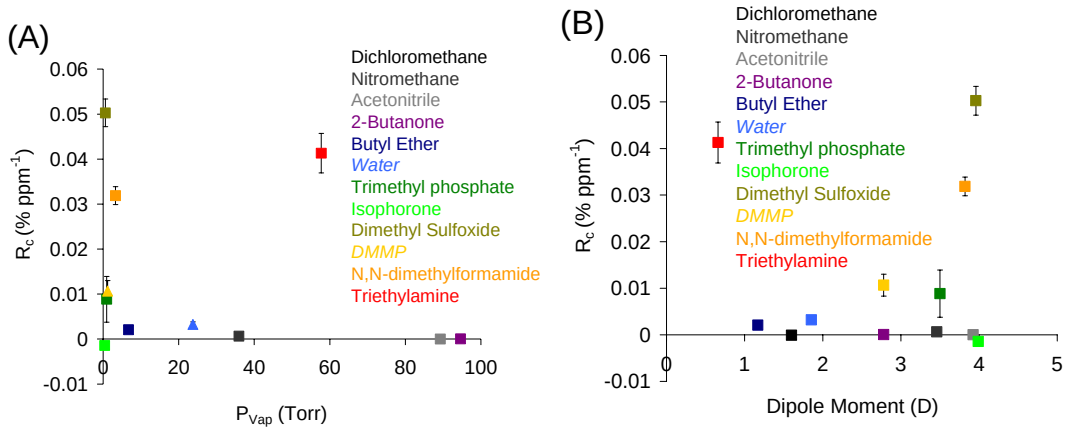

Figure 3-6 CoPc response slopes R_C as a function of (A) vapor pressure and (B) dipole moment, showing the lack of correlation.

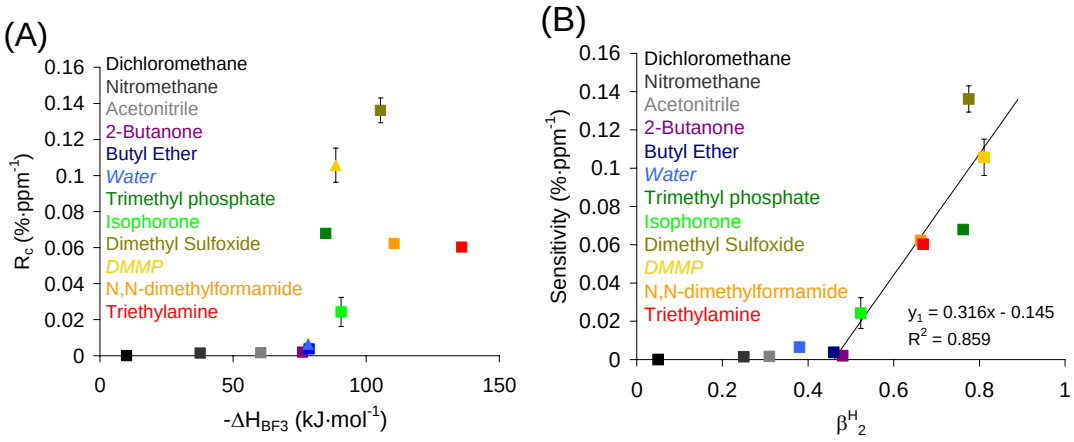

Figure 3-7 H_2Pc response slopes R_C as a function of (A) Lewis basicity $-\Delta H^o_{BF_3}$ and (B) hydrogen bond basicity β_2^H. Error bars are less than the size of the data points in most cases.

3.4.4 H_2Pc Sensitivity

The H_2Pc sensors generally gave much lower currents. In contrast to CoPc, the H_2Pc R_C values do not correlate well with $-\Delta H^o_{BF_3}$, as can be seen in Figure 3-7A. However, the H_2Pc R_C values do correlate bilinearly (R^2 = 0.905) with analyte β_2^H (Figure 3-7B) with a critical threshold of 0.46 units. This threshold behavior is again

postulated to arise from a transition from physisorption to chemisorption as described above; however, chemisorption in this case arises from hydrogen bonding between analyte and the interior N-H hydrogens of H_2Pc molecules on the sensor film surface. In Table 3-2, the analyte values for both basicity scales are summarized along with the sensor responses of both Pcs next to the appropriate scale. The results of the CoPc and H_2Pc response studies lend support to a model that the molecular core is the primary source of chemical interaction in the Pc films for more strongly basic analytes. CoPc sensor response is dominated by analyte coordination chemistry, and H_2Pc is dominated by analyte hydrogen bonding interactions. The presence of a critical threshold for this behavior may reflect when the entropic cost of specific ordered surface binding is offset by a favorable enthalpy of binding.

Table 3-2 Sensor responses and appropriate basicity scales for each phthalocyanine and analyte.

Analyte	$-\Delta H^{o}_{BF_3}$ **(kJ·mol^{-1})**	**CoPc Sensor Response R_C (%·ppm^{-1}) *10^{-3}**	β_2^H	**H_2Pc Sensor Responses R_C (%·ppm^{-1}) *10^{-3}**
Dichloromethane	10.0	-8.7 *10^{-2}	0.05	0
Nitromethane	37.63	0.6	0.25	1.5
Acetonitrile	60.39	5.7 *10^{-3}	0.31	1.7
2-Butanone	76.07	3.7*10^{-2}	0.48	2.0
Di-*n*-butyl ether	78.57	2.1	0.46	3.8
Trimethyl phosphate	84.79	8.8	0.76	67.9
Water	--	3.2	0.38	6.5
Isophorone	90.56	-1.4	0.52	24.3
DMMP	--	10.7	0.81	105.7
DMSO	105.34	50.3	0.78	136.2
DMF	110.49	31.9	0.66	62.3
Triethylamine	135.87	41.3	0.67	60.3

3.4.5 Oxygen Effects on Sensor Behavior

The influence of O_2 on the sensing behavior of the Pc films was explored by using either air or nitrogen as the carrier gas. Conductivity in Pc thin films arises by oxidation of the Pc film by O_2 (Scheme 3-1). The model gives two predictions for dosing in a nitrogen atmosphere: (a) before exposure to analyte, the nitrogen atmosphere will cause O_2 to gradually desorb from the film, decreasing the current; (b)

upon exposure to analytes, analytes will displace residual O_2 irreversibly from the film, leading to incomplete recovery of current after dosing. The kinetically slower process of oxygen displacement makes these processes more important in longer exposure dosing. To test these hypotheses, CoPc and H_2Pc IDEs were dosed with 225 ppm of water for 40 min, with a recovery period of 180 min (18% duty cycle), using air as the carrier gas; this dosing was repeated using nitrogen. Figure 3-8 compares the time-dependent CoPc current plots for doses in both gases; H_2Pc behaves qualitatively similarly.

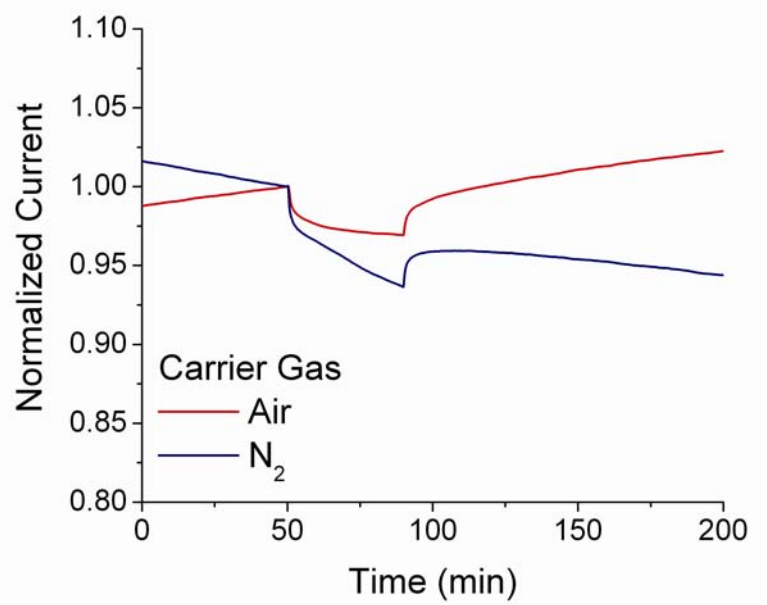

Figure 3-8 Normalized CoPc sensor responses to 225 ppm doses of water in UHP N_2 and zero grade air.

In this figure several results can be seen. The sensor drift changes in the two different carrier gases; in nitrogen the drift is -1.94% per hour, while in air the drift is +1.46% per hour. This suggests that the film is gradually losing the dopant (and conductivity) when the carrier gas is O_2 free. There is also a stronger sensor response

to water in nitrogen (6.7 ± 1.0% CoPc, 6.65 ± 1.9% H_2Pc) than in air (3.4 ± 0.4% CoPc, 2.6 ± 1.4% H_2Pc). These results can be attributed to reduced analyte-O_2 competition in the nitrogen atmosphere; the air dose still has O_2 present to compete with analyte for the binding sites, reducing the analyte effect on the film. Finally, in air the sensor eventually completely recovers over time from the dose, but in nitrogen the sensor never recovers completely (even over several days). In nitrogen, the fast component (C, Figure 3-1) is almost completely recovered, but the slower component (D, Figure 3-1) is not, suggesting that the slow effect arises from displacement of O_2. From a practical point of view, device operation is more stable and reproducible when operated in dry air. These results support the model that analytes both bind to free Pc sites and compete for O_2-bound Pc sites (Scheme 3-1).

3.5 CONCLUSION

The gas sensing behaviors of cobalt phthalocyanine (CoPc) and metal-free phthalocyanine (H_2Pc) thin films were investigated with respect to analyte basicity. There was a transition from physisorption to chemisorption once the analyte exceeded a critical basicity. It was found that the device response for CoPc increased significantly with analyte Lewis basicity and for H_2Pc sensor response increased significantly with analyte hydrogen-bond basicity. These results support the model that the analyte-phthalocyanine interaction is dominated by the central cavity of the phthalocyanine; coordination chemistry governs CoPc responses, and hydrogen bonding interactions govern H_2Pc responses. The interactions of the two

phthalocyanines with analytes were found to follow first order kinetics. The influence of O_2 on the film response was examined, and it was found that competitive binding between analytes and O_2 significantly affects film response and recovery.

These films may be candidates for application as robust detectors. For example, EPA guidelines for exposure to Sarin gas (isopropyl methylphosphonofluoridate) list concentrations for disabling and lethal exposures; disabling exposures occur above 15 ppb for 10 min of exposure, while lethal exposures occur above 64 ppb for 10 min of exposure.[55] The responses reported above for DMMP detection suggest that with modest improvements in sensitivity they have potential to be used as part of a cross-reactive sensor array[5] or when interfaced with a micro gas chromatograph.[56]

3.6 ACKNOWLEDGEMENT

Chapter 3 is a reprint in full of the material as it appears in the *Journal of the American Chemical Society*, **2007**, *129*(*17*), 5640-5646. Coauthors included A. Sharoni, C. Colesniuc, J. Park, I. K. Schuller, A. C. Kummel, and W. C. Trogler.

3.7 REFERENCES

(1) Snow, A. W.; Barger, W. R. Phthalocyanine Films in Chemical Sensors. *Phthalocyanines: Properties and Applications;* Lever, A. B. P., Ed; John Wiley and Sons: New York, 1989; Vol. 1, p. 341.

(2) Wright, J. D. *Prog. Surf. Sci.* **1989**, *31,* 1-60.

(3) Guillaud, G.; Simon, J.; Germain, J. *Coord. Chem. Rev.* **1998**, *178,* 1433-1484.

(4) Gould, R. D. *Coord. Chem. Rev.* **1996**, *156,* 237-274.

(5) Albert, K. J.; Lewis, N. S.; Schauer, C. L.; Sotzing, G. A.; Stitzel, S. E.; Vaid, T. P.; Walt, D. R. *Chem. Rev.* **2000**, *100,* 2595-2626.

(6) Eley, D. *Nature* **1948**, *162,* 819.

(7) Wilson, A.; Collins, R. A. *Sens. Actuators* **1987**, *12,* 389-403.

(8) Kerp, H. R.; Westerdui, K. T.; van Veen, A. T.; van Faassen, E. E. *J. Mater. Res.* **2001**, *16(2),* 503-511.

(9) de Haan, A.; Debliquy, M.; Decroly, A. *Sens. Actuators, B* **1999**, *57,* 69-74.

(10) Simon, J.; Andre, J. J. *Molecular Semiconductors* Springer-Verlag, Berlin, **1985**, pp. 73-149.

(11) Ho, K. C.; Tsou, Y. H. *Sens. Actuators, B* **2001**, *77,* 253-259.

(12) Zwart, J.; Van Wolput, J. H. M. C. *J. Molec. Cat.* **1979**, *5,* 51-64.

(13) Yahiro, H.; Naka, T.; Kuramoto, J.; Kurohagi, K.; Okada, G.; Shiotani, M. *Microporous Mesoporous Mater.* **2005**, *79,* 291-297.

(14) Lundstrom, I. *Sens. Actuators, B* **1996,** *35,* 11-19.

(15) Fleischer, M.; Meixner, H. *J. Vac. Sci. Technol., A* **1999,** *17,* 1866-1872.

(16) Nakata, S.; Okunishi, H. *Appl. Surf. Sci.* **2005,** *240,* 366-374.

(17) Barsan, N.; Schweizer-Berberich, M.; Gopel, W. *Fresenius J. Anal. Chem.* **1999,** *365,* 287-304.

(18) Gopel, W. *Sens. Actuators, B* **1995,** *24-25,* 17-32.

(19) Dunbar, A. D. F.; Richardson, T. H.; McNaughton, A. J.; Hutchinson, J.; Hunter, C. A. *J. Phys. Chem. B* **2006,** *110,* 16646-16651.

(20) Armstrong, N. R. *J. Porphyrins Phthalocyanines* **2000,** *4*, 414-417.

(21) Nieuwenhuizen, M. S.; Nederlof, A. J.; Barendsz, A. W. *Anal. Chem.* **1988,** *60,* 230-235.

(22) Bekyarova, E.; Davis, M.; Burch, T.; Itkis, M. E.; Zhao, B.; Sunshine, S.; Haddon, R. C. *J. Phys. Chem. B* **2004,** *108,* 19717-19720.

(23) Grate, J. W.; Abraham, M. H. *Sens. Actuators, B* **1991,** *3,* 85-111.

(24) Grate, J. W. *Chem. Rev.* **2000,** *100,* 2627-2648.

(25) Hierlemann, A.; Ricco, A. J.; Bodenhofer, K.; Gopel, W. *Anal. Chem.* **1999,** *71,* 3022-3035.

(26) Lee, Y. L.; Hsiao, C. Y.; Chang, C. H.; Yang, Y. M. *Sens. Actuators, B* **2003**, *94,* 169-175.

(27) Liu, C.J.; Hsieh, J. C.; Ju, Y. H. *J. Vac. Sci. Technol., A* **1996**, *14(3),* 753-756.

(28) Zhou, Q.; Gould, R. D. *Thin Solid Films* **1998**, *317,* 436-439.

(29) Sadaoka, Y.; Jones, T. A.; Gopel, W. *Sens. Actuators, B* **1990**, 148-153.

(30) Germain, J. P.; Pauly, A.; Maleysson, C.; Blanc, J. P.; Schollhorn, B. *Thin Solid Films* **1998,** *333,* 235-239.

(31) Schollhorn, B.; Germain, J. P.; Pauly, A.; Maleysson, C.; Blanc, J. P. *Thin Solid Films* **1998**, *326,* 245-250.

(32) Orti, E.; Bredas, J. L. *J. Am. Chem. Soc.* **1992,** *114,* 8669-8675.

(33) Shihub, S. I.; Gould, R. D. *Thin Solid Films* **1995,** *254,* 187-193.

(34) Schlettwein, D.; Hesse, K.; Gruhn, N. E.; Lee, P. A.; Nebesny, K. W.; Armstrong, N. R. *J. Phys. Chem. B* **2001,** *105,* 4791-4800.

(35) Taft, R. W.; Gurka, D.; Joris, L.; Schleyer, P. von R.; Rakshys, J. W. *J. Am. Chem. Soc.* **1969,** *91,* 4801-4808.

(36) Kamlet, M. J.; Taft, R. W. *J. Am. Chem. Soc.* **1976,** *98,* 377-383.

(37) Abraham, M. H.; Grellier, P. L.; Prior, D. V.; Morris, J. J.; Taylor, P. J. *J. Chem. Soc. Perkins Trans 2* **1990,** 521-529.

(38) Gutmann, V. *Electrochim. Acta* **1976,** *21,* 661-670.

(39) Gutmann, V. *Coord. Chem. Rev.* **1976,** *18,* 225-255.

(40) Gritzner, G. *J. Mol. Liquids* **1997,** *73,* 487-500.

(41) Maria, P. C.; Gal, J. F. *J. Phys. Chem.* **1985,** *89,* 1296-1304.

(42) Pearson, R. G. *Hard and Soft Acids and Bases;* Dowden, Hutchinson, and Ross: Stroudsville, PA, 1973.

(43) Miller, C. W.; Sharoni, A.; Liu, G.; Colesniuc, C. N.; Fruhberger, B.; Schuller, I. K. *Phys. Rev. B* **2005,** *72,* 104113.

(44) Marrs, T. C. *Pharmac. Ther.* **1993,** *58,* 51-66.

(45) Lide, D. R., Frederikse, H. P. R., Eds. *CRC Handbook of Chemistry and Physics,* 74th ed.; CRC Press: Ann Arbor, 1993; Section 9.

(46) Miller, K. A.; Yang, R. D.; Hale, M. J.; Park, J.; Fruhberger, B.; Colesniuc, C. N.; Schuller, I. K.; Kummel, A. C.; Trogler, W. C. *J. Phys. Chem, B* **2006,** *110,* 361-366.

(47) Lee, Y. L.; Tsai, W. C.; Maa, J. R. *Appl. Surf. Sci.* **2001,** *173,* 352-361.

(48) Chen, J. C.; Ju, Y. H.; Liu, C. J. *Sens. Actuators, B* **1999,** *60,* 168-173.

(49) Kolesar, E. S.; Wiseman, T. M. *Anal. Chem.* **1989,** *61,* 2355-2361.

(50) Tongpool, R.; Yoriya, S. *Thin Solid Films* **2005**, *109,* 7878-7882.

(51) Atkins, P.; Jones, L. *Chemistry: Molecules, Matter, and Change 4th Ed.* W. H. Freeman and Co.: New York, 2000.

(52) Herrebout, W. A.; van der Veken, B. J. *J. Am. Chem. Soc.* **1997,** *119,* 10446-10454.

(53) Passard, M.; Pauly, A.; Blanc, J.-P.; Dogo, S.; Germain, J.-P.; Maleysson, C. *Thin Solid Films* **1994,** *237,* 272-276.

(54) Steed, J. W.; Atwood, J. L. *Supramolecular Chemistry* J. Wiley and Sons, Ltd.: New York, 2000.

(55) National Research Council. *Acute Exposure Guideline Levels for Selected Airborne Chemicals, Volume 3.* The National Academies Press: Washington, DC, 2003.

(56) Lu, C. J.; Whiting, J.; Sacks, R. D.; Zellers, E. T. *Anal. Chem.* **2003,** *75,* 1400-1409.

CHAPTER IV

COMPARATIVE GAS SENSING IN COBALT, NICKEL, COPPER, ZINC, AND METAL-FREE PHTHALOCYANINE CHEMIRESISTORS

4.1 ABSTRACT

The sensitivities of metallophthalocyanine (MPcs: M = Co, Ni, Cu, Zn, and H_2) chemiresistors to vapor phase electron donors were examined using 50 nm MPc films deposited on interdigitated electrodes. Sensor responses were measured as changes in current at constant voltage. Analytes were chosen to span a broad range of Lewis base and hydrogen bond base strengths. The MPc sensor responses were correlated exponentially with binding enthalpy. These exponential fits were consistent with the van't Hoff equation and standard free energy relationships. Sensor recovery times were found to agree with Arrhenius behavior. Relative sensitivities of all MPcs were compared via two-way ANOVA analysis. Array response patterns were differentiated via linear discriminant analysis, and analyte identification was achieved over a range of concentrations with 96.7% classification accuracy for the strong binding analytes. The ability to distinguish among different analytes, regardless of their concentration, through normalization of the responses to a reference sensor is particularly noteworthy.

4.2 INTRODUCTION

Phthalocyanines (Pcs), both metalated (MPcs) and metal-free (H_2Pc), are metal-organic semiconductors that have been applied as chemiresistive sensors.[1-3] MPc sensitivity to vapor-phase molecules may be tuned by manipulation of the metal center and by substitution of functional groups on the organic ring.[1-4] Conductivity in MPc films depends strongly on atmospheric chemical species, particularly oxidants and reductants.[5-6] P-type MPcs are insulating in dark, high-vacuum environments and become semiconducting on exposure to air.[7-9] This air-induced conductivity has been attributed to coordination of O_2 to surface MPc metal centers, forming superoxide adducts which extract electrons, generating charge carriers (holes) in the bulk film.[10-12] Superoxide adducts have been detected directly through EPR studies.[13-15] Oxygen adsorption on H_2Pc has been reported as occurring on the four *meso*-nitrogens, leading to weaker conductivity gains.[16] Other oxidizing gases (O_3, NO_X, Cl_2, and others) induce similar conductivity gains in p-type MPc films through charge transfer or redox reactions which generate holes in the film.[17-20]

MPc interactions with electron donating (reducing) gases, including Lewis bases such as NH_3, have the opposite effect. Current losses reported on dosing with Lewis bases have been attributed to hole trapping within the p-type film by electrons donated from the chemisorbed analyte.[5] Sensor interactions with electron donating analytes may be understood by using linear solvation energy relationships (LSER), which account for weak intermolecular forces such as dispersion interactions (van der Waals forces and π–π interactions), polarizability, dipolarity, and hydrogen bond

acidity and basicity.[21-22] Though not included in general LSER theory, metal coordinative bonds are potentially the strongest intermolecular binding force for adsorption of Lewis bases onto MPcs.[23] As a surface dopant, O_2 occupies only a fraction of the binding sites on the film;[10] therefore strong Lewis bases could bind either to oxygen-free surface metal centers or could compete with O_2 for occupied metal surface sites (Scheme 4-1).[24] Non-coordinating weak bases may be physisorbed on the organic regions of the MPc molecule through van der Waals forces and polarization interactions.

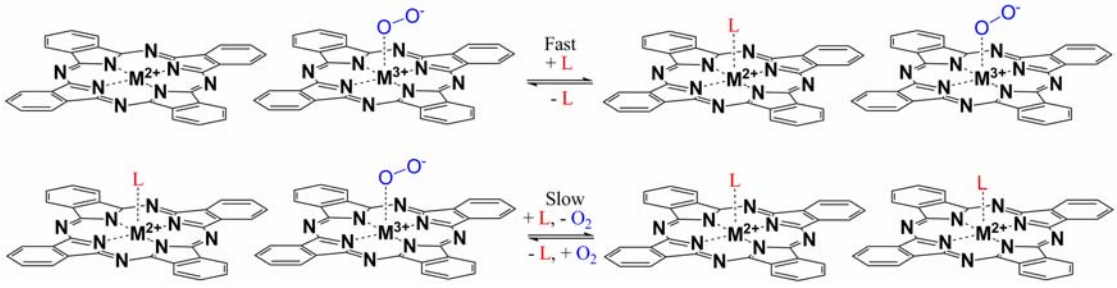

Scheme 4-1 Model of chemisorption onto MPc film by coordinating analyte L. Analytes may bind at open metal sites or may compete for oxygen bound sites.

Detection of electron donating analytes by CoPc was found to be governed primarily by coordination to the metal center.[24] CoPc sensor responses to these analytes were correlated bilinearly to the Lewis basicity of the analyte, described by the binding enthalpy scale $-\Delta H^{o}_{BF_3}$.[25] The $-\Delta H^{o}_{BF_3}$ scale was determined from calorimetrically measured enthalpies of formation (kJ mol^{-1}) of 1:1 adducts of Lewis bases to the Lewis acid BF_3 in dichloromethane, and thereby directly probes basicity through the free energy of binding. Detection of electron donors by H_2Pc was

bilinearly correlated with the hydrogen bond basicities of the analytes as tabulated in the β_2^H scale.[26] Values for the β_2^H scale were determined using log *K* values (dm^3 mol^{-1}) of the complexation of bases with reference acids such as 4-fluorophenol in CCl_4. Therefore, the β_2^H scale is an indirect probe of basicity and binding enthalpy through reaction equilibria.

Arrays of MPc sensors (VOPc, TiOPc, CoPc, NiPc, CuPc, ZnPc, and PbPc) have been used to detect various analytes, including strongly basic analytes such as pyridine and piperidine,[27-28] hydrocarbons and aromatic compounds (hexane, benzene, and toluene),[28-29] polar[30] and protic[31] solvents (acetonitrile, THF, methanol, and isopropanol), and strong oxidants such as NO and NO_2.[32] However, none of these studies examines a spectrum of analytes with a broad range of binding strengths. In the present study the sensitivities of an array of MPc chemiresistors (M = Co, Ni, Cu, Zn, and H_2) are examined with respect to a series of analytes spanning a range of both Lewis basicities ($-\Delta H^o_{BF_3}$) and hydrogen bond basicities (β_2^H). Sensor kinetics are examined to determine the dependence of sensor recovery on analyte basicity. The MPc device sensitivities are compared via two-way ANOVA analysis. Linear discriminant analysis is employed for analyte identification for a range of concentrations and normalization is shown to provide a concentration independent method for analyte identification.

4.3 EXPERIMENTAL

4.3.1 Sensor Fabrication

Chemiresistive metallophthalocyanine (MPc) sensors were prepared as reported previously.[24] 50 nm thick Au interdigitated electrodes (IDEs) were prepared by standard photolithography and processing on 1 μm-thick SiO_2 over (100) Si substrates; the IDEs contained 45 finger pairs with a channel length of 5 μm and a width of 2 mm. Six IDEs were fabricated per substrate for reproducibility. CoPc (Aldrich, 97%), NiPc (Aldrich, 85%), CuPc (Aldrich, 97%), ZnPc (Acros, 98%), and H_2Pc (Aldrich, 98%) were purified by multiple zone sublimations at 400 ^oC and 10^{-5} Torr. The 50 nm thick sensor films of MPcs were deposited on IDEs in a UHV chamber (base pressure 2 x 10^{-10} Torr) using organic molecular beam epitaxy (deposition pressure 5 x 10^{-9} Torr, deposition rate 0.2 – 0.5 Å s^{-1}). Deposition rate and film thickness were monitored by QCM. Substrate temperature during deposition was held constant at 25.0 ± 0.1 ^oC to maintain constant film morphology across all sensors. Film thickness and structure were characterized by low angle XRD measurements (Rigaku RU-200B diffractometer, Cu K_α radiation) and AFM (Nanoscope IV Scanning Microscope, Mikromasch NSC15 325 kHz probe).[33] The devices were aged at 10 mTorr for 48 h before use.

4.3.2 Device Measurements

Sensor responses of MPc chemiresistors were measured as reported previously.[24] Each array of six IDEs was wirebonded to leads in a dual in-line ceramic

package purchased from Spectrum Semiconductor Materials, Inc. (Figure 4-1). Two sensor arrays were mounted simultaneously in a SiO_2-passivated stainless steel chamber (15 cm^3 internal volume). Sensors were monitored by a Keithley 6517/6521 multi-channel electrometer used as both voltage source and ammeter. Residual sensor photoconductivity was allowed to decay for 24 h before testing. During dosing, the chamber temperature was maintained at 50.0 ± 0.1 ^oC by a Haake F8 constant temperature bath. Zero grade air was used as the carrier gas for dosing studies, with a constant flow rate of 500 sccm (standard cm^3 per min). Analyte vapors were introduced into the chamber by mass flow controllers (MKS Instruments, Inc. Model 1497A, 10 and 1000 sccm) in conjunction with impinger flasks. Analyte concentrations in ppm were calculated from published vapor pressure data[34] using the Clausius-Clapeyron equation; dose concentrations were determined by flask temperature, flow rate through the flask, and dose dilution in the carrier gas. Solenoid valves were placed before and after the impinger flasks to prevent analyte cross-contamination, and a four-way valve was placed before the sensor chamber in order to saturate the gas line with analyte vapor before introduction into the chamber. A Labview VI program was used to control all instruments and record data.

Analytes were chosen to span both $-\Delta H^o_{BF_3}$ and β_2^H basicity scales. These included dichloromethane, nitromethane, acetonitrile, 2-butanone, di-*n*-butyl ether, trimethyl phosphate, water, isophorone, dimethyl methylphosphonate (DMMP), dimethyl sulfoxide (DMSO), *N*,*N*-dimethylformamide (DMF), and triethylamine (Table 4-1).

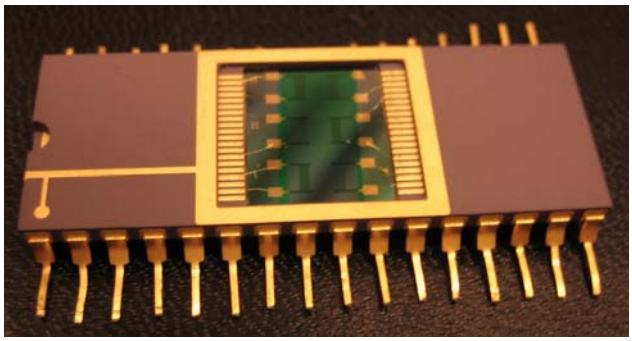

Figure 4-1 An MPc sensor array containing six chemiresistors (50 nm thick Au electrodes, 45 interdigitated pairs of fingers, 5 μm channel spacing, on a 1 μm thick SiO_2 substrate) wirebonded in a dual-inline ceramic package.

Analytes were dried over 4 Å molecular sieves (Fisher) before use. Dichloromethane, nitromethane, acetonitrile, and 2-butanone were dosed at concentrations of 225, 450, 675, and 900 ppm. Di-*n*-butyl ether, trimethyl phosphate, water, isophorone, DMMP, DMSO, DMF, and triethylamine were dosed at 90, 135, 180, and 225 ppm concentrations. The devices were annealed at 70.0 ± 0.1 ^{o}C for 1 h before dosing.

Sensor responses were determined from time-dependent current plots at constant voltage. The devices were operated in the space charge limited conduction (SCLC) regime at 8V. Sensor responses were calculated as the percent current change during the dose ($\Delta I/I_{baseline}$ x 100) with negative responses for current losses and positive responses for current gains. Sensor responses have been shown to be first order with analyte concentration, so MPc sensitivities to analytes are defined as the slope of the sensor response vs. analyte concentration (% ppm^{-1}).[24,35]

Table 4-1 Lewis basicities $-\Delta H^{o}_{BF_3}$ and hydrogen bond basicities β_2^H for analytes studied. Colors listed corresponded to color labeling in all figures.

Analyte	Color Label		$-\Delta H^{o}_{BF_3}$	β_2^H
Dichloromethane	Black	■	10.0	0.05
Nitromethane	Dark Grey	■	37.6	0.25
Acetonitrile	Light Grey	■	60.4	0.31
2-Butanone	Purple	■	76.1	0.48
Di-n-butyl ether	Royal Blue	■	78.6	0.46
Water[a]	Light Blue	■	*82.1 ± 4.3*	0.38
Trimethyl Phosphate	Green	■	84.8	0.76
Isophorone	Chartreuse	■	90.6	0.52
DMMP[b]	Yellow	■	*104.1 ± 12.9*	0.81
DMSO	Orange	■	105.3	0.78
DMF	Red	■	110.5	0.66
Triethylamine	Wine	■	135.9	0.67

[a] The $-\Delta H^{o}_{BF_3}$ value for water was determined from fits of the experimental data for all MPcs in the present study.

[b] The $-\Delta H^{o}_{BF_3}$ value for DMMP was also determined from experimental fits of all MPcs in the present study; the β_2^H value was estimated from experimental values for dimethyl ethylphosphonate and diethyl methylphosphonate.

4.3.3 Statistical Methods

All correlation coefficients were determined from linear and non-linear curve fits in OriginPro 7.5. Recovery time t'_{90} data were determined from raw sensor data. Two-way ANOVAs were performed with OriginPro 7.5 using the Tukey method at a significance level of 0.05.[36] Linear discriminant analysis was performed using the R-2.6.2 environment (LDA function, MASS library).

4.4 RESULTS AND DISCUSSION

4.4.1 MPc Sensor Characterization

MPc (M = Co, Ni, Cu, Zn, and H_2) surface morphologies were determined by atomic force microscopy (AFM). The MPcs show differences in granular structure due to variances in crystal lattice; these differences may be caused by metal center or by temperature-induced crystal phase transitions.[16] Granular variability was suppressed in the current study by holding the substrate temperature constant at 25.0 ± 0.1°C during deposition and closely monitoring the deposition rate (0.2 to 0.5 Å s^{-1}). All MPc films were found to be textured α phase with ellipsoidal grains of 50 nm average diameter on the long axis.[33] *I-V* measurements showed good ohmic behavior at low voltages in all sensors, with space charge limited conductivity (SCLC) occurring in general above 5 V. Operation of MPc IDE sensors in the SCLC regime removes the influence of contact resistance between the MPc film and the electrodes on relative sensor responses (% current change); all sensors were operated at 8 V, well within the SCLC regime.[37]

Sensor responses are reported as the change in sensor current at constant voltage on dosing with analytes. Steady state MPc sensor responses have been found to occur within 30 min of dose exposure.[38-40] Sensor responses and recoveries generally exhibit an initial fast region (~ 5 min), accounting for the largest change in sensor current, followed by a slow saturation region. We have proposed a model assigning the fast (kinetic) region of the response and recovery to adsorption of analyte primarily at O_2-free metal centers, and the slow (saturation) response region to competitive displacement of O_2-bound metal centers.[24] It was demonstrated that sensor responses in the 5 min regime for basic physisorption and chemisorption interactions obey first order kinetics. This behavior dictates that the sensor responses to analytes depend linearly on analyte concentration.[35] In the present study sensor responses ($\Delta I/I_{baseline}$ x 100) were determined from 5 min doses of analytes at varied concentrations. Figure 4-2 displays sensor response data for all MPcs dosed with water. MPc sensitivities (% ppm^{-1}) to individual analytes are thus determined as the slope of the linear fit of the sensor responses versus analyte concentration (Appendix, Figure 4-7).[24] These sensitivities are tabulated (Appendix, Table 4-3).

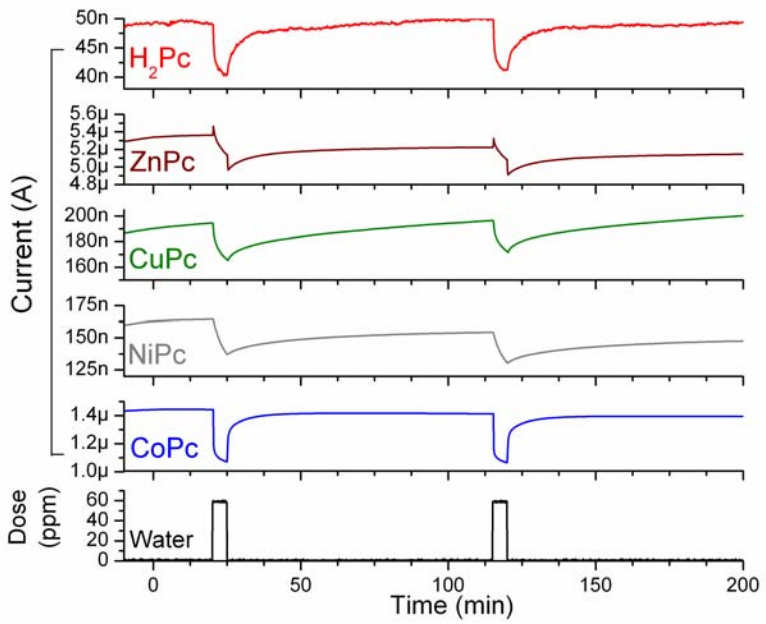

Figure 4-2 Sensor data for all MPcs (M = Co, Ni, Cu, Zn, H_2) on exposure to doses of 60 ppm water.

4.4.2 Comparison of MPc Sensitivities

Sensitivities (% ppm^{-1}) of all MPcs to all analytes were correlated with the $-\Delta H^{o}_{BF_3}$ scale (and the β_2^H scale in the case of H_2Pc). These data are plotted in Figure 4-3. There is an approximate exponential dependence of sensitivity on Lewis basicity $-\Delta H^{o}_{BF_3}$ for CoPc, NiPc, CuPc, and ZnPc. Lewis basicity values ($-\Delta H^{o}_{BF_3}$) for DMMP and water are unavailable in the literature, and so were derived from exponential sensitivity fits of these four MPcs to all analytes. H_2Pc sensing behavior correlates with hydrogen bond basicity, showing a better exponential fit to β_2^H values than to $-\Delta H^{o}_{BF_3}$ values. The significance of these exponential dependences will be discussed (*vide infra*).

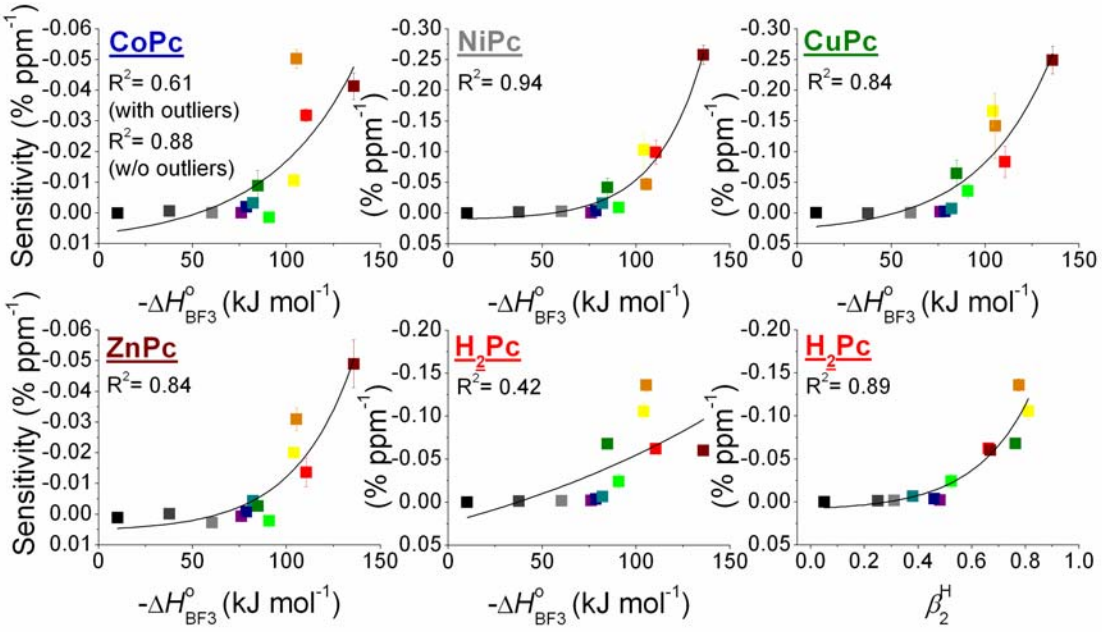

Figure 4-3 MPc sensitivities plotted versus basicity for all analytes. Good exponential fits are seen for all MPcs to Lewis basicity $-\Delta H^{o}_{BF_3}$ with the exception of H_2Pc, which is better correlated to hydrogen bond basicity β_2^H. Color coding of analytes is found in Table 4-1; error bars are present for all points.

CoPc sensitivities have been reported previously,[24] with DMSO and isophorone noted as outliers from the general trend of increasing sensitivity with increasing basicity. The unusual sensitivity of CoPc to DMSO ($-\Delta H^{o}_{BF_3}$ = 105.34 kJ mol^{-1}) was attributed to hard-soft acid-base properties.[41] The tendency of the soft, electron-rich sulfur of DMSO to bind to the relatively soft cobalt(II) center of CoPc differs from binding of DMSO to the hard Lewis acid BF_3, which would be more likely to bind to the oxygen of DMSO, leading to the noted disparity in relative binding strength. The binding enthalpy of isophorone (3,5,5-trimethyl-2-cyclohexene-1-one, $-\Delta H^{o}_{BF_3}$ = 90.56 kJ mol^{-1}) represents a potential flaw in the $-\Delta H^{o}_{BF_3}$ scale. In

contrast to cyclohexanone ($-\Delta H^{o}_{BF_3}$ = 76.37 kJ mol^{-1}), isophorone is overestimated in basicity due to the ability of BF_3 to also bind to the alkene moiety with an enthalpy of 11.8 kJ mol^{-1}.[42]

NiPc, CuPc, and ZnPc follow an exponential dependence on $-\Delta H^{o}_{BF_3}$ much more closely than observed in CoPc; they exhibit similarly weak responses to isophorone, but are much less sensitive to DMSO. In general Ni^{2+}, Cu^{2+}, and Zn^{2+} are harder acids than Co^{2+}; they have smaller ionic radii (Co^{2+} = 0.75 Å, Ni^{2+} = 0.69 Å, Cu^{2+} = 0.65 Å, Zn^{2+} = 0.68 Å)[43] and no easily accessible higher oxidation states, while Co^{2+} may be further oxidized to Co^{3+}. Examination of molecular orbital diagrams shows that, on axial binding of electron donors to the metal center, the LUMO of CoPc has d_{z^2} character, while the LUMOs of NiPc, CuPc, and ZnPc have d_{π} character.[44] These characteristics make NiPc, CuPc, and ZnPc more likely to form π-bonding interactions with the oxygen in DMSO, while CoPc can form stronger σ-bonding interactions with the sulfur.

4.4.3 Exponential Dependence of Sensitivity on $-\Delta H^{o}_{BF_3}$

It was argued that the analyte sensitivities of CoPc and H_2Pc follow a bilinear dependence on $-\Delta H^{o}_{BF_3}$ and β_2^H, respectively.[24] This was attributed to a transition from physisorption to chemisorption at a relative analyte basicity of 73.7 kJ mol^{-1} ($-\Delta H^{o}_{BF_3}$) for CoPc and 0.46 units (β_2^H) for H_2Pc. For strong binders ($-\Delta H^{o}_{BF_3}$ greater than 73.7 kJ mol^{-1}), chemisorption and coordination at the metal center (CoPc)

or the internal protons (H_2Pc) was proposed as the dominant mechanism of sensing. For weak binders ($-\Delta H^o_{BF_3}$ less than 73.7 kJ mol^{-1}), it is unclear whether chemisorption to the metal center/internal protons or physisorption on the organic ring is the dominant interaction. However, the weak sensor responses observed are consistent with limited charge transfer, whether it arises from weak coordination interactions or physisorption on the organic.

Statistically, the data can be fit equally well by bilinear fits or exponential fits. Exponential fits are consistent with standard models of surface coverage and binding energy. The $-\Delta H^o_{BF_3}$ scale is a direct measurement of the binding enthalpy of analytes to the Lewis acid BF_3 used as a relative measurement of electron donation/basicity to other Lewis acids.[25] The β_2^H scale is a relative scale that relies indirectly on the binding enthalpy of electron-donating analytes to reference hydrogen-bond acids.[26] The ligand-to-metal binding event (Scheme 4-1) may be represented by equation (1).

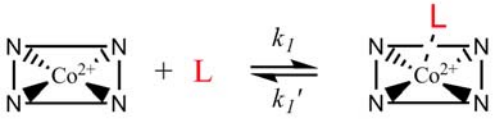

(1)

The equilibrium constant K for this binding event should be exponentially related to the enthalpy of binding using the van't Hoff equation[45] and the standard free energy of reaction (eq. 2).[46]

$$K = \exp(-\Delta G^o/RT) \quad (2)$$

$$\Delta G^o = \Delta H^o - T\Delta S^o \quad (3)$$

The entropy change on binding should be approximately equal for all analyte binding interactions; therefore, at constant temperature the equilibrium constant of the reaction is exponentially dependent on the enthalpy of binding (eq. 3). Thus, an analyte with a high enthalpy of binding would favor the products side of eq. 1, leading to a strong sensor response, which exponentially depends on $-\Delta H^{o}_{BF_3}$ or β_2^H.

4.4.4 Exponential Dependence of Sensor Recovery on $-\Delta H^{o}_{BF_3}$

Application of the Arrhenius equation (4) to the interaction proposed in (1) implies that the reaction rate k_1 and the reverse rate $k_1^{'}$, and by extension the response and recovery times, are also exponentially dependent on the binding enthalpy.[47]

$$k = A\exp(-\Delta G^{o}/RT) \qquad (4)$$

A large binding enthalpy would imply a fast adsorption rate and a slow desorption rate; in the present study recovery times were probed as an indirect measurement of desorption rate. The recovery time $t_{90}^{'}$ (min) is defined as the time required to recover 90% of the steady-state sensor current.[48] CoPc $t_{90}^{'}$ values for 225 ppm doses of each analyte are plotted against $-\Delta H^{o}_{BF_3}$ in Figure 4-4A; $t_{90}^{'}$ values are plotted against CoPc sensitivities (% ppm^{-1}) in Figure 4-4B.

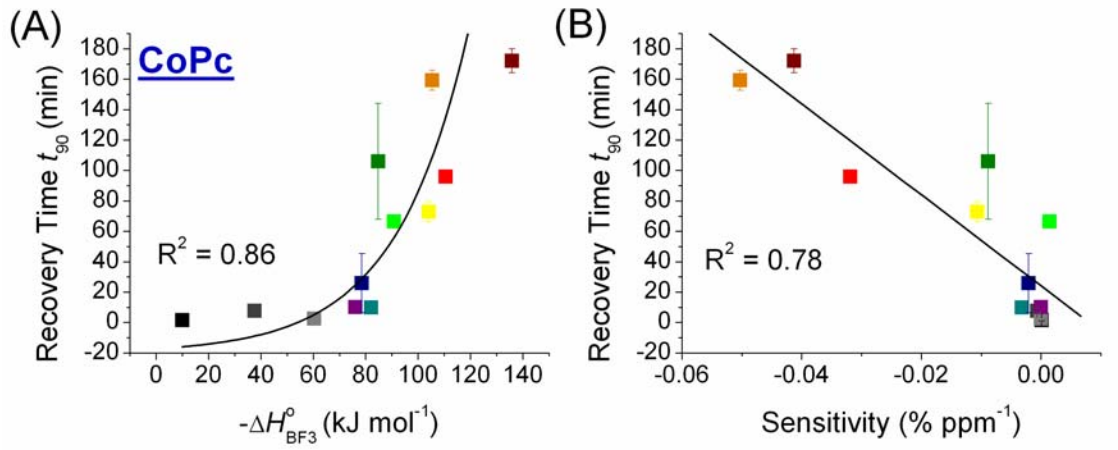

Figure 4-4 (A) Exponential dependence of CoPc recovery times t'_{90} for 225 ppm doses of each analyte on Lewis basicity $-\Delta H^o_{BF_3}$. B) Linear dependence of CoPc recovery times t'_{90} on CoPc sensitivity (% ppm^{-1}). Color coding of analytes is found in Table 4-1.

CoPc t'_{90} values are exponentially dependent on the enthalpy of binding; this translates to a linear relationship with CoPc sensitivities. The exponential dependence of t'_{90} for analyte dissociation on binding enthalpy is evident for all MPcs in this study (Appendix, Figure 4-8). Correlation constants are tabulated (Appendix, Table 4-4), as are recovery times t'_{90} (Appendix, Table 4-5). All MPcs show reasonably good correlation of t'_{90} with exponential of the binding enthalpy or basicity, and a good linear correlation of t'_{90} to sensitivity, with the exception of H_2Pc.

4.4.5 ANOVA of all MPcs

Cross-reactive sensor array applications demand sensors that respond to a broad range of analytes and vary in their relative responses; these sensors are analyzed

with pattern-recognition software to identify analytes.[49] MPc sensor data were compared in cross correlation plots (Appendix, Figure 4-9), and analyzed with a two-way ANOVA (analysis of variance) program. Correlation coefficients for all MPcs are presented in Table 4-2. CoPc and H_2Pc show the greatest variance from all the other MPcs ($R^2 = 0.25 \leq x \leq 0.78$), while NiPc, CuPc, and ZnPc are all quite similar to one another ($R^2 = 0.80 \leq x \leq 0.90$). This behavior agrees with previously mentioned HOMO-LUMO arguments of binding to electron donors (CoPc bonds through d_σ orbitals while NiPc, CuPc, and ZnPc bond through d_π orbitals) rather than with classical inorganic binding models such as the Irving-Williams series, which suggests that ZnPc should agree more closely with CoPc behavior.[50]

Table 4-2 Correlation constants for linear fits of two-MPc sensitivity comparisons (Appendix, Figure 4-9).

	CoPc	NiPc	CuPc	ZnPc	H_2Pc
H_2Pc	0.61	0.25	0.59	0.48	1
ZnPc	0.78	0.80	0.90	1	0.48
CuPc	0.63	0.84	1	0.90	0.59
NiPc	0.48	1	0.84	0.80	0.25
CoPc	1	0.48	0.63	0.78	0.61

4.4.6 Linear Discriminant Analysis

A variety of methods have been explored to selectively identify analytes with cross reactive sensor arrays, including probabilistic and artificial neural networks (PNN and ANN), linear discriminant analysis (LDA), principal component analysis (PCA), and nearest neighbor (NN) pattern recognition algorithms.[51] Of these, LDA and PCA are among the most popular due to their analysis speed, ease of use, low memory requirements, and statistical accuracy. LDA is generally more useful than PCA because it is a self-consistent method capable of producing greater differentiation and less overlap.[52] In general, LDA and PCA analyses have limited success separating analytes at varied concentrations due to the overlap of sensor responses, particularly if those analytes have similar interaction mechanisms.[51-56] Incorporation of orthogonal sensing modes, such as the combination of mass spectrometry and surface acoustic wave devices, can help to discriminate between analytes at variable concentrations.[55] Otherwise, significant overlap between analytes may occur in the LDA plot.[54,56]

We have developed a novel route to remove concentration dependence from the responses of our sensing array to improve the selectivity of our LDA. One well-behaved ZnPc sensor was removed from the LDA, and its concentration-dependent sensor responses were used to normalize all other sensors (Figure 4-5), thereby removing the concentration dependence of the sensor responses. This method was used to identify analytes over a range of concentrations using all MPc sensors. The independent variable to be differentiated by LDA was the analyte identity; the dependent variable consisted of a linear combination of all MPc sensor responses.

Good separation was achieved for trimethyl phosphate, isophorone, DMMP, and triethylamine; significant overlap remained for the remaining analytes.

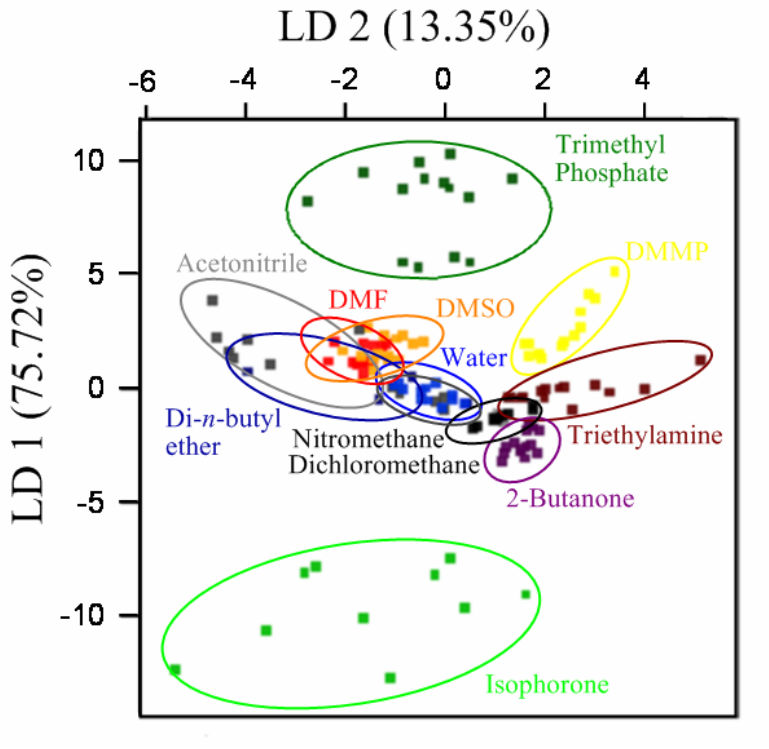

Figure 4-5 Concentration-independent linear discriminant analysis (LDA) of MPc array sensor responses to all analytes, achieved by normalization to a single ZnPc sensor.

Weak binders provide most of the overlap within the LDA. These analytes can be identified by recovery time, which can be two to one hundred times faster than the strong binders (Figure 4-4A). After identification by recovery time, separate LDA analyses can be performed for the strong and weak binders. Initial separation by recovery time results in an LDA with excellent analyte separation for the strong binders; the only overlapping analytes are DMSO and DMF (Figure 4-6A). LDA of

the weak binders alone shows that significant overlap remains (Figure 4-6B). We note that initial separation by recovery time is a practical technique since the sensors are operated in pulsed mode (kinetic regime) to reduce the effects of drift on sensor measurement.

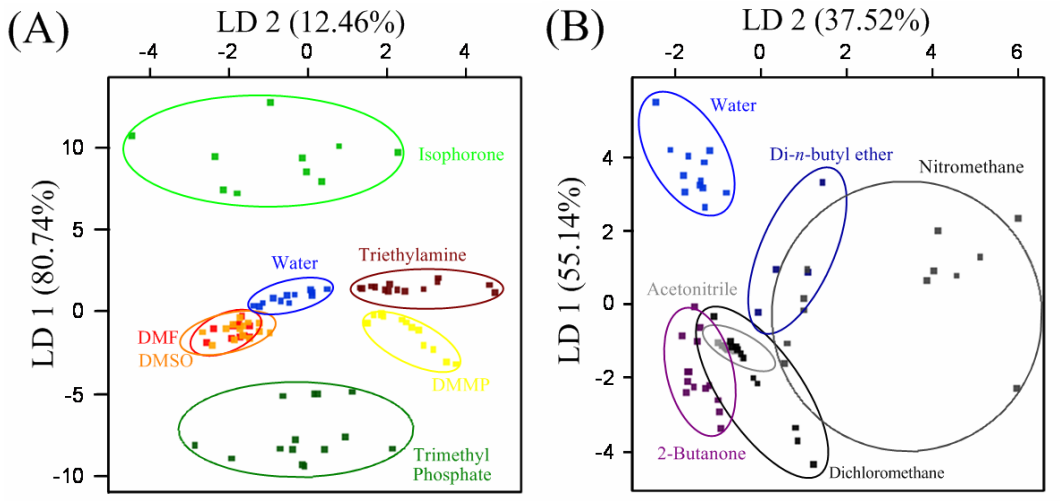

Figure 4-6 (A) Normalized LDA of MPc array sensor responses to strong binding analytes. (B) Normalized LDA of MPc array sensor responses to weak binding analytes.

4.5 CONCLUSION

MPc sensitivities to vapor phase electron donors were found to correlate exponentially with binding enthalpy, consistent with the van't Hoff equation and standard free energy of reaction. MPc sensitivities correlated best with the Lewis base enthalpy scale $-\Delta H^{o}_{BF_3}$, while H_2Pc sensitivities correlated best with the hydrogen bond base enthalpy scale β_2^H. Sensor recovery times t'_{90}, used as an indirect probe of

the analyte desorption rate, were also found to depend exponentially on $-\Delta H^{o}_{BF_3}$ (CoPc, NiPc, CuPc, and ZnPc) and β_2^H (H_2Pc). This behavior is in agreement with the Arrhenius equation. The MPc sensitivities showed significant variance among the different analytes. Sensitivities were compared via two-way ANOVA analysis, and it was found that all MPcs vary from one another in a statistically significant way, consistent with electronic structure arguments. Linear discriminant analysis was used to identify analytes. Single sensor normalization of analyte concentration leads to excellent discrimination and identification of analytes. This technique may be expanded by including a concentration- or mass-specific sensor (such as a QCM or SAW) in the sensor array. MPc sensors show promise as robust, inexpensive chemiresistors for incorporation into electronic-nose type applications.[57]

4.6 ACKNOWLEDGEMENT

Chapter 4 is a reprint in full of the material as it appears in the *Journal of the American Society*, **2008**, *submitted*. Coauthors included C. Colesniuc, J. Park, M. E. Ruidiaz, I. K. Schuller, A. C. Kummel, and W. C. Trogler.

4.7 REFERENCES

(1) Snow, A. W.; Barger, W. R. Phthalocyanine Films in Chemical Sensors. *Phthalocyanines: Properties and Applications;* Lever, A. B. P., Ed; John Wiley and Sons: New York, 1989; Vol. 1, p. 341.

(2) Eley, D. *Nature* **1948**, *162,* 819.

(3) Gould, R. D. *Coord. Chem. Rev.* **1996**, *156,* 237-274.

(4) Guillaud, G.; Simon, J.; Germain, J. *Coord. Chem. Rev.* **1998**, *178,* 1433-1484.

(5) Schollhorn, B.; Germain, J. P.; Pauly, A.; Maleysson, C.; Blanc, J. P. *Thin Solid Films* **1998**, *326,* 245-250.

(6) Germain, J. P.; Pauly, A.; Maleysson, C.; Blanc, J. P.; Schollhorn, B. *Thin Solid Films* **1998,** *333,* 235-239.

(7) Martin, M.; Andre, J. J.; Simon, J. *J. Appl. Phys.* **1983**, *54*, 2792-2794.

(8) Pankow, J. W.; Arbour, C.; Dodelet, J. P.; Collins, G. E.; Armstrong, N. R. *J. Phys. Chem.* **1993**, *97*, 8485-8494.

(9) Hiller, S.; Schlettwein, D.; Armstrong, N. R.; Wohrle, D. *J. Mater. Chem.* **1998**, *8*, 945-954.

(10) Kerp, H. R.; Westerduin, K. T.; van Veen, A. T.; van Faassen, E. E. *J. Mater. Res.* **2001**, *16,* 503-511.

(11) Simon, J.; Andre, J. J. *Molecular Semiconductors* Springer-Verlag: Berlin, **1985**; pp 73-149.

(12) Ho, K. C.; Tsou, Y. H. *Sens. Actuators, B* **2001**, *77,* 253-259.

(13) Zwart, J.; Van Wolput, J. H. M. C. *J. Molec. Cat.* **1979**, *5,* 51-64.

(14) Yahiro, H.; Naka, T.; Kuramoto, J.; Kurohagi, K.; Okada, G.; Shiotani, M. *Microporous Mesoporous Mater.* **2005**, *79,* 291-297.

(15) Barbon, A.; Brustolon, M.; van Faassen, E. E. *Phys. Chem. Chem. Phys.* **2001**, *3*, 5342-5347.

(16) Wright, J. D. *Prog. Surf. Sci.* **1989**, *31,* 1-60.

(17) Lee, Y. L.; Tsai, W. C.; Chang, C. H.; Yang, Y. M. *Appl. Surf. Sci.* **2001**, *172*, 191-199.

(18) Sadaoka, Y.; Jones, T. A.; Gopel, W. *Sens. Actuators, B* **1990**, 148-153.

(19) Miyata, T.; Minami, T. *Appl. Surf. Sci.* **2005**, *244*, 563-567.

(20) Sadaoka, Y.; Jones, T. A.; Gopel, W. *J. Mater. Sci. Lett.* **1989**, *8*, 1288-1290.

(21) Grate, J. W.; Abraham, M. H. *Sens. Actuators, B* **1991,** *3,* 85-111.

(22) Grate, J. W. *Chem. Rev.* **2000,** *100*, 2627-2648.

(23) Liao, M. S.; Kar, T.; Gorun, S. M.; Scheiner, S. *Inorg. Chem.* **2004**, *43*, 7151-7161.

(24) Bohrer, F. I.; Sharoni, A.; Colesniuc, C.; Park, J.; Schuller, I. K.; Kummel, A. C.; Trogler, W. C. *J. Am. Chem. Soc.* **2007**, *129*, 5640-5646.

(25) Maria, P. C.; Gal, J. F. *J. Phys. Chem.* **1985,** *89,* 1296-1304.

(26) Abraham, M. H.; Grellier, P. L.; Prior, D. V.; Morris, J. J.; Taylor, P. J. *J. Chem. Soc. Perkins Trans 2* **1990,** 521-529.

(27) Spadavecchia, J.; Ciccarella, G.; Rella, R. *Sens. Actuators, B* **2005**, *106*, 212-220.

(28) Sibrina, G. V.; Blokhina, S. V.; Ol'kovich, M. V., Borovkov, N. Yu. *Russ. J. Gen. Chem.* **1997**, *67(3)*, 479-484.

(29) Sibrina, G. V.; Blokhina, S. V.; Ol'kovich, M. V., Borovkov, N. Yu. *Russ. J. Gen. Chem.* **1997**, *67(3)*, 439-444.

(30) Bora, M.; Schut, D.; Baldo, M. A. *Anal. Chem.* **2007**, *79*, 3298-3303.

(31) Yang, R. D.; Fruhberger, B.; Park, J.; Kummel, A. C. *Appl. Phys. Lett.* **2006**, *88*, 074104/1-3.

(32) Chen, J. C.; Ju, Y. H.; Liu, C. J. *Sens. Actuators, B* **1999**, *60*, 168-173.

(33) Miller, C. W.; Sharoni, A.; Liu, G.; Colesniuc, C. N.; Fruhberger, B.; Schuller, I. K. *Phys. Rev. B* **2005,** *72,* 104113/1-6.

(34) Lide, D. R., Frederikse, H. P. R., Eds. *CRC Handbook of Chemistry and Physics,* 74th ed.; CRC Press: Ann Arbor, 1993; Section 9.

(35) Tongpool, R.; Yoriya, S. *Thin Solid Films* **2005**, *109,* 7878-7882.

(36) Armstrong, R. A.; Eperjesi, F.; Gilmartin, B. *Ophthal. Physiol. Opt.* **2002**, *22*, 248-256.

(37) Miller, K. A.; Yang, R. D.; Hale, M. J.; Park, J.; Fruhberger, B.; Colesniuc, C. N.; Schuller, I. K.; Kummel, A. C.; Trogler, W. C. *J. Phys. Chem, B* **2006,** *110,* 361-366.

(38) Kolesar, E. S.; Wiseman, T. M. *Anal. Chem.* **1989,** *61,* 2355-2361.

(39) Lee, Y. L.; Tsai, W. C.; Maa, J. R. *Appl. Surf. Sci.* **2001,** *173,* 352-361.

(40) de Haan, A.; Debliquy, M.; Decroly, A. *Sens. Actuators, B* **1999**, *57,* 69-74.

(41) Gritzner, G. *J. Mol. Liquids* **1997,** *73,* 487-500.

(42) Herrebout, W. A.; van der Veken, B. J. *J. Am. Chem. Soc.* **1997,** *119,* 10446-10454.

(43) Shannon, R. D. *Acta Cryst.* **1976**, *A32*, 751-767.

(44) Liao, M. S.; Scheiner, S. *J. Chem. Phys.* **2001**, *114*, 9780-9791.

(45) Garrone, E.; Areán, C. O. *Chem. Soc. Rev.* **2005**, *34*, 846-857.

(46) Espenson, J. H. *Chemical Kinetics and Reaction Mechanisms* McGraw-Hill, Inc.: New York, 1981.

(47) Atkins, P.; Jones, L. *Chemistry: Molecules, Matter, and Change 4th Ed.* W. H. Freeman and Co.: New York, 2000.

(48) Liu, C.J.; Hsieh, J. C.; Ju, Y. H. *J. Vac. Sci. Technol., A* **1996**, *14(3),* 753-756.

(49) Albert, K. J.; Lewis, N. S.; Schauer, C. L.; Sotzing, G. A.; Stitzel, S. E.; Vaid, T. P.; Walt, D. R. *Chem. Rev.* **2000**, *100,* 2595-2626.

(50) Irving, H.; Williams, R. J. P. *Nature* **1948**, *162*, 746-747.

(51) Shaffer, R. E.; Rose-Pehrsson, S. L.; McGill, R. A. *Anal. Chim. Acta* **1999**, *384*, 305-317.

(52) Greene, N. T.; Morgan, S. L.; Shimizu, K. D. *Chem. Commun.* **2004**, 1172-1173.

(53) Shaffer, R. E.; Rose-Pehrsson, S. L.; McGill, R. A. *Field Anal. Chem. Tech.* **1998**, *2*, 179-192.

(54) Szczurek, A.; Maciejewska, A. *Talanta* **2004**, *64*, 609-617.

(55) Feldhoff, R.; Saby, C. A.; Bernadet, P. *Analyst* **1999**, *124*, 1167-173.

(56) Pardo, M.; Sisk, B. C.; Sberveglieri, G.; Lewis, N. S. *Sens. Actuators, B* **2006**, *115*, 647-655.

(57) Slater, J. M.; Paynter, J.; Watt, E. J. *Analyst* **1993**, *118*, 379-384.

4.8 APPENDIX

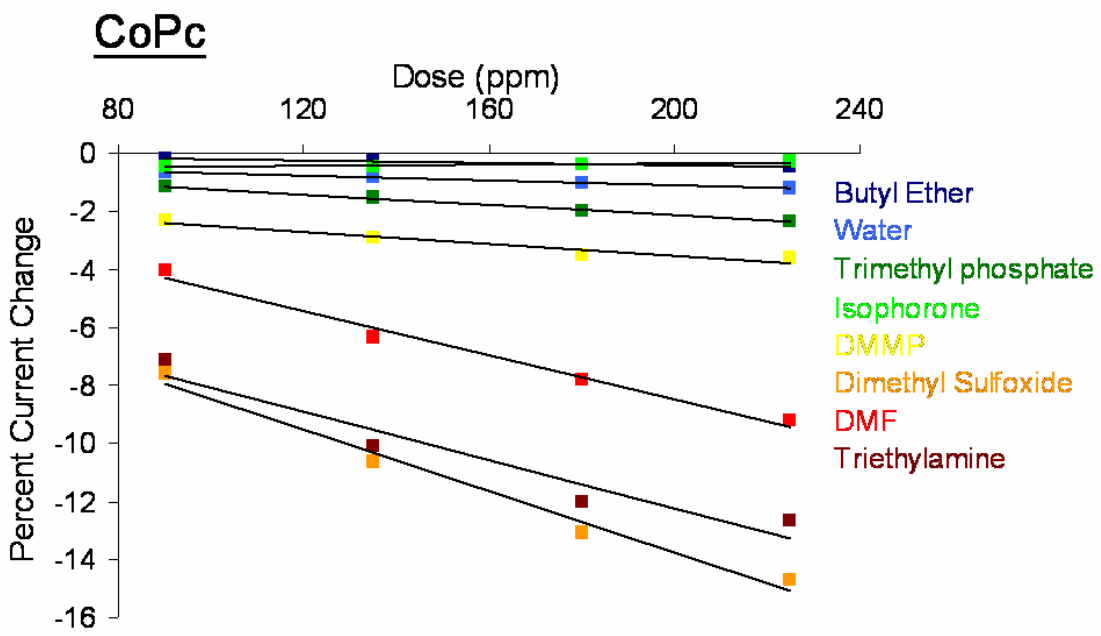

Figure 4-7A CoPc sensor responses correlate linearly with analyte concentration; the slopes (%·ppm^{-1}, $R^2 \geq 0.97$) are defined as the CoPc sensitivity to that analyte. Some analytes have been omitted for clarity.

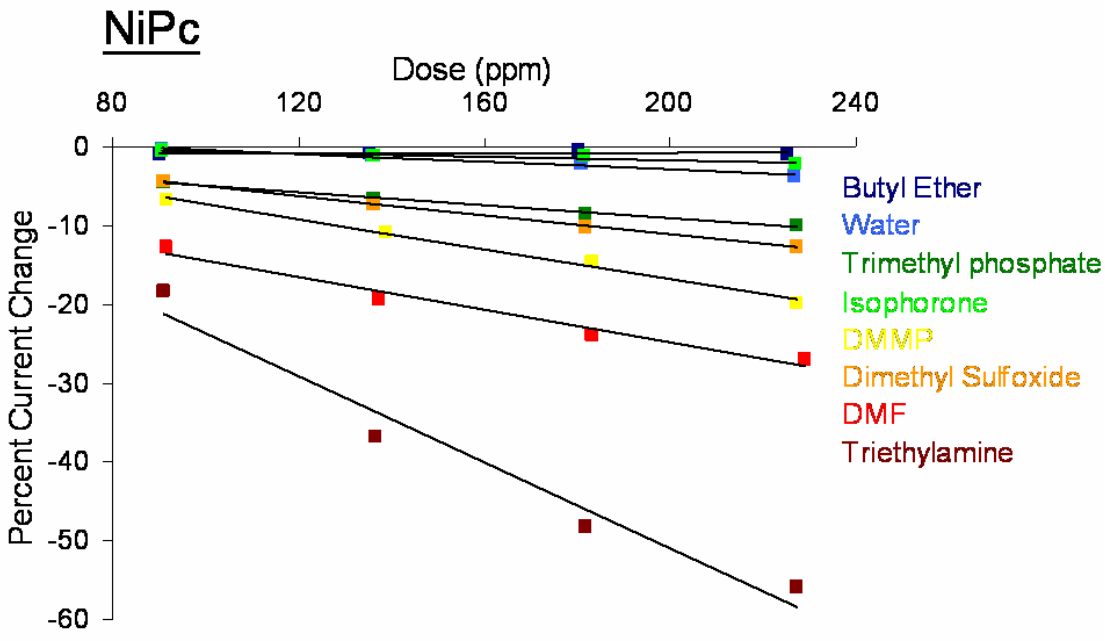

Figure 4-7B NiPc sensor responses correlate linearly with analyte concentration; the slopes (%·ppm^{-1}, $R^2 \geq 0.97$) are defined as the NiPc sensitivity to that analyte. Some analytes have been omitted for clarity.

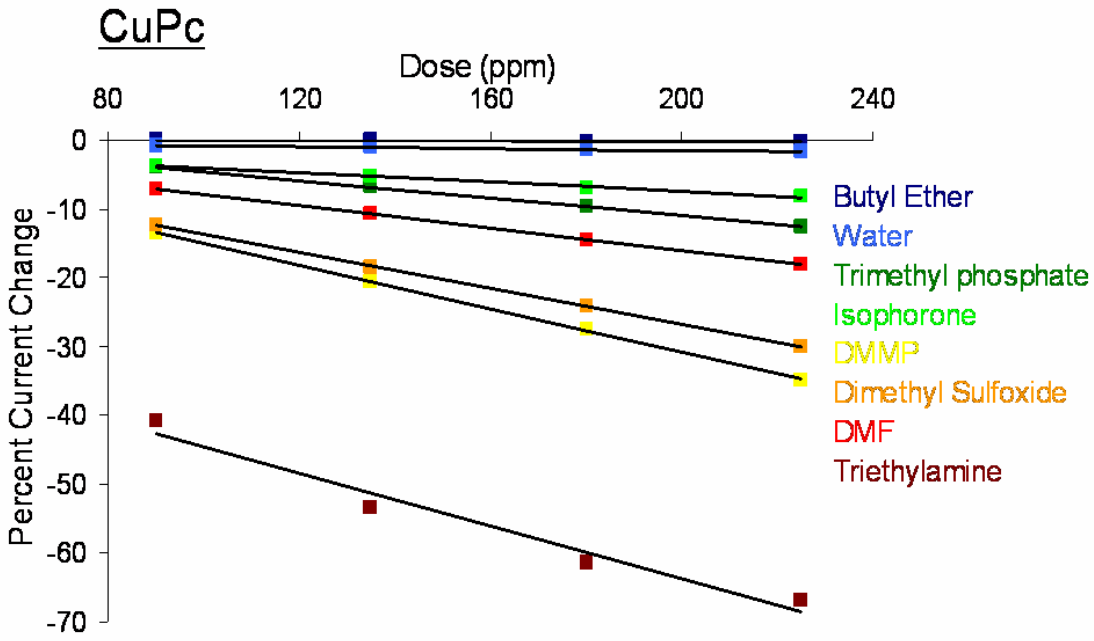

Figure 4-7C CuPc sensor responses correlate linearly with analyte concentration; the slopes (%·ppm^{-1}, $R^2 \geq 0.97$) are defined as the CuPc sensitivity to that analyte. Some analytes have been omitted for clarity.

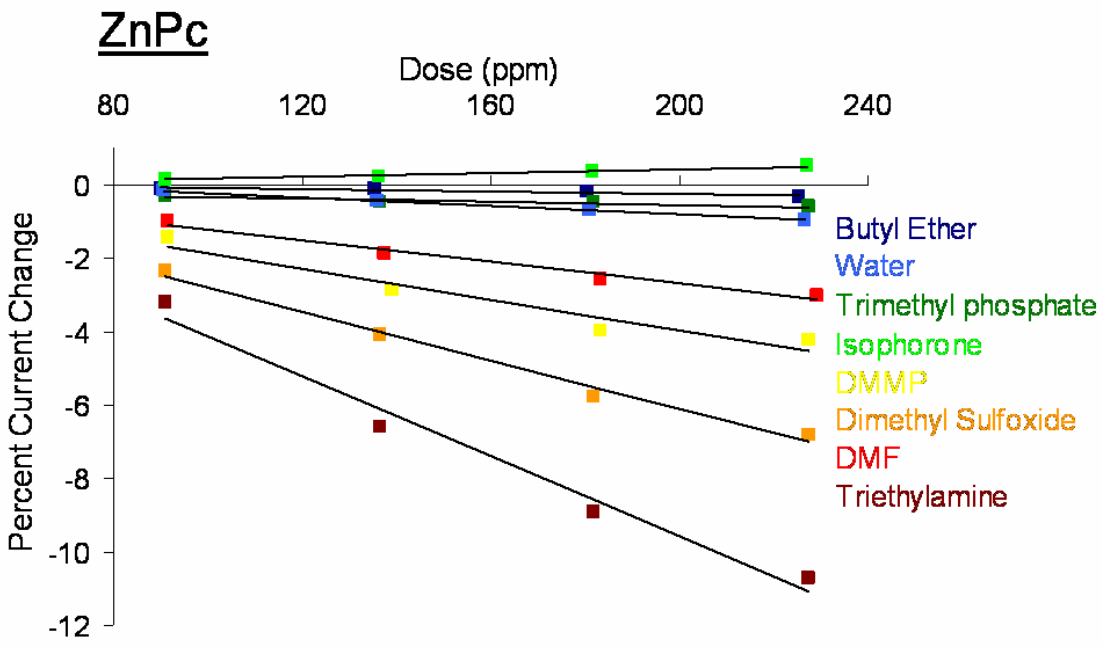

Figure 4-7D ZnPc sensor responses correlate linearly with analyte concentration; the slopes (%·ppm^{-1}, $R^2 \geq 0.97$) are defined as the ZnPc sensitivity to that analyte. Some analytes have been omitted for clarity.

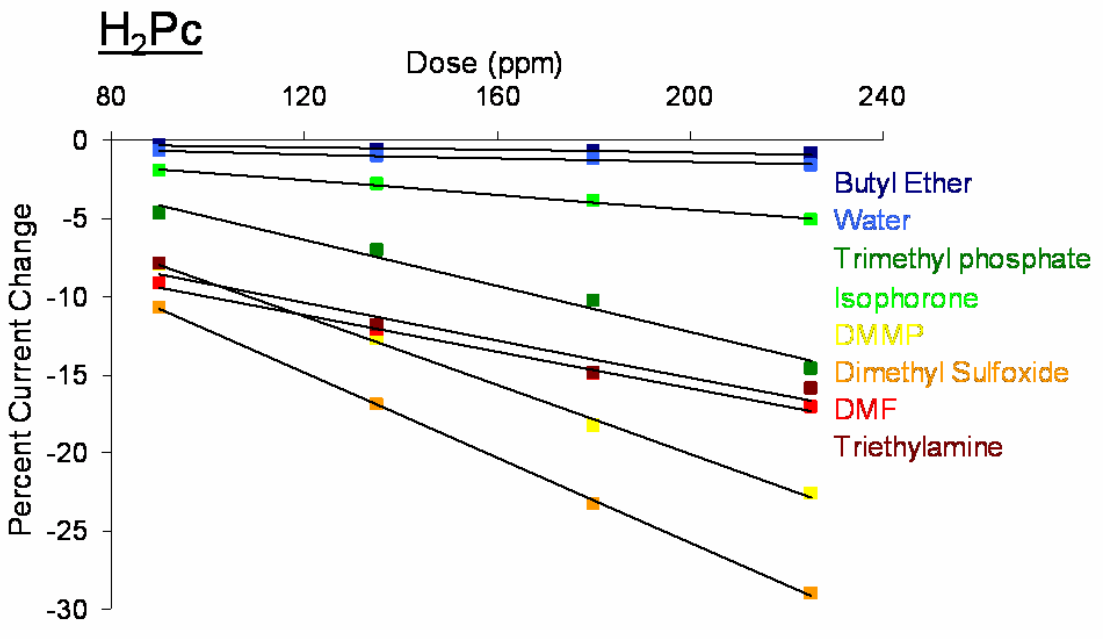

Figure 4-7E H_2Pc sensor responses correlate linearly with analyte concentration; the slopes (%·ppm^{-1}, $R^2 \geq 0.97$) are defined as the H_2Pc sensitivity to that analyte. Some analytes have been omitted for clarity.

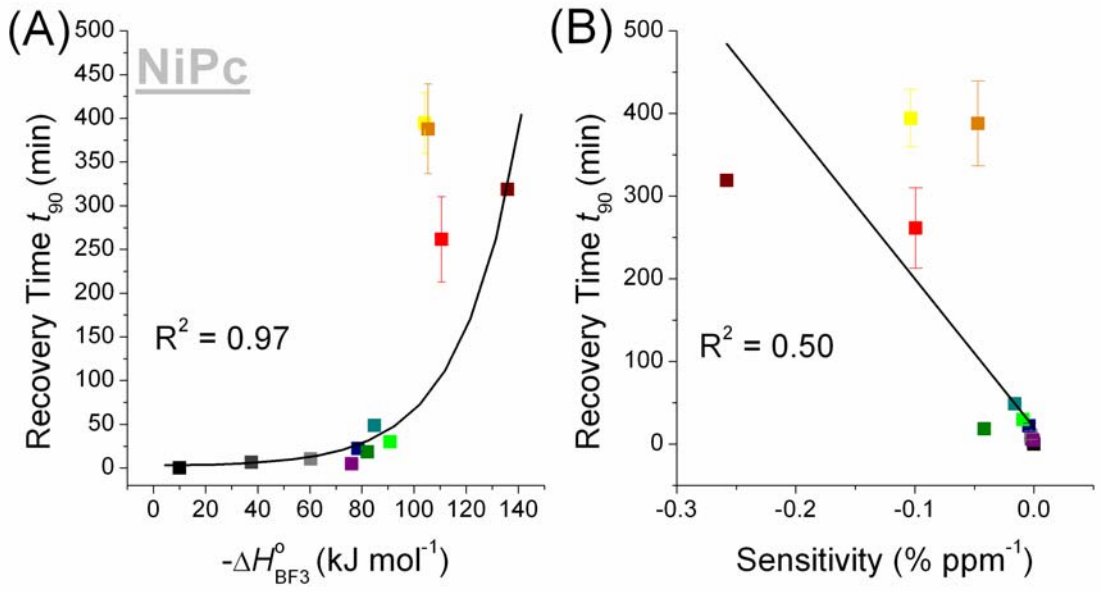

Figure 4-8A (A) Exponential dependence of NiPc recovery times $t_{90}^{'}$ on Lewis basicity $-\Delta H^{o}_{BF_3}$. (B) Linear dependence of NiPc recovery times $t_{90}^{'}$ on NiPc sensitivity (% ppm^{-1}). Color coding of analytes is found in Table 4-1.

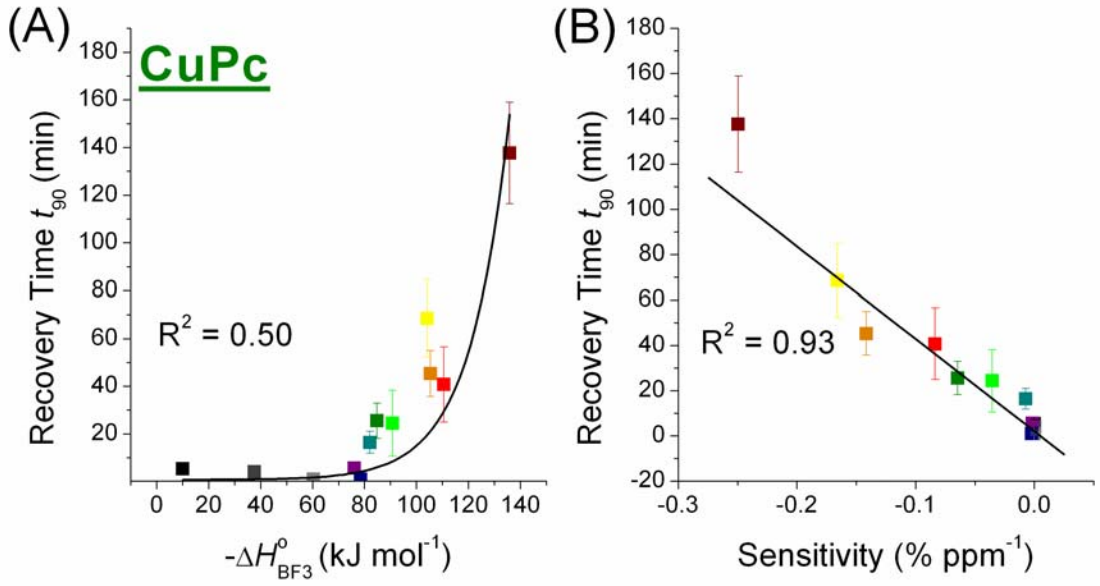

Figure 4-8B (A) Exponential dependence of CuPc recovery times $t_{90}^{'}$ on Lewis basicity $-\Delta H^{o}_{BF_3}$. (B) Linear dependence of CuPc recovery times $t_{90}^{'}$ on CuPc sensitivity (% ppm^{-1}). Color coding of analytes is found in Table 4-1.

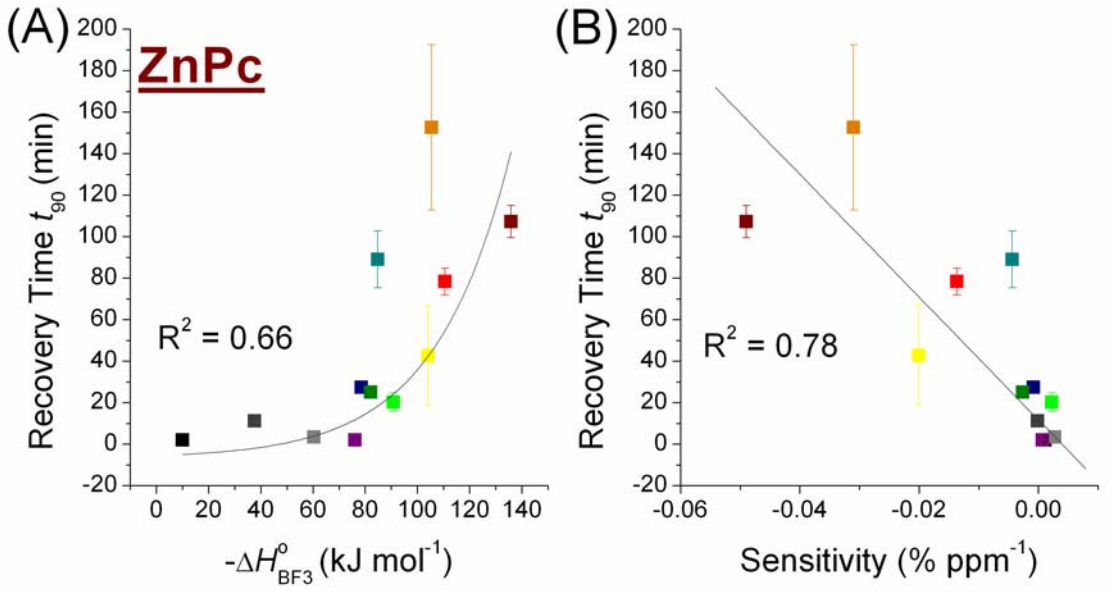

Figure 4-8C (A) Exponential dependence of ZnPc recovery times $t_{90}^{'}$ on Lewis basicity $-\Delta H^{o}_{BF_3}$. (B) Linear dependence of ZnPc recovery times $t_{90}^{'}$ on ZnPc sensitivity (% ppm^{-1}). Color coding of analytes is found in Table 4-1.

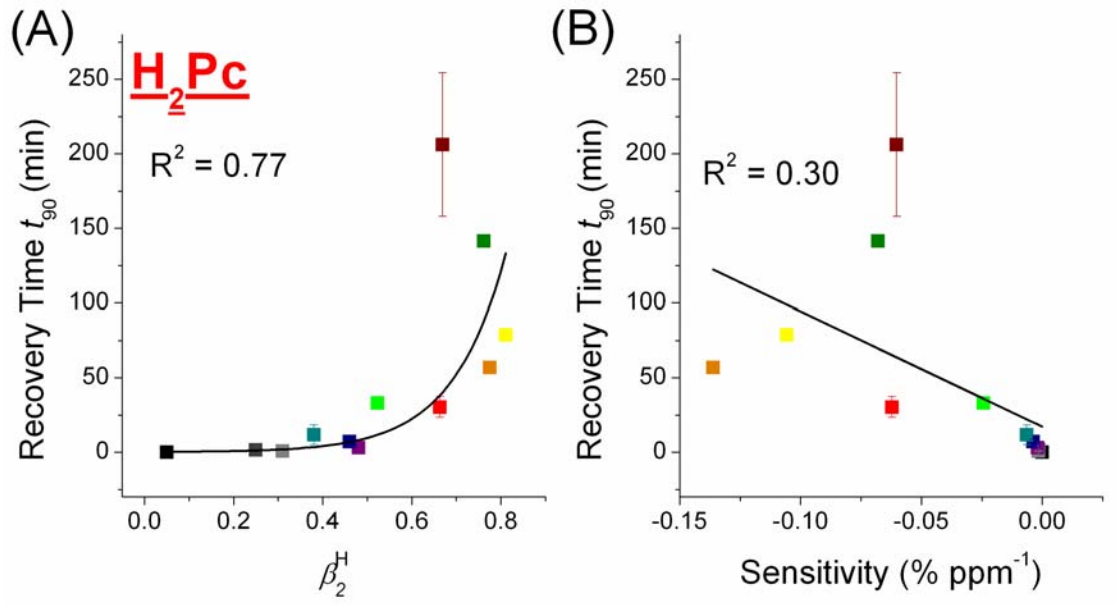

Figure 4-8D (A) Exponential dependence of H_2Pc recovery times $t_{90}^{'}$ on hydrogen bond basicity β_2^H. (B) Linear dependence of H_2Pc recovery times $t_{90}^{'}$ on H_2Pc sensitivity (% ppm^{-1}). Color coding of analytes is found in Table 4-1.

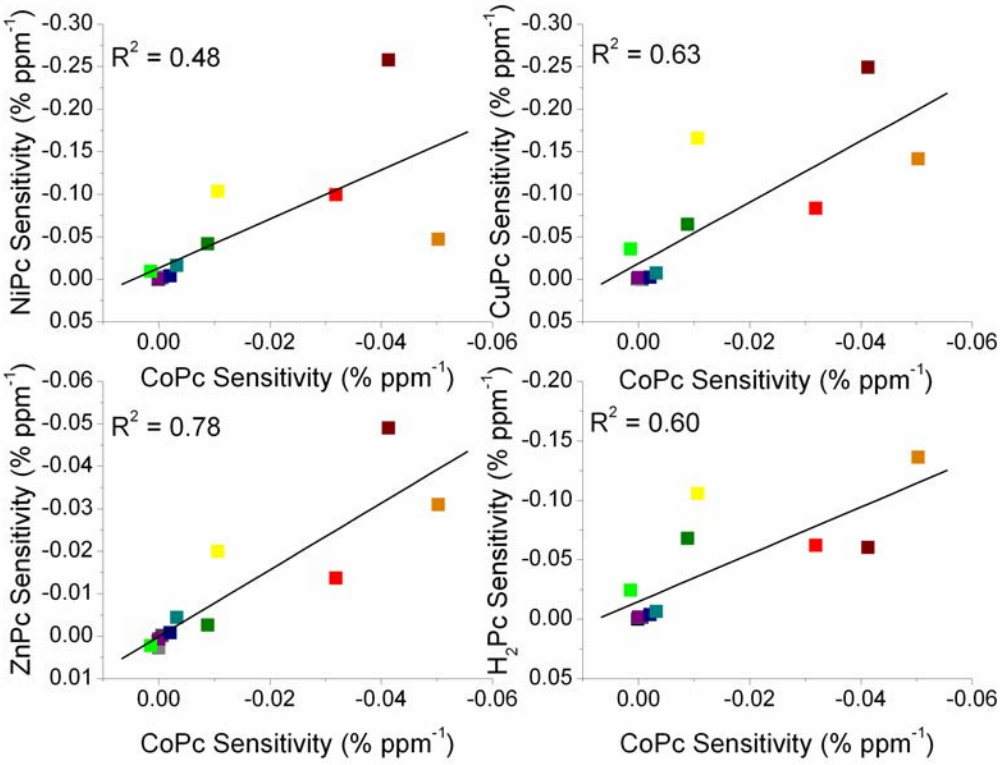

Figure 4-9A Comparison of CoPc sensitivities (% ppm^{-1}) versus sensitivities of other MPcs. Color coding of analytes is found in Table 4-1.

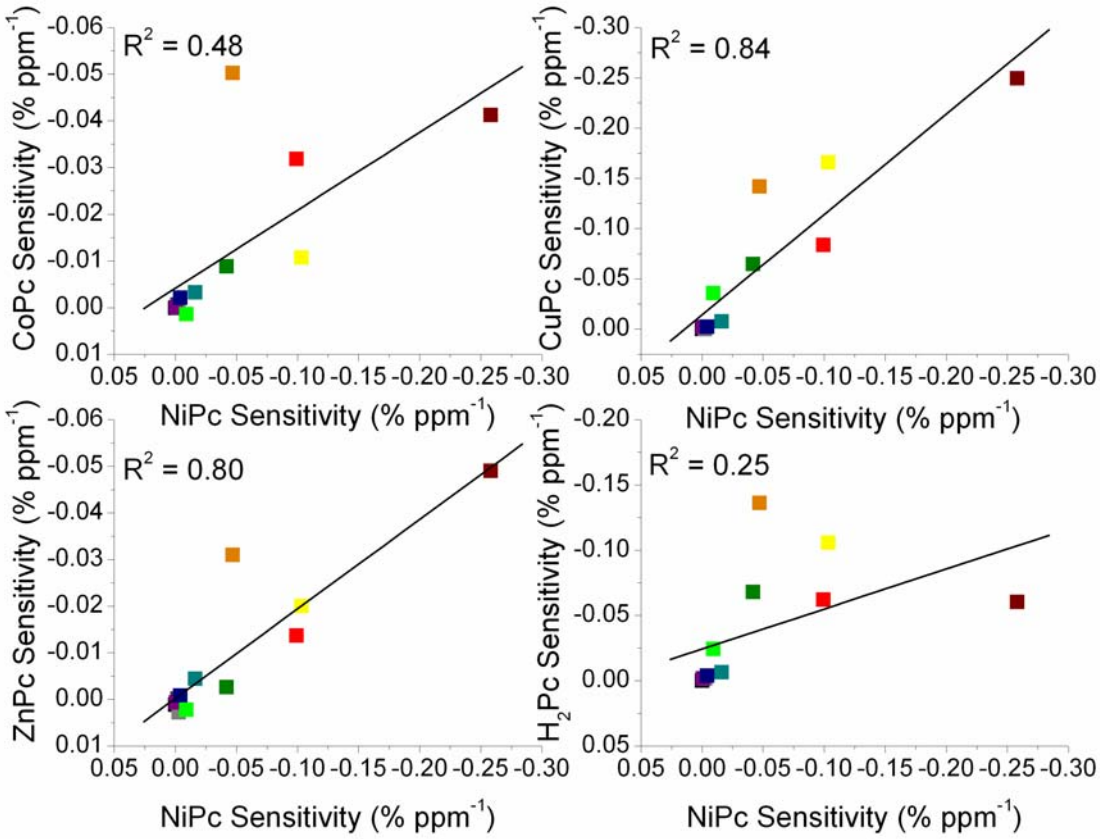

Figure 4-9B Comparison of NiPc sensitivities (% ppm^{-1}) versus sensitivities of other MPcs. Color coding of analytes is found in Table 4-1.

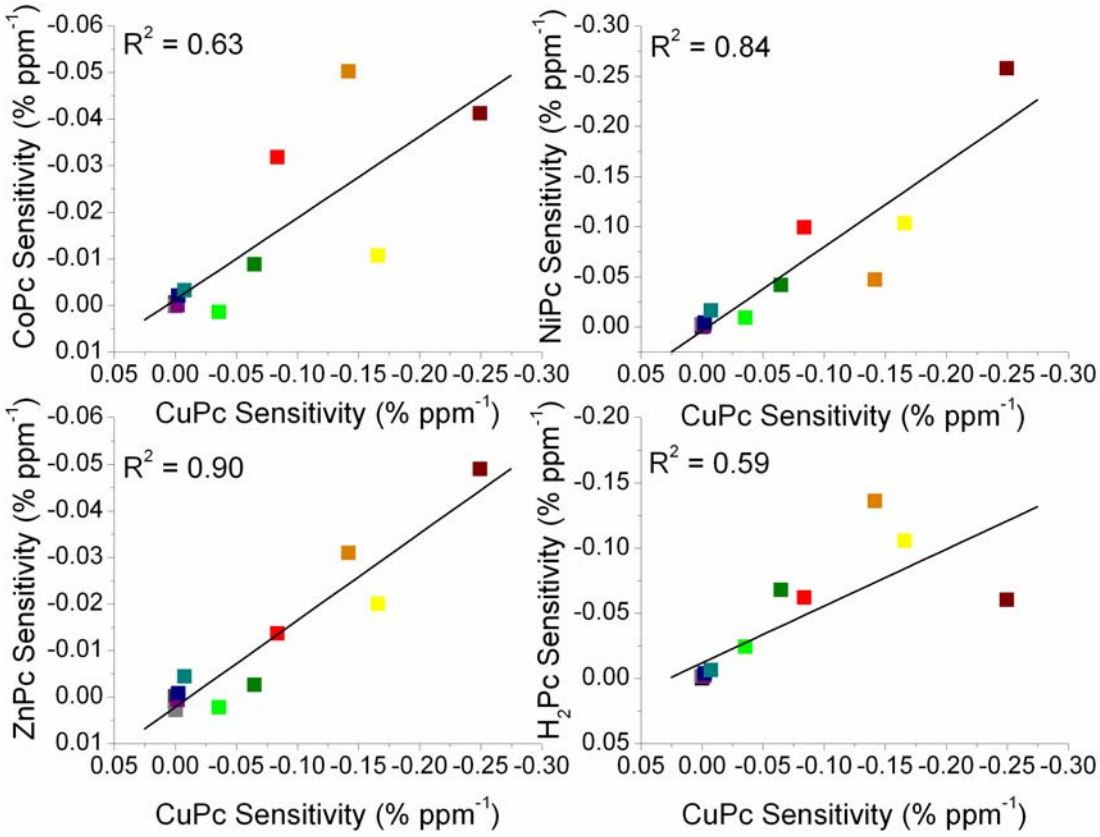

Figure 4-9C Comparison of CuPc sensitivities (% ppm^{-1}) versus sensitivities of other MPcs. Color coding of analytes is found in Table 4-1.

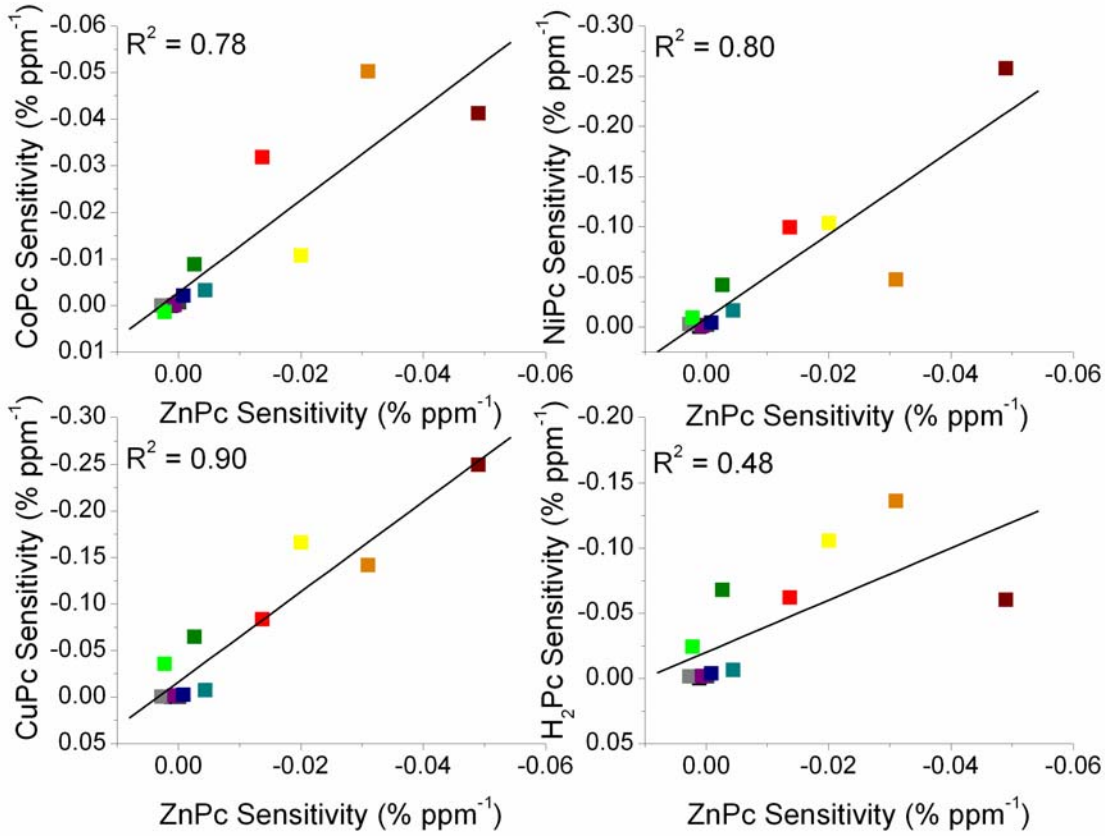

Figure 4-9D Comparison of ZnPc sensitivities (% ppm^{-1}) versus sensitivities of other MPcs. Color coding of analytes is found in Table 4-1.

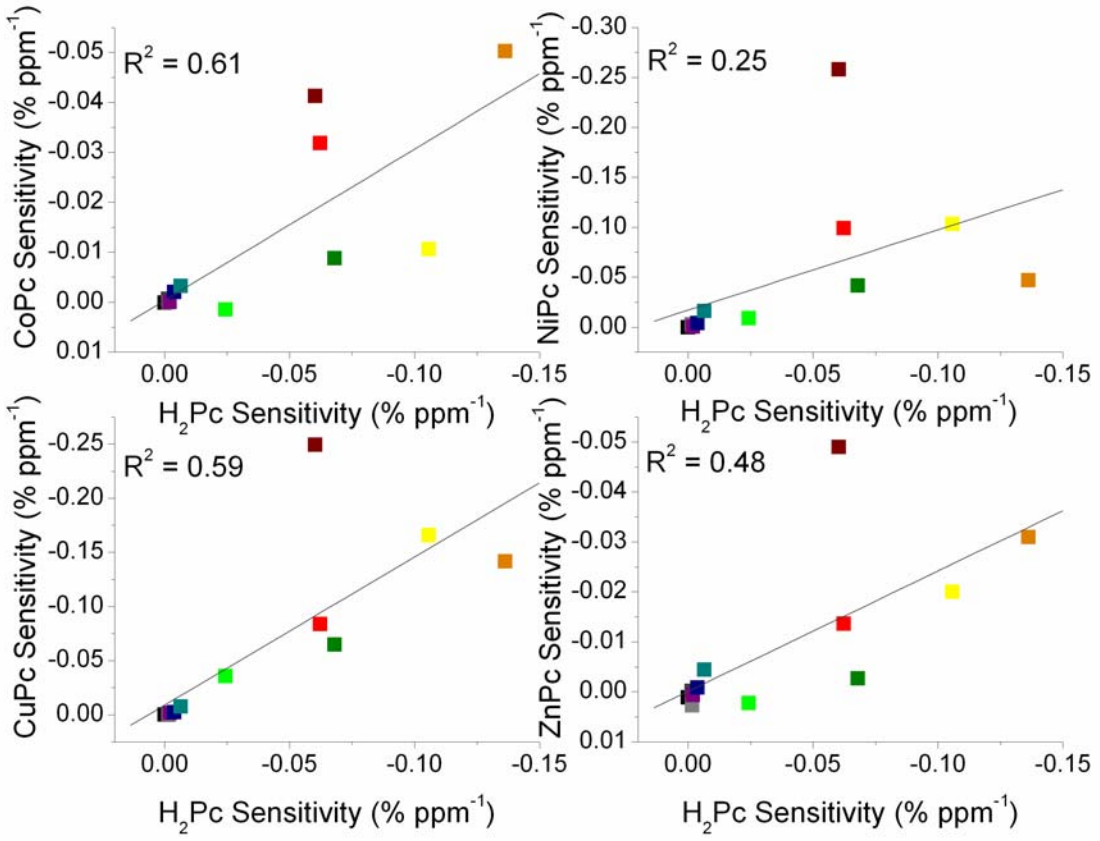

Figure 4-9E Comparison of H_2Pc sensitivities (% ppm^{-1}) versus sensitivities of other MPcs. Color coding of analytes is found in Table 4-1.

Table 4-3 Sensitivities (% ppm^{-1}) of all MPcs to all analytes; data presented in Figure 4-3 tabulated.

Analyte	**CoPc (% ppm^{-1}) x 10^{-3}**	**NiPc (% ppm^{-1}) x 10^{-3}**	**CuPc (% ppm^{-1}) x 10^{-3}**	**ZnPc (% ppm^{-1}) x 10^{-3}**	**H_2Pc (% ppm^{-1}) x 10^{-3}**
Dichloromethane	0.09 ± 0.01	0	-0.1 ± 0.1	1.1 ± 0.08	0
Nitromethane	-0.6 ± 0.05	-1.93 ± 0.4	0.04 ± 0.06	-0.2 ± 0.06	-1.5 ± 0.2
Acetonitrile	-0.01 ± 0.01	-2.73 ± 0.5	-0.3 ± 0.01	2.8 ± 0.1	-1.7 ± 0.07
2-Butanone	-0.04 ± 0.04	-1.17 ± 0.2	-1.8 ± 0.4	0.8 ± 0.1	-2.0 ± 0.1
Di-n-butyl ether	-2.1 ± 0.3	-4.13 ± 0.2	-2.4 ± 0.1	-0.4 ± 0.1	-3.8 ± 0.9
Trimethyl Phosphate	-8.8 ± 5.1	-44.6 ± 15.7	-64.7 ± 21.2	-2.7 ± 0.6	-67.9 ± 2.1
Water[c]	-3.2 ± 0.5	-16.2 ± 1.6	-7.4 ± 2.2	-4.4 ± 0.2	-6.5 ± 0.5
Isophorone	1.4 ± 0.2	-17.7 ± 7.4	-35.6 ±11.7	2.2 ± 0.4	-24.3 ± 8.1
DMMP[d]	-10.7 ± 2.3	-134.8 ± 27.3	-165.9 ± 24.1	-18.3 ± 1.4	-105.7 ± 9.5
DMSO	-50.3 ± 3.1	-56.5 ± 9.8	-141.7 ± 53.0	-31.0 ± 3.4	-136.2 ± 6.9
DMF	-31.9 ± 2.0	-120.8 ± 19.8	-83.6 ± 25.5	-13.7 ± 4.7	-62.3 ± 0.6
Triethylamine	-41.3 ± 4.4	-272.4 ± 15.6	-249.4 ± 22.6	-49.0 ± 7.8	-60.3 ± 1.6

[c] The $-\Delta H^{o}_{BF_3}$ value for water was determined from fits of the experimental data for all MPcs in the present study.

[d] The $-\Delta H^{o}_{BF_3}$ value for DMMP was also determined from experimental fits of all MPcs in the present study; the β_2^H value was estimated from experimental values for dimethyl ethylphosphonate and diethyl methylphosphonate.

Table 4-4 Correlation constants for dependence of MPc recovery times $t_{90}^{'}$ on analyte basicity (Figure 4-4A) and on MPc sensitivity (Figure 4-4B).

MPc	R^2 (recovery time $t_{90}^{'}$ vs. basicity)	R^2 (recovery time $t_{90}^{'}$ vs. MPc sensitivity)
CoPc ($-\Delta H_{BF_3}^{o}$)	0.86	0.78
NiPc ($-\Delta H_{BF_3}^{o}$)	0.94	0.79
CuPc ($-\Delta H_{BF_3}^{o}$)	0.50	0.93
ZnPc ($-\Delta H_{BF_3}^{o}$)	0.72	0.83
H_2Pc ($-\Delta H_{BF_3}^{o}$)	0.70	
H_2Pc (β_2^H)	0.77	0.30

Table 4-5 Recovery times $t_{90}^{'}$ (min) for 225 ppm doses for each analyte (Figures 4-4, 4-8).

Analyte	CoPc $t_{90}^{'}$	NiPc $t_{90}^{'}$	CuPc $t_{90}^{'}$	ZnPc $t_{90}^{'}$	H_2Pc $t_{90}^{'}$
Dichloromethane	1.60 ± 0.60	0	5.36 ± 1.79	2.06 ± 0.98	0
Nitromethane	7.73 ± 1.14	6.53 ± 0.51	4.09 ± 1.42	11.23 ± 1.98	1.51 ± 0.01
Acetonitrile	2.48 ± 0.17	10.56 ± 5.18	1.04 ± 0.47	3.50 ± 0.15	0.725 ± 0.36
2-Butanone	10.09 ± 4.09	4.77 ± 1.73	5.64 ± 0.69	2.08 ± 1.26	3.06 ± 1.06
Di-n-butyl ether	25.94 ± 19.34	22.19 ± 3.14	0.98 ± 0.77	27.40 ± 2.19	7.045 ± 1.65
Trimethyl Phosphate	105.94 ± 38.05	48.86 ± 1.43	25.53 ± 7.38	89.08 ± 13.72	141.51 ± 3.83
Water	9.99 ± 2.12	18.57 ± 4.27	16.43 ± 4.56	25.09 ± 0.85	11.69 ± 6.48
Isophorone	66.48 ± 0.44	29.79 ± 3.03	24.40 ± 13.83	20.27 ± 4.55	33.06 ± 1.53
DMMP	72.94 ± 6.84	394.35 ± 34.67	68.46 ± 16.19	42.75 ± 24.05	78.8 ± 4.36
DMSO	159.45 ± 6.64	387.83 ± 51.24	45.28 ± 9.59	152.70 ± 39.79	56.98 ± 0.12
DMF	95.96 ± 4.05	261.44 ± 48.79	40.73 ± 15.75	78.35 ± 6.46	30.27 ± 6.96
Triethylamine	172.06 ± 7.91	318.84 ± 2.77	137.64 ± 21.29	107.32 ± 7.71	206.16 ± 48.24

CHAPTER V

SELECTIVE VAPOR-PHASE DETECTION OF PEROXIDES WITH CHEMIRESISTIVE METAL PHTHALOCYANINE NANOFILMS

5.1 ABSTRACT

The use of hydrogen peroxide as a precursor for improvised explosives has made peroxide detection a topic of critical importance. Chemiresistor arrays consisting of 50 nm thick films of metallophthalocyanines (MPcs, M = Fe, Co, Ni, Cu, Zn, and H_2) are shown to be redox selective vapor sensors of H_2O_2 and di-*t*-butyl peroxide. MPc sensor films were deposited on interdigitated gold electrodes by organic molecular beam epitaxy and measured in the space-charge limited current regime at constant voltage while dosing the films with peroxide vapor. The sensor responses were analyzed in both the kinetic regime (5 min doses) and the saturation regime (30 min doses). H_2O_2 was shown to decrease currents in CoPc sensors while it increased currents in FePc, NiPc, CuPc, and H_2Pc sensors, with a detection limit of 50 ppb. All films were stable against bulk decomposition in the presence of H_2O_2 with the exception of FePc, which degraded slowly at long exposures. Di-*t*-butyl peroxide was shown to decrease currents in CoPc sensors and increase currents in FePc, NiPc, CuPc, and ZnPc sensors, with a detection limit of 250 ppb. This study presents the first example of analytes that can both decrease and increase current in an array of MPc sensors by variation of the metal center. Oxidation and reduction of peroxides

via catalysis at the phthalocyanine surface is consistent with the pattern of sensor responses. Differential analysis by redox contrast of a small array of sensors thus uniquely identifies peroxide vapors. Metallophthalocyanine chemiresistors offer a potential advantage over existing peroxide vapor detection technologies in durability and selectivity in a greatly decreased sensor package size.

5.2 INTRODUCTION

Vapor phase monitoring of peroxides is of critical importance for military and industrial safety applications. Hydrogen peroxide (H_2O_2) is a common oxidant, used for paper bleaching and specialty chemical manufacture, as well as a chemical disinfectant.[1] Hydrogen peroxide is quite toxic; in the vapor phase 75 ppm (which may be present in the vapor over 30% aqueous H_2O_2) is immediately hazardous to health, and the OSHA permissible exposure limit (PEL) for an 8 hour period is 1 ppm.[2-3] Recent incidents in England and Germany involving improvised peroxide based explosives, and the employment of H_2O_2 in liquid explosive mixtures, have made peroxide detection crucial to counterterrorism efforts.[4-6] Current detection methods of peroxide based explosives, such as triacetone triperoxide (TATP) and hexamethylene triperoxide diamine (HMTD), rely on the photochemical reaction of the organic peroxide with UV light (λ = 254 nm) to form H_2O_2. The samples are then analyzed through the use of HPLC in combination with FTIR or fluorescence detectors,[7-8] enzymatic fluorochemical assays[9] (often interfaced with HPLC),[10-11] or amperometric (solution-phase) detection;[12] however, these systems are generally limited to solid and

liquid samples. Therefore, there is an urgent need for rapid vapor-phase detection of peroxides with a simple electronic sensor.

Phthalocyanines, both metalated (MPcs; M = p-, d-, and f-block metals) and metal-free (H_2Pc), are a class of organic p-type semiconductors that have been explored widely as inexpensive, robust chemiresistive sensors.[13-16] MPcs exhibit a potential for chemical selectivity through variation of the metal center[17] and through substitution of functional groups on the organic ring.[18-19] Conductivity in MPc films is strongly influenced by oxidizing[20] and reducing[21] gases. It has been shown that p-type MPcs are insulating in dark high vacuum environments and become semiconducting upon exposure to air.[22-24] This conductivity has been attributed to the formation of charge transfer complexes by coordination of O_2 to MPc metal centers at the air/phthalocyanine boundary, forming MPc^+ and O_2^- species and injecting charge carriers (holes) into bulk phthalocyanine.[25-27] These superoxide adducts have been detected for multiple MPcs via EPR studies.[28-30] In H_2Pc, this conductivity has been attributed to O_2 adsorption on the inner *meso*-nitrogens, leading to more modest conductivity increases.[15] This type of chemical sensitivity has direct bearing on the mechanism of chemical sensing in MPcs.

The majority of MPc sensing studies have focused on the detection of oxidizing gases such as ozone, NO_X, and Cl_2.[31-38] MPc (M = H_2, Pb, Fe, Co, Ni, Cu, Zn, and others) films universally exhibit current increases upon exposure to these gases; the films are easily oxidized, forming charge-transfer complexes which inject holes and increase film currents. These oxidants have been proposed to bind at the

metal center and on the outer carbons of the organic rings.[15] Exposure of MPc films to electron-donating (reducing) gases such as H_2O and NH_3 results in the opposite effect, a decrease in current upon analyte binding.[16,18,21] Previously, we have shown that the sensor responses of CoPc films to electron-donating analytes correlate with the Lewis basicity of the analyte, while the sensor responses of H_2Pc films to these same analytes correlate with the hydrogen-bond basicity of the analyte.[39] This strongly suggests that electron donor gases coordinate to the central cavity of the phthalocyanine, donating electron density into the film and thereby acting as counter dopants to O_2. At longer exposure times, O_2 may be displaced from the sensor film, irreversibly destroying charge carriers.

The interactions of MPcs with hydrogen peroxide have been extensively studied using solution-phase electrochemical techniques, but vapor sensing has not been explored. Most previous research was focused on detection of biomolecules in complex solutions; these molecules were exposed to their respective oxidases and chemically modified electrodes (CMEs) incorporating MPcs were used to detect the peroxide products.[40-41] For example, CMEs with surface CoPc molecules have been used to both oxidize and reduce hydrogen peroxide at positive and negative potentials, respectively.[42-43] The mechanism of CoPc-catalyzed decomposition of H_2O_2 has been explored, and it has been proposed that redox-active cobalt metal centers (Co^{3+}, Co^{2+}, and a transient Co^{+} state) are responsible for this activity.[42,44] Isotopic studies have shown that the peroxide O-O bond remains intact on oxidation, suggesting a catalase-type model for reactivity supported by the fact that the reaction is second-order with

respect to H_2O_2.[44-45] A similar mechanism has been proposed for FePc,[46] which has been shown to be an even more potent catalyst for H_2O_2 oxidation and reduction.[47-48] Other MPcs (M = H_2, Zn, Cu, Ni, Mn, Cr, Ru, and Pb) have been explored as possible catalysts for the oxidation of H_2O_2, but showed minimal activity in voltammetric studies.[49]

Few studies are available examining the interactions of MPcs with organic peroxides, which are useful as mimics for peroxide based explosives such as TATP and HMTD. Voltammetric studies of FePc modified carbon electrodes were shown to catalytically reduce some alkyl hydroperoxides, but showed minimal activity towards dialkyl peroxides.[50] Similar studies of CoPc modified carbon electrodes reported oxidation of alkyl hydroperoxides.[51] EPR studies of ZnPc and AlPc were consistent with the cleavage of dialkyl peroxides into highly reactive alkoxy radicals, which is promising for the chemiresistive detection of these peroxides.[52]

In this report, chemiresistors using 50 nm thick films of metallophthalocyanines (M = Fe, Co, Ni, Cu, Zn, and H_2) are examined as sensors for vapor phase peroxides. Sensor currents were measured at constant voltage during exposure to doses of 30% H_2O_2(aq) and di-*t*-butyl peroxide vapor. In order to separate the water response from the hydrogen peroxide response, constant humidity was maintained for some experiments. Sensor responses were analyzed in the kinetic (5 min dose) and saturation (30 min dose) regimes to determine relative sensitivities and detection limits. The mechanism of interaction between vapor phase peroxides and MPcs is proposed.

5.3 EXPERIMENTAL

5.3.1 Sensor Fabrication

Metallophthalocyanine sensors were fabricated as reported previously[39] using Au interdigitated electrodes (IDEs) prepared by standard photolithography and lift-off processing on thermally grown SiO_2 (thickness of 1 μm) on (100) Si substrates. The electrodes consist of 45 pairs of fingers with 5 μm channel spacing and an electrode width of 2 mm. Six IDEs were fabricated on each substrate, with excellent sensor reproducibility. FePc (Aldrich, 90%), CoPc (Aldrich, 97%), NiPc (Aldrich, 85%), CuPc (Aldrich, 97%), ZnPc (Acros, 98%), and H_2Pc (Aldrich, 98%) were purified via multiple zone sublimations at 400 ^oC and 10^{-5} Torr. Films of 50 nm thickness were deposited on IDEs via organic molecular beam epitaxy (OMBE) in a UHV chamber with a base pressure of $2x10^{-10}$ Torr. Film growth rate and thickness were monitored by QCM. Substrate temperature during deposition was held constant at 25.0 ± 1.0 ^oC. The devices were stored at 10^{-3} Torr for 48 h until use. Because air doping is essential for conductivity, fresh devices have lower conductivities, and the 48 h waiting period significantly increased (~5x) the sensor conductivity. Film thickness was confirmed by low angle XRD measurements on a Rigaku RU-200B diffractometer using Cu K_α radiation.[53]

5.3.2 Device Measurements

Chemical responses of the MPc sensors were measured in a testing chamber as previously reported.[39] The IDEs were wire-bonded to gold leads on ceramic chip mounts purchased from Spectrum Semiconductor Materials Inc. (Figure 5-1). Two sensor arrays could be simultaneously placed in the chamber, for a total of twelve sensors. The internal temperature of the chamber was controlled by coolant lines connected to a Haake F8 constant temperature bath; during dosing the chamber temperature was maintained at 50.0 ± 0.1 ^{o}C. A Keithley 6517/6521 multi-channel electrometer was used both as voltage source and ammeter. Photoconductivity was allowed to decay for 24 h before testing.

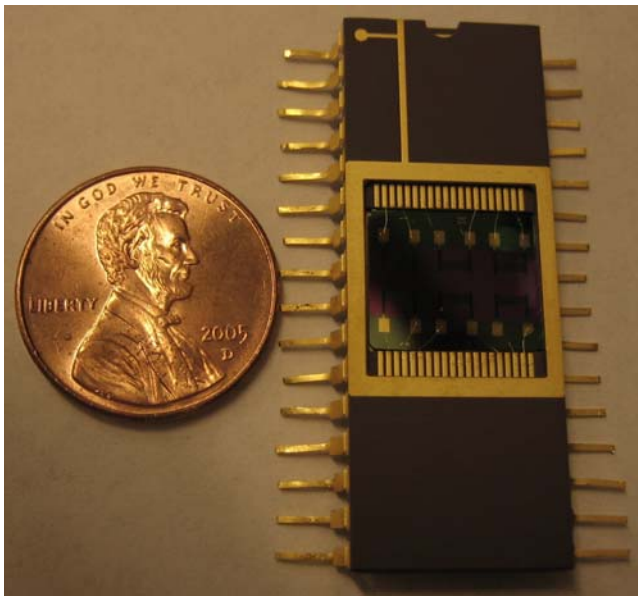

Figure 5-1 Image of a CoPc sensor array containing six microsensors (50 nm thick Au electrodes, 45 interdigitated pairs of fingers, 5 μm channel spacing, on a 1 μm thick SiO_2 substrate) wirebonded in a ceramic package.

Zero grade air was used as the carrier gas with a constant flow rate of 500 sccm (standard cm^3 per minute) applied during the dosing/purging cycle. Mass flow controllers (MKS Instruments, Inc. Model 1479A, 10 sccm and 1000 sccm) were used in conjunction with impinger flasks to introduce known concentrations of analytes into the sensor chamber. Analyte concentrations were controlled by temperature, flow rate, and dilution in the carrier gas. Solenoid valves were placed before and after each bubbler to prevent cross contamination of analytes, and a four-way valve was used to saturate the carrier gas with analyte vapor before introduction into the chamber. A Labview VI program was used to control all instruments and record data.

The analytes measured in the present study included hydrogen peroxide and di-*t*-butyl peroxide. Pure hydrogen peroxide is unavailable commercially due to the fact that it is toxic (OSHA permissible exposure limit = 1 ppm, NIOSH immediately dangerous to life and health limit = 75 ppm),[2] an explosion hazard,[54] and hygroscopic.[55] Therefore, 30 wt% H_2O_2 in water (Acros) was used for vapor dosing. 30% H_2O_2(aq) was used as purchased with a fresh solution for every dosing run. Hydrogen peroxide solutions were assayed via iodometric titration and the average peroxide weight percentage was 27.1% ± 2.0%. Vapor-phase concentrations of hydrogen peroxide over 27% H_2O_2(aq) were derived from published data.[56-57] Hydrogen peroxide was dosed at concentrations of 15, 30, 45, 60, and 75 ppm, accompanied by 1650, 3300, 4950, 6600, and 8250 ppm of water, respectively. Di-*t*-butyl peroxide (Aldrich, 98%) was used as purchased, and stored at 2-6 ^oC under inert gas. Dosing concentrations for di-*t*-butyl peroxide were calculated from reported

values[58] using the Clausius-Clapeyron equation. Di-*t*-butyl peroxide was dosed at concentrations of 150, 225, 300, 375, and 450 ppm. Before dosing, the devices were annealed at 70.0 ^{o}C for 1 h in order to drive off any adsorbed molecules and achieve a stable baseline current.

5.3.3 UV/Vis Measurements

Films of purified MPcs were deposited on clean glass slides by sublimation at 450 ^{o}C and 10^{-3} Torr. UV/Vis spectra of the films were recorded after deposition on a Hewlett Packard 8452A spectrophotometer; all slides were oriented identically during consecutive scans to remove variance in film absorption. The slides were suspended over a solution of 5% H_2O_2(aq) solution (approx. 24 ppm hydrogen peroxide vapor) and changes in the UV/Vis spectra were monitored hourly for seven hours.

5.4 RESULTS AND DISCUSSION

5.4.1 Film Characterization

The morphologies of the MPc films were determined by AFM using a Nanoscope IV Scanning Microscope in tapping mode with a Mikromasch NSC15 325 kHz probe. Films were uniformly composed of a granular structure with ellipsoidal grains of approximately 50 nm diameter on the long axis and an RMS roughness of 5 nm. Low angle X-ray diffraction studies revealed the films deposited at 25 ^{o}C to be textured α phase.[53] I-V measurements (voltage range = 10V to -10V, 0.1V increments) were recorded in the test chamber at 5 degree increments in a range from 5 to 50 ^{o}C.

The devices were allowed to equilibrate at each temperature and voltage. All devices reported showed ohmic behavior at low voltages, with space charge limited conductivity (SCLC) occurring above approximately 5 V. Miller and coworkers showed that operation of MPc IDEs in the SCLC regime yields sensing results independent of the metal contacts.[59] Device responses were measured at 8 V, which is well within the SCLC regime. The consensus in the literature is that 30 minutes is a sufficient time to reach the chemical saturation region of the sensor response.[60-64] Additionally, we have previously demonstrated that sensors can be operated in the kinetic regime (i.e. under 5 minutes) for basic physisorption and chemisorption interactions due to the first order kinetic behavior of sensor response.[39] In this study sensors were dosed in both the saturation (30 min) and kinetic (5 min) regimes.

5.4.2 Sensor Responses to Hydrogen Peroxide

Responses of FePc, CoPc, NiPc, CuPc, ZnPc, and H_2Pc sensors were determined from time-dependent current plots at constant voltage on dosing with 27% H_2O_2(aq). Sensors were dosed multiple times with identical concentrations of 27% H_2O_2(aq) to determine the repeatability of the responses. The devices were examined in the kinetic regime (5% approximate duty cycle: 5 min doses with 90 min recoveries) and in the saturation regime (25% duty cycle: 30 min doses with 90 min recoveries). Data in the kinetic and saturation regimes for each sensor are shown in Figure 5-2. The doses were composed of 45 ppm of hydrogen peroxide, accompanied by 4950 ppm of water (approximately 17% relative humidity); these data can be seen

in the upper trace of each panel (Figure 5-2). The sensors were also dosed identically (45 ppm hydrogen peroxide) at constant humidity (17% RH) in order to distinguish the sensor response of hydrogen peroxide from the sensor response to water. The data for the constant humidity runs are presented in the middle trace of each panel (Figure 5-2).

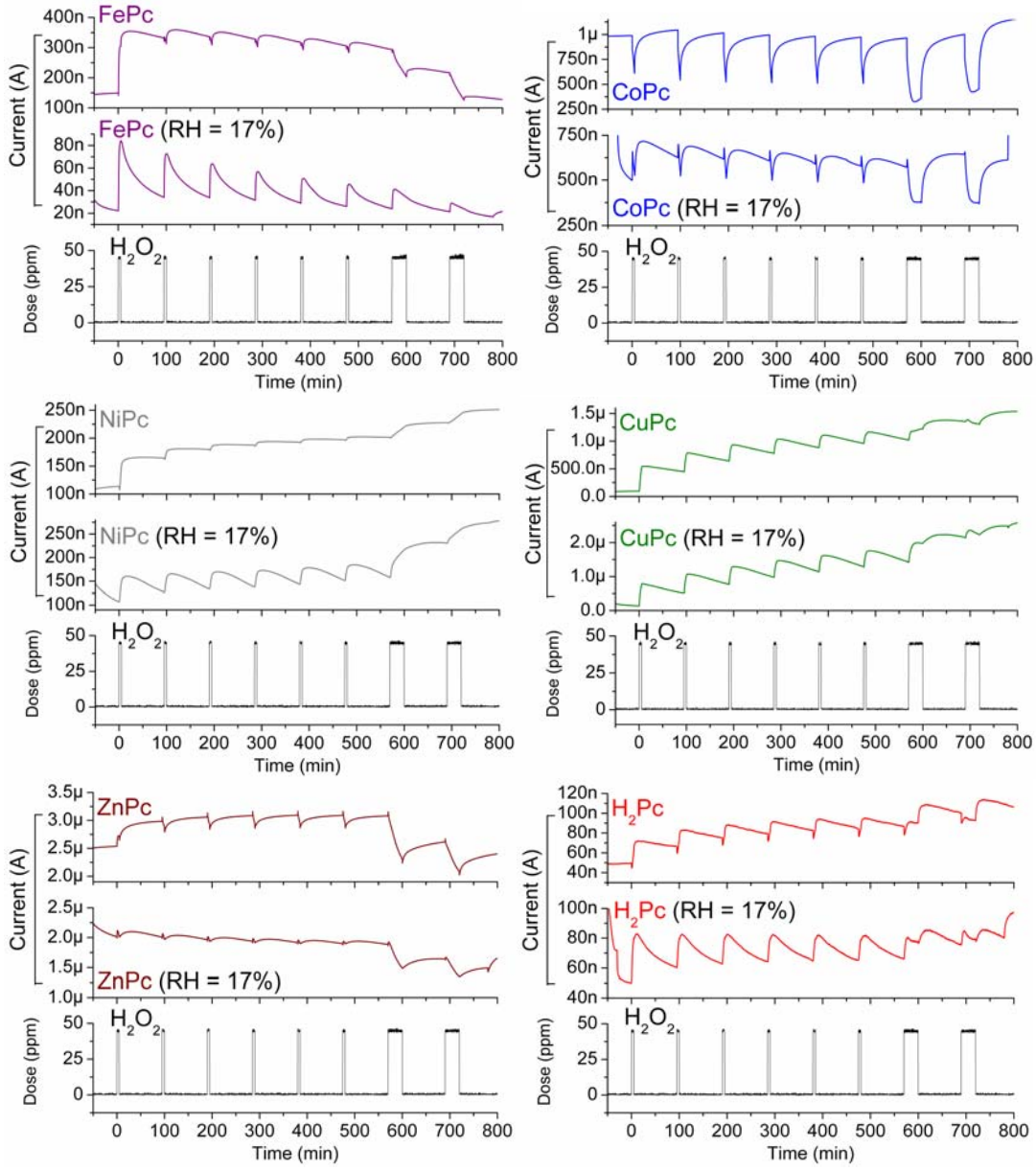

Figure 5-2 Sensing data for FePc (purple), CoPc (blue), NiPc (grey), CuPc (green), ZnPc (wine), and H_2Pc (red) measured at 8V and 50 ^{o}C, on exposure to 27% H_2O_2(aq) doses (black) in the presence (middle trace) and absence (upper trace) of humidity. Relative humidity present (RH) = 17%.

The sensors respond within the mixing time of the dosing system (< 15 s) on exposure of the films to peroxide vapors. When FePc is dosed with 27% H_2O_2(aq),

the first pulse induces a strong initial current increase, but subsequent doses induce only minimal changes in current. When FePc is dosed with 27% H_2O_2(aq) at constant humidity, current gains are observed for each peroxide pulse. FePc responses to solely 27% H_2O_2(aq) are consistent with initial film oxidation (with related current increase) by hydrogen peroxide followed by current losses from film interaction with water present in the subsequent doses. The superior response data at constant humidity are consistent with the FePc film being reduced by water between doses and reoxidized by the 27% H_2O_2(aq) doses.

CoPc responds with significant current losses to each pulse of 27% H_2O_2(aq) with and without constant humidity, in both the kinetic and saturation regimes. As shown with the long pulses, the CoPc sensors reach the maximum sensor response within 10 min. ZnPc responds to 27% H_2O_2(aq) in a manner similar to FePc; the first pulse induces a current increase but subsequent pulses induce small current losses. Conversely, at constant humidity, the ZnPc sensor responses are minimal, suggesting that water dominates the observed sensor response. NiPc, CuPc and H_2Pc exhibit current gains to 27% H_2O_2(aq) in the presence and absence of constant humidity; at constant humidity these films appear to be reduced by water between doses in a manner similar to FePc. In the saturation regime, these films appear to reach maximum sensor response within 10 min. The complex behavior seen for FePc, CuPc, and H_2Pc in response to saturation doses may be attributed to competing redox effects of hydrogen peroxide (oxidizing the film) and water (reducing the film).

Qualitatively, there are some differences between runs performed with and without constant humidity (e.g. H_2Pc sensors exhibit an initial current drop to each dose that is lost when constant humidity is applied) but, with the exception of FePc and ZnPc, the overall behavior is nearly identical with and without humidity. It has been previously reported that phthalocyanine sensors exhibit a decrease in current upon exposure to water vapor.[39,59,65] This was confirmed by exposing the various MPcs used in this study to 4950 ppm doses of water (5% duty cycle, Figure 5-3).

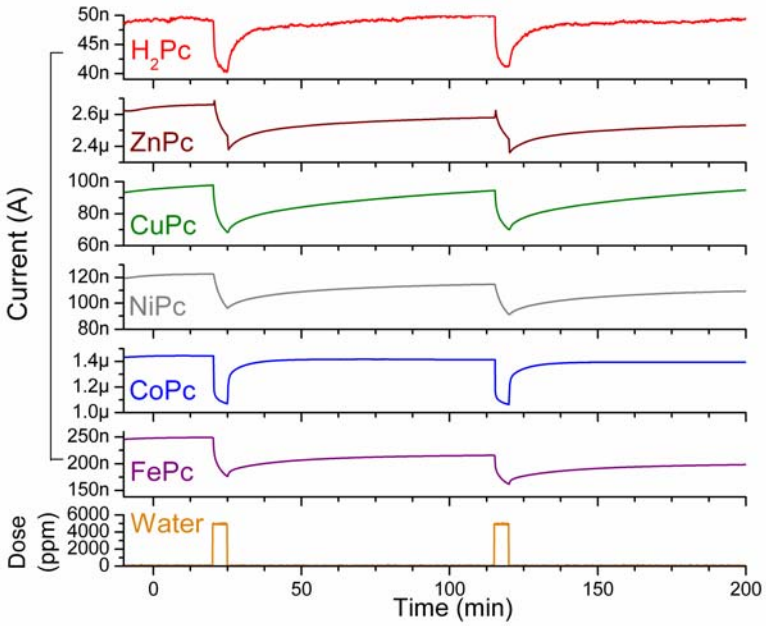

Figure 5-3 Sensing data for MPcs (M = Fe, Co, Ni, Cu, Zn, H_2) exposed to doses of 4950 ppm water (5% duty cycle, carrier gas: zero grade air, operating temp 50 ^{o}C, 8V).

Water doses cause current losses for all MPc films. However, the data presented in Figure 5-2 demonstrates that, with the exception of ZnPc, the hydrogen peroxide interaction with the MPcs is dominant, even at a concentration of water that is 3 orders of magnitude greater than the concentration of the peroxide. Because H_2O_2

is known to be both an oxidant and a reductant, the data is consistent with CoPc being reduced and FePc, NiPc, CuPc, and H_2Pc being oxidized; this model will be elaborated (*vide infra*). The varied sensor responses allow differential response analysis with a small MPc sensor array to be used to uniquely identify exposure to hydrogen peroxide vapor. Other oxidants, such as Cl_2, O_3, and NO_2 are known to all cause current increases for FePc, CoPc, NiPc, CuPc, ZnPc, and H_2Pc. Hydrogen peroxide is unique in showing current losses for CoPc concurrent with current gains on other MPc films. Therefore, a CoPc sensor could be paired with a NiPc, CuPc, or H_2Pc sensor for a peroxide specific sensor array.

It has been reported that sensor responses of MPcs exhibit first order kinetics and therefore are linear with respect to analyte concentration for physisorption and chemisorption interactions.[66-67] This behavior was examined for 27% H_2O_2(aq) by varying the dose concentration (15, 30, 45, 60, and 75 ppm hydrogen peroxide). Each MPc was dosed with 27% H_2O_2(aq) in the kinetic regime (5% duty cycle) and in the saturation regime (25% duty cycle). In addition, the sensor responses were analyzed quantitatively by calculating the percent current change for each dose (sensor response = $\Delta I/I_{baseline}$*100).[68] If the sensor exhibits a current increase, the response will be positive; likewise, if the sensor exhibits a current decrease, the response will be negative.

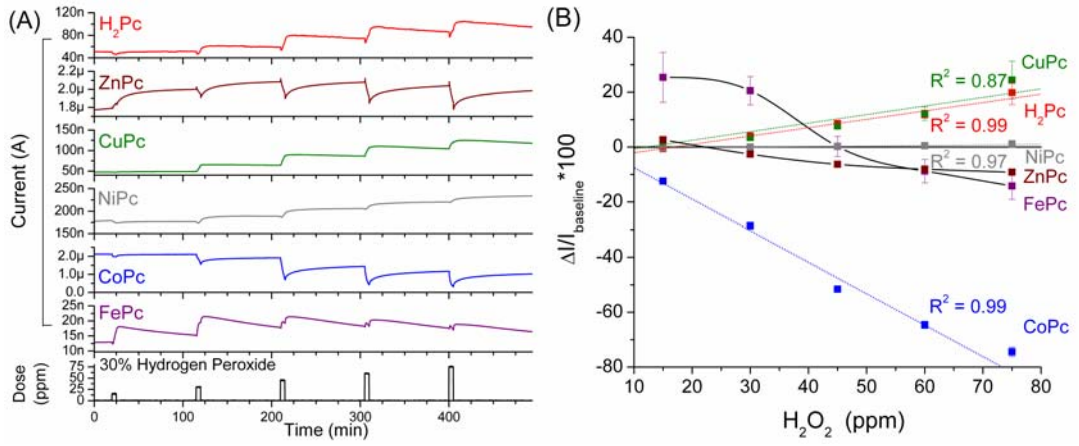

Figure 5-4 (A) Sensing data for MPcs (M = Fe, Co, Ni, Cu, Zn, H_2) exposed to 27% H_2O_2(aq) doses (5% duty cycle, carrier gas: zero grade air, operating temp 50 ^oC, 8V). (B) Sensor responses ($\Delta I/I_{baseline}$*100) for each dose, with best fit lines (dashed) for determining sensitivities and detection limits. The solid nonlinear traces are for FePc and ZnPc responses to 27% H_2O_2(aq).

Figure 5-4 shows data for all MPcs dosed with 27% H_2O_2(aq) in the kinetic regime at varied concentrations, as well as the quantitative sensor responses for each dose. The quantitative data shows that sensor responses for CoPc, NiPc, CuPc, and H_2Pc are linear with concentration, while responses for FePc and ZnPc are not. As seen in Figure 5-2, ZnPc responds to the first dose with a current increase, followed by current losses for subsequent doses. The non-linear response of ZnPc to hydrogen peroxide would be consistent with the 27% H_2O_2(aq) responses by ZnPc being dominated by the response to water rather than peroxide. The sensitivities of the MPcs to hydrogen peroxide may be defined as the slope (% ppm^{-1}) of the sensor. The linear fits of responses versus concentration show modest non-ideal behavior in that the intercepts are non-zero; this is likely due to influence of the water present in each dose, which acts as an offset. Sensitivities are presented in Table 5-1.

Table 5-1 Sensitivities (% ppm^{-1}) for MPcs (M = Fe, Co, Ni, Cu, Zn, H_2) to 27% H_2O_2(aq) and di-*t*-butyl peroxide vapors in the kinetic dosing regime at 50 ^oC and 8 V.

MPc	Hydrogen peroxide sensitivities (% ppm^{-1}) x 10^{-2}	Di-*t*-butyl peroxide sensitivities (% ppm^{-1}) x 10^{-2}
FePc[a]	N/A	6.2 ± 0.8
CoPc	-103.2 ± 3.3	-0.3 ± 0.1
NiPc	2.3 ± 0.9	0.3 ± 0.1
CuPc	31.2 ± 8.3	3.9 ± 1.5
ZnPc[b]	N/A	0.5 ± 0.2
H_2Pc	27.6 ±5.2	0

Figure 5-5 depicts MPc sensor behavior toward 27% H_2O_2(aq) in the saturation regime. The sensor responses do not correlate linearly with hydrogen peroxide concentration but instead depend on dosing history. This unusual behavior is consistent with a chemical or electrochemical reaction modifying the sensor film, rather than simple physisorption or chemisorption (*vide infra*). While CuPc, ZnPc, and H_2Pc exhibit significant current gains when initially exposed, on subsequent dosing the sensor responses saturate at what appears to be a maximum film oxidation. For successive doses, minor current losses occur, which can be attributed to the sensors responding to the water present in each dose. Conversely, NiPc displays current gains to each dose, suggesting that NiPc films take longer to reach oxidative

[a] FePc kinetic regime responses to 27% H_2O_2(aq) are nonlinear.
[b] ZnPc responses to 27% H_2O_2(aq) are overshadowed by water exposure.

saturation than films of CuPc, ZnPc, and H_2Pc. Both CoPc and FePc exhibit somewhat ill defined responses to the first large peroxide dose; however, the films respond to subsequent doses with significant current decreases. Like H_2Pc and CuPc, CoPc appears to reach sensor response saturation, but at maximum film reduction rather than oxidation. FePc sensor behavior differs in that sensor current decreases on exposure to long pulses of 27% H_2O_2(aq) with no recovery after the doses, so that by the end of the run the sensor current is negligible. This irreversible behavior may be due either to the formation of the μ-oxo dimer of FePc[69] or the catalytic breakdown of the film. This was further explored by UV/Vis spectroscopy.

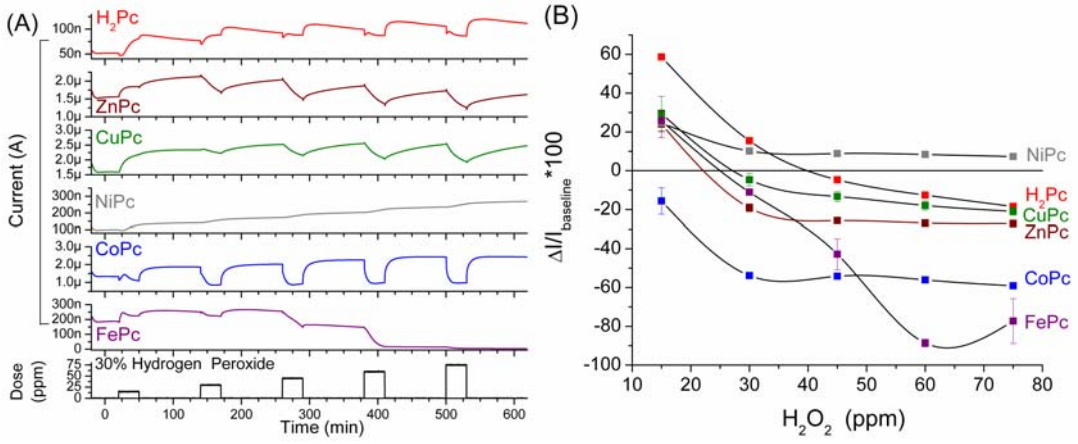

Figure 5-5 (A) Sensing data for MPcs (M = Fe, Co, Ni, Cu, Zn, H_2) exposed to 27% H_2O_2(aq) doses (25% duty cycle, carrier gas: zero grade air, operating temp 50 ^oC, 8V). (B) Sensor responses ($\Delta I/I_{baseline}$*100) for each dose.

5.4.3 UV/Vis Absorption Studies

Two major absorption bands are present in the UV/Vis spectra of MPcs, which give rise to the characteristic blue color of phthalocyanine dyes: the Soret band (λ =

300-350nm) and the Q band (λ = 600-700nm).[70] Changes in MPc oxidation state have been detected by monitoring these spectra.[71-73] Thin films of the MPcs were sublimed onto glass slides (no visible absorption above 300 nm); the slides were exposed to vapors from 5% H_2O_2(aq) solution (approx. 24 ppm hydrogen peroxide) and changes in the UV/Vis spectra were monitored for seven hours (Figure 5-6).

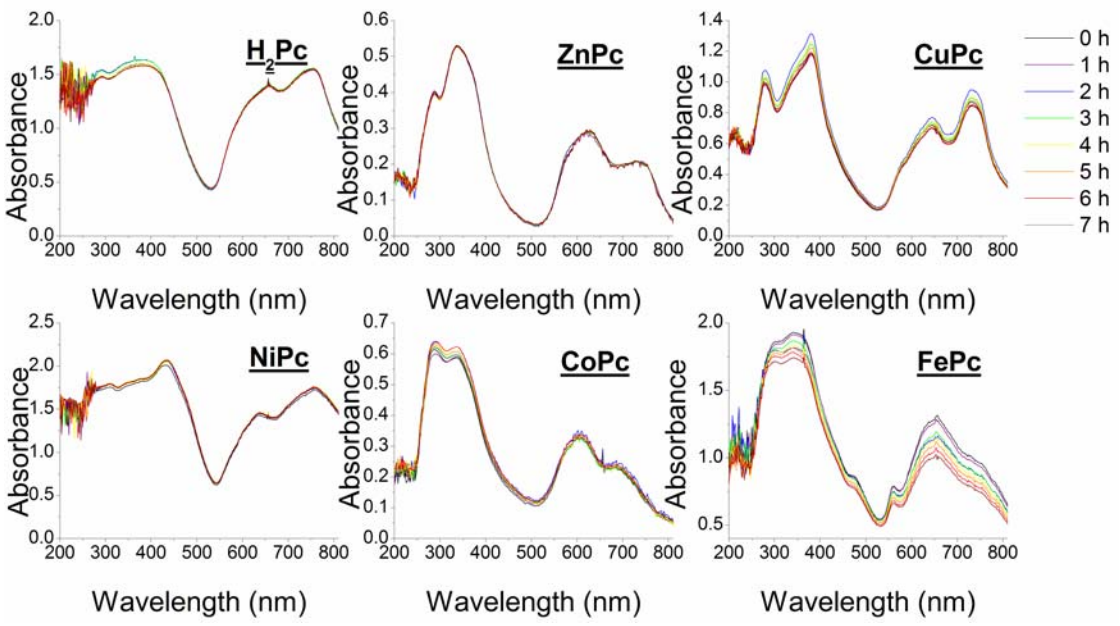

Figure 5-6 UV/Vis absorption spectra of thin evaporated films of MPcs on glass. The films were exposed to vapors of 5% H_2O_2(aq) solution (~24 ppm H_2O_2) at room temperature and spectra were taken hourly. FePc was the only film that showed a marked decrease in intensity with H_2O_2 exposure.

Negligible changes are evident in the spectra of CoPc, NiPc, CuPc, ZnPc, and H_2Pc, suggesting that changes of MPc oxidation states are too small to be monitored by this method. However, the absorption spectrum of FePc diminishes in intensity during the exposure time. To examine this further, an FePc film was exposed to the

vapor from 27% H_2O_2(aq) solution (approx. 381 ppm hydrogen peroxide). The absorption spectrum of FePc decreased drastically over time, and visual observation confirmed that the blue color of the film nearly disappeared. The instability of FePc films to H_2O_2 exposure explains the irreversible decrease in FePc sensor current: the FePc film degrades to the point of being nonconductive.

5.4.4 Mechanism of Hydrogen Peroxide Detection

The redox properties of the most common MPcs (M = Fe, Co, Ni, Cu, Zn, and H_2) have been thoroughly studied in the scientific literature with theoretical and experimental techniques. Experimental studies of MPcs with redox-active metal centers (M = Fe, Co) have shown that their redox activity is based on the metal; Co^{3+}, Co^{2+}, and transient Co^{+} states have been identified,[71] and Fe^{2+} and Fe^{3+} phthalocyanine species are well known.[73] Similar studies of MPcs with less redox-active metal centers (M = Ni, Cu, Zn) and of H_2Pc have shown that oxidations and reductions occur on the organic ring rather than the metal center.[75-76] These results have been supported by theoretical work and DFT calculations.[77-78] From these electronic properties, it may be predicted that MPc reactions with H_2O_2 and corresponding sensor behavior may be divided into redox-active metal and redox-inactive metal groups.

Catalytic decomposition of H_2O_2 by MPcs has been explored using electrochemical techniques, oxygen evolution studies, and various spectrometric techniques.[42-45] Both FePc and CoPc have been demonstrated to be potent catalysts for H_2O_2 oxidation and reduction at positive and negative potentials, respectively.[42-48] The

oxidation of H_2O_2 by MPcs follows a second order catalase-type mechanism; the lack of linearity between sensor response and H_2O_2 concentration in the saturation regime can be explained by this model.[44-48] It is inferred from the current losses observed for CoPc in Figures 5-4 and 5-5 that the cobalt-catalyzed oxidation of H_2O_2 is occurring (with concurrent film reduction), leading to a catalytic saturation of sensor response. The catalase-type reaction can be written as follows (adapted from Gilmartin et al):[42]

$$2Co^{3+/2+}Pc + H_2O_2 \rightarrow 2Co^{2+/+}Pc + 2H^+ + O_2 \quad (1)$$

$$2Co^{2+/+}Pc \rightarrow 2Co^{3+/2+}Pc + 2e^- \quad (2)$$

$$H_2O_2 \rightarrow 2H^+ + O_2 + 2e^- \quad \textit{overall reaction} \quad (3)$$

The mechanism of the FePc-H_2O_2 reaction is more difficult to characterize. In the kinetic regime, the FePc sensor exhibits current gains consistent with H_2O_2 reduction and FePc film oxidation, while in the saturation regime the FePc sensor current decreases in an irreversible fashion. Deactivation of FePc electrodes in the presence of H_2O_2 has previously been reported;[79] the UV/Vis data presented here is consistent with deactivation and current loss resulting from oxidative destruction of the FePc film. Oxidative breakdown of the conductive film by H_2O_2 results in irreversible current loss and probably occurs through the generation of $^{\bullet}OH$ radicals during the reduction of hydrogen peroxide.

The reaction between H_2O_2 and MPcs with non-redox-active metal centers has been less extensively researched.[49] Voltammetric studies of a variety of MPcs revealed no electrocatalytic behavior for Ni, Cu, Zn, and H_2Pc in the presence of H_2O_2,[49] but EPR studies of optically excited ZnPc solutions revealed the presence of $^{\bullet}OH$ radicals,

suggesting homolytic cleavage of H_2O_2.[52] The presence of a small amount of hydroxyl radicals during dosing accounts for H_2O_2 oxidation of Ni, Cu, and H_2Pc films, leading to the observed sensor responses. The marked similarity of ZnPc responses to water and H_2O_2 suggests that the oxidation of ZnPc by H_2O_2 is negligible and overshadowed by the sensor interaction of ZnPc with water. This can be seen in the saturation regime (Figure 5-5) where ZnPc is weakly oxidized on the first dose and exhibits current losses on subsequent exposures. ZnPc will thus be disregarded with respect to detection of hydrogen peroxide. The reaction of NiPc, CuPc, ZnPc, and H_2Pc with hydrogen peroxide can be portrayed as a radical reaction (4) or as a charge transfer process following coordination (5):[52]

$$MPc + HOOH \rightarrow MPc^{\bullet +} + OH^- + {}^{\bullet}OH \quad (4)$$

$$MPc + HOOH \rightarrow [MPc \text{ --- } HOOH \leftrightarrow MPc^{\delta +} \text{ --- } HOOH^{\delta -}] \quad (5)$$

5.4.5 Sensor Responses to Di-*t*-butyl Peroxide

FePc, CoPc, NiPc, CuPc, ZnPc, and H_2Pc sensors were exposed to doses of di-*t*-butyl peroxide and sensor responses were recorded as time-dependent current plots. Dose concentrations were varied to examine sensor responses at 150, 225, 300, 375, and 450 ppm exposures. Devices were analyzed in the kinetic regime (5% duty cycle, 5 min doses with 90 min recovery) and in the saturation regime (25% duty cycle, 30 min doses with 90 min recovery). Data for the kinetic regime is displayed in Figure 5-7; data for the saturation regime is displayed in Figure 5-8.

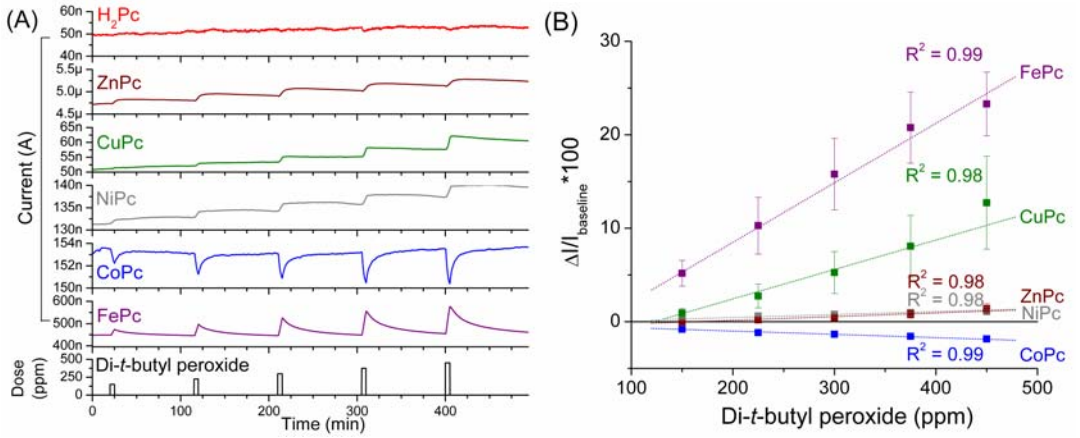

Figure 5-7 (A) Sensing data for MPcs (M = Fe, Co, Ni, Cu, Zn, H_2) exposed to di-*t*-butyl peroxide doses (5% duty cycle, carrier gas: zero grade air, operating temp 50 ^{o}C, 8V). (B) Sensor responses ($\Delta I/I_{baseline}$*100) for each dose, with best fit lines (dashed) for determining sensitivities and detection limits. H_2Pc was neglected due to lack of sensitivity.

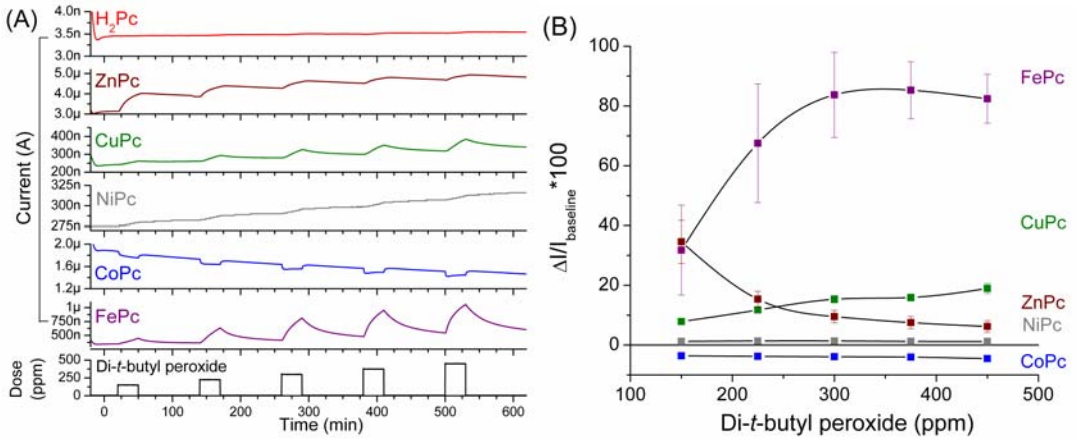

Figure 5-8 (A) Sensing data for MPcs (M = Fe, Co, Ni, Cu, Zn, H_2) exposed to di-*t*-butyl peroxide doses (25% duty cycle, carrier gas: zero grade air, operating temp 50 ^{o}C, 8V). (B) Sensor responses ($\Delta I/I_{baseline}$*100) for each dose.

There is significant variance in the sensor responses of the different MPcs. H_2Pc shows no response to di-*t*-butyl peroxide. CoPc films display current losses upon dosing with di-*t*-butyl peroxide consistent with CoPc film reduction by the

peroxide. FePc, NiPc, CuPc, and ZnPc films show an increase in current to each pulse of di-*t*-butyl peroxide consistent with the films being oxidized by exposure to the organic peroxide; these responses were weak for NiPc, moderate for ZnPc and CuPc, and strong for FePc. In the kinetic regime, the sensor responses of all MPcs to di-*t*-butyl peroxide are linear with concentration. Sensitivities (% ppm^{-1}) were calculated for each MPc and are displayed in Table 5-1. However, in the saturation regime the sensor responses to di-*t*-butyl peroxide do not follow first order kinetics and are again dependent on dosing history consistent with irreversible chemical reactions.

5.4.6 Mechanism of Di-*t*-butyl Peroxide Detection

Catalytic reactions of MPcs with organic peroxides have been the subject of limited prior study. In voltammetric studies, FePc modified carbon electrodes have been shown to catalyze the reduction of organic hydroperoxides, hydrogen peroxide, and peroxy acids at low positive potentials (0.1-0.2V); however, minimal responses were seen for dialkyl peroxides.[50] This mechanism is consistent with the FePc sensors responses observed in the present study. Conversely, CoPc has been reported to catalyze the oxidation of organic hydroperoxides and dialkyl peroxides at low positive potentials consistent with the current losses/film reductions observed in the present study.[51] Organic peroxide catalytic decomposition with NiPc and CuPc has not been reported. However, EPR studies of ZnPc and AlPc provided evidence for the reductive cleavage of dialkyl peroxides into highly reactive alkoxy radicals, which can then extract electrons from the MPc film leading to peroxide reduction and MPc

oxidation.[52] The behavior of Ni, Cu, and ZnPc in the current study suggests a similar type of mechanism in thin sensor films. The analogous mechanisms of di-*t*-butyl peroxide reactions for the various MPcs are suggested as follows.[80]

FePc: $Fe^{2+}Pc + {}^{t}BuOO^{t}Bu \rightarrow Fe^{3+}Pc + O^{t}Bu^{-} + {}^{\bullet}O^{t}Bu$ (7)

CoPc: $2Co^{3+/2+}Pc + {}^{t}BuOO^{t}Bu \rightarrow 2Co^{2+/+}Pc$ + complex breakdown products (8)

Ni, Cu, ZnPc: $MPc + {}^{t}BuOO^{t}Bu \rightarrow MPc^{\bullet+} + O^{t}Bu^{-} + {}^{\bullet}O^{t}Bu$ (9)

(7) and (9) generate holes and are expected to increase conductivity, while (8) reduces holes and leads decreased conductivity.

5.4.7 Detection Limits

MPc chemiresistive sensors offer potential advantages over existing commercial vapor-phase peroxide detection methods. Colorimetric methods suffer from a lack of quantifiable data and cross-reactivity with Cl_2 and NO_2,[81-82] while IR detection systems are bulky and have high power demands.[83] In addition to the problem of cross-reactive interferents, electrochemical sensors must rely on an electrolyte solution, which limits their operating temperature range from 0 ^{o}C to 65 ^{o}C.[84] In contrast, MPc chemiresistors are compact, with low power demands; they are robust, with a large operating temperature range (up to 150 ^{o}C); and they are selective for peroxides.

Detection limits of the above commercial hydrogen peroxide sensors range from 0.1 ppm to 1 ppm. No vapor phase detection limits are available for di-*t*-butyl peroxide. Detection limits for the chemiresistive MPc sensors examined in this study

were calculated from the MPc sensitivities determined from kinetic regime sensing data (Table 5-1). The detection limits were calculated as the peroxide dose concentration at which the sensors exhibit a signal to noise ratio of 3 (Table 5-2). Sensor noise was low, ranging from 0.01% to 0.3%. The influence of water was considered in the calculation of the limits for H_2O_2; for CuPc and H_2Pc the x-intercept of the linear fit of kinetic regime data (Figure 5-4) marks the point where the water present in the 27% hydrogen peroxide solution overcomes the peroxide response, and detection limits were calculated at S/N = 3 in the positive y direction. For CoPc, the y-intercept (linear fit, Figure 5-4) marks the point where only the water response is observed and the detection limit was calculated at S/N = 3 above this level. The detection limits for di-*t*-butyl peroxide had no interference from water, and were calculated at S/N = 3. CoPc is the most sensitive material for detecting peroxides, with a lower detection limit of 50 ppb for hydrogen peroxide and 250 ppb for di-*t*-butyl peroxide; its sensitivity is an improvement on the state of the art.[85] These detection limits may be further improved by incorporation of a preconcentrator[10] or an ultrathin ChemFET geometry, which have been shown to increase MPc film sensitivities.[86]

Table 5-2 Detection limits for each MPc to H_2O_2 and di-*t*-butyl peroxide, calculated at a sensor signal to noise ratio of 3.

MPc (Response at S/N =3)	Hydrogen peroxide detection limit (ppm)	Di-*t*-butyl peroxide detection limit (ppm)
FePc (0.3%)	N/A	53.0
CoPc (0.03%)	0.05	0.25
NiPc (0.2%)	40.1	101.1
CuPc (0.03%)	12.2	146.5
ZnPc (0.06%)	N/A	188.2
H_2Pc (0.9%)	11.7	N/A

5.5 CONCLUSION

Hydrogen peroxide and organic peroxide vapors may be selectively detected in ppb amounts by contrasting oxidation/reduction behavior in nanoscale chemiresistive films of metallophthalocyanines. This study presents the first example of a series of MPc vapor sensors showing both oxidation and reduction to the same analyte based on the specific metal center of the MPc, which may be attributed to electrocatalytic processes in the sensor film. When exposed to 27% H_2O_2(aq), FePc, NiPc, CuPc, and H_2Pc all show current gains, while CoPc demonstrates marked current losses. When exposed to di-*t*-butyl peroxide H_2Pc shows a minimal response, CoPc again shows current losses, and FePc, NiPc, CuPc and ZnPc show current gains. Therefore, differential response analysis can be used to uniquely identify the presence of hydrogen peroxide or organic peroxides through the combination of two sensors (e.g.,

CoPc and CuPc) with opposite sensor responses. Device characteristics and detection limits may be improved by incorporating a preconcentrator and an ultrathin ChemFET geometry. This study represents a new approach to selective analyte detection: catalytic redox contrast in a sensor array.

5.6 ACKNOWLEDGEMENT

Chapter 5 is a reprint in full of the material as it appears in the *Journal of Materials Chemistry*, **2008**, *submitted*. Coauthors included C. Colesniuc, J. Park, I. K. Schuller, A. C. Kummel, and W. C. Trogler.

5.7 REFERENCES

(1) Jacobs, P. T.; Lin, S. M. Gas Plasma Sterilization. *Irradiation of Polymers: Fundamentals and Technological Applications*; Clough, R. L., Shalaby, S. W., Eds.; ACS Symposium Series 620; American Chemical Society: Washington, DC, 1996; pp 216-39.

(2) Occupational Safety and Health Administration Website, Chemical Sampling Information: Hydrogen Peroxide. http://www.osha.gov/dts/chemicalsampling/data/CH_246600.html (accessed May 2007).

(3) Dickson, K. F.; Caravati, E. M. *J. Toxicol. Clin. Toxicol.* **1994**, *32*, 705-14.

(4) Bellamy, A. J. *J. Forensic Sci.* **1999**, *44*, 603-608.

(5) *Report of the Official Account of the Bombings in London on 7th July 2005.* HC series, 2005-06 1087; House of Commons, Parliament, Great Britain; Stationary Office, London, 2006.

(6) Landler, Mark. German police arrest 3 in terrorist plot. *New York Times* 09/06/07; http://www.nytimes.com/2007/09/06/world/europe/06germany.html

(7) Schulte-Ladbeck, R.; Kolla, P.; Karst, U. *Anal. Chem.* **2003**, *75*, 731-735.

(8) Schulte-Ladbeck, R.; Edelmann, A.; Quintas, G.; Lendl, B.; Karst, U. *Anal. Chem.* **2006**, *78*, 8150-8155.

(9) Schulte-Ladbeck, R.; Kolla, P.; Karst, U. *Analyst* **2002**, *127*, 1152-1154.

(10) Schulte-Ladbeck, R.; Karst, U. *Anal. Chim. Acta* **2003**, *482*, 183-188.

(11) Hong, J.; Maguhn, J.; Freitag, D.; Kettrup, A. *Fresenius J. Anal. Chem.* **1998**, *361*, 124-128.

(12) Lu, D.; Cagan, A.; Munoz, R. A. A.; Tangkuaram, T.; Wang, J. *Analyst* **2006**, *131*, 1279-1281.

(13) Snow, A. W.; Barger, W. R. Phthalocyanine Films in Chemical Sensors. *Phthalocyanines: Properties and Applications;* Lever, A. B. P., Ed.; John Wiley and Sons: New York, 1989; Vol. 1, p. 341.

(14) Eley, D. *Nature* **1948**, *162*, 819.

(15) Wright, J. D. *Prog. Surf. Sci.* **1989**, *31*, 1-60.

(16) Guillaud, G.; Simon, J.; Germain, J. *Coord. Chem. Rev.* **1998**, *178*, 1433-1484.

(17) Chen, J. C.; Ju, Y. H.; Liu, C. J. *Sens. Actuators, B* **1999,** *60*, 168-173.

(18) Schollhorn, B.; Germain, J. P.; Pauly, A.; Maleysson, C.; Blanc, J. P. *Thin Solid Films* **1998**, *326*, 245-250.

(19) Germain, J. P.; Pauly, A.; Maleysson, C.; Blanc, J. P.; Schollhorn, B. *Thin Solid Films* **1998,** *333*, 235-239.

(20) Zhou, Q.; Gould, R. D. *Thin Solid Films* **1998**, *317*, 436-439.

(21) Bora, M.; Schut, D.; Baldo, M. A. *Anal. Chem.* **2007**, *79*, 3298-3303.

(22) Martin, M.; Andre, J. J.; Simon, J. *J. Appl. Phys.* **1983**, *54*, 2792-2794.

(23) Pankow, J. W.; Arbour, C.; Dodelet, J. P.; Collins, G. E.; Armstrong, N. R. *J. Phys. Chem.* **1993**, *97*, 8485-8494.

(24) Hiller, S.; Schlettwein, D.; Armstrong, N. R.; Wohrle, D. *J. Mater. Chem.* **1998**, *8*, 945-954.

(25) Kerp, H. R.; Westerduin, K. T.; van Veen, A. T.; van Faassen, E. E. *J. Mater. Res.* **2001**, *16*, 503-511.

(26) Simon, J.; Andre, J. J. *Molecular Semiconductors* Springer-Verlag: Berlin, **1985**; pp 73-149.

(27) Ho, K. C.; Tsou, Y. H. *Sens. Actuators, B* **2001**, *77*, 253-259.

(28) Zwart, J.; Van Wolput, J. H. M. C. *J. Molec. Cat.* **1979**, *5*, 51-64.

(29) Yahiro, H.; Naka, T.; Kuramoto, J.; Kurohagi, K.; Okada, G.; Shiotani, M. *Microporous Mesoporous Mater.* **2005**, *79*, 291-297.

(30) Barbon, A.; Brustolon, M.; van Faassen, E. E. *Phys. Chem. Chem. Phys.* **2001**, *3*, 5342-5347.

(31) Lee, Y. L.; Hsiao, C. Y.; Chang, C. H.; Yang, Y. M. *Sens. Actuators, B* **2003**, *94*, 169-175.

(32) Lee, Y. L.; Tsai, W. C.; Chang, C. H.; Yang, Y. M. *Appl. Surf. Sci.* **2001**, *172*, 191-199.

(33) Liu, C. J.; Hsieh, J. C.; Ju, Y. H. *J. Vac. Sci. Technol., A* **1996**, *14(3)*, 753-756.

(34) Sadaoka, Y.; Jones, T. A.; Gopel, W. *Sens. Actuators, B* **1990**, 148-153.

(35) Brunet, J.; Pauly, A.; Mazet, L.; Germain, J. P.; Bouvet, M.; Malezieux, B. *Thin Solid Films* **2005**, *490*, 28-35.

(36) Miyata, T.; Minami, T. *Appl. Surf. Sci.* **2005**, *244*, 563-567.

(37) Bouvet, M.; Guillaud, G.; Leroy, A.; Maillard, A.; Spirkovitch, S.; Tournilhac, F. G. *Sens. Actuators, B* **2001**, *73*, 63-70.

(38) Sadaoka, Y.; Jones, T. A.; Gopel, W. *J. Mater. Sci. Lett.* **1989**, *8*, 1288-1290.

(39) Bohrer, F. I.; Sharoni, A.; Colesniuc, C.; Park, J.; Schuller, I. K.; Kummel, A. C.; Trogler, W. C. *J. Am. Chem. Soc.* **2007**, *129*, 5640-5646.

(40) Wring, S. A.; Hart, J. P.; Birch, B. J. *Electroanalysis* **1992**, *4*, 299-309.

(41) Wang, J.; Golden, T.; Li, R. *Anal. Chem.* **1988**, *60*, 1642-1645.

(42) Gilmartin, M. A. T.; Ewen, R. J.; Hart, J. P.; Honeybourne, C. L. *Electroanalysis* **1995**, *7*, 547-555.

(43) Mashazi, P. N.; Ozoemena, K. I.; Nyokong, T. *Electrochim. Acta* **2006**, *52*, 177-186.

(44) Korzhenevskii, A. B.; Shikova, T. G.; Bykova, V. V.; Koifman, O. I. *Russ. J. Gen. Chem.* **2002**, *72*, 1123-1127.

(45) Tarasevich, M. R.; Zakharkin, G. I. *React. Kinet. Catal. Lett.* **1977**, *6*, 77-82.

(46) Hadasch, A.; Sorokin, A.; Rabion, A.; Meunier, B. *New J. Chem.* **1998**, *22*, 45-51.

(47) Linders, C. R.; Vincke, B. J.; Patriarche, G. J. *Anal. Lett.* **1986**, *19*, 1831-1837.

(48) Kozawa, A.; Zilionis, V. E.; Brodd, R. J. *J. Electrochem. Soc.* **1970**, *117*, 1470-1474.

(49) Gilmartin, M. A. T.; Ewen, R. J.; Hart, J. P. *J. Electroanal. Chem.* **1996**, *401*, 127-137.

(50) Qi, X.; Baldwin, R. P. *Electroanalysis* **1993**, *5*, 547-554.

(51) Wang, J.; Angnes, L.; Liang, C.; Evans, O. *Talanta* **1991**, *38*, 1077-1081.

(52) Gantchev, T. G.; Sharman, W. M.; Lier, J. E. *Photochem. Photobiol.* **2003**, *77*, 469-479.

(53) Miller, C. W.; Sharoni, A.; Liu, G.; Colesniuc, C. N.; Fruhberger, B.; Schuller, I. K. *Phys. Rev. B* **2005,** *72*, 104113/1-6.

(54) Proud, W. G.; Field, J. E. *AIP Conference Proceedings* **1999**, *505*, 937-940.

(55) Maass, O.; Hatcher, W. H. *J. Am. Chem. Soc.* **1920**, *42*, 2548-2569.

(56) Scatchard, G.; Kavanagh, G. M.; Ticknor, L. B. *J. Am. Chem. Soc.* **1952**, *74*, 3715-3720.

(57) Manatt, S. L.; Manatt, M. R. R. *Chem. Eur. J.* **2004**, *10*, 6540-6557.

(58) Diogo, H. P.; Minas de Piedade, M. E.; Martinho Simoes, J. A.; Nagano, Y. *J. Chem. Thermodynamics* **1995**, *27*, 597-604.

(59) Miller, K. A.; Yang, R. D.; Hale, M. J.; Park, J.; Fruhberger, B.; Colesniuc, C. N.; Schuller, I. K.; Kummel, A. C.; Trogler, W. C. *J. Phys. Chem, B* **2006,** *110*, 361-366.

(60) de Haan, A.; Debliquy, M.; Decroly, A. *Sens. Actuators, B* **1999**, *57*, 69-74.

(61) Lee, Y. L.; Hsiao, C. Y.; Hsiao, R. H. *Thin Solid Films* **2004**, *468*, 280-284.

(62) Lee, Y. L.; Chang, C. H. *Sens. Actuators, B* **2006,** *119*, 174-179.

(63) Lee, Y. L.; Tsai, W. C.; Maa, J. R. *Appl. Surf. Sci.* **2001,** *173*, 352-361.

(64) Kolesar, E. S.; Wiseman, T. M. *Anal. Chem.* **1989,** *61*, 2355-2361.

(65) de Haan, A.; Decroly, A. *Sens. Actuators, B* **1996**, *30*, 143-150.

(66) Wilson, A.; Collins, R. A. *Sens. Actuators* **1987**, *12*, 389-403.

(67) Tongpool, R.; Yoriya, S. *Thin Solid Films* **2005**, *477*, 148-152.

(68) Patel, S. V.; Mlsna, T. E.; Fruhberger, B.; Klaassen, E.; Cemalovic, S.; Baselt, D. R. *Sens. Actuators, B* **2003**, *96*, 541-553.

(69) Ercolani, C.; Gardini, M.; Monacelli, F.; Pennesi, G.; Rossi, G. *Inorg. Chem.* **1983**, *22*, 2584-2589.

(70) Edwards, L.; Gouterman, M. *J. Mol. Spectrosc.* **1970**, *33*, 292-310.

(71) Rollmann, L. D.; Iwamoto, R. T. *J. Am. Chem. Soc.* **1968**, *90*, 1455-1463.

(72) Cahill, A. E.; Taube, H. *J. Am. Chem. Soc.* **1951**, *73*, 2847-2851.

(73) Lever, A. B. P.; Pickens, S. R.; Minor, P. C.; Licoccia, S.; Ramaswamy, B. S., Magnell, K. *J. Am. Chem. Soc.* **1981**, *103*, 6800-6806.

(74) Kennedy, B. J.; Murray, K. S.; Zwack, P. R.; Homborg, H.; and Kalz, W. *Inorg. Chem.* **1985**, *24*, 3302-3305.

(75) Clack, D. W.; Hush, N. S.; Woolsey, I. S. *Inorg. Chim. Acta.* **1976**, *19*, 129-132.

(76) Wolberg, A.; Manassen, J. *J. Am. Chem. Soc.* **1970**, *92*, 2982-2991.

(77) Toman, P.; Nespurek, S.; Yakushi, K. *Macromol. Symp.* **2004**, *212*, 327-334.

(78) Liao, M. S.; Scheiner, S. *J. Chem. Phys.* **2001**, *114*, 9780-9791.

(79) Melendres, C. A.; Feng, X. *J. Electrochem. Soc.* **1983**, *130*, 811-814.

(80) Workentin, M. S.; Maran, F.; Wayner, D. D. M. *J. Am. Chem. Soc.* **1995**, *117*, 2120-2121.

(81) AFT International, Inc. Website, Dräger Safety Short Term Detector Tubes: Hydrogen Peroxide. http://www.afcintl.com/pdf/draeger/8101041.pdf (accessed July 2007).

(82) Centanni, M. A. Visual detector for vaporized hydrogen peroxide. U. S. Patent 7,186,373, July 22, 2003.

(83) McVey, I. F. Non-dispersive mid-infrared sensor for vaporized hydrogen peroxide. U. S. Patent 7,157,045, July 9, 2002.

(84) Dräger Inc. Safety Website, DrägerSensor® H_2O_2 LC Chemical Sensor Data Sheet. http://www.draeger.com/ST/internet/pdf/Master/En/gt/9023492_h2o2lc_d_e.pdf (accessed July 2007).

(85) Regarding a H_2O_2 selective sensor array comprised of CuPc and CoPc sensors: while CuPc is only sensitive to 12 ppm of H_2O_2 it does not raise the effective detection limit of 50 ppb, since CuPc sensors are more sensitive to the broad class of electron donor analytes that cause current losses in both CoPc and CuPc sensors. Thus, a 50 ppb dose of H_2O_2 would cause a decrease in the CoPc sensor, but a weak or undetectable decrease in CuPc sensor; however, an electron donor analyte would cause a decrease in both sensors, with the effect being larger for CuPc.

(86) Yang, R. D.; Gredig, T.; Colesniuc, C. N.; Park, J.; Schuller, I. K.; Trogler, W. C.; Kummel, A. C. *Appl. Phys. Lett.* **2007**, *90*, 263506/1-3.

CHAPTER VI

FIELD EFFECT TRANSISTORS OF ZINC PHTHALOCYANINE

6.1 ABSTRACT

Chemically sensitive field-effect transistors (ChemFETs) of zinc phthalocyanine (ZnPc) were fabricated and evaluated for use as organic transistors and vapor sensors. Bottom-gate FETs were prepared using standard photolithography and lift-off processing. The semiconducting channel consisted of 50 nm thick sensing films of ZnPc, which were deposited using organic molecular beam epitaxy. Average device mobilities were 1.3×10^{-4} cm^2 V^{-1} s^{-1}, comparable to previously reported phthalocyanine mobility values. ZnPc ChemFETs were found to display persistent photoconductivity lasting up to 1.5 months. This photoconductivity induced significant baseline drift which may be partially suppressed by using a pulsed gate bias. Persistent photoconductivity and the ensuing baseline current instability require improvements to the ZnPc ChemFET architecture before its implementation in vapor sensors.

6.2 INTRODUCTION

Organic field-effect transistors (OFETs) are of interest for chemical sensing of vapor-phase compounds due to the dependence of charge transport within the organic channel on environmental chemical species. Field-effect transistors consist of a

semiconducting channel contacted by source and drain electrodes; charge transport within the channel is modulated by use of a gate electrode separated from the channel by a thin dielectric layer. When the gate is biased, the electric field produced can either attract or repel carriers in the channel, and control of the current flow can be achieved.[1] Silicon-based FETs are used widely in electronics and computer processors; these include metal-oxide-semiconductor FETs (MOSFETs) and metal-insulator-semiconductor FETs (MISFETs).[2] The semiconducting channel is the bottom layer of the MOSFET, generally composed of p-type silicon with doped n-type regions where the source and drain electrodes contact (Figure 6-1A). An oxide layer over the channel forms the insulating dielectric between the metal gate electrode and the channel.

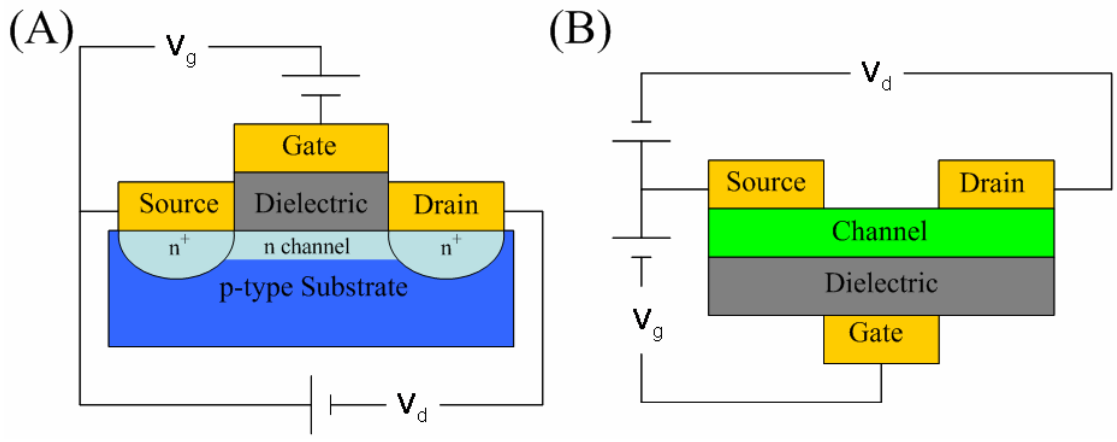

Figure 6-1 Device geometries of (A) MOSFET and (B) OFET.

OFETs are of interest for applications such as flexible displays,[3] chemical sensors,[4] and large-scale electronic applications.[5] The geometry of an OFET differs from a MOSFET in that the semiconducting channel is the top layer of the device,

deposited on the insulating dielectric with source and drain electrodes either above or below the channel (Figure 6-1B). Semiconducting materials used in OFETs are generally p-type and include pentacene, polythiophenes, phthalocyanines, poly(phenylene ethynylene), and polyaniline.[4-6] N-type organic materials are also being developed, and include fluorinated phthalocyanines and oligothiophenes as well as heterocyclic aromatics.[7]

Current output curves for standard p-type OFET operation are shown in Figure 6-2A. OFETs operate in accumulation mode, where the drain bias (V_d) and gate bias (V_g) are both negative. The result is that the charge carriers (holes) are pulled down to the channel/dielectric interface. In the linear regime (low V_d) the drain current (I_d) is proportional to V_d. When V_d is increased, I_d approaches a finite maximum value; this is denoted the saturation regime.[8] The charge carrier mobility may be approximated from transfer curves (I_d recorded at constant V_d while V_g is swept, Figure 6-2B). These curves may be recorded in the linear or saturation regimes. The mobility is extracted from the linear regime I_d by equation (1) and from the saturation regime I_d by equation (2).[9]

$$I_d = (Z/L)C_i\mu[(V_g - V_0)V_d - (V_d^2/2)] \quad (1)$$

$$I_{dsat} = (Z/2L)C_i\mu(V_g - V_0)^2 \quad (2)$$

In equations (1) and (2) Z and L are the channel width and length, C_i is the dielectric capacitance, V_0 is the threshold voltage, and μ is the mobility of the charge carriers. Average mobilities in silicon MOSFETs are 1 $cm^2\ V^{-1}\ s^{-1}$; OFET mobilities are generally 3 to 4 orders of magnitude lower, although recently progress has been made,

with mobilities approaching those of silicon MOSFET.[8,10] Threshold voltages in these devices arise from gate-dependent mobility in the accumulation region and can lead to significant currents at low gate bias.[11]

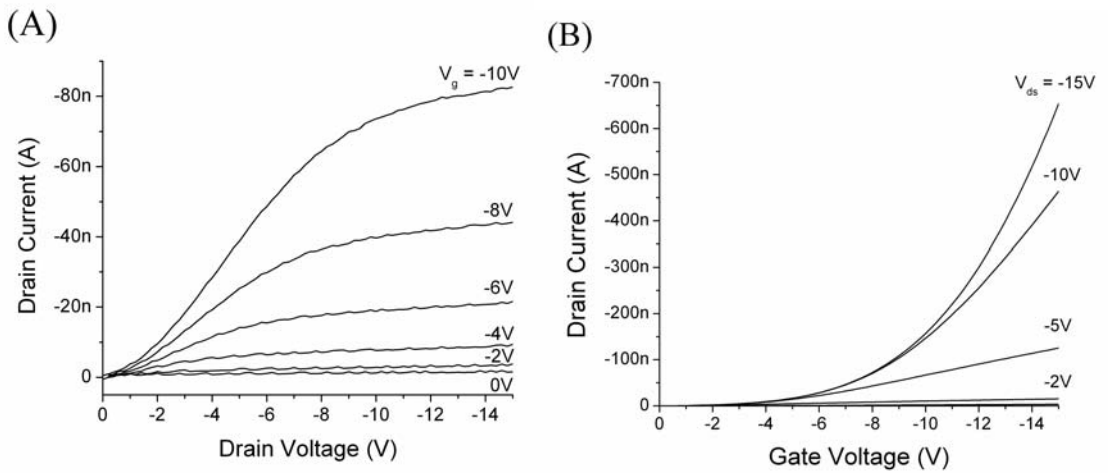

Figure 6-2 (A) Output and (B) transfer curves for a copper phthalocyanine (CuPc) FET.

Field-effect transistors with chemically sensitive channels have been demonstrated to be reliable sensors.[12-20] MOSFETs have been adapted for limited use as chemFETs for potentiometric sensor applications in conducting liquids.[13] OFETs exhibit potential for use as vapor sensors because the organic semiconductor films are generally sensitive to weak intermolecular interactions with vapor-phase molecules and have channels that may be easily exposed to air (Figure 6-1B).[14-15] ChemFETs have been developed using a variety of organics, most often oligo- and poly-thiophenes,[16] phthalocyanines,[17] and pentacene.[18-19] The chemically sensitive layer may also be applied to the gate; exposure of a polymer gate to vapor-phase analytes modifies the FET threshold voltage.[20]

Metallophthalocyanines (MPcs) are useful channel materials for chemFETs. MPcs have been extensively studied for gas sensing applications, and the sensing mechanisms are now well-understood.[21-23] Mobilities of copper phthalocyanine (CuPc) FETs approach those of amorphous Si (0.02 $cm^2\ V^{-1}\ s^{-1}$).[24-25] CuPc chemFETs offer excellent sensitivity to analytes such as ozone, with detection limits of 10 ppb.[26] Ultrathin sensing films of CuPc (3.8 monolayers, or approximately 6 nm), while exhibiting relatively modest mobilities ($1.0x10^{-4}\ cm^2\ V^{-1}\ s^{-1}$), display excellent sensing behavior, including rapid response and recovery, stable baseline currents, and high sensitivity.[27-28] Zinc phthalocyanine (ZnPc) is another phthalocyanine of interest for sensing applications; zinc porphyrins and phthalocyanines are photoconductive and show high sensitivity to volatile amines and other strong binders.[29-33] ZnPc chemFETs have been investigated with respect to volatile solvents, but not for more strongly binding analytes.[34]

In the following chapter electrical characteristics of ZnPc ChemFETs are explored. It was found that ZnPc FETs exhibit non-ideal FET behavior which gradually corrected itself over an extended period (approximately 1 month). This behavior has been attributed to persistent photoconductivity in the photoactive ZnPc semiconductor layer.[33,35] This photoconductivity renders ZnPc unfit for sensor studies, as it causes the baseline current to drift significantly. This extended period of photoinduced conductivity decay exacerbates the problem.

6.3 EXPERIMENTAL

6.3.1 Device Fabrication

ChemFETs were fabricated using interdigitated electrodes (IDEs) as source and drain contacts, ZnPc films as the semiconducting channels, and n-type Si substrates as gates, with backside Au gate contacts. IDEs were prepared by standard photolithography and lift-off processing on thermally grown SiO_2 (100 nm thick) on highly doped n^+ Si wafers. The electrodes consist of 45 pairs of fingers with a channel length of 5 μm and an electrode width of 2 mm. The electrodes were deposited by electron beam evaporation; an adhesion layer of 5 nm Ti was applied first, followed by 45 nm of Au, for a total electrode thickness of 50 nm. The backside oxide was removed by buffered oxide etching (BOE) and 100 nm of gold was evaporated onto the clean silicon to form the gate contact. Six pairs of IDEs were grown on each substrate to verify sensor reproducibility and increase yield.

Sensing films were deposited by organic molecular beam epitaxy (OMBE). ZnPc (Aldrich, 97%) was purified via multiple zone sublimations at 400 ^oC and 10^{-5} Torr. 50 nm thick films were deposited onto the FETs in a UHV chamber with a base pressure of $2x10^{-10}$ Torr. The deposition rate ranged from 0.2 to 0.5 Å s^{-1}, and the deposition pressure was $5x10^{-9}$ Torr. Film growth rate and thickness were monitored with a quartz crystal microbalance (QCM). The FETs were mounted on a temperature-controlled stage monitored with two thermocouples. Substrate temperature during deposition was held constant at 25.0 ± 1.0 ^oC. After deposition, the devices were stored under vacuum at 10^{-3} Torr for 48 h until use. The thickness of

the films was confirmed by low angle XRD measurements performed on a Rigaku RU-200B diffractometer using Cu K_α radiation.[36]

6.3.2 Device Characterization

ZnPc films were imaged with a Nanoscope IV Scanning Microscope in tapping mode with a Mikromasch NSC15 325 kHz probe (Figure 6-3). The films had a granular structure with ellipsoidal grains of approximately 50 nm diameter on the long axis and an RMS roughness of 5 nm. Low angle XRD measurements performed on a Rigaku RU-200B diffractometer using Cu K_α radiation revealed the films to be textured α phase.[36]

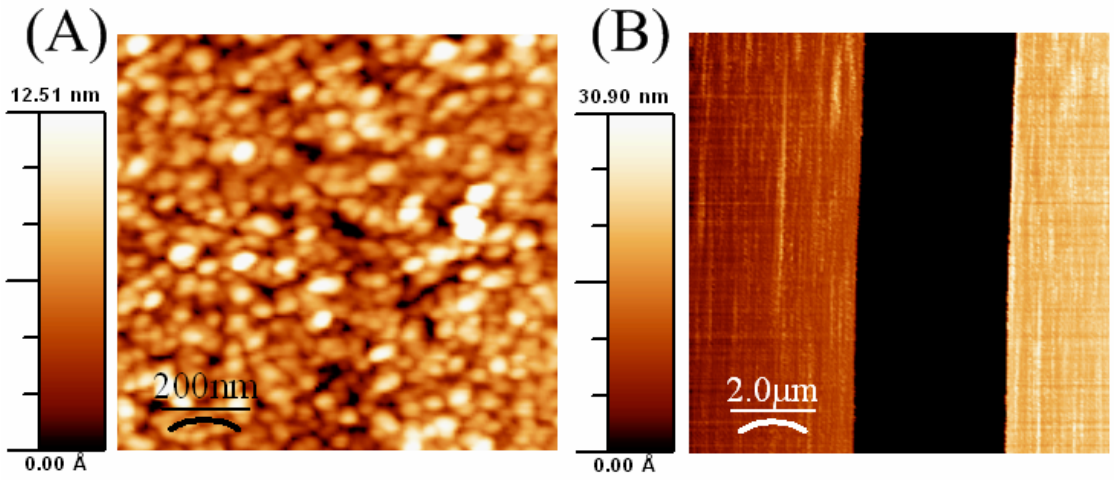

Figure 6-3 AFM images of ZnPc films (A) 1 µm x 1 µm (channel) and (B) 10 µm x 10 µm (electrodes surrounding channel).

6.3.3 Device Measurements

ZnPc chemFETs were analyzed inside a stainless steel test chamber with an internal volume of 50 cm^3. The FETs were mounted on PCB packages and electrical

contacts were made with indium solder points. The PCB package was connected to the voltage supplies and picoammeter through a DB-25 adapter in the test chamber wall. The internal temperature of the chamber was monitored by a thermocouple and maintained at 25.0 ± 0.1 ^{o}C by coolant lines connected to a Haake F8 constant temperature bath. Agilent E3641A and E3631A DC power supplies were used to bias the gate and drain electrodes, respectively. A Keithley 6485 picoammeter was used to monitor the source-drain current. Current-voltage characteristics were studied using a Labview VI program.

6.4 RESULTS AND DISCUSSION

6.4.1 Field Effect Behavior

ZnPc ChemFETs were characterized in an optically isolated chamber at 25 ^{o}C in dry air. The sensors were isolated in this chamber for at least one month to allow photoconductivity to decay and remove the effects of ambient humidity on the films. Output curves were recorded by applying a fixed gate bias and monitoring I_d while sweeping V_d. Transfer curves were recorded by applying a fixed drain bias and monitoring I_d while sweeping V_g. Typical output and transfer curves are displayed in Figure 6-4A and 6-4B, respectively. The output curves showed well-defined saturation behavior with relatively low currents (less than 1 μA). Carrier mobility was calculated from transfer data; the average mobility was 1.3×10^{-4} cm^2 V^{-1} s^{-1}, similar to previously reported MPc mobility values.[28,37]

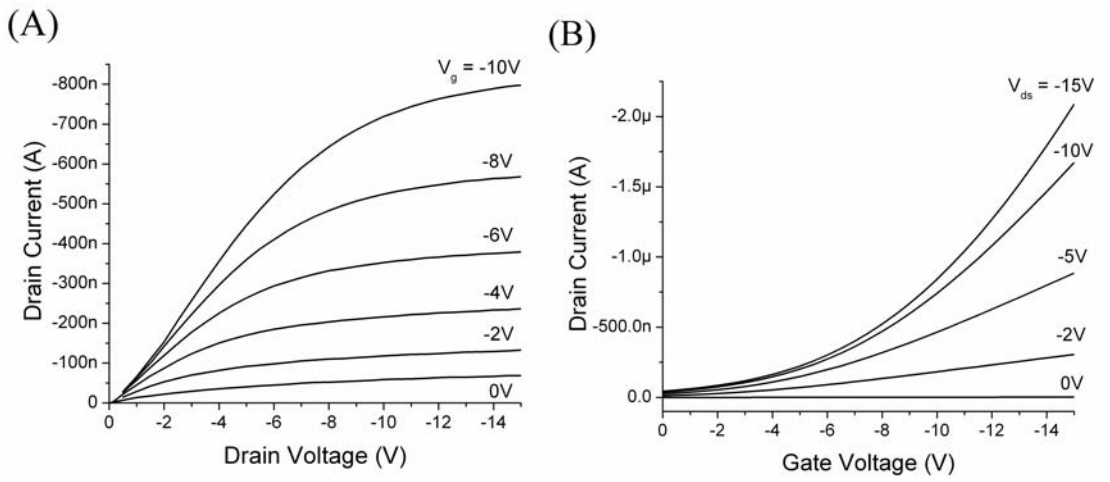

Figure 6-4 Typical (A) output and (B) transfer curves for a ZnPc ChemFET.

6.4.2 Photoconductivity

ZnPc chemFETs display high currents and non-saturation output behavior when measured in the presence of light or within one day of optical isolation (Figure 6-5A). This is attributed to photogenerated charge carriers overwhelming the field-effect. Upon continued optical isolation and monitoring, these currents were gradually reduced. One hour after isolation the ZnPc chemFET current (V_d = -15V, V_g = -10V) was -2.1 µA; after 6 days the current at the same drain and gate bias had been reduced to approximately -600 nA (Figure 6-5B). The field-effect of the gate electrode was gradually recovered over a period of 42 days; saturation output behavior improved over this time (Figure 6-5C, D).

This behavior is attributed to persistent photoconductivity with the ZnPc film. Zinc phthalocyanines and porphyrins are well-known to be photoactive and photoconductive.[29-34] Persistent photoconductivity has been well documented in semiconductors and FETs.[35] The I-V characteristics presented (Figure 6-5A-D)

generally resemble persistent photoconductivity in MOSFETs, including suppression of the field-effect of the gate and a lack of saturation behavior.[38] The slow decay of persistent photoconductivity has been modeled by Queisser and Theodorou: assuming hole-electron pair recombination through wave function overlap, the closest charge pairs recombine and the recombination probability exponentially decreases with distance, slowing the decay process considerably over long time scales and leading to extremely long-lived photoconductivity in ZnPc devices.[39]

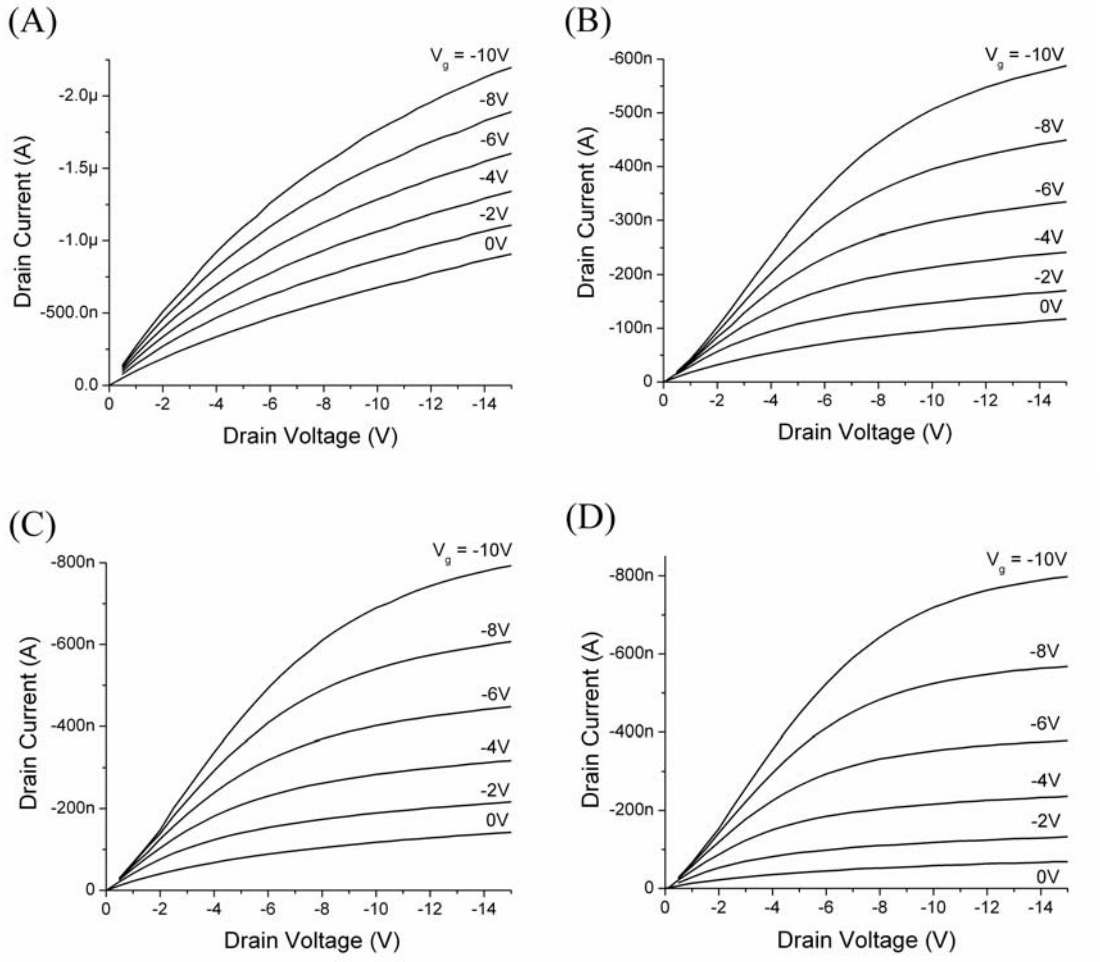

Figure 6-5 Output curves for a ZnPc FET taken (A) one hour after isolation in a dark, dry air environment; (B) six days after isolation; (C) 12 days after isolation; (D) 42 days after isolation.

6.4.3 Baseline Drift in ZnPc ChemFETs

The baseline currents of ZnPc ChemFETs were examined for drift. Stable baseline currents have been obtained in CuPc ChemFETs by pulsing V_g, energizing the gate only briefly while recording I_d and allowing the film to relax between pulses.[28] Optimal drift suppression was achieved using a 1% gate duty cycle (V_g applied for 100 ms every 10 s). This type of pulsed gating was applied to ZnPc. Baseline drifts were recorded in the saturation regime (Figure 6-6A, V_d = -10V) at various gate voltages (V_g = -2V, -4V, -6V, -8V). V_g = -4V gave the lowest baseline current drift, 0.5% h^{-1} (Figure 6-6B).

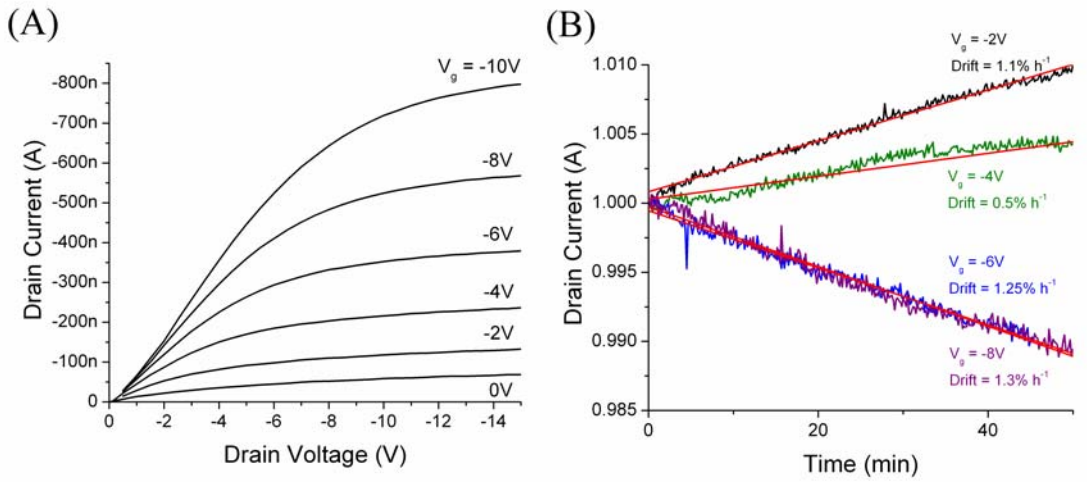

Figure 6-6 (A) Output curves and (B) baseline current drifts at various V_g for a ZnPc ChemFET.

The baseline drifts of the ZnPc ChemFETs were moderate to reasonably good for 50 nm films.[28] A major drawback, however, was that considerable settling time (~8 h) was required for the ChemFETs to reach these stable drift baselines. Over this

settling time the drift was often much larger and nonlinear. Settling times may be mitigated in a variety of ways: better temperature control of the sensing chamber, improved device contacts through wire-bonding, and annealing the films before use. Temperature control would be improved through the use of a smaller testing chamber.[23]

6.5 CONCLUSION

ChemFETs using chemiresistive ZnPc films as the channel layer were fabricated and characterized. Device mobilities were comparable to other organic thin film transistors, with average mobilities of 1.3×10^{-4} cm^2 V^{-1} s^{-1}. ZnPc films exhibited persistent photoconductivity lasting for approximately 1.5 months; this photoconductivity masked the field effect and led to non-saturation output behavior from the FET. A result of this photoconductivity was significant baseline current drift, which could be partially suppressed by application of pulsed gate bias. Further device optimization is necessary before implementation of ZnPc ChemFETs as practical organic transistors and vapor sensors, but it may be more practical to use other channel materials.

6.6 ACKNOWLEDGEMENT

The author would like to thank Dr. Richard Yang for insights and assistance with the work presented above.

6.7 REFERENCES

(1) Sze, S. M. *Physics of Semiconductor Devices 2nd Ed.* John Wiley and Sons: New York, 1981: Chapter 8.

(2) Zolper, J. C. *Solid-State Electron.* **1998**, *42*, 2153-2156.

(3) Shirota, Y.; Kageyama, H. *Chem. Rev.* **2007**, *107*, 953-1010.

(4) Mabeck, J. T.; Malliaras, G. G. *Anal. Bioanal. Chem.* **2006**, *384*, 343-353.

(5) Dimitrakopoulos, C. D.; Malenfant, P. R. L. *Adv. Mater.* **2002**, *14*, 99-117.

(6) *Semiconducting Polymers : Chemistry, Physics, and Engineering*; Hadziioannou, G., van Hutten, P. F., Eds.; Wiley VCH: New York, 2000.

(7) Newman, C. R.; Frisbie, C. D.; da Silva Filho, D. A.; Bredas, J. L.; Ewbank, P. C.; Mann, K. R. *Chem. Mater.* **2004**, *16*, 4436-4451.

(8) Horowitz, G. *Mol. Cryst. Liq. Cryst.* **1998**, *322*, 63-70.

(9) Horowitz, G.; Hajlaoui, M. E.; Hajlaoui, R. *J. Appl. Phys.* **2000**, *87*, 4456-4463.

(10) Laquindanum, J. G.; Katz, H. E.; Lovinger, A. J.; Dodabalapur, A. *Chem. Mater.* **1996**, *8*, 2542-2544.

(11) Horowitz, G.; Hajlaoui, R.; Bouchriha, H.; Bourguiga, R.; Hajlaoui, M. *Adv. Mater.* **1998**, *10*, 923-927.

(12) Someya, T.; Katz, H. E.; Gelperin, A.; Lovinger, A. J.; Dodabalapur, A. *Appl. Phys. Lett.* **2002**, *81*, 3079-3081.

(13) Domansky, K.; Janata, J.; Josowicz, M.; Petelenz, D. *Analyst* **1993**, *118*, 335-340.

(14) Grate, J. W.; Abraham, M. H. *Sens. Actuators, B* **1991,** *3,* 85-111.

(15) Grate, J. W. *Chem. Rev.* **2000,** *100*, 2627-2648.

(16) Torsi, L.; Tanese, M. C.; Cioffi, N.; Gallazzi, M. C.; Sabbatini, L.; Zambonin, P. G.; Raos, G.; Meille, S. V.; Giangregorio, M. M. *J. Phys. Chem., B* **2003**, *107*, 7589-7594.

(17) Touda, H.; Tada, H.; Matsushige, K. *Mol. Cryst. Liq. Cryst.* **1999**, *327*, 287-290.

(18) Wang, L.; Fine, D.; Sharma, D.; Torsi, L.; Dodabalapur, A. *Anal. Bioanal. Chem.* **2006**, *384*, 310-321.

(19) Huang, J.; Miragliotta, J.; Becknell, A.; Katz, H. E. *J. Am. Chem. Soc.* **2007**, *129*, 9366-9376.

(20) Covington, J. A.; Gardner, J. W.; Briand, D.; de Rooij, N. F. *Sens. Actuators, B* **2001**, *77*, 155-162.

(21) Guillaud, G.; Simon, J.; Germain, J. *Coord. Chem. Rev.* **1998**, *178*, 1433-1484.

(22) Wright, J. D. *Prog. Surf. Sci.* **1989**, *31*, 1-60.

(23) Bohrer, F. I.; Sharoni, A.; Colesniuc, C.; Park, J.; Schuller, I. K.; Kummel, A. C.; Trogler, W. C. *J. Am. Chem. Soc.* **2007**, *129*, 5640-5646.

(24) Bao, Z.; Lovinger, A. J.; Dodabalapur, A. *Appl. Phys. Lett.* **1996**, *69*, 3066-3068.

(25) Ofuji, M.; Ishikawa, K.; Takezoe, H.; Inaba, K.; Omote, K. *Appl. Phys. Lett.* **2005**, *86*, 062114/1-3.

(26) Bouvet, M.; Guillaud, G.; Leroy, A.; Maillard, A.; Spirkovitch, S.; Tournilhac, F. G. *Sens. Actuators, B* **2001**, *73*, 63-70.

(27) Yang, R. D.; Gredig, T.; Colesniuc, C. N.; Park, J.; Schuller, I. K.; Trogler, W. C.; Kummel, A. C. *Appl. Phys. Lett.* **2007**, *90*, 263506/1-3.

(28) Yang, R. D.; Park, J.; Colesniuc, C. N.; Schuller, I. K.; Trogler, W. C.; Kummel, A. C. *J. Appl. Phys.* **2007**, *102*, 034515/1-7.

(29) Kerp, H. R.; Westerduin, K. T.; van Veen, A. T.; van Faassen, E. E. *J. Mater. Res.* **2001**, *16*, 503-511.

(30) Dunbar, A. D. F.; Richardson, T. H.; McNaughton, A. J.; Hutchinson, J.; Hunter, C. A. *J. Phys. Chem. B* **2006**, *110*, 16646-16651.

(31) Spadavecchia, J.; Ciccarella, G.; Stomeo, T.; Rella, R.; Capone, S.; Siciliano, P. *Chem. Mater.* **2004**, *16*, 2083-2090.

(32) Winkelmann, C. B.; Ionica, I.; Chevalier, X.; Royal, G.; Bucher, C.; Bouchiat, V. *Nano Lett.* **2007**, *7*, 1454-1458.

(33) Gantchev, T. G.; Sharman, W. M.; Lier, J. E. *Photochem. Photobiol.* **2003**, *77*, 469-479.

(34) Bora, M.; Schut, D.; Baldo, M. A. *Anal. Chem.* **2007**, *79*, 3298-3303.

(35) Nathan, M. I. *Solid-State Electron.* **1986**, *29*, 167-172.

(36) Miller, C. W.; Sharoni, A.; Liu, G.; Colesniuc, C. N.; Fruhberger, B.; Schuller, I. K. *Phys. Rev. B* **2005,** *72*, 104113/1-6.

(37) Gould, R. D. *Coord. Chem. Rev.* **1996**, *156*, 237-274.

(38) Lehovec, K.; Seeley, W. G. *Solid-State Electron.* **1971**, *14*, 1077-1086.

(39) Queisser, H. J.; Theodorou, D. E. *Phys. Rev. B* **1986**, *33*, 4027-4033.

CHAPTER VII

DISSERTATION SUMMARY, CONCLUSIONS, AND FUTURE DIRECTIONS

The sensitivity of metallophthalocyanine conduction to atmospheric chemical species makes MPcs ideal candidates for gas sensing applications. As p-type molecular semiconductors, MPcs are sensitive to both electron donor and acceptor gases, which tune the film current by trapping and generating charge carriers, respectively. MPcs have little intrinsic conductivity, and their observed conduction arises from doping by environmental oxidants such as oxygen, ozone, and nitrogen oxides. The metal center of the phthalocyanine molecule determines the molecular orbital structure, which in turn influences the interaction of the MPc with gaseous analytes. This metal center is the most energetically favorable site for analyte binding, and may also be involved in catalytic processes. These attributes render phthalocyanines highly useful for gas sensing applications.

A broad array of research is available examining the dependence of MPc sensing on metal center, organic functionalization, crystal phase, film mesostructure, and analyte identity. Research presented in this dissertation seeks to elucidate the mechanism of MPc sensing of gas-phase analytes of military, industrial, and medical relevance, including volatile peroxides, organophosphate neurotoxins, and other volatile organic compounds. Analyte identification by a cross-reactive array of MPc sensors is of particular interest.

Chapter 2 describes the syntheses of a wide range of MPcs, including such metals as Ti(IV), V(IV), Mn(II), Fe(II), Co(II), Ni(II), Cu(II), and Pd(II). Organically modified MPcs were prepared, incorporating methyl-, *tert*-butyl-, and 1,1,1,3,3,3-hexafluoropropan-2-ol (HFIP) functional groups. This last functional group was unavailable commercially, and so required the development of a novel synthetic method. To this end, hexafluoracetone was added to the 4-position of 2-bromoaniline through a Friedel-Crafts reaction. 4-HFIP-phthalonitrile was derived from 4-HFIP-2-bromoaniline by conversion of the amino group to the nitrile through the Sandmeyer reaction (diazotization), followed by replacement of the bromo group with the nitrile by the Rosenmund-von Braun reaction. 4-HFIP-phthalonitrile was cyclized around a copper(II) center to form $Cu(HFIP)_4Pc$ as a pH-sensitive, dark blue-purple solid in good yield (66%)

Film morphology was studied by depositing 50 nm thick films by organic molecular beam epitaxy (OMBE) and spin-coating. Textured α-phase films were deposited by OMBE; these films had an ellipsoidal granular structure with a grain diameter of 50 nm on the long axis. The identity of the MPc metal center had minimal effect on film morphology, but the substrate deposition temperature drastically affected both film crystal phase and grain structure. Films deposited at a substrate temperature of 25 ^{o}C had stable film currents and reproducible sensing behaviors. Spin-coating was explored as a cost-effective alternative to OMBE for production of uniform films of soluble, functionalized phthalocyanines. Tetrasubstituted MPcs with *t*-butyl and HFIP groups were spin-coated from toluene and trifluoroethanol,

respectively, forming highly uniform amorphous films. These films suffered from extremely low conductivity due to the lack of molecular ordering.

Future investigation into sensing applications of functionalized phthalocyanines is warranted, as these functional groups show promise for analyte selectivity and improved device kinetics. Increased currents in amorphous MPc films may be produced by operating the MPc sensors at elevated temperatures (50 to 70 ^{o}C), thereby promoting charge carrier generation and hopping. Synthesis and spin-coating of mesogenic (liquid crystal) MPcs can lead to higher solid state ordering and concomitant conductivity gains. Field effect transistors offer another pathway to increase currents in amorphous MPc films, as application of a gate potential can improve charge carrier mobility.

Chapter 3 explores the differing mechanisms of sensing in H_2Pc and CoPc with respect to electron-donating (basic) analytes. CoPc sensor responses correlate bilinearly to the analyte Lewis basicity, while H_2Pc sensor responses correlate bilinearly to the analyte hydrogen bond basicity. This suggests that the analyte-phthalocyanine interaction is dominated by binding to the central cavity of the phthalocyanine, with metal coordination interactions determining CoPc sensor responses and hydrogen bonding interactions governing H_2Pc sensor responses. The interactions between the phthalocyanine films and analytes were found to follow first order kinetics. The influence of O_2 on the film response was examined, and it was found that competitive binding between analytes and O_2 significantly affects film response and recovery.

Chapter 4 furthers this investigation by increasing the number of MPcs studied to include CoPc, NiPc, CuPc, ZnPc, and H_2Pc. MPc sensitivities to vapor phase electron donors were found to correlate exponentially with analyte basicity as described by binding enthalpy, consistent with the van't Hoff equation and standard free energy of reaction; this contradicts earlier results which suggested bilinear dependence. As seen in chapter 3, MPc sensitivities correlated best with the Lewis basicity, while H_2Pc sensitivities correlated best with the hydrogen bond basicity. Sensor recovery times $t_{90}^{'}$, used as an indirect probe of the analyte desorption rate, were also found to depend exponentially on binding enthalpy, in agreement with the Arrhenius equation. Linear discriminant analysis (LDA) was used to identify analytes. Single sensor normalization of analyte concentration leads to excellent discrimination and identification of analytes.

Results from this array of MPcs show promise for future investigations into practical detection of analytes. Normalization of an array of MPc sensors to a single well-behaved device can remove analyte concentration dependence from the data, enabling analyte identification with LDA. Incorporation of a mass-sensitive device (SAW, QCM) as the normalizing factor may lead to greater discrimination between analytes. The MPc sensor array may be expanded to include such dissimilar metal centers as titanium, lead, silicon, or any of a number of lanthanide bis(phthalocyanine) sandwich compounds. These complexes offer different electronic and physical structures from the MPcs used in the present array, and may lead to an improvement in analyte identification.

Chapter 5 expands MPc array detection to vapor-phase peroxides, which are relevant to industrial safety and counterterrorism efforts. Chemiresistor arrays comprised of 50 nm thick films of metallophthalocyanines (MPcs, M = Fe, Co, Ni, Cu, Zn, and H_2) are redox-selective vapor sensors of hydrogen peroxide and di-*t*-butyl peroxide. These peroxides cause current losses in CoPc sensors and current gains in FePc, NiPc, CuPc, ZnPc, and H_2Pc sensors. Detection limits of 50 ppb and 250 ppb were achieved for hydrogen peroxide and di-*t*-butyl peroxide, respectively. The sensitivity of these films to peroxide analytes shows promise for the detection of peroxide-based explosives such as TATP and HMTD. This study presents the first example of a series of MPc vapor sensors showing both oxidation and reduction to the same analyte based on the specific metal center of the MPc, which may be attributed to electrocatalytic processes in the sensor film.

Further studies of improvised explosives detection are warranted. Explosive compounds are generally strongly oxidizing, leading to energetic instability and a tendency to react violently with reducing media. This strong redox behavior can lead to sensitive detection by MPc chemiresistors. Ammonium nitrate is a hygroscopic salt used to make ANFO, an improvised explosive used in a variety of terrorist acts, including the Oklahoma City bombing. Upon exposure to water, ammonium nitrate may hydrolyze to form nitric acid (an oxidant) and ammonia (a reductant). These redox-active components may in turn be detected by an MPc sensing array.

Chapter 6 investigates the use of ZnPc chemFETs for detection of analytes; chemFETs show promise for increased sensitivity and faster device kinetics. Device

mobilities were comparable to other organic thin film transistors, with average mobilities of $1.3x10^{-4}$ cm^2 V^{-1} s^{-1}. ZnPc films exhibited persistent photoconductivity lasting for approximately 1.5 months; this photoconductivity led to suppression of the field effect and non-saturation output behavior. This resulted in significant baseline current drift, which could be partially suppressed by application of pulsed gate bias. Further device optimization is necessary before implementation of ZnPc ChemFETs as practical organic transistors and vapor sensors.

ChemFET device parameters require improvement before continued study of vapor sensing. The current state of technology requires contacts be made via indium soldering, which is relatively unstable. An improved contact method would be wirebonding, which has been shown to make physically strong contacts with minimal resistance. Once this improvement has been made, then further exploration of photoconductivity across a range of MPcs would allow identification of MPcs with minimal photoconductivity and stable baseline currents. Reduction of photoconductivity and stabilization of drift are necessary before beginning array studies like those in chapter 4.

Metallophthalocyanines have been shown to be excellent candidates for chemiresistive sensors of vapor-phase analytes. MPcs are chemically sensitive to electron donors and acceptors in the low ppm range, and arrays of MPcs can specifically identify analytes. MPcs show potential for commercial use as sensitive detectors of peroxide-based improvised explosives and chemical warfare agents.